Nonequilibrium fluctuations and conversion processes

Gatien Verley

université
PARIS-SACLAY

Nonequilibrium fluctuations and conversion processes

Habilitation à diriger des recherches
de l'Université Paris-Saclay

Présentée et soutenue à Orsay, le 8 juillet 2024, par

Gatien VERLEY

Composition du jury :

Yannick De Decker Professeur, CENOLI, Université Libre de Bruxelles	Rapporteur
Cécile Monthus Directrice de recherche, CNRS, CEA, IPhT, Université Paris Saclay	Rapportrice
Frédéric Van Wijland Professeur, Laboratoire MSC, Université Paris Cité	Rapporteur
Bart Cleuren Professeur, Theory Lab, Université de Hasselt	Examinateur
Grégory Schehr Directeur de recherche, LPTHE, Sorbonne Université	Examinateur

Habilitation à diriger desrecherches

Contents

List of tables and figures

List of Acronyms

List of my publications

[1] G. Verley, K. Mallick, and D. Lacoste. Modified fluctuation-dissipation theorem for non-equilibrium steady states and applications to molecular motors. *Europhys. Lett.*, 93:10002, 2011.

[2] G. Verley, R. Chétrite, and D. Lacoste. Modified fluctuation-dissipation theorem for general non-stationary states and application to the Glauber-Ising chain. *J. Stat. Mech: Theory Exp.*, 10:P10025, 2011.

[3] G. Verley and D. Lacoste. Fluctuation theorems and inequalities generalizing the second law of thermodynamics out of equilibrium. *Phys. Rev. E*, 86:051127, 2012.

[4] G. Verley and D. Lacoste. Fluctuations and response from a Hatano and Sasa approach. *Phys. Scr.*, 86:058505, 2012.

[5] Gatien Verley. Nonequilibrium thermodynamic potentials for continuous-time markov chains. *Phys. Rev. E*, 93:012111, 2016.

[6] G. Verley and D. Lacoste. Fluctuation relations and fluctuation-response for molecular motors. In *AIP Conf. Proc.*, volume 1332, pages 247–248, 2011.

[7] G. Verley, R. Chétrite, and D. Lacoste. Inequalities generalizing the second law of thermodynamics for transitions between non-stationary states. *Phys. Rev. Lett.*, 108:120601, 2012.

[8] Hadrien Vroylandt, Massimiliano Esposito, and Gatien Verley. Collective effects enhancing power and efficiency. *Europhys. Lett.*, 120(3):30009, nov 2017.

[9] Hadrien Vroylandt, David Lacoste, and Gatien Verley. Degree of coupling and efficiency of energy converters far-from-equilibrium. *J. Stat. Mech: Theory Exp.*, 2018.

[10] Hadrien Vroylandt, David Lacoste, and Gatien Verley. An ordered set of power-efficiency trade-offs. *J. Stat. Mech: Theory Exp.*, 2019(5):054002, may 2019.

[11] Paul Raux, Christophe Goupil, and Gatien Verley. Thermodynamic circuits i: Association of devices in stationary nonequilibrium. September 2023.

[12] Hadrien Vroylandt and Gatien Verley. Non-equivalence of dynamical ensembles and emergent non-ergodicity. *J. Stat. Phys.*, 174(2):404–432, Jan 2018.

[13] G. Verley, T. Willaert, C. Van den Broeck, and M. Esposito. The unlikely carnot efficiency. *Nat. Commun.*, 5:4721, 2014.

[14] G. Verley, T. Willaert, C. Van den Broeck, and M. Esposito. Universal theory of efficiency fluctuations. *Phys. Rev. E*, 90:052145, 2014.

[15] M. Polettini, G. Verley, and M. Esposito. Efficiency statistics at all times: Carnot limit at finite power. *Phys. Rev. Lett.*, 114:050601, 2015.

[16] H. Vroylandt, A. Bonfils, and G. Verley. Efficiency fluctuations of small machines with unknown losses. *Phys. Rev. E*, 93:052123, 2016.

[17] Hadrien Vroylandt, Massimiliano Esposito, and Gatien Verley. Efficiency fluctuations of stochastic machines undergoing a phase transition. *Phys. Rev. Lett.*, 124(25), jun 2020.

[18] Gatien Verley. Dynamical equivalence classes for markov jump processes. *J. Stat. Mech: Theory Exp.*, 2022(2):023211, 2022.

[19] Lydia Chabane, Raphaël Chétrite, and Gatien Verley. Periodically driven jump processes conditioned on large deviations. *J. Stat. Mech: Theory Exp.*, 2020(3):033208, mar 2020.

[20] Lydia Chabane, Alexandre Lazarescu, and Gatien Verley. Effective hamiltonians and lagrangians for conditioned markov processes at large volume. *J. Stat. Phys.*, 187(1), feb 2022.

[21] G. Verley, C. Van den Broeck, and M. Esposito. Modulated two-level system: Exact work statistics. *Phys. Rev. E*, 88:032137, 2013.

[22] G. Verley, C. Van den Broeck, and M. Esposito. Work statistics in stochastically driven systems. *New J. Phys.*, 16(9):095001, 2014.

[23] S. Tusch, A. Kundu, G. Verley, T. Blondel, V. Miralles, D. Démoulin, D. Lacoste, and J. Baudry. Energy versus information based estimations of dissipation using a pair of magnetic colloidal particles. *Phys. Rev. Lett.*, 112:180604, 2014.

Chapter A

Introduction

Contents

A.1 Foreword

This professorial thesis manuscript summarizes the research I have produced since my doctoral thesis in 2012, which is entitled "Fluctuations and response of non-equilibrium systems". Since then, I have worked in stochastic thermodynamics, essentially on energy conversion, irreversible phenomena, and large deviation theory. This introductory Chapter A provides an overview of my works and field of research without going into much detail. Other chapters have a very different structure: Chapter B is almost an introductory lecture to stochastic thermodynamics and conversion processes, Chapter C collects unpublished works providing alternative points of view on my research, while Chapter D summarizes a coherent subset of my publications. Within stochastic thermodynamics, I have been interested in operational applications and theoretical developments. Most often, mean behaviors are sufficient for applications on the physics of coupled currents (which is a broader topic than energy conversion). However, it turned out that studying fluctuations was also inspiring for more applied topics. This is not surprising: Thermodynamics has always progressed through constant dialogue between theory and applications.

The title of this thesis, "Nonequilibrium fluctuations and conversion processes", emphasizes my objective during this first part of my career of modeling non-equilibrium phenomena by studying the coupling between and the fluctuations of physical currents in the simplest possible ways: I have worked on Markov jump processes mainly, on simple models with few states, on elementary interactions between many simple systems when working on the macroscopic limit, etc. Stochastic thermodynamics has allowed this approach by giving solid grounds to the thermodynamics of small (and hence simple) systems. A great merit of stochastic thermodynamics is its top-down construction. Just assuming modeling using stochastic processes, its core reasoning is to infer a constraint on the process dynamics (called Local Detailed Balance (LDB)) from the basic principles of thermodynamics. Since thermodynamics also deals with far-from-equilibrium transformations, such as gas mixtures, gas expansions, etc., the inferred constraints must hold far from equilibrium. The fact that the same constraints also arise from a perturbative analysis strengthens this theory. There is no contradiction: This does not reduce the realm of application, for instance, by rejecting its ability to describe far-from-equilibrium phenomena. In simple words, what can do more can do less. I will follow this line of thought when introducing the main ingredients of stochastic thermodynamics in Chapter B. This chapter will be devoted to the physics of coupled currents and conversion processes at the mean level (no fluctuations).

Even within the simplifying framework of stochastic thermodynamics, the difficulty of non-equilibrium physics prevents building a non-equilibrium statistical physics framework as achieved as the one for equilibrium systems (even when focusing on Non-Equilibrium Stationary State(s) (NESS)). Apart from the nonlinearity arising far from equilibrium, the main difficulty comes from the interplay between time anti-symmetric observables (physical currents) and time-symmetric ones (e.g., activity that gives the frequency of the exchanges with the environment). Large deviation theory offers a complete and successful framework for an asymptotically large number of degrees of freedom, for asymptotically large durations of observation, and for both at the same time. For instance, it allows us to assess the symmetries of current fluctuations at the global scale due to the LDB constraints on the dynamics. However, it often requires considering a number of physical observables that grows with the number of accessible states instead of a finite number of observables and (so-called) equations of states relating them. Chapter C presents a subset of my works in large deviation theory, focusing on different topics such as ensemble equivalence for given observation time or activity (unpublished), equivalence between equilibrium and non-equilibrium dynamics, and quadractic bounds for the LDF of physical currents for systems in TiPS with a connection to nonlinear conductance matrices (unpublished).

Combining the stochastic thermodynamics of converters with methods of large deviation theory leads to the natural question of efficiency fluctuations. The efficiency of a stochastic converter fluctuates on a large interval. The ratio of stochastic currents displays interesting large deviations with a structure different from the one observed for extensive variables (in time or size). Fluctuations can even lead a con-

verter to switch operating mode (e.g., for a heat engine going from mechanical power generation to heat pumping). In Chapter D, I summarize the logic behind the various papers I have published on the consequence of Fluctuations-Relation (FR) on efficiency statistics. Sometimes, as for the study of non-equilibrium phase transitions in energy converters with ergodicity breaking, we will see that several preliminary works were required before concluding. I take advantage of writing this thesis to emphasize the connections between them.

A.2 Co-authors and Ph.D. students

The works presented in this manuscript are the result of my fruitful collaborations with the following co-authors (number of joint publications in parenthesis)

- Hadrien Vroylandt (6), Ph.D. student from 2015 to 2018,
- Lydia Chabane (2), Ph.D. student from 2018 to 2021,
- Paul Raux (1), Ph.D. student from 2021-2024,

- Jean Baudry (1),
- Thibaud Blondel (1)
- Anthony Bonfils (1)
- Raphaël Chétrite (3),
- Damien Démoulin (1),
- Massimiliano Esposito (7),
- Christophe Goupil (1),
- Anupam Kundu (1),
- David Lacoste (9),
- Alexandre Lazarescu (1),
- Kirone Mallick (1),
- Vincent Miralles (1),
- Matteo Polettini (1),
- Simon Tusch (1),
- Christian Van den Broeck (4),
- Tim Willaert (2).

I thank them for our inspiring discussions about these joint works. Creative thinking in physics is enthusiastic, I hope we'll find many other occasions of collaborations.

A.3 Overview of research topics

I have already distinguished three research directions in my foreword (physics of coupled currents, large deviation theory, efficiency fluctuations). A more precise classification of my scientific works yields

A.3.1 Non-equilibrium response theory [1, 2, 3, 4, 5]
A.3.2 Fluctuation relations [4, 6, 7]
A.3.3 Energy converters [1, 8, 9]
A.3.4 Non-equilibrium conductance matrix [9, 10, 11]
A.3.5 Dynamical phase transitions [8, 12]
A.3.6 Efficiency fluctuations [13, 14, 15, 16, 17]
A.3.7 Doob transformation and rectification [5, 18, 19, 20]
A.3.8 Relating equilibrium and nonequilibrium dynamics [5, 12, 18]
A.3.9 Exact computation of Cumulant Generating Function (CGF) [21, 22]
A.3.10 Thermodynamic uncertainty relation, inequality of convexity [7, 23, 10]
A.3.11 TiPS [21, 14, 19]

These topics are enumerated in the order of this chapter's sections, giving an overview of each of them. Citations refer to the publication list in the starting matter and at the end of this manuscript. Some publications appear several times due to the many topic overlaps. In Table A.1, I list some of the above topics considered for different dynamics and time regimes, as explained in the caption. This table helps identify future research directions.

	Topic	Finite time	Stationary	Periodic
Linear	Response	Relaxation ✓	×	✓
	Fluctuation relations	Relaxation ✓	×	✓
	Efficiency fluctuations	Gaussian currents ✓	✓	✓
	Doob transformation	×	×	✓
	Conductance Matrix		✓	∼
Non-linear	Doob transformation		✓	∼
	Efficiency Fluctuations		Model Study ✓	

Table A.1: Tables of topics that have been studied by myself ✓ (not exclusively!), by others but not by myself ×, or roughly done but unpublished in peer-reviewed journals ∼. The columns separate studies in finite times (e.g., system undergoing a relaxation), at infinite time for stationary states (system under constant forces), and for periodic states (systems under periodic forcing). The lines are divided into studies using linear operators (markov generators of jump or diffusive processes) or nonlinear operators associated with Hamiltonians. The keyword "relaxation" refers to a quenched initial condition.

Below I provide an overview of the above research fields with many references to the literature and to my works. I try to describe the general framework, to make the connection between the various topics, and to indicate possible directions of research.

In this manuscript, my research works have all the lowest citation numbers, from

[1] to [23].

A.3.1 Non-equilibrium response theory

Response theory is a conventional technique used to study the effect of a perturbation on the evolution (or on the state) of a system whose evolution (or state) is well-known without the perturbation. For both time-dependent and independent systems, this technique is particularly well established in many fields of physics: for time-independent systems, simple and exact formulas exist for the first and second-order perturbation of the spectrum and the eigenstates of a quantum mechanical system under a perturbation of its energy levels [24]. First and second-order perturbation theory is also relatively simple in analytical mechanics when perturbing an integrable system (in the adiabatic case). In this case, one can prepare the perturbation analysis by finding a canonical set of angle-action variables that simplifies the integrable Hamiltonian and apply the same scheme for the perturbation part of the Hamiltonian [25]. Using the appropriate set of variables is crucial to avoid the fast divergence of the perturbative approach with increasing time. In the framework of stochastic processes, the linear response of a system submitted to a time-dependent perturbation is given by the Fluctuations-Dissipation Theorem (FDT), see Ref. [26, 27]. Its time-independent version is at the core of linear irreversible thermodynamics. We quickly discuss this in the sections on the physics of coupled currents A.3.3 and B.2.1. Although perturbation theory is an old research topic, it is still an active research field because it is convenient and universal as many systems remain in the linear regime (Ohm's law, Fourier's law, Fick law, etc.). Some of its drawbacks also provide directions of research or refinement [28]. For instance, in analytical mechanics, different perturbation approaches exist (adiabatic, resonant, or chaotic), e.g., the adiabatic perturbation requires that the structure of the phase space is not significantly modified after perturbation. Similar criteria must be established for the perturbation theory of stochastic processes.

Perturbation theory is also connected to the recent investigations on Thermodynamic Uncertainty Relations (TUR)s that originate from Gaussian bounds on the large deviation functions of physical currents [29, 30, 31]. TURs translate results of perturbative analysis into inequalities that are true non-perturbatively. Other inequalities can likely be found inspired by conventional results of linear response theory. For instance, regarding the response of physical currents to a time-dependent perturbation on thermodynamics forces, is it possible to write a Fluctuations-Dissipations Inequality that would saturate into the FDT when approaching a close-to-equilibrium regime? This would generalize the result of Ref. [32] and [33] that should be considered now with the viewpoint of TURs since answering the previous question relies on the possibility to extend to finite time large deviation results leading to TUR. An interesting point is also to determine how this fluctuations-dissipation inequality would relate to the generalized FDT (see Ref. [1, 2, 3, 4, 5]) giving the time-dependent linear response close to arbitrary non-equilibrium states [34, 35, 36, 37]. Would tighter inequalities exist when considering simpler forms of the generalized

FDT? Finally, the non-linear modeling with Hamiltonian of stochastic processes in the large volume limit, see [20], opens possibilities to relate the response of stochastic processes that I studied during my Ph.D. to the conventional approach of analytical mechanics.

A.3.2 Fluctuation relations

FRs are at the foundation of stochastic thermodynamics. They are equivalent at the global scale to the constraint on the dynamics imposed by the LDB at the microscopic scale. In words, a fluctuation relation says that during a trajectory, under a time-dependent driving, positive entropy production is exponentially more likely with the entropy produced than to destroy this entropy during the time-reversed trajectory (with time-reversed driving). Historically, the first FR was obtained for fluids under stationary shear [38, 39, 40], then for jump processes [41] and diffusive processes [42], with many following developments, see for instance [43, 44, 45, 46]. My work on the topic extends the FR of Hatano and Sasa for NESS to the case of TiPS and aging systems. I have related the fluctuation relations I found (and their integrated version) to the linear response close to an arbitrary non-equilibrium state [2]. This was also the occasion to improve the theory of linear response close to NESS of Seifert and Speck [47, 48], more precisely regarding the definition of the so-called local velocity of a Markov jump process.

LDB generalizes to non-equilibrium states the notion of detailed balance attached to equilibrium states. It is so fundamental, both at the transitions level or at the global level in the form of FR, that I expect future works will continue to appear on the topic. For instance, Lazarescu has recently obtained a new kind of FR that requires an exchange of the reservoirs [49]. Harunari, Garilli, and Polettini have obtained a FR for partial entropy production [50], i.e., restricted to a subset of transitions when time is counted according to the number of these considered transitions. This shows that a FR can hold even with hidden degrees of freedom and that estimating entropy production with hidden degrees of freedom is possible [51].

A.3.3 Energy converters

The physics of coupled currents is omnipresent in valuable technologies but also in nature in the form of various couplings (Peltier effect, electro-osmosis, osmosis, etc.). In many frameworks, such as energy conversion, uranium enrichment, biochemical conversion, and many more, the aim is always to generate an entropy-destroying current (this is sometimes called negative response in perturbation theory [52, 53]). This is only possible when using another entropy-producing process, thereby satisfying the second principle.

The study of individual converters displays a rich phenomenology [54], with many different working points (pure dissipator regime, regime of active reduction of a flow, stalling point, normal regime with current opposed to its conjugated force, etc). Although the physics at stake is universal, the characterization of individual

converters is often specific to each application (e.g., for water turbines, using level lines of efficiency in the space of output power and water flow). In our lecture notes on the physics of energy conversion, we stress that a universal characterization is possible. We illustrate this point with some examples of power–efficiency trade-off beyond the framework of stochastic thermodynamics at the end of Chapter B. Given this universality, improvements in this characterization seem accessible through various graphical representations of the coupling between the currents, the forces, the input or output powers, and the overall efficiency. The description of individual converters becomes slightly more complex when considering boundary conditions [55, 56, 57, 58, 59], as in nodal thermodynamics [60, 61, 62, 63]. Neumann (fixed current) or Dirichlet (fixed potential) conditions are often assumed. However, mixed boundary conditions (where both current and potential achieve non-prescribed stationary values) are significant due to the feedback of the current onto the potential seen by the converter [64]. For instance, these mixed boundary conditions appear due to a resistance in the system-environment coupling [60]. They also appear in any practical application involving a network of thermodynamic devices [65], e.g., in the serial connection of two thermo-electric generators [62, 11]. Stability analysis due to these feedback effects should be studied and, if possible, compared to the textbook results on electric circuits.

Beyond the framework of energy conversion, the coupling of general thermodynamic circuits as we considered in Ref. [11] seems promising to decompose complex systems into simpler sub-circuits. In the long term, it could be a tool for studying realistic circuits such as those found in intra-cellular biochemical reaction networks. Our method generalizes the theory of steady-state electric circuits to an arbitrary number of conserved quantities (energy, charge, matter) and thermodynamic potentials (temperature, chemical or electrochemical potential, etc.). However, this method applies neither to strongly coupled systems nor to circuit connections leading to current loops. In practice, loops are a form of strong coupling and can produce under-determined sets of equations, i.e., floating local potentials. More importantly, a systems dynamics is needed to compute the non-equilibrium conductance (relating physical currents of the thermodynamic device) on which is based our theory of equivalent impedance for thermodynamic circuits. Finding a numerical or experimental way of determining a non-equilibrium conductance matrix would improve the operational use of our theory. In the same idea, developing an algorithm that automates the computation of the working point of the circuits and the global equivalent impedance would be valuable to proceed with systems of increasing complexity.

A.3.4 Non-equilibrium conductance matrix

As aforementioned, the first-order perturbation theory of systems at equilibrium provides the response matrix linking currents and thermodynamic forces. As such, it could also be named a close-to-equilibrium conductance matrix. The fact that it is proportional to the covariance matrix of currents is a central result of statistical physics for close-to-equilibrium systems. This result has different names, depending

on the context: Stokes-Einstein-Sutherland's equation (link between mobility and diffusion coefficient) [66, 67], Onsager's reciprocity relations (stationary framework with crossed effects) [68, 69], or the fluctuation-dissipation theorem formulated by Green and Kubo (time-dependent framework) [70].

In our recent works [9, 10, 11], we have introduced a real matrix, symmetrically defined and positive (or semi-positive) definite, which we call the out-of-equilibrium conductance matrix, and which generalizes the Onsager response matrix for out-of-equilibrium stationary states. This matrix is no longer a response matrix, as it depends non-linearly on the thermodynamic forces. On the other hand, low-force development obviously produces the Onsager response matrix [71]. This non-equilibrium conductance matrix contains more information about the dynamics of the system than the non-linear functions giving each physical current in term of the thermodynamic forces. Indeed, there are n such functions for a system with n currents, whereas the conductance matrix has $n(n+1)/2$ non-linear coefficients functions of thermodynamic forces.

As an illustration of this point, let's consider a thermo-electric generator with two independent currents: energy and electric currents. The conductance matrix has three independent components. This makes possible to calculate a determinant of the conductance matrix and thus a degree of coupling between the currents: a zero determinant is synonymous of "strong coupling" between the currents. This corresponds to a null thermal conductivity at zero electric current: heat transfer takes place with electron transfer only, necessarily producing electric work. Before introducing non-equilibrium conductances, it was only possible to say if a system was in strong coupling or not, without giving the degree of this coupling as was possible for close-to-equilibrium systems [55].

A.3.5 Dynamical phases transitions

Dynamical ensemble theory transposes the equilibrium ensemble theory to trajectory ensembles, defined as the ensembles of different realizations of a stochastic process. In the so-called "microcanonical" dynamic ensemble, the value of a dynamic observable is constrained to a given value. In the "canonical" ensemble, an exponential bias on the probability of the process trajectories is introduced to shift the mean value of this observable. As with the ensemble theory of statistical physics, equivalence between the two ensembles means that performing calculations in either ensemble has no effect on the result, except of course for the considered observable, which fluctuates in the "canonical" dynamic ensemble and remains constant in the "microcanonical" ensemble. In our work on these issues [12], we study the physical conditions associated with ensemble equivalence and the consequences of non-equivalence. For Markov jump processes in continuous time, we show that ergodicity guarantees ensemble equivalence. For non-ergodic systems, we adapt a method developed for equilibrium ensembles [72] to compute the asymptotic probabilities of the observable under consideration, taking into account the initial condition that influences the long-time fluctuations due to the ergodicity breaking. We illustrate our

results on the Ising infinite range model, characterizing magnetization and activity fluctuations. We discuss the emergence of non-ergodicity by showing that the initial condition is forgotten only after a time that scales exponentially with the number of spins. In a work focusing on the mean behavior of a non-equilibrium version of this model, called Brownian donkey model [8], we have shown that the dynamical phase transition can lead to emergent tight coupling between two currents of a converter enhencing its efficiency.

A.3.6 Efficiency fluctuations

I have unveiled in Ref. [13] the properties of fluctuating efficiencies, based on four hypothesis: stationarity of dynamics, limit of long observation time of currents, converter with two independent currents, absence of phase transition. For each hypothesis made in Ref. [13], I have now published an article going beyond this hypothesis. We studied efficiency fluctuations for a converter in TiPS [14]. We considered the fluctuations of efficiency at finite time for a model with Gaussian fluctuations of currents [15]. We extended our work to a converter with more than two independent currents [16]. Finally, our aforementioned work on dynamical ensembles is motivated by the study of energy conversion in systems undergoing a phase transition [17]. To this end, we studied the Brownian donkey model, defined as a stochastic heat engine made up of N interacting uni-cyclic two-state machines. This model presents a phase transition in the macroscopic limit due to emergent ergodicity breaking [73]. Depending on N and observation time, the N-machine heat engine may or may not explore its entire phase space. This affects the engine's efficiency, which fluctuates strongly over a wide range of equiprobable efficiencies (ergodic case) or fluctuates close to several most probable values (non-ergodic case). For this model, we were able to prove that even with a phase transition, the decay rate of the efficiency probability distribution is maximum at the reversible efficiency, although other efficiencies may now decay just as rapidly. This work concludes a cycle of research started in 2013 during my post-doctorate at the University of Luxembourg. Chapter D reviews with more details my works on efficiency fluctuations.

A.3.7 Doob transformation and rectification

As already mentioned in section A.3.5, when studying stochastic processes it is often interesting to ask how these systems behave given that certain observables take on a prescribed value. This conditioning problem is well understood in the linear operator formalism [74, 75, 76], i.e. for systems described by transition rate matrices or Fokker-Planck type dynamics of many independent random walkers. For those generators, it is possible to bias the dynamics to explore the statistics of chosen observables. One can also rectify the dynamics using the so-called Doob transform to determine the typical process associated with some rare fluctuations [77]. Indeed, relying on certain spectral properties of biased linear operators, guaranteed by the Perron-Frobenius theorem, an effective process can be found such that its path

probability is equivalent to the conditional path probability. An extension of these results to the non-linear Markov processes that arise when the many random walkers are no longer independent is developed in Ref. [20]. In this case, the large-volume limit makes it possible to define the dynamics using the Lagrangian-Hamiltonian formalism [78, 71, 79, 80]. The Lagrangian and Hamiltonian are interpreted respectively as the LDF and the CGF of these currents. For non-linear processes, the spectral problem of the linear operator formalism to be solved in order to determine the effective process becomes an Hamilton-Jacobi equation associated with an appropriately biased Hamiltonian. Our work on various examples (see Fig. A.2) has enabled us to conjecture that there are two special global solutions to this Hamilton-Jacobi equation. This conjecture replaces the Perron-Frobenius theorem concerning the positivity of the dominant eigenvector (left and right). It applies to a specific class of Hamiltonians called "statistic Hamiltonians" to differentiate them with quantum Hamiltonians. In our conjecture, the positive nature of the eigenvector is replaced by the global nature of the solution, i.e. it exists on the whole state space, while the stable or unstable nature of the solution replaces the notion of left/right eigenvectors. On the basis of this conjecture, we were able to design a rectification procedure producing the effective process and its Hamiltonian. This rectification procedure extends Doob's transform to the Hamiltonian and Lagrangian formalism. It is based on a canonical gauge transformation of the biased Hamiltonian, producing effective dynamics in line with the original conditioning. In the framework developed, we were able to interpret the notion of dual dynamics as the rectification of the dynamics obtained by time reversal. We were also able to show that a Hamiltonian symmetry known as the "fluctuation relation", responsible for the positivity of the mean Entropy Production Rate (EPR), is transmitted to the biased and effective Hamiltonians. Finding a proof of our conjecture (that goes beyond a continuous limit) seems challenging for a physicist as an expertise on the geometry of simplectic manifold is probably needed. Another possible extension is to define the rectification of periodically driven non-linear processes, as done for TiPS of Markov jump processes [19] and diffusive processes [79]. Here again the challenge is to guarantee that solutions of the time dependent Hamilton-Jacobi equation exist globally with appropriate stability. Finally, we defined in this work extended Lagrangians and Hamiltonians for which the space of position and current (or moments) are not of the same dimension. Fundamental results of analytical mechanics need to be extended to this peculiar case in future works (e.g. Noether theorem, canonical transformations and associated generating functions).

A.3.8 Relating equilibrium and nonequilibrium dynamics

Non-equilibrium stationary states (described for instance by Oono [81]) are significantly different from equilibrium stationary states: the existence of physical currents and thermodynamic forces increases the number of conjugate variables. These conjugated variables are enough to determine the entropy production rate in the stationary state, but they do not form a complete set characterizing the fluctuations of

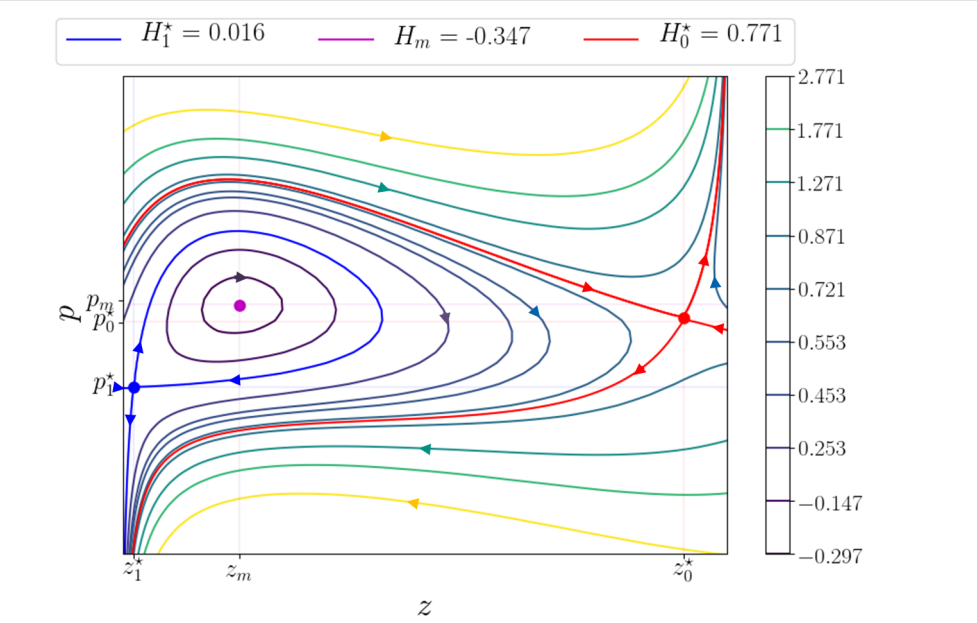

Figure A.2: Trajectory in phase space for the Hamiltonian $H_\gamma(p, z)$ in the case of the Brownian donkey model [20], see A.3.7. $z \in [0, 1]$ is the proportion of the machine in the highest-energy state. The moment conjugate to z is denoted by p. The red, magenta and blue points correspond to the fixed points of the system. Red is the trajectory at the value of the Hamiltonian at the dominant saddle point. This trajectory is indeed a global solution of the Hamilton-Jacobi equation. There is a single stable global solution and a single unstable global solution that does not diverge on the edges of the state space in either the increasing or decreasing time direction.

the system as it is the case in equilibrium statistical mechanics. Indeed, in the same configuration space, many different dynamics share equal probability currents with different [82] or equal state probabilities [83]. In any case, higher order cumulants always differ in general [84]. In view of making equilibrium and nonequilibrium statistical mechanics as comparable as possible, it would be interesting to connect the equilibrium fluctuations of a system to those of the same system subjected to finite thermodynamic forces generated by different reservoirs (of heat, matter, etc). This would be an extension beyond linear order of Onsager's regression hypothesis. In Ref. [5] and for a dynamics with Arrhénius rates, I found a set of observables that allow to map exactly the equilibrium and nonequilibrium dynamics via biasing and Doob transformation of the dynamics (see section C.2.2 for a detailed summary). This set of observables includes the physical currents, the activity of the exchange with the reservoirs and the states occupancy (which is not volume extensive). The role of time-reversal symmetrical observables (occupancies and activities) has also been raised by others [85] and motivates the introduction of nonequilibrium equivalence classes in a more recent work [18]. In this work focusing on jump processes (continuous time) on multigraphs, I have shown that dynamics belonging to the same equivalence class share the same currents fluctuations. Equivalence classes are defined from an equivalence relation based on an edgewise symetrization of the rate matrices leading to an equilibrium representative of the class, see [86, 87] for similar symetrization procedures. Interestingly, the freedom to move inside an equivalence class comes from the different ways of splitting the thermodynamic forces on the possible transitions. This freedom also plays a fundamental role in the local detailed balance and in the decomposition of thermodynamic forces into a potential and a non-conservative part [88, 89]. Another remark is that the equilibrium dynamics from which we start (and that is driven out of equilibrium using LDB to reach the nonequilibrium dynamics) is different from the equilibrium representative of an equivalence class. It differs at least by the escape rates from the various states (if not by some symmetric factors in the rate matrix). The possibility of relating those two equilibrium dynamics via a conditioning should be considered, for instance using the recent results of Ref. [90].

A.3.9 Exact computation of CGF

To illustrate many of the aforementioned results, I have determined the CGF of several models. For instance, the CGF of the work received from a piecewise-constant driving by a modulated two level system is obtained in [21]. The initial model is purely dissipative: all the work is dumped as heat into a single thermostat. This model was used in the following works for

- studying efficiency fluctuations of a heat engine in TiPS [14]. In this work, we used a LDB dynamics and also extended the number of jumps of the modulated driving.

- comparing deterministic and stochastic driving in [22], where the notion of

work source is precisely defined as an energy source with no contribution to the second law. Our work was further extended in Ref.[91].

– determining an effective process associated to the conditioning of a system in TiPS [19].

Another model is transversal in my research work: The Brownian donkey model introduced by C. Van den Broeck and B. Cleuren [73]. This is a long-range Ising model extended to nonequilibrium using a LDB involving two heat reservoirs and a non-conservative force. Each two-level system of this model is in fact a uni-cyclic heat engine with strongly coupled currents: it was introduced for studying negative response. The all to all interaction energy (and the existence of an activation barrier) leads to a spontaneous ergodicity breaking in the large volume limit (i.e. large number of two-states engines). This model allowed my to study

– the role of collective effects and emergent strong coupling of an machine efficiency in [17]. The interaction between the heat engine suppresses the strong coupling of each single engine. The large volume limit reintroduce this coupling.

– the efficiency fluctuation of an engine undergoing a phase transition [17],

– the computation of non-convex LDF using subdominant eigenvalues in [12], a work that extends to path ensemble Ref. [72],

– the conditioning and rectification of non-linear processes (extension of Doob transformation in the large volume case) [20].

A.3.10 Thermodynamic uncertainty relations

The first TUR derived in [29] were obtained by finding lower bounds for the CGF of physical currents. These bounds on the CGF lead to bounds on the current variance when computing the second cumulant from the exact CGF and from the lower bound. Indeed, the CGF bound is quadratic in the mean current times the conjugated counting field. It is also proportional to the inverse of the entropy production rate. As a result, the current variance is higher than twice the square currents divided by the entropy production rate. In other words, to make possible low values of a current variance one needs to produce entropy (so that the variance lower bound is small). A proof of the quadratic bound on the CGF was given in [30] the same year of the first publication on TUR. Many works followed providing bounds on the efficiency of heat engines [92] and molecular motors [93], or on the precision of a Brownian clock [94]. During his Ph.D. under my supervision, H. Vroylandt provided the best quadratic bound on the CGF in Ref. [9]. This bound is actually given by the quadratic form that is based on the nonequilibrium conductance matrix. With this conductance matrix describing an energy converter, we were able to improve the upper bound for the thermodynamic efficiency. The latter is smaller than a universal function depending solely on the degree of coupling between the input and output

currents, generalizing beyond the linear case the work of Kedem and Caplan [55]. Finally, we have shown using an ordered set of TUR that the lower bound on the CGF becomes more accurate with the information provided on the dynamics [10]. Ultimately, with the full knowledge of the dynamics, one can obviously compute the exact CGF.

In connection with the next section, TUR have been generalized to TiPS in Ref. [95]. However, this TUR can be made tighter using a nonequilibrium conductance matrix for TiPS that we introduce in section C.3 for physical currents (different from the work done by conservative forces).

A.3.11 Time Periodic States

An expression of the large deviation function of occupancy and currents exists for diffusive processes [96] and jump processes [97]. However, time translation invariance is generally assumed when studying the aforementioned (see section A.3.7) "microcanonical" dynamical ensembles with conditioned observables and "canonical" dynamical ensembles with exponential bias on trajectory probabilities to shift the mean value of the observable under consideration [75, 76]. With L. Chabane and R. Chétrite, we have studied the conditioning of jump processes whose transition rates are functions of the (time) period T. For sake of simplicity, we focused on an observable A defined using a time integral of periodic functions of the same period T. These periodic functions depend on the state of the system or the transitions performed. The optimization, constrained by the value of A, of the large deviations function characterizing the asymptotic fluctuations of the occupancy of each state and of empirical currents between states (after many periods) leads to the effective Markov process. This unconstrained process typically presents the chosen value of A. Alternatively, this effective process can be determined by solving a time-dependent linear differential equation (that replaces the spectral problem of the stationary case). All these results generalize to the periodic case, the notion of Doob transformation specific to autonomous systems [75].

In future work, I plan to study the rectification of biased system in TiPS and at large volume. Beyond the general case, an illustration of the rectification procedure could be done on Brownian Donkey model submitted to a piecewise-constant driving. The piecewise nature of the driving may allow to solve the time-dependent Hamilton-Jacobi equation. The method will be to solve separately for each constant value of the driving and then to associate the solutions via a matching of the boundary conditions.

Chapter B

Physics of energy conversion

Contents

Energy is an abstract concept that quantifies the capacity to modify the state of a system (e.g., to increase the speed of one of its elements). According to the first principle of thermodynamics, one of its main characteristics is to be conserved when exchanged between two parts, albeit with a propensity to disperse in microscopic degrees of freedom. In mechanical terms, energy transfer is the work a force performs when moving an object, for example, in a downward gravitational field. The product of the displacement and the force of gravity gives the work done by the weight as it falls. At the end of the operation, the gravitational potential energy has been reduced by the corresponding work. This potential energy is converted into kinetic energy during the fall, and in contact with the ground, kinetic energy is itself transformed into heat, i.e., the disordered agitation of the atoms of the object and the ground (energy dispersion).

Therefore, the form of energy is of prime importance: utility increases with the concentration of energy in a few degrees of freedom. The production of useful energy is about converting diluted energy by concentrating it in a few degrees of freedom. This doesn't happen spontaneously, and by the second principle of thermodynamics, it's necessary to use a spontaneous flow (i.e., flowing in the dispersing direction) to drive another coupled flow against a force, producing work.

Energy on a macroscopic scale is either kinetic or potential. For a small number of degrees of freedom, these energies are directly accessible (e.g., flywheel). They can be converted with an efficiency close to unity, as is the case with the turbines of hydroelectric power stations. However, at the microscopic level and when dispersed on many degrees of freedom, kinetic energy corresponds to thermal energy. Concentrating it again can only be done with loss. Likewise, potential energy can be distributed in numerous bonds (physical or chemical) and cannot be collected directly. For instance, a thermal engine must be used to convert the potential energy of gasoline into mechanical work.

Energy is useful when concentrated and is often available in a dilute form. Spontaneous flows tend to dilute energy onto many degrees of freedom, expanding the phase space of the system, i.e., its number of configurations. The dual concept of entropy formalizes this tendency. Entropy provides an extensive characterization of the number of configurations. By definition, extensivity implies entropy additivity when two different macroscopic subsystems are merged. By combinatorial analysis, the number of configurations of a system made up of two subsystems is the product of the number of configurations of each subsystem. Then, extensivity implies the logarithmic growth of entropy with the number of system configurations.

The above discussion informally introduces the dual concepts of energy and entropy. Those are central in thermodynamics, the physics of coupled currents, and, more specifically, the physics of energy conversion. In this chapter, we quickly introduce the stochastic thermodynamics of a Markov jump process on a simple connected graph. We develop formally how energy conservation (first law) and positive entropy production (second law) constrain the dynamics of the process (that can model an energy converter). This constraint is called LDB in stochastic thermodynamics [98, 99]. It allows us to define forces at the elementary transition level and in far-from-equilibrium conditions. Then, before considering conversion arbitrarily far from equilibrium, we describe the physics of coupled currents in the linear regime. We revisit the seminal work of Kedem and Caplan [55], emphasizing the universal trade-off between efficiency and power. Finally, we comment how the two selected publications for this chapter [9, 11] generalize some materials of this chapter and open many possibilities for the study of complex networks of converters.

B.1 Stochastic thermodynamics of Markov jump processes

B.1.1 States, transitions, and their graphical representation

We consider a system with a finite number V of states. States are labeled by integers, generically denoted with x, y, or z. Transitions between states are denoted $e = (xy, \nu)$ where ν indexes the channels that give different ways of moving from state y to state $x \neq y$. For example, we can switch from one state to another by exchanging energy with a cold reservoir or hot reservoir (the index ν, in this case, can be associated with a heat reservoir), see Fig. B.1. In a graphical representation of the system, states are represented by points called *vertices* and allowed transitions between states by lines called *edges*. Edges are arbitrarily oriented, with an arrow defining the positive orientation. Microreversibility means that a transition existing in one direction must also exist in the opposite direction. Edges are, therefore, bidirectional. If this is not the case, the dynamic is said to be totally irreversible, a situation excluded in stochastic thermodynamics. In general, not all transitions are possible, i.e., some transitions are forbidden in both directions. If not, the graph is totally connected: reaching any state from any state with just one transition is possible. In a *connected graph*, finding a succession of edges connecting any pair of states is always possible. It is customary to consider only systems with connected graphs (disconnected subparts of a non-connected graph representing different systems).

B.1.2 Markovian dynamics on a graph

For jump processes, the durations between transitions follow an exponential law. The escape rate from a state (at time t), say x, is given by the sum of all jump rates $k_{(yx,\nu)}$ for transitions reaching y by any channel. If any, the time dependence of jump rates is implicit in the notation. Then, a probability conservation balance reads

$$p_x(t+dt) = \left(1 - \sum_{y\neq x,\nu} k_{(yx,\nu)} dt\right) p_x(t) + \sum_{y\neq x,\nu} k_{(xy,\nu)} p_y(t) dt. \tag{B1}$$

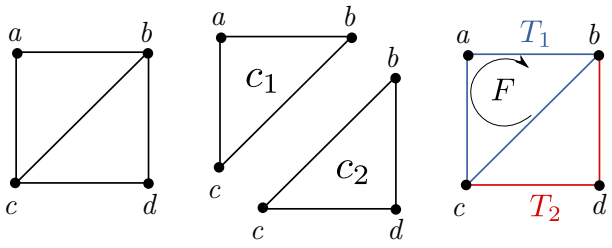

Figure B.1: Four-state model for a system in contact with two heat reservoirs at temperature T_1 and T_2, and subjected to a non-conservative force F on cycle c_1.

Accordingly, the probability of state x, denoted $p_x = p_x(t)$, evolves in time according to the master equation

$$\frac{dp_x}{dt} = \sum_{y,\nu} k_{(xy,\nu)} p_y. \tag{B2}$$

The matrix $\sum_\nu \boldsymbol{k}_\nu$ of xy component $\sum_\nu k_{(xy,\nu)}$ is a Markov matrix: the sum of the column elements is zero. The off-diagonal elements are positive or null, while the diagonal elements are negative. To emphasize that the above equation is a continuity equation, we introduce the probability current

$$j_{(xy,\nu)} = k_{(xy,\nu)} p_y - k_{(yx,\nu)} p_x \tag{B3}$$

so that

$$\frac{dp_x}{dt} = \sum_{y,\nu} j_{(xy,\nu)} = \sum_e D_{x,e} j_e \tag{B4}$$

since $\sum_{y,\nu} k_{(yx,\nu)} = 0$. We have used the incidence matrix $\boldsymbol{D}$, which is such that

$$D_{z,(xy,\nu)} = \begin{cases} +1 \text{ if } z = x, \\ -1 \text{ if } z = y, \\ 0 \text{ otherwise.} \end{cases} \tag{B5}$$

We sum over all oriented edges in B4: the incidence matrix provides the correct orientation given the arbitrary orientation of edge e so that we count the probability flow towards vertex x. The matrix $\boldsymbol{D}$ is a divergence operator on a graph $\dot{\boldsymbol{p}} = \boldsymbol{D}\boldsymbol{j}$.

B.1.3 LDB from the (mean) 1st and 2nd principles

The first principle of thermodynamics ensures the conservation of energy. Since the energy of the system is a state variable, we can associate an energy $\varepsilon_x = \varepsilon_x(t)$ (possibly time-dependent) with each state x of the system. Given $p_x = p_x(t)$ the probability of state x at time t solving Eq. B4, the variation of the mean energy with respect to time is written

$$\begin{aligned}
\frac{d}{dt}\langle \varepsilon \rangle &= \frac{d}{dt} \sum_x p_x \varepsilon_x, && \text{(B6)} \\
&= \sum_x \left(\frac{dp_x}{dt} \varepsilon_x + p_x \frac{d\varepsilon_x}{dt} \right), && \text{(B7)} \\
&= \sum_{x,y,\nu} j_{(xy,\nu)} \varepsilon_x + \sum_x p_x \frac{d\varepsilon_x}{dt}, && \text{(B8)} \\
&= \frac{1}{2} \sum_{x,y,\nu} j_{(xy,\nu)} (\varepsilon_x - \varepsilon_y) + \sum_x p_x \frac{d\varepsilon_x}{dt}, && \text{(B9)} \\
&= \sum_\nu \langle q_\nu \rangle + \langle w \rangle, && \text{(B10)}
\end{aligned}$$

where we use the antisymmetry $j_{(xy,\nu)} = -j_{(yx,\nu)}$ of the probability current. The first term in Eq. B10 corresponds to the heat currents per unit of time (positive

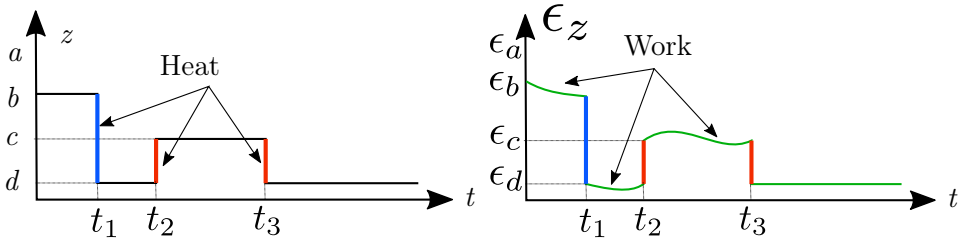

Figure B.2: (Left) The state $z = z(t)$ of the four-state system of Fig. B.1 as a function of time: the system undergoes three transitions during which it supplies energy to the cold reservoir at t_1, then receives heat from the hot reservoir at t_2, which it returns to the same reservoir at t_3. (Right) The energy of the same four-state system as a function of time: the variation in energy is broken down into heat exchange during jumps and work exchange during the displacement of energy levels. For example, at the start of the trajectory, the system in state b supplies work as its ε_b energy decreases.

when) received from the reservoirs, and the second to the work done by conservative forces per unit of time (positive when received by the system). In the presence of non-conservative forces, this energy balance is completed so that

$$\langle q \rangle = \sum_{x,y>x,\nu} j_{(xy,\nu)}(\varepsilon_x - \varepsilon_y - w^{\rm nc}_{(xy,\nu)}), \tag{B11}$$

$$\langle w \rangle = \sum_x p_x \frac{d\varepsilon_x}{dt} + \sum_{x,y>x,\nu} j_{(xy,\nu)} w^{\rm nc}_{(xy,\nu)}, \tag{B12}$$

where $w^{\rm nc}_e$ is the work (positive when) supplied by non-conservative forces to the system during transition e. This work appears with an opposite sign in the heat, as it reduces the energy required from the heat reservoir to achieve the transition. Alternatively, when $w^{\rm nc}_e$ is negative, the opposite is true: more heat is required to transition to a higher energy state than just the energy difference, and the system produces some non-conservative work. Let us emphasize that the first principle helps to identify work and heat in the conservative case as the exchanges due to modification of the energy levels for the first and those due to the jumps for the second, see Fig.B.2.

The second principle guarantees that entropy production is positive. We start with the entropy variation of the system and try to find an expression with a strictly positive quantity and the heat flow identified in Eq. B11. The system's entropy includes, as usual, a Shannon entropy part based on the state's probabilities and a part associated with the internal entropy of each state. This internal entropy is due to the possibility for state x to have some internal and equilibrated degrees of freedom, made up, for example, of Ω_x equiprobable and indistinguishable states, see [8] for a concrete example. In this case $S^{\rm int}_x \equiv \ln \Omega_x$. Thus, taking units where

$k_B = 1$, entropy reads

$$\langle s(t) \rangle = \sum_x p_x(t)[S_x^{\text{int}} - \ln p_x(t)]. \tag{B13}$$

Internal entropy enables maintaining the same theoretical structure despite changes in the scale of description by eliminating internal degrees of freedom assumed to be at equilibrium [100]. For example, it is possible to construct a system with a discrete number of states from a continuous system separated into different zones associated with potential wells. The volume of the phase space associated with the equilibrium states in each zone may be different and thus associated with a different internal entropy. For autonomous systems (i.e., time-independent dynamics), the internal entropy of the states is constant in time. The time derivative of the mean entropy is

$$\begin{aligned}
\frac{d}{dt}\langle s(t) \rangle &= \sum_x \frac{dp_x}{dt}[S_x^{\text{int}} - \ln p_x] - \sum_x \frac{p_x}{p_x}\frac{dp_x}{dt}, && \text{(B14)}\\
&= \sum_{x,y,\nu} k_{(xy,\nu)} p_y [S_x^{\text{int}} - \ln p_x], && \text{(B15)}\\
&= \sum_{x,y,\nu} \left[k_{(xy,\nu)} p_y - k_{(yx,\nu)} p_x\right] [S_x^{\text{int}} - \ln p_x], && \text{(B16)}\\
&= \frac{1}{2} \sum_{x,y,\nu} \left[k_{(xy,\nu)} p_y - k_{(yx,\nu)} p_x\right] \left[-\ln \frac{p_x}{p_y} + S_x^{\text{int}} - S_y^{\text{int}}\right], && \text{(B17)}\\
&= \frac{1}{2} \sum_{x,y,\nu} j_{(yx,\nu)} \left[\ln \frac{p_y}{p_x} + S_x^{\text{int}} - S_y^{\text{int}}\right], && \text{(B18)}
\end{aligned}$$

where we have used the master equation and the anti-symmetry of probability currents. We now move the internal entropy term in the left-hand member and also add and subtract on the left and right sides the logarithm of the ratio of forward and backward transition rates:

$$\begin{aligned}
\frac{d}{dt}\langle s(t) \rangle + \sum_{x,y>x,\nu} j_{(xy,\nu)} \left[S_y^{\text{int}} - S_x^{\text{int}} + \ln \frac{k_{(xy,\nu)}}{k_{(yx,\nu)}}\right] = \\
\sum_{x,y>x,\nu} \left[k_{(xy,\nu)} p_y - k_{(yx,\nu)} p_x\right] \ln \frac{k_{(xy,\nu)} p_y}{k_{(yx,\nu)} p_x} = \sigma \geq 0 \quad \text{(B19)}
\end{aligned}$$

The last term, called EPR and denoted σ, is positive or zero. Indeed, if the probability current is positive, then the ratio in the logarithm is greater than 1, and the logarithm is therefore positive as well. Otherwise, the ratio is smaller than 1, the logarithm is negative, as is the current, and their product is positive. All summed terms are, therefore, positive. Such a general conclusion on the sign of σ is not accidental: its positivity in all situations supports the interpretation of an entropy production term. The entropy balance, in full connection with the heat definition arising from the first principle, achieves this reasoning: The first term on the left-hand side of Eq. B19 is the system entropy increase. Then, the second term must

be the rate of reservoir entropy production, which is the sum over ν of minus the heat flows from reservoir ν to the system divided by T_ν. Given that we already have a definition of heat from the first principle, cf. Eq. (B11), we find the following constraint on the transition rates

$$\ln \frac{k_{(xy,\nu)}}{k_{(yx,\nu)}} = -\frac{1}{T_\nu}\left(\varepsilon_x - \varepsilon_y - T_\nu S_x^{\rm int} + T_\nu S_y^{\rm int} - w^{\rm nc}_{(xy,\nu)}\right). \tag{B20}$$

This equation is called the canonical LDB (no exchange of matter). Note that the canonical LDB involves the non-conservative force and the difference in free energy (based on internal entropy only) $\varepsilon_x - T_\nu S_x^{\rm int}$ between the two states x and y. Alternatively, the edge forces

$$f_{(xy,\nu)} \doteq \ln \frac{k_{(xy,\nu)} p_y}{k_{(yx,\nu)} p_x} = -\frac{1}{T_\nu}\left[(\varepsilon_x - T_\nu s_x) - (\varepsilon_y - T_\nu s_y) - w^{\rm nc}_{(xy,\nu)}\right]. \tag{B21}$$

involves instead the difference in non-equilibrium free energy $\varepsilon_x - T_\nu s_x$. The latter is not a state function as it is defined for each reservoir separately. Here, the entropy of state x is $s_x \doteq S_x^{\rm int} - \ln p_x$ using the probability p_x. Its mean value reproduces the system entropy defined in Eq. (B13).

With the constraint of Eq. (B20), the square bracket on the left side of Eq. B19 is exactly the heat sent to reservoir ν during transition (xy, ν). Therefore, we arrive at the crucial fact that the *LDB is the dynamical statement of the second principle of classical thermodynamics*

$$\frac{d}{dt}\langle s(t)\rangle - \sum_\nu \frac{\langle q_\nu\rangle}{T_\nu} = \langle \sigma\rangle \geq 0. \tag{B22}$$

This principle provides an entropy balance of a non-equilibrium system in contact with several heat reservoirs. Generalization to open systems in the grand canonical ensemble is available in the literature [89].

B.2 Exoreversible and stationary linear converters

As we have laid the foundations of stochastic thermodynamics, we proceed with the physics of energy conversion in its standard formulation: in the linear regime. The physics of energy conversion is a sub-field of the physics of coupled currents when (i) considering only two independent currents and (ii) when the output current is a rate of work extraction. However, removing assumption (ii) leads to the same physics, which already has many applications and universality. Indeed, one must deal with a power-efficiency trade-off in many activities: in information technology (fast versus efficient computers leading to two very different CPU architectures: x86 or ARM), in economics (quick and cheap, but natural resource wasting versus slow and expensive, but natural resource preserving, e.g., in slate production), in logistic (fast versus efficient parcel delivery), etc.

For simplicity, we focus on exoreversible machines (no dissipation through imperfect connection with the reservoirs) in a close-to-equilibrium stationary state.

Machines working close to equilibrium are, by definition, weakly irreversible, which gives them a clear advantage in terms of efficiency. Their internal entropy production is low due to low thermodynamic forces, making it possible to linearize the expression of currents as a function of forces. In rare cases, the relationship between current and force is linear without needing a low-force approximation. Thanks to the machine's linearity, we can determine the exact efficiency-power trade-off by obtaining an expression relating efficiency to output power normalized by maximum power. We did not find alssewhere in the literature this result (Eq. (B54) below) relating efficiency and power in the linear regime, although the study of linear conversion is a textbook topic [101]. Ref. [9] generalizes this approach to stationary and non-linear converters: the same trade-off between power and efficiency exists, although providing their general relation requires assuming some current-force characteristics.

B.2.1 Currents and forces in linear regime

The flux-force relationship (phenomenological or from a close-to-equilibrium linearization) writes

$$I_1 = L_{11}A_1 + L_{12}A_2, \tag{B23}$$
$$I_2 = L_{21}A_1 + L_{22}A_2, \tag{B24}$$

where I_i for $i = 1, 2$ is the ith (fundamental) current, A_i is the conjugated (foundamental) force, and $L_{ij} = L_{ji}$ is the ij component of the Onsager conductance matrix. The Onsager matrix is symmetrical as it relates to the covariance matrix of stationary currents [102]. Total EPR writes as the sum of two partial EPRs

$$\sigma = \sigma_1 + \sigma_2 \geq 0, \tag{B25}$$

with $\sigma_i = A_i I_i$. An entropy production has the dimension of an entropy (Joule per Kelvin), while entropy production rates have the dimension of an entropy per unit time (Joule per Kelvin per second). Total entropy production is the quadratic form

$$\sigma = \begin{pmatrix} A_1 & A_2 \end{pmatrix} \cdot \begin{pmatrix} L_{11} & L_{21} \\ L_{21} & L_{22} \end{pmatrix} \cdot \begin{pmatrix} A_1 \\ A_2 \end{pmatrix} \tag{B26}$$

This entropy production must always be positive or zero. As the matrix L is symmetrical, it is diagonalizable: we can perform a basis change using an orthogonal transition matrix $\boldsymbol{P}^T = \boldsymbol{P}^{-1}$ so that entropy production is written as a sum of squares $\sigma = (\boldsymbol{PA})^T \boldsymbol{D} (\boldsymbol{PA})$ where $\boldsymbol{D}$ is the diagonal matrix of eigenvalues. This implies that the eigenvalues of L are positive or zero so that for any choice of force A_i, we have $\sigma \geq 0$. Since the determinant of $\boldsymbol{L}$ is equal to the product of the eigenvalues, it is positive or zero as well:

$$\mathrm{Det}\, \boldsymbol{L} \geq 0 \tag{B27}$$

We speak of *strong coupling* between the currents when this determinant is zero. Strong coupling of two physical currents means that the ratio of the currents is force-independent. Without strong coupling, entropy production is a positive definite quadratic form of the forces. On the other hand, all forces need not be zero to cancel entropy production in the case of strong coupling: since the currents are related by $I_1 = \alpha I_2$ for a constant α, we have

$$\sigma = A_1 I_1 + A_2 I_2 = (A_1 \alpha + A_2) I_2 \tag{B28}$$

that is null if $A_1\alpha + A_2 = 0$, which does not require that neither forces nor currents are null. This apparently contradicts the definition of equilibrium states (that have null currents and null EPR). We resolve this contradiction by considering that strong coupling is a mathematical limit that some models can fulfill, although as an idealization (in the same line as the reversible limit)..

B.2.2 Machine regime and efficiency

With two partial entropy productions, there are three possibilities for their respective signs

- Both positive, purely dissipating device: $\sigma_1 \geq 0$ and $\sigma_2 \geq 0$, the system operates as a complete heat sink, and both processes are spontaneous. (*dud engine*)
- Opposite sign, functional device: $\sigma_1 \geq 0$ and $\sigma_2 \leq 0$, the system operates in machine mode, with one spontaneous process destroying entropy for the second process (idem in the $1 \leftrightarrow 2$ exchange). (*engine and inverse modes*)
- Both negative: $\sigma_1 \leq 0$ and $\sigma_1 \leq 0$ is forbidden by the second law of thermodynamics.

The reversible case corresponds to $\sigma_1 = -\sigma_2$ for which the second principle of inequality (B25) is saturated. Arbitrarily, we decide that the output current is I_2 and the input current is I_1. Then, $\sigma_2 < 0$, and entropy is destroyed by the output flow (force opposing the current), while entropy is produced by the input flow $\sigma_1 > 0$ (force aligned with the current). With those conventions, the type II efficiency is defined by

$$\eta \equiv -\frac{I_2 A_2}{I_1 A_1} = -\frac{\sigma_2}{\sigma_1}. \tag{B29}$$

Type II efficiencies are dimensionless and bounded by the reversible type II efficiency

$$\eta_{\text{rev}} = -\frac{\sigma_2}{\sigma_1} \leq \frac{\sigma_1}{\sigma_1} = 1. \tag{B30}$$

Efficiency is positive for an operational machine and is negative for a dud engine. For example, a refrigerator operating at high outside temperatures may no longer be able to extract heat from the inside to the outside. The point at which heat

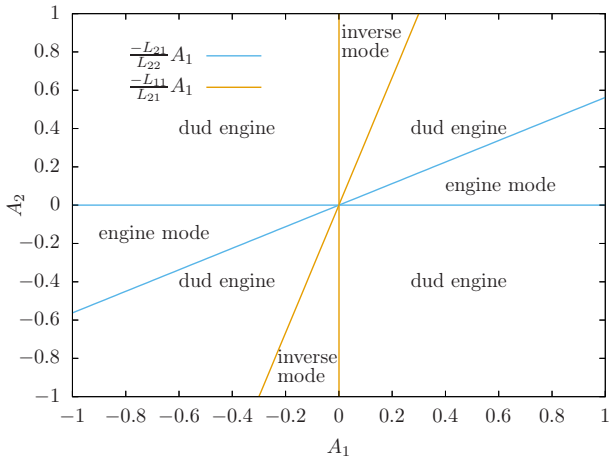

Figure B.3: Operation diagram of a linear machine. Three modes can be distinguished: the engine mode where $\sigma_2 < 0$ while $\sigma_1 > 0$, the inverse mode where $\sigma_2 > 0$ while $\sigma_1 < 0$, and the purely dissipating mode where $\sigma_2 > 0$ and $\sigma_1 > 0$ (dud engine).

extraction reaches zero is called a *stalling point*. In the general case, this point corresponds to the cancellation of the I_2 flow at large force A_2.

To fix ideas, we choose $A_1 > 0$, $I_1 > 0$ and $A_2 > 0$, $I_2 < 0$. In this case, the type II efficiency corresponds to the type I efficiency $-I_2/I_1$ divided by the reversible type I efficiency A_1/A_2. We also have $L_{12} = L_{21} < 0$, but the diagonal terms L_{ii} of the Onsager matrix are positive so that in the absence of the other force, entropy production remains positive. For example, at $A_2 = 0$ we have $I_1 = L_{11}A_1$ and therefore $\sigma = A_1 I_1 = L_{11}A_1^2 \geq 0$ which imposes $L_{11} \geq 0$.

B.2.3 Operation diagram

The operation diagram is a graph in the space of forces A_1 and A_2 that indicates the different operating modes of the device; see Fig. B.3. It is obtained by plotting the implicit function $\sigma_2 = 0$ (light blue lines) and $\sigma_1 = 0$ (light yellow lines). In the case of linear machines, we find trivially

$$\sigma_2 = A_2 I_2 = A_2 \left(L_{21}A_1 + L_{22}A_2\right) = 0, \tag{B31}$$

$$\sigma_1 = A_1 I_1 = A_1 \left(L_{11}A_1 + L_{21}A_2\right) = 0. \tag{B32}$$

The machine is in *engine mode* for $\sigma_2 < 0$ and $\sigma_1 > 0$, and hence for forces

- $0 < A_2 < -\frac{L_{21}}{L_{22}}A_1$ for positive output and input forces A_2 and A_1,
- $0 > A_2 > -\frac{L_{21}}{L_{22}}A_1$ for negative output and input forces A_2 and A_1,

when keeping in mind that $L_{21} < 0$. The machine is in *inverse mode* for $\sigma_2 > 0$ and $\sigma_1 < 0$, and hence for forces

- $0 < A_1 < -\frac{L_{21}}{L_{11}} A_2$ for positive output and input forces A_2 and A_1,
- $0 > A_1 > -\frac{L_{21}}{L_{11}} A_2$ for negative output and input forces A_2 and A_1.

The operation diagram of the linear machine is simple: the corresponding structure with functional, inverse, and dud modes exist in any device in the close-to-equilibrium limit, for instance, Ref. [103] for an operation diagram including far from equilibrium conditions and the expected structure at weak thermodynamics forces.

B.2.4 Current-force characteristic

One way of characterizing the operation of a converter is to consider the curve relating output current and force (at constant partial entropy production for the input process). This curve, called current-force characteristic, is obtained by varying the load (here the force A_2) against which the converter works: at low force, the current can take high values, but the power remains low ($-\sigma_2 = -A_2 I_2$ is small); at high force, the converter approaches the stalling point at which the current is zero (the converter stalls), and the power is also low.

We start by determining a relationship between the two forces, thanks to the fact that we're working with constant partial input entropy production

$$\sigma_1 = L_{11} A_1^2 + L_{12} A_1 A_2, \tag{B33}$$

which we solve for A_1

$$A_1 = \frac{-L_{12} A_2 \pm \sqrt{(L_{12} A_2)^2 + 4 L_{11} \sigma_1}}{2 L_{11}}. \tag{B34}$$

This leads to the output current

$$I_2 = L_{12} \left[\frac{-L_{12} A_2 \pm \sqrt{(L_{12} A_2)^2 + 4 L_{11} \sigma_1}}{2 L_{11}} \right] + L_{12} A_2. \tag{B35}$$

Fig. B.4 shows this current-force characteristic for a linear machine.

B.2.5 Degree of coupling and other parameters

We introduce the following parameters:

$$\Pi \equiv L_{1,1} A_1^2, \quad \varphi \equiv \sqrt{\frac{L_{2,2} A_2^2}{L_{1,1} A_1^2}}, \quad \text{and} \quad \xi \equiv \frac{L_{1,2}}{\sqrt{L_{1,1} L_{2,2}}} \operatorname{sign}(A_1 A_2). \tag{B36}$$

Π is the intrinsic entropy production of the input process, φ is the entropy production of the output process relative to the input process (called asymmetry in [101]), and ξ is the degree of coupling which is related to the determinant of the Onsager matrix:

$$\xi \equiv \frac{L_{12}}{\sqrt{L_{11} L_{22}}} = \pm \sqrt{1 - \frac{\operatorname{Det} L}{L_{11} L_{22}}} \quad \text{since} \quad \operatorname{Det} L = L_{11} L_{22} - L_{12}^2 = L_{11} L_{22} (1 - \xi^2). \tag{B37}$$

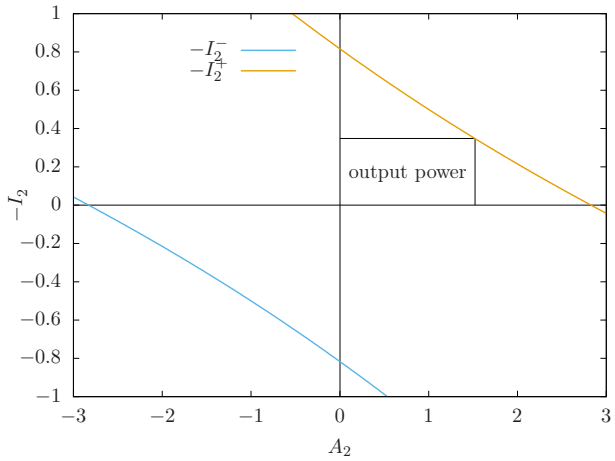

Figure B.4: Opposite of output current (i.e. $-I_2$) versus output force A_2. The area of a square between the curve and the abscissa and ordinate axes gives the output power (partial entropy production $-\sigma_2$). For this figure, we take dimensionless currents and forces with $L_{11} = 3$, $L_{12} = -1$, $L_{22} = 0.5$, $\sigma_1 = 2$, $\xi = -0.82$.

The degree of coupling is, therefore, ± 1 when the determinant is zero (at strong coupling). Of these three parameters, only the degree of coupling is independent of the machine's operating point (for linear converters only). Therefore, it characterizes the machine in a fairly universal way. The degree of coupling determines the possibility for a machine to reach the maximum efficiency: reversibility is a necessary but not sufficient condition.

B.2.6 Trade-off between power and efficiency

Partial entropy destruction σ_2 is maximum (highest flux-force product, i.e., maximum output power $-\sigma_2 = -A_2 I_2$) when

$$\frac{\partial(-\sigma_2)}{\partial A_2} = -\frac{\partial}{\partial A_2}(L_{21}A_1 + L_{22}A_2)A_2, \tag{B38}$$

$$0 = -(L_{21}A_1 + 2L_{22}A_2), \tag{B39}$$

$$A_2^* = -\frac{L_{12}A_1}{2L_{22}} \geq 0. \tag{B40}$$

The maximum output power is then

$$-\sigma_2^* = -(L_{21}A_1 + L_{22}A_2^*)A_2^*, \tag{B41}$$

$$-\sigma_2^* = L_{21}A_1\frac{L_{12}A_1}{2L_{22}} - L_{22}\left(\frac{L_{12}A_1}{2L_{22}}\right)^2, \tag{B42}$$

$$\sigma_2^* = \frac{(L_{12}A_1)^2}{2L_{22}} - \frac{(L_{12}A_1)^2}{4L_{22}}, \tag{B43}$$

$$\sigma_2^* = \frac{(L_{12}A_1)^2}{4L_{22}} \geq 0. \tag{B44}$$

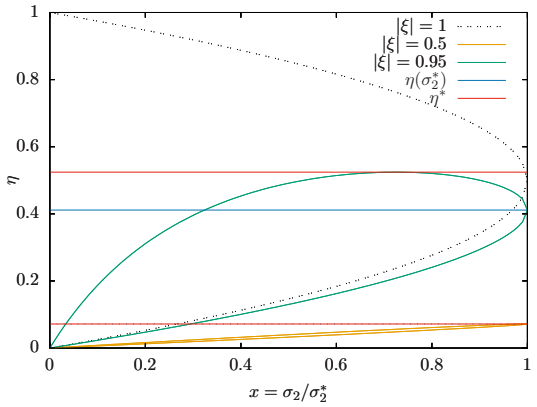

Figure B.5: Type II efficiency η as a function of the power ratio x for a linear machine with degrees of coupling $|\xi| = 1, 0.95, 0.5$. The blue horizontal line indicates the efficiency at maximum power for $\xi = 0.95$. The red horizontal lines are the maxima of the lobe-shaped curves and give the maximum efficiency at power below the maximum power. The lobes flatten rapidly as $|\xi|$ decreases towards 0.

We can also determine the value of the force A_2 for a given value of partial entropy production $\sigma_2 = (L_{21}A_1 + L_{22}A_2)A_2$ that is a polynomial of the second degree in A_2 with solution

$$A_2^{\pm} = \frac{-L_{12}A_1 \pm \sqrt{(L_{12}A_1)^2 + 4L_{22}\sigma_2}}{2L_{22}}, \tag{B45}$$

$$A_2^{\pm} = A_2^* \pm \frac{|L_{12}A_1|}{2L_{22}}\sqrt{1 + \frac{4L_{22}\sigma_2}{(L_{12}A_1)^2}}, \tag{B46}$$

$$A_2^{\pm} = A_2^* \pm |A_2^*|\sqrt{1 - \frac{\sigma_2}{\sigma_2^*}}, \tag{B47}$$

$$A_2^{\pm} = A_2^*\chi_{\pm}(x) \quad \text{with power ratio} \quad x \doteq \frac{\sigma_2}{\sigma_2^*}. \tag{B48}$$

Thus, the force against which the machine works is a function of the force at maximum power and the ratio x of operating power and maximum power. We have introduced the function

$$\chi_{\pm}(x) = 1 \pm \sqrt{1 - x}. \tag{B49}$$

Let's now calculate a linear machine's efficiency $\eta(x)$ as a function of the ratio x of operating power and maximum power. This efficiency writes in terms of the

coefficients of the Onsager matrix and the forces

$$\eta = \frac{-L_{12}A_1A_2 - L_{22}A_2^2}{L_{12}A_2A_1 + L_{11}A_1^2} \tag{B50}$$

$$\eta = \frac{-L_{12}A_1A_2^*\chi_\pm - L_{22}F_2^{*2}\chi_\pm^2}{L_{12}A_1A_2^*\chi_\pm + L_{11}A_1^2} \tag{B51}$$

$$\eta = \frac{L_{12}A_1\frac{L_{12}A_1}{2L_{22}}\chi_\pm - L_{22}\left(\frac{L_{12}A_1}{2L_{22}}\right)^2\chi_\pm^2}{-L_{12}A_1\frac{L_{12}A_1}{2L_{22}}\chi_\pm + L_{11}A_1^2} \tag{B52}$$

$$\eta = \frac{\frac{\xi^2}{2}\chi_\pm - \frac{\xi^2}{4}\chi_\pm^2}{-\frac{\xi^2}{2}\chi_\pm + 1} \tag{B53}$$

where we used Eqs. (B48, B40). We conclude that efficiency is a bivalued function of the machine output power

$$\eta(x) = \frac{\chi_\pm(1 - \chi_\pm/2)}{2/\xi^2 - \chi_\pm} \tag{B54}$$

The corresponding power-efficiency graph of a linear machine is shown in Fig. B.5 for different degrees of coupling ξ. Such graphs are, in fact, typical for energy converters even beyond the linear hypothesis. As illustrations borrowed from my lectures on energy conversion, we provide in Fig. B.6 the power-efficiency graphs for two simplified models of non-linear converters: a Francis turbine and an asynchronous electric motor. It is striking that it is possible, in principle, to match the maximum efficiency with the efficiency at maximum power in a Francis turbine. This is the case when the turbine is adapted to the maximal flow, i.e. without quadratic dissipation when the flow is maximal. In other words, when the flow is lower, the dissipation is quadratic in the distance to the maximal flow (chosen as the adapted flow). For the electric motor, we consider the Joule dissipation in the stator only. Without this dissipation ($\alpha = 0$) the motor displays strong coupling.

Let's emphasize that normalizing power by the maximum power allows us to compare trade-offs between the power and efficiency of very different machines, but absolute maximum powers may differ by several orders of magnitude. This is the case for Francis turbines, which operate at a very high power compared to electric motors.

B.2.7 Efficiency at maximum power and maximum efficiency

Efficiency at maximum power depends solely on the degree of coupling [104]. It is obtained by taking $\chi_\pm = 1$ in Eq. (B54)

$$\eta(\sigma_2^*) = \frac{\xi^2}{4 - 2\xi^2}. \tag{B55}$$

For strong coupling between input and output flows, the degree of coupling is $\xi = -1$. The efficiency at maximum power is $\eta(\sigma_2^*) = 1/2$, i.e. half the maximum

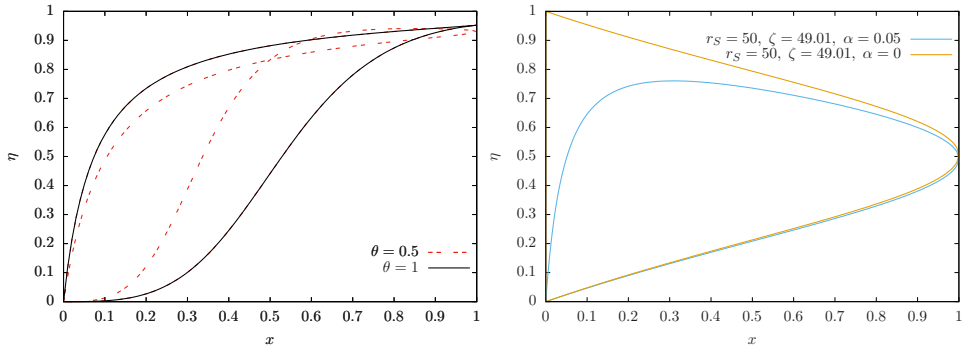

Figure B.6: Type II efficiency η as a function of the power ratio x for (Left) a Francis turbine and (Right) an asynchronous electric motor. For the turbine, the parameter θ is the fraction of the flow with respect to the maximal flow. For the motor, r_S is a scaled pulsation of the stator current with $\zeta = -1 \pm \sqrt{1 + r_S^2}$, and α is a parameter related to the degree of coupling that is proportional to the Joule dissipation in the stator.

efficiency. Optimization of the efficiency with respect to σ_2 is also possible, although a little more computationally demanding, leading to the *maximum efficiency*

$$\eta^* = \left(\frac{1 - \sqrt{1 - \xi^2}}{\xi} \right)^2 = \frac{1 - \sqrt{1 - \xi^2}}{1 + \sqrt{1 - \xi^2}}. \tag{B56}$$

The second equality arises from multiplying the numerator and denominator of the fraction on the right by $1 - \sqrt{1 - \xi^2}$. Fig. B.5 shows that the reversible efficiency $\eta = 1$ is out of reach when the degree of coupling is $-1 < \xi < 1$. In the case of $|\xi| = 1$, the curve is open: it is not a lobe anymore. Maximum efficiency is achieved at zero power only. This is the expected result for a reversible machine: for example, a Carnot cycle is completed in infinite time so that the power supplied per unit time is zero. The fact that power-efficiency curves are bivalued is intuitive: a unique pair of conjugated variables exists at maximum power; in all other cases, two pairs of conjugated variables can lead to the same output power (high current and low force, or low current and high force).

B.3 Stationary converters

Ref. [9] generalizes the results of the previous section to stationary and non-linear converters modeled by Markov jump processes. We assume knowing the state probability in NESS. We also use the decomposition of edge currents on cycle currents and similarly the decomposition of physical currents on fundamental currents [105, 106, 107, 108]. We supplement in this section the result of Ref. [9] by providing some elements on state probabilities and the decomposition of currents in NESS.

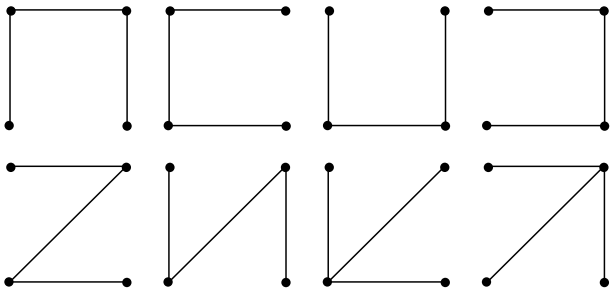

Figure B.7: All spanning trees of the four-state model of Fig. B.1.

B.3.1 Stationary probability

The stationary probability $p_y^{\rm st}$ is a solution of

$$\sum_{y,\nu} k_{(xy,\nu)} p_y^{\rm st} = 0. \tag{B57}$$

This stationary probability for state y is obtained by selecting an arbitrary row x (always the same, whatever the value of y) and isolating the minors (xy).

$$p_y^{\rm st} = \frac{(-1)^{y+x}}{Z} {\rm Det} \left(\sum_\nu \boldsymbol{k}_\nu \right)_{xy}, \tag{B58}$$

where the subscript indicates xy minor of the matrix $\sum_\nu \boldsymbol{k}_\nu$. We denote by Z a normalization constant. Remark that a Markov matrix has a null determinant: its largest eigenvalue is zero with the associated right (resp. left) eigenvector being $\boldsymbol{p}^{\rm st}$ [resp. $(1, \dots, 1)$]. By Perron-Froebenius theorem, all other eigenvalues have negative real parts so that the finite time probability eventually relaxes to the stationary one (for finite V). Relaxation from a given initial condition of the solution of the master equation can, therefore, be pure damping or damped oscillations, but will always converge to $p^{\rm st}$. Let's verify Eq. (B57) for the probability vector of Eq. (B58):

$$\sum_{y,\nu} k_{(xy,\nu)} p_y^{\rm st} = \frac{1}{Z} \sum_{y,\nu} k_{(xy,\nu)} (-1)^{y+x} {\rm Det} \left(\sum_\nu k_\nu \right)_{xy} = \frac{1}{Z} {\rm Det} \sum_\nu k_\nu = 0. \tag{B59}$$

The vector $\boldsymbol{p}^{\rm st}$ is the Froebenius eigenvector: its components are all positive, as required for a probability vector. Indeed, the Markov generator is of rank $V-1$ and hence has non-null minors. In principle, the Perron-Froebenius theorem applies to matrices with positive coefficients. An extension exists for irreducible matrices whose coefficients are positive or zero. Irreducibility is associated with strongly connected graphs (i.e., there is always a path from one vertex to another and vice versa). If the graph is unconnected, the probability of one of the disconnected parts may be zero.

An alternative formula from graph theory exists for stationary probability; see [109]. It is called the spanning tree formula. A spanning tree is a subset of the edge

set that includes $V-1$ edges connecting all vertices; see Fig. B.7. Choosing a root vertex x for the spanning tree T implies orienting tree edges toward the root. We denote the rooted spanning tree T_x. Then, the spanning tree formula reads

$$p_x^{\rm st} = \frac{1}{Z}\sum_{T_x}\prod_{e\in T_x} k_e, \tag{B60}$$

where the sum runs on all spanning trees rooted in x. The product covers all edges in T_x. Then, the numerator of Eq. (B60) includes all the products of $V-1$ different transition rates. The same is true of the minors of the rate matrix that, by definition, are homogeneous of degree $V-1$ in the transition rates, with product involving transition rates all connecting different pairs of states. This statement is enough to relate Eqs. (B59-B60). We emphasize that the spanning tree formula applies to multigraphs, i.e., graphs with different edges connecting the same pair of vertices. Since $k_{xy} \doteq \Sigma_\nu k_{xy,\nu}$, the number of spanning trees increases with the number of channels. This higher number of trees corresponds to the supplemental products of rates appearing in the minors formula when developing the sum over ν in the transition rates.

The spanning tree formula is easy to interpret as all the probability flows toward the root, contributing positively to the probability of the corresponding state. It is easy to calculate for systems with a low number of states V, while the minor formula is more straightforward for systems with large V. The stationary probability replaces the Gibbs-Boltzman probability of systems at equilibrium. However, it is not sufficient to study the thermodynamics of non-equilibrium systems beyond average behavior. We finally remark that the spanning tree formula leads to the Boltzmann probability under the detailed balance condition (Eq. (B20) when all temperatures are equal and without non-conservative forces).

B.3.2 Decomposition of stationary currents and forces

There is often a linear dependence between currents due to conservation laws, either at the microscopic level for probability currents or at the macroscopic level for the currents of physical quantities. This linear dependence allows using a reduced set of currents and conjugated forces to describe a physical system without losing anything about it as long as one knows the existing conservation laws. In table B.9, we summarize the various notations for the current and forces used in this section. Cycle currents or fundamental currents are obtained by selecting an independent set of currents beyond the edge currents or the physical currents respectively. Given the similarity between the procedure at the microscopic or macroscopic level, we use different letters for these two cases but switch from lower to upper case when reducing the number of independent variables.

Microscopic level– In the NESS, we write the *edge forces* f_e as logarithms of the probability ratio of stationary transition probability for e and $-e$

$$f_{(xy,\nu)} \equiv \ln \frac{k_{(xy,\nu)}p_y^{\rm st}}{k_{(yx,\nu)}p_x^{\rm st}}. \tag{B61}$$

The *edge probability current* along $e = (xy, \nu)$ is the net current along the edge

$$j_{(xy,\nu)} \equiv k_{(xy,\nu)} p_x^{\mathrm{st}} - k_{(yx,\nu)} p_y^{\mathrm{st}}. \tag{B62}$$

Given probability conservation, it is unsurprising that those currents are linearly dependent (Kirchhoff currents law at each vertex). Taking one spanning tree introduced in the previous section allows us to identify cycles. Starting from the spanning tree and adding one edge of the graph creates a cycle, i.e., a path of edges making a unique loop. The added edge is called a chord and uniquely identifies its associated fundamental cycle; see Fig. B.8. The orientation of the chord c defines the orientation of the associated cycle, also denoted c. It is obvious then that the set of chords is a subset of edges. The choice of spanning tree defines a basis of fundamental cycles (different trees lead to different bases). Each basis includes a number of fundamental cycles equal to the number of edges in the graph that do not belong to the spanning tree. Based on this observation, the formula relating the number of edges E, of vertices V and of fundamental cycles C is

$$E = V - 1 + C \tag{B63}$$

By definition of a basis, it is possible to combine the fundamental cycles to form any other graph cycle (edges common to both graphs and of opposite orientations are removed from the final cycle). This explains the use of the word "fundamental" cycles as those cycles that create a basis for all cycles. In practice, a cycle c is a vector in edge space such that the components of this vector are

$$c_e = \begin{cases} +1 \text{ if } e \in c \text{ with the same orientation} \\ -1 \text{ if } e \in c \text{ with the opposite orientation} \\ 0 \text{ otherwise} \end{cases} \tag{B64}$$

Let's call $\boldsymbol{\mathcal{C}}$ the matrix whose columns are fundamental cycle vectors. Therefore, the matrix $\boldsymbol{\mathcal{C}}$ is of dimension $E \times C$. Note that the fundamental cycles are a basis of the kernel of the incidence matrix, so $\boldsymbol{D\mathcal{C}} = 0$, and the cycles are its right null eigenvectors.

Each fundamental cycle labeled by chord c is associated with a stationary *cycle current* J_c equal to the chord current of cycle c. By definition, a chord belongs to only one fundamental cycle. Edges that are not chords belong to one or several cycles and must sustain the sum of the currents of all the cycles they belong to. They are linear combinations of cycle currents where the coefficients of this linear combination are 1 or -1 according to the relative orientation of the edge and cycles:

$$j_e = \sum_c \mathcal{C}_{ec} J_c \quad \Rightarrow \quad \boldsymbol{j} = \boldsymbol{\mathcal{C}} \boldsymbol{J} \tag{B65}$$

Furthermore, we define the *cycle force* of c by the sum of the forces on the edges belonging to cycle c:

$$F_c^{\mathrm{T}} = \sum_e f_e^{\mathrm{T}} \mathcal{C}_{ec} \quad \Rightarrow \quad \boldsymbol{F}^T = \boldsymbol{f}^{\mathrm{T}} \boldsymbol{\mathcal{C}} \tag{B66}$$

	Full set	Reduced set
Micro	Edge current $\boldsymbol{j}$ Edge force $\boldsymbol{f}$	Cycle current $\boldsymbol{J}$ Cycle force $\boldsymbol{F}$
Macro	Physical current $\boldsymbol{i}$ Local potential $\boldsymbol{a}$	Fundamental current $\boldsymbol{I}$ Fundamental force $\boldsymbol{A}$

Table B.9: Notation for the current and forces at the different levels of description, from the microscopic level of edges and cycles to the macroscopic level of physical currents exchanged with the environment and the reduced set of fundamental currents. Lower case letters are for the full set of variables and upper case letters are for the reduced set of variables. We follow here the usual convention that $\boldsymbol{j}$ are local currents and $\boldsymbol{i}$ are integrated currents. Ref. [11] is at the macroscopic level only and uses the notations of this table. In Ref. [9], the notations are different; for instance, lowercase letters are for fluctuating variables.

where T indicates transposition. This choice guarantees the unicity of the entropy production rate expressed using edge or cycle variables

$$\sigma = \boldsymbol{f}^{\mathrm{T}}\boldsymbol{j} = \boldsymbol{f}^{\mathrm{T}}\boldsymbol{\mathcal{C}}\boldsymbol{J} = \boldsymbol{F}^{\mathrm{T}}\boldsymbol{J} \tag{B67}$$

where the first equality is a restatement of Eq. (B19) using edge currents and forces.

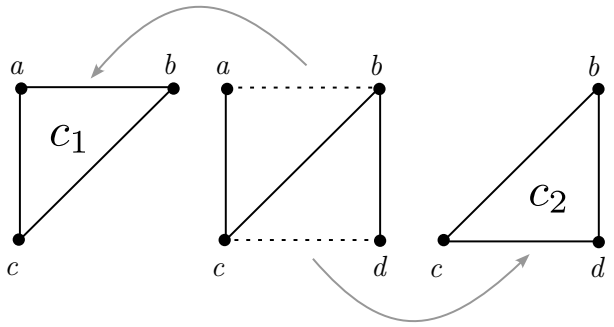

Figure B.8: Spanning tree leading to cycle c_1 by adding chord ab and to cycle c_2 by adding chord cd.

Macroscopic level– The above reasoning applies equally at the macroscopic level. Let's first define the physical currents as the sum over all cycles of the cycle currents J_c times Φ_{Xc} the amount of xth physical quantity ($x = 1, \ldots, N$) received by the system when performing cycle c:

$$i_X = \sum_{c=1}^{C} \Phi_{Xc} J_c \quad \Rightarrow \quad \boldsymbol{i} = \boldsymbol{\Phi}\boldsymbol{J} \tag{B68}$$

The local potentials a_X associated with each reservoir (i.e. forces at the physical

level) are related to cycle forces by

$$F_c^{\mathrm{T}} = \sum_{X=1}^{N} a_X^{\mathrm{T}} \Phi_{Xc} \quad \Rightarrow \quad \boldsymbol{F}^{\mathrm{T}} = \boldsymbol{a}^{\mathrm{T}} \boldsymbol{\Phi}, \tag{B69}$$

so that the EPR remains the same whether expressed using edges, cycles, or physical currents and their conjugated forces:

$$\sigma = \boldsymbol{F}^{\mathrm{T}} \boldsymbol{J} = \boldsymbol{a}^{\mathrm{T}} \boldsymbol{\Phi} \boldsymbol{J} = \boldsymbol{a}^{\mathrm{T}} \boldsymbol{i}. \tag{B70}$$

Due to conservation of physical quantities (such as energy and matter), the physical currents are often linearly dependent according to $\boldsymbol{\ell}_\alpha \boldsymbol{i} = 0$ where $\boldsymbol{\ell}_\alpha$ are line vectors ($\alpha = 1, \ldots, \lambda$) with a number of columns (labeled by x) corresponding to the total number of physical currents received from the reservoirs. The matrix $\boldsymbol{\ell}$ with components $\ell_{\alpha X}$ encodes all the system's conservation laws. Then, we choose a subset of $N - \lambda$ physical currents, called fundamental currents, that are linearly independent according to

$$i_X = \sum_{Y=1}^{N-\lambda} S_{XY} I_Y \quad \Rightarrow \quad \boldsymbol{i} = \boldsymbol{S} \boldsymbol{I}, \tag{B71}$$

where the selection matrix satisfies $\boldsymbol{\ell} \boldsymbol{S} = 0$. The column vectors of the selection matrix define a basis of the kernel of the matrix of conservation laws. In other words, the selection matrix reconstructs the physical currents from the fundamental currents. It selects which currents in the basis are necessary to reconstruct each physical current according to the conservation laws. It also selects the local potentials to create fundamental forces according to

$$\boldsymbol{A}^{\mathrm{T}} = \boldsymbol{a}^{\mathrm{T}} \boldsymbol{S}, \tag{B72}$$

where again the EPR is the same at the physical and fundamental levels

$$\sigma = \boldsymbol{a}^{\mathrm{T}} \boldsymbol{i} = \boldsymbol{a}^{\mathrm{T}} \boldsymbol{S} \boldsymbol{I} = \boldsymbol{A}^{\mathrm{T}} \boldsymbol{I}. \tag{B73}$$

B.3.3 Nonlinear conductance matrices

In order to define non-linear conductances (or resistances), we now use the relations between the currents at the various levels of description obtained in the previous section. We start by defining a trivial relation between edge forces and currents and export it to the higher levels. In Ref. [9], we skip the level of physical currents as in the linear regime since Onsager's response matrix is often given at the fundamental level.

In the steady state, we first define the *edge resistance* along e transition by

$$r_e \equiv \frac{f_e}{j_e} > 0, \tag{B74}$$

so that the edge force is given by $\boldsymbol{f} = \boldsymbol{r} \boldsymbol{j}$, i.e. applying the resistance matrix $\boldsymbol{r}$, diagonal with diagonal components r_e, on the edge current $\boldsymbol{j}$. The positivity of

local resistance arises for the same reason as the positivity of entropy production in Eq. (B19). Moreover, entropy production can be written as a quadratic form of the currents or forces on the edges, where r_e are the coefficients, which must therefore be positive. Note that r_e is not defined when the edge current is zero.

Then the *cycle resistance matrix* defined by

$$\boldsymbol{R} = \boldsymbol{\mathcal{C}}^{\mathrm{T}} \boldsymbol{r} \boldsymbol{\mathcal{C}} \tag{B75}$$

relates cycle currents and forces since

$$\boldsymbol{F} = \boldsymbol{\mathcal{C}}^{\mathrm{T}} \boldsymbol{f} = \boldsymbol{\mathcal{C}}^{\mathrm{T}} \boldsymbol{r} \boldsymbol{j} = (\boldsymbol{\mathcal{C}}^{\mathrm{T}} \boldsymbol{r} \boldsymbol{\mathcal{C}}) \boldsymbol{J} = \boldsymbol{R} \boldsymbol{J}. \tag{B76}$$

The matrix $\boldsymbol{R}$ is a square symmetric matrix of dimension $C \times C$ given that $\boldsymbol{r}$ is a square diagonal matrix of dimension $E \times E$. Like for $\boldsymbol{r}$, the cycle resistance matrix is defined positive in accordance with the positivity of the EPR, written as a quadratic form of the currents or forces. Hence, there is an inverse matrix called *cycle conductance matrix* $\boldsymbol{R}^{-1}$ such that

$$\boldsymbol{J} = \boldsymbol{R}^{-1} \boldsymbol{F}. \tag{B77}$$

Proceeding similarly to the level of physical currents and forces leads to the *physical conductance matrix* $\boldsymbol{g} = \boldsymbol{\Phi} \boldsymbol{R}^{-1} \boldsymbol{\Phi}^{\mathrm{T}}$

$$\boldsymbol{i} = \boldsymbol{\Phi} \boldsymbol{J} = \boldsymbol{\Phi} \boldsymbol{R}^{-1} \boldsymbol{F} = (\boldsymbol{\Phi} \boldsymbol{R}^{-1} \boldsymbol{\Phi}^{\mathrm{T}}) \boldsymbol{a} = \boldsymbol{g} \boldsymbol{a}. \tag{B78}$$

and to the *fundamental conductance matrix* $\boldsymbol{G} = \boldsymbol{S}^{+} \boldsymbol{g} \boldsymbol{S}^{+\mathrm{T}}$.

$$\boldsymbol{I} = \boldsymbol{S}^{+} \boldsymbol{i} = \boldsymbol{S}^{+} \boldsymbol{g} \boldsymbol{a} = (\boldsymbol{S}^{+} \boldsymbol{g} \boldsymbol{S}^{+\mathrm{T}}) \boldsymbol{A} = \boldsymbol{G} \boldsymbol{A}, \tag{B79}$$

where $\boldsymbol{S}^{+}$ is the Moore-Penrose inverse of matrix $\boldsymbol{S}$ that exists since its columns are independent. We stress that the nonlinear conductance matrix is a function of the macroscopic forces $\boldsymbol{A}$ explaining why even though the current-force relation looks linear it is in fact nonlinear. This dependence appears in the transition rates k_e via the LDB. However, the linear relationship between macroscopic forces and currents arises naturally when developing the nonlinear conductance at first order in fundamental forces.

The crucial point is that the nonlinear conductance matrix includes more information about the system than simply giving currents as a function of macroscopic forces. For instance, the determinant of the non-linear conductance matrix at the fundamental level is accessible, enabling the generalization of the degree of coupling between the currents (cf. B.3.4). This is impossible without nonlinear conductance matrix when using the non-linear currents as a function of the forces. Moreover, we have shown in Ref. [11] that given the fundamental conductances of two different devices put in connection, one can compute the fundamental conductance of the resulting device. This allows decomposing complex problems into several simpler pieces that can be characterized independently and assembled together (cf. B.3.5).

Journal of Statistical Mechanics: Theory and Experiment
An IOP and SISSA journal

PAPER: Classical statistical mechanics, equilibrium and non-equilibrium

Degree of coupling and efficiency of energy converters far-from-equilibrium

Hadrien Vroylandt[1], **David Lacoste**[2] **and Gatien Verley**[1]

[1] Laboratoire de Physique Théorique (UMR8627), CNRS, Univ. Paris-Sud, Université Paris-Saclay, 91405 Orsay, France
[2] Laboratoire de Physico-Chimie Théorique—UMR CNRS Gulliver 7083, PSL Research University, ESPCI 10 rue Vauquelin, F-75231 Paris, France
E-mail: david.lacoste@espci.fr

Received 6 December 2017
Accepted for publication 15 January 2018
Published 15 February 2018

Online at stacks.iop.org/JSTAT/2018/023205
https://doi.org/10.1088/1742-5468/aaa8fe

Abstract. In this paper, we introduce a real symmetric and positive semi-definite matrix, which we call the non-equilibrium conductance matrix, and which generalizes the Onsager response matrix for a system in a non-equilibrium stationary state. We then express the thermodynamic efficiency in terms of the coefficients of this matrix using a parametrization similar to the one used near equilibrium. This framework, then valid arbitrarily far from equilibrium allows to set bounds on the thermodynamic efficiency by a universal function depending only on the degree of coupling between input and output currents. It also leads to new general power-efficiency trade-offs valid for macroscopic machines that are compared to trade-offs previously obtained from uncertainty relations. We illustrate our results on an unicycle heat to heat converter and on a discrete model of a molecular motor.

Keywords: large deviations in non-equilibrium systems, stationary states, transport processes / heat transfer, molecular motors

1742-5468/18/023205+25$33.00

Contents

Introduction

The second law of thermodynamics prevents the thermodynamic efficiency of energy converters to exceed the reversible efficiency [1], thus ruling out perpetual motion. The energy converters operating close to reversible efficiency have been widely studied [2–5]. Historically, these questions were first addressed within the framework of weakly irreversible thermodynamics developed by Onsager for purely resistive systems [6, 7], i.e. systems with fluxes and affinities instantaneously related. This theory assumes local equilibrium and expresses physical currents (e.g. energy currents, matter currents) as non-linear functions of the affinities and local intensive parameters [1].

J. Stat. Mech. (2018) 023205

In the linear response regime near equilibrium, currents become linear function of the affinities, which defines the so-called Onsager response matrix. The framework based on this response matrix has been very successful to describe thermoelectric effects [8, 9], to determine the degree of coupling between influx and outflux [2, 10, 11], or to predict the efficiency at maximum power [12, 13]. This framework can also be extended to cover mesoscopic and nanoscale systems [14]. A key result of the response matrix framework is Onsager's reciprocity relations which can be deduced from a more general symmetry property called fluctuation theorems [15–17]. Previous attempts to generalize the notion of Onsager matrix to non-equilibrium stationary states lead to non-symmetric Onsager matrices, so that many properties were lost for that reason [18].

In this paper, building on the work of Polettini *et al* [19, 20], we introduce precisely a non-equilibrium conductance matrix that is symmetric just as the Onsager response matrix, but whose coefficients are now functions of the affinities. Intuitively, such a conductance matrix should exist at the macroscopic scale, because it can be constructed by associating conductances between every pair of states from the microscopic scale up to the macroscopic scale. Naturally, the question whether a symmetric matrix can be constructed in this way even when the system is in a non-equilibrium stationary state requires a more careful analysis.

For this reason, we assume in a first step that such a non-equilibrium conductance matrix can be constructed disregarding the issue of possible non-unicity of this matrix. We then show that a parametrization of the thermodynamic efficiency introduced by Kedem and Caplan [2] for machines near equilibrium still applies to a machine operating far from equilibrium. This parametrization involves the degree of coupling ξ between the influx and outflux, which together with the functions Π and φ characterize the dissipation and therefore also the efficiency of a machine. Using this parametrization which is linked to the chosen non-equilibrium conductance matrix, we show that the efficiency admits a general upper bound valid arbitrarily far from equilibrium, which only depends on the degree of coupling. We also deduce from our framework power-efficiency inequalities that set bounds on the output power as a function of the machine efficiency.

In a second step, we construct the non-equilibrium conductance matrix from a framework based on the large deviation function (LDF) of currents. In the linear regime near equilibrium, this LDF has a quadratic form, which is related to central results of Statistical Physics such Onsager relations and the Fluctuation-Dissipation theorem. In this framework, response and current fluctuations are connected through an equality. Near a non-equilibrium stationary state, the relation between fluctuations and response takes instead the form of an inequality, which states that currents fluctuations near a non-equilibrium stationary state are always more likely than those predicted by linear response analysis close to this point [21, 22]. We show that a consequence of this property is an inequality between the non-equilibrium conductance matrix and the matrix of covariances of currents, for a certain matrix order among symmetric matrices [23]. Remarkably, our result contains various interesting power-efficiency trade-offs [24, 25]. Hence, our approach provides a unifying framework for studying and optimizing machine performance, and illustrates the relevance of the concept of the non-equilibrium conductance matrix.

J. Stat. Mech. (2018) 023205

To summarize, in the first section, we use standard thermodynamics to constrain the form of the non-equilibrium conductance matrix and then we exploit a parametrization originally developped for equilibrium systems to describe the efficiency of macroscopic thermodynamic machines operating far from equilibrium. In the second section, we derive an explicit formula for this non-equilibrium conductance matrix at the stochastic level. In the third section, we obtain various power-efficiency inequalities from that framework which we illustrate with two examples: a three state model of heat to heat converter with strongly coupled heat fluxes and a discrete model of molecular motor [26, 27].

1. From non-equilibrium conductance matrix to constraints on power and efficiency

1.1. The non-equilibrium conductance matrix

Machines are systems that produce on average a current against an external force, usually called thermodynamic affinity. This is achieved by using another current generated by its own affinity. Hence, a machine generically involves two affinities F_1 and F_2 associated with two physical currents J_1 and J_2. In terms of the physical currents and affinities, the mean entropy production rate can be written as

$$\sigma = F_1 J_1 + F_2 J_2, \tag{1}$$

which is the sum of two partial entropy production rates denoted by $\sigma_x = F_x J_x$. We focus here on the steady-state regime of the machine, where all quantities introduced so far are time-independent. Throughout the paper, we use $k_B = 1$ which means that entropy production rates have the dimension of inverse time. Physical observables, including currents J_x, affinities F_x, and partial entropy production rates σ_x, are labeled with index $x = 1, 2$. Close to equilibrium, physical currents are linear functions of the affinities:

$$\begin{pmatrix} J_1 \\ J_2 \end{pmatrix} = \begin{pmatrix} L_{1,1} & L_{1,2} \\ L_{2,1} & L_{2,2} \end{pmatrix} \begin{pmatrix} F_1 \\ F_2 \end{pmatrix}, \tag{2}$$

where $L_{X,Y}$ are the components of the Onsager matrix $\boldsymbol{L}$ [6]. This matrix has real and symmetric coefficients which are independent of the affinities.

Beyond the linear regime, the physical currents become non-linear functions of the affinities but it is not known whether the concept of Onsager matrix can still be used for systems in non-equilibrium stationary state. Let us assume for the moment that such a generalization exists, which we call the non-equilibrium conductance matrix $\boldsymbol{G}$. By similarity with the Onsager matrix, we assume a relation of the type

$$\begin{pmatrix} J_1 \\ J_2 \end{pmatrix} = \begin{pmatrix} G_{1,1} & G_{1,2} \\ G_{2,1} & G_{2,2} \end{pmatrix} \begin{pmatrix} F_1 \\ F_2 \end{pmatrix}, \tag{3}$$

with again real and symmetric coefficients. An important difference with the previous case is that the coefficients of the matrix $\boldsymbol{G}$ are now necessarily functions of the affinities

F_1 and F_2 unlike the constant coefficients of the Onsager matrix $\boldsymbol{L}$. Importantly these assumptions together with equation (3) still do not define a unique matrix $\boldsymbol{G}$.

We now specialize to a thermodynamic machine by assuming (without loss of generality) that the first process is the driving process and the second process is the output process. Hence the partial entropy production rate of the first process verifies $\sigma_1 \geqslant 0$ while $\sigma_2 \leqslant 0$ for the second process. The thermodynamic efficiency reads

$$\eta = \frac{-\sigma_2}{\sigma_1}. \tag{4}$$

The second law imposes the positivity of the total entropy production rate $\sigma = \sigma_1 + \sigma_2 \geqslant 0$, which implies $0 \leqslant \eta \leqslant 1$, where 0 is reached when there is no output current and 1 is reached for a reversible operation of the machine with vanishing entropy production rate σ. Now, using the above properties of the non-equilibrium conductance matrix, we get for the partial entropy production rates

$$\sigma_1 = J_1 F_1 = G_{1,1} {F_1}^2 + G_{1,2} F_1 F_2, \tag{5}$$

$$\sigma_2 = J_2 F_2 = G_{2,1} F_1 F_2 + G_{2,2} {F_2}^2. \tag{6}$$

We choose the affinity dependent matrix to be positive semi-definite to guarantee the validity of the second law for arbitrary affinities. Since $G_{1,2} = G_{2,1}$ this means:

$$G_{1,1} G_{2,2} \geqslant {G_{1,2}}^2, \tag{7}$$

for all possible affinities. Using equations (5) and (6) combined with the conditions $\sigma_1 \geqslant 0$ and $\sigma_2 \leqslant 0$ leads to the inequalities

$$G_{1,1} F_1^2 \geqslant -G_{1,2} F_1 F_2 \geqslant G_{2,2} F_2^2 \geqslant 0, \tag{8}$$

which are also valid for arbitrary affinities.

The question of the existence of a non-equilibrium conductance matrix with the above properties can be resolved by exhibiting a particular solution. It is simple to check that the matrix

$$\boldsymbol{G}_{\min} \equiv \frac{1}{\sigma} \begin{pmatrix} J_1^2 & J_1 J_2 \\ J_1 J_2 & J_2^2 \end{pmatrix}, \tag{9}$$

satisfies equation (3) by construction and is positive semi-definite because its trace is positive and its determinant is zero. The reason for the subscript 'min' for this matrix, can be understood once we introduce a matrix order for symmetric matrices, called Loewner partial order [23]. This is defined in such a way that $\boldsymbol{A} \geqslant \boldsymbol{B}$ means that $\boldsymbol{A} - \boldsymbol{B}$ is a positive semi-definite matrix. This property implies that for two symmetric $n \times n$ matrices $\boldsymbol{A}$ and $\boldsymbol{B}$:

$$\boldsymbol{A} \geqslant \boldsymbol{B} \Leftrightarrow \forall \boldsymbol{x} \in \mathbb{R}^n, \quad \boldsymbol{x}^{\mathrm{T}} \cdot \boldsymbol{A} \cdot \boldsymbol{x} \geqslant \boldsymbol{x}^{\mathrm{T}} \cdot \boldsymbol{B} \cdot \boldsymbol{x}. \tag{10}$$

Now, using equations (1), (3) and (8), one can show explicitly that the matrix $\boldsymbol{G} - \boldsymbol{G}_{\min}$ is also a positive semi-definite matrix, because its trace is again positive and its determinant is zero. Therefore, we have the general property

$$\boldsymbol{G} \geqslant \boldsymbol{G}_{\min}, \tag{11}$$

which justifies the name $\boldsymbol{G}_{\min}$ for a matrix which represents a minimum among all conductance matrices for the specific matrix order defined above.

1.2. General parametrization of the efficiency

Thanks to the above properties of the non-equilibrium conductance matrix, we can introduce the functions

$$\Pi \equiv G_{1,1}F_1^2, \quad \varphi \equiv \sqrt{\frac{G_{2,2}F_2^2}{G_{1,1}F_1^2}}, \quad \text{and} \quad \xi \equiv \frac{G_{1,2}}{\sqrt{G_{1,1}G_{2,2}}}\,\mathrm{sign}(F_1F_2). \tag{12}$$

These functions are direct generalizations of the ones used in the close-to-equilibrium regime [2]. The parameter $\Pi = \Pi(F_1, F_2)$ determines the dissipation of the driving process when there is no output process coupled to the driving process or when there is one but we choose to ignore it. In the following, we call this quantity the intrinsic dissipation of the driving process. Then $\varphi = \varphi(F_1, F_2)$ is the relative intrinsic dissipation of the output process with respect to the driving process, and finally $\xi = \xi(F_1, F_2)$ quantifies the *degree of coupling* [2, 4, 10, 13, 14]. From the constraints of equations (7) and (8), these functions are bounded by

$$\Pi \geqslant 0, \quad \xi \in [-1, 0[, \quad \varphi \in [0, -\xi], \tag{13}$$

for the system to operate as a machine. If it does not, the above parametrization could still be used but with a modified range of the parameters, namely $\varphi \geqslant 0$ and $\xi \in [-1, 1]$. Note that we have also excluded the value $\xi = 0$ from our analysis which corresponds to having independent driving and output processes for which $G_{1,2} = 0$. In this case, the system cannot work as a machine because its efficiency would be negative with $\eta = -\varphi^2 \leqslant 0$. Note also that in the literature on thermoelectricity [2, 14], it is customary to use the figure of merit ZT instead of the degree of coupling. The two notions are simply related by $ZT = \xi^2/(1 - \xi^2)$, so that ZT is a real positive number which goes to infinity when ξ tends to -1.

Restricting ourselves to a working machine, we use equations (5) and (6) in the definition (4) of thermodynamic efficiency to obtain

$$\eta = -\frac{G_{1,2}F_1F_2 + G_{2,2}F_2^2}{G_{1,1}F_1^2 + G_{1,2}F_1F_2}, \tag{14}$$

which can be turned into

$$\eta = -\frac{\varphi^2 + \xi\varphi}{1 + \xi\varphi}, \tag{15}$$

with the aid of equation (12). We emphasize that with this new parametrization, the machine efficiency does not to depend explicitly on the intrinsic dissipation Π, but only depends on the relative intrinsic dissipation φ and on the degree of coupling ξ. The specific dependence of the efficiency on the affinities is then completely transferred to φ and ξ. As we shall see below, this new parametrization of the efficiency provides useful insights into the machine properties. One important benefit in particular is the ability to bound the machine efficiency and output power.

J. Stat. Mech. (2018) 023205

1.3. Tight coupling far from equilibrium

In this section, we discuss the notion of tight coupling far-from-equilibrium based on the non-equilibrium conductance matrix and the (Π, φ, ξ) parametrization. Tight coupling between two entropy fluxes means that the elementary steps must produce entropy in constant proportion. In other words, the physical quantities corresponding to the driving and output processes must be always exchanged in the same proportion in such a way that the two equations in (3) are linearly dependent. The latter condition implies that the matrix $\boldsymbol{G}$ is of rank one, which means that it can be written in the form

$$\boldsymbol{G} = \begin{pmatrix} G_{1,1} & G_{1,2} \\ G_{2,1} & G_{2,2} \end{pmatrix} = G_{1,1} \begin{pmatrix} 1 & \alpha \\ \alpha & \alpha^2 \end{pmatrix}, \tag{16}$$

in terms of a real coefficient α. Using equation (3), one finds $J_1 = \alpha J_2$, thus α is precisely the proportionality factor between the two currents. Then using equation (9), one finds $\boldsymbol{G} = \boldsymbol{G}_{\min}$. Thus $\boldsymbol{G}_{\min}$ is the non-equilibrium conductance matrix of the system if it operates in the tight coupling regime. Furthermore, this shows that the inequality of equation (11) becomes saturated in the tight coupling regime.

Now, from equations (12) and (15), the coupling parameter reaches the value $\xi = \mathrm{sign}(F_1 F_2 \alpha) = -1$, because $\xi \in [-1, 0[$, and $\eta = \varphi = |\alpha F_2 / F_1|$. Thus, in the tight coupling regime, the degree of coupling reaches its minimum value.

Going back to the general case, one deduces from equation (15) that

$$\left.\frac{\partial \eta}{\partial \xi}\right|_{\varphi} = -\frac{\varphi(1-\varphi^2)}{(1+\xi\varphi)^2}, \tag{17}$$

which is always negative since $\varphi \in [0, 1]$. Therefore, the efficiency monotonously increases when ξ decreases, and the maximum value of the efficiency at fixed value of φ is reached when $\xi = -1$, i.e. at tight coupling.

1.4. Maximum efficiency as function of the degree of coupling

We now bound the efficiency $\eta = \eta(\xi, \varphi)$ of equation (15) by looking at the value of the function φ that yields the maximum efficiency in equation (15) at a fixed degree of coupling ξ. The condition $\partial\eta/\partial\varphi|_{\xi} = 0$ leads to a simple second degree polynomial equation

$$\xi\varphi^2 + 2\varphi + \xi = 0. \tag{18}$$

Multiplying the numerator and denominator of equation (15) by $2 + \xi\varphi$ and using (18), we find that the maximum efficiency becomes $\eta_{\max} = -\xi\varphi/(2 + \xi\varphi)$. Using the solution of equation (18) in this expression of $\eta_{\max}$, we obtain the maximal machine efficiency in terms of the degree of coupling function ξ,

$$\eta_{\max}(\xi) \equiv \frac{1 - \sqrt{1-\xi^2}}{1 + \sqrt{1-\xi^2}}, \tag{19}$$

which is such that

$$\eta_{\max}(\xi) \geqslant \eta(\xi, \varphi) \tag{20}$$

for all ξ and φ in the allowed range. This inequality is illustrated in figure 4 for the model of molecular motor studied in section 4. As expected from the previous section, equation (19) also confirms that the maximum of the curve $\eta_{\max}(\xi)$ is reached when the condition of tight coupling holds namely $\xi = -1$ since at this point $\eta_{\max} = 1$.

Since the maximum efficiency depends only on the degree of coupling ξ, it is possible to bound the efficiency by measuring the degree of coupling. For instance, if it is known that $\xi_{\min} \leqslant \xi$ for all conditions of operation of the machine, then we can deduce from equation (20) that $\eta \leqslant \eta_{\max}(\xi_{\min})$. Note that the bound itself is not unique because ξ is constructed from the non-equilibrium conductance matrix which is not uniquely defined by equation (3); nevertheless the dependance of $\eta_{\max}$ versus ξ is universal.

1.5. Power-efficiency relations

In this section we derive two upper bounds for the entropy production rate of the output process, a quantity which is the product of the output power of the machine with its affinity. These bounds are functions of the efficiency and hence are called power-efficiency relations, since they represent a constraint for reaching both high power and high efficiency.

To obtain the first bound, we factorize $G_{1,1}F_1^2$ in equation (6):

$$-\sigma_2 = -G_{1,1}F_1^2\left(\frac{G_{1,2}F_2}{G_{1,1}F_1} + \frac{G_{2,2}F_2^2}{G_{1,1}F_1^2}\right) = -\Pi\left(\xi\varphi + \varphi^2\right). \tag{21}$$

From equation (15) we have $-(\xi\varphi + \varphi^2) = \eta(1 + \xi\varphi)$ and therefore

$$-\sigma_2 = \Pi\eta\left(1 + \xi\varphi\right), \tag{22}$$

then using again equation (15), we can express φ in terms of η and ξ as

$$\varphi^{\pm} = -\frac{\xi\left(\eta + 1\right)}{2} \pm \frac{1}{2}\sqrt{(\eta+1)^2\xi^2 - 4\eta}, \tag{23}$$

where we have used equations (19) and (20) to guarantee that φ is real. Inserting these two solutions in equation (22), we obtain

$$-\sigma_2^{\pm} = \Pi\eta\left(1 - \xi^2\frac{1+\eta}{2} \mp \xi\sqrt{\frac{\xi^2}{4}(1+\eta)^2 - \eta}\right). \tag{24}$$

This equation shows that the relation between the output entropy production rate $-\sigma_2$ and the efficiency is in general bi-valued, which means that there are two possible values of the output entropy production rate for the same value of the efficiency. This relation becomes single-valued when $\xi = -1$, i.e. for tight coupling, since in this case $-\sigma_2^-$ is equal to zero, and only $-\sigma_2^+$ remains.

In the general case of arbitrary coupling, it is enough to upper bound $-\sigma_2^+$ to obtain a general bound on the output entropy production rate because $-\sigma_2^+ \geqslant -\sigma_2^-$ for $\xi \in [-1, 0[$. Since one can also show that $-\sigma_2^+$ is always a decreasing function of ξ at fixed η, its maximum value is reached at $\xi = -1$, which corresponds to the tight coupling condition. When inserting $\xi = -1$ into the expression of $-\sigma_2^+$, we obtain the first inequality:

J. Stat. Mech. (2018) 023205

$$-\sigma_2 \leqslant \Pi\eta(1-\eta). \tag{25}$$

Alternatively, one can start from equation (6) and factorize $G_{2,2}F_2^2$ which leads to $\sigma_2 = G_{2,2}F_2^2(1+\xi/\varphi)$. Then, using again the explicit solution of φ as a function of ξ and η, one obtains an expression which when evaluated at $\xi = -1$ leads to the second inequality

$$-\sigma_2 \leqslant G_{2,2}F_2^2\frac{1-\eta}{\eta}. \tag{26}$$

Despite the apparent similarities between equations (25) and (26) with the bounds recently derived in [25], we would like to stress that equations (25) and (26) represent a different result because our bounds are based on the non-equilibrium conductance matrix using classical thermodynamics in a macroscopic and deterministic setting. In contrast to that, the bounds of [25] have been derived in a stochastic setting based on uncertainty relations. The introduction of the non-equilibrium conductance matrix, the parametrization of the efficiency and equations (25) and (26) represent our first main results. In the following, we explain how to reconcile both bounds within a formalism of large deviation of currents.

2. Construction of the non-equilibrium conductance matrix from a large deviation function framework

So far, our analysis was based primarily on classical thermodynamics, where currents are deterministic quantities. In contrast to that, we introduce in the following a stochastic thermodynamics description, in which currents become random variables. As far as the microscopic dynamics is concerned, we assume that it can be described as a Markov jump process. This Markovian dynamics admits a non-equilibrium stationary state. In the following, by exploiting a quadratic bound of the LDF of currents near this non-equilibrium stationary state, we show how to define uniquely the NE conductance matrix.

We denote with upper case letters average quantities and with lower case letters the corresponding fluctuating quantities; then the subscript indicates the level of description, (x, y) for an edge, $c = c_1, c_2, \ldots$ for cycles and $x = 1, 2$ for the physical quantities.

2.1. Physical, cycle and edge currents and affinities

The probability per unit time to jump from the state y to state x of the machine is given by the rate matrix of components $k_{(x,y)} \geqslant 0$. We call the couple of states (x, y) an oriented edge when $k_{(x,y)} > 0$. We assume that if the jump from y to x is possible then the reverse jump also exists, i.e. $k_{(x,y)} > 0$ implies that $k_{(y,x)} > 0$. The stationary probability of x, denoted π_x, verifies by definition $\sum_y k_{(x,y)}\pi_y = 0$. The number of oriented edges is $|E|$. The average probability current along edge (x, y) in the stationary state is

$$J_{(x,y)} \equiv k_{(x,y)}\pi_y - k_{(y,x)}\pi_x, \tag{27}$$

J. Stat. Mech. (2018) 023205

and the edge affinity

$$F_{(x,y)} \equiv \ln \frac{k_{(x,y)}\pi_y}{k_{(y,x)}\pi_x}. \tag{28}$$

Another level of description is that of cycles which consist of several edges connected together. Cycle currents are linearly connected to edge currents [11] as:

$$J_{(x,y)} \equiv \sum_{c\in C} A_{(x,y),c} J_c, \tag{29}$$

where $\boldsymbol{A}$ is an $|E| \times |C|$ matrix, such that $A_{(x,y),c}$ is zero if the edge (x, y) does not belongs to the cycle c, or ± 1 if it belongs to it with the sign providing the orientation. The columns of $\boldsymbol{A}$ form a basis of vectors called fundamental cycles, and the ensemble of fundamental cycles is denoted C with cardinal $|C|$. This set is called fundamental because it is a minimal set of linearly independent cycles that can generate any cycle of the graph [28].

Each physical thermodynamic force involved in the interaction of the machine with its environment has a corresponding physical (also called sometimes operational for this reason) current associated with it. These currents are also linearly related to the cycle currents as:

$$J_X \equiv \sum_{c\in C} \phi_{X,c} J_c, \tag{30}$$

where $\phi_{X,c}$ represents the amount of the physical quantity x which is exchanged with the environment when the cycle c is run once. Note that by construction the coefficients of the matrix $\boldsymbol{\phi}$ are dimension full, depending on the choice of physical currents, unlike the coefficients of the matrix $\boldsymbol{A}$ which are dimensionless.

The entropy production takes the same value on these three levels, thus

$$\sigma = \sum_{(x,y)} J_{(x,y)} F_{(x,y)} = \sum_c J_c F_c = \sum_X J_X F_X. \tag{31}$$

This allows to connect the edge, cycle and physical affinities through dual forms of equations (29) and (30) [11, 19]:

$$F_c = \sum_{(x,y)} F_{(x,y)} A_{(x,y),c}, \tag{32}$$

$$F_c = \sum_X F_X \phi_{X,c}. \tag{33}$$

2.2. Quadratic bound on large deviations

In a stochastic description of the machine, all the currents introduced above at the various levels become stochastic quantities. Let us denote $j_{(x,y)}$ as the edge current associated to the net number of transitions from y to x per unit time during a trajectory of duration t. These edge currents $\{j_{(x,y)}\}$ are fluctuating quantities which are assumed to obey a large deviation principle. This means that the probability P of observing them in a total time t decays as

J. Stat. Mech. (2018) 023205

$$P(\{j_{(x,y)}\}) \simeq_{t\to+\infty} \mathrm{e}^{-tI(\{j_{(x,y)}\})}, \tag{34}$$

where $I(\{j_{(x,y)}\})$ is the large deviation function (LDF) of the currents also called rate function [29].

After some manipulations of equation (3) of [22][3], a quadratic bound for the LDF of edge currents can be written in the form

$$I(\{j_{(x,y)}\}) \leqslant \frac{1}{4}\sum_{(x,y)}(j_{(x,y)} - J_{(x,y)})^2 \bar{R}_{(x,y)}, \tag{35}$$

where

$$\bar{R}_{(x,y)} \equiv \frac{F_{(x,y)}}{J_{(x,y)}} \tag{36}$$

represents the components of a diagonal resistance matrix, i.e. an edgewise resistance. Now, the cycle currents j_c are connected to the edge currents $j_{(x,y)}$ by the stochastic version of equation (29). Let us introduce $\tilde{\boldsymbol{j}} \equiv (j_{c_1}, j_{c_2}, \ldots, j_{c_{|C|}})^{\mathrm{T}}$ the vector of the cycle currents and $\tilde{\boldsymbol{J}}$ its mean value. When using equation (29) as a change of variable into equation (35), we obtain

$$I(\tilde{\boldsymbol{j}}) \leqslant \frac{1}{4}(\tilde{\boldsymbol{j}} - \tilde{\boldsymbol{J}})^{\mathrm{T}} \cdot \tilde{\boldsymbol{R}} \cdot (\tilde{\boldsymbol{j}} - \tilde{\boldsymbol{J}}), \tag{37}$$

where $\tilde{\boldsymbol{R}}$ is the cycle resistance matrix of components

$$\tilde{R}_{c,c'} \equiv \sum_{(x,y)} A_{(x,y),c} A_{(x,y),c'} \frac{F_{(x,y)}}{J_{(x,y)}}. \tag{38}$$

By contracting equation (37) over cycle currents, one obtains an upper bound for the LDF of physical currents j_1, j_2. The LDF we are interested in reads

$$I_{\mathrm{quad}}(\boldsymbol{j}) = \frac{1}{4}\min_{\{..\}}\left(\tilde{\boldsymbol{j}} - \tilde{\boldsymbol{J}}\right)^{\mathrm{T}} \cdot \tilde{\boldsymbol{R}} \cdot \left(\tilde{\boldsymbol{j}} - \tilde{\boldsymbol{J}}\right), \tag{39}$$

where $\{..\}$ denotes the minimum over currents $\tilde{\boldsymbol{j}}$ such that $\boldsymbol{j} = \boldsymbol{\phi} \cdot \tilde{\boldsymbol{j}}$, with $\boldsymbol{j}$ the vector of physical currents (j_1, j_2). Since the function to be minimized is quadratic and the constraints are linear, this contraction can be achieved exactly as follows: The function to be minimized is

$$f_{\mathrm{quad}} = \frac{1}{4}\left(\tilde{\boldsymbol{j}} - \tilde{\boldsymbol{J}}\right)^{\mathrm{T}} \cdot \tilde{\boldsymbol{R}} \cdot \left(\tilde{\boldsymbol{j}} - \tilde{\boldsymbol{J}}\right) - \boldsymbol{\lambda}^{\mathrm{T}} \cdot \left(\boldsymbol{j} - \boldsymbol{\phi} \cdot \tilde{\boldsymbol{j}}\right), \tag{40}$$

where $\boldsymbol{\lambda}$ is a Lagrange multiplier. After minimizing f_{quad} with respect to $\tilde{\boldsymbol{j}}$, one obtains an expression of $\tilde{\boldsymbol{j}}$ as a function of $\boldsymbol{\lambda}$. Then using again the constraint $\boldsymbol{j} = \boldsymbol{\phi} \cdot \tilde{\boldsymbol{j}}$, one finds

$$\boldsymbol{\lambda} = -\frac{1}{2}\left[\boldsymbol{\phi} \cdot \tilde{\boldsymbol{R}}^{-1} \cdot \boldsymbol{\phi}^{\mathrm{T}}\right]^{-1} \cdot (\boldsymbol{j} - \boldsymbol{J}). \tag{41}$$

[3] More precisely, one needs to express the term $\sigma^{\pi}(y,z)$ of equation (3) of [22] as $j^{\pi}(y,z)F(y,z)$ and divide $j^{\pi}(y,z)$ out to obtain equation (35).

J. Stat. Mech. (2018) 023205

Inserting this expression into $\tilde{\boldsymbol{j}}$ and using it into $I_{\rm quad}$, one obtains

$$I_{\rm quad}(\boldsymbol{j}) = \frac{1}{4}\left(\boldsymbol{j}-\boldsymbol{J}\right)^{\rm T}\cdot\boldsymbol{R}\cdot\left(\boldsymbol{j}-\boldsymbol{J}\right), \tag{42}$$

where we have introduced $\boldsymbol{R}$ as the 2×2 resistance matrix in the basis of physical currents

$$\boldsymbol{R} \equiv \left(\boldsymbol{\phi}\cdot\tilde{\boldsymbol{R}}^{-1}\cdot\boldsymbol{\phi}^{\rm T}\right)^{-1}. \tag{43}$$

In the end, we obtain the following inequality for the LDF of physical currents:

$$I(\boldsymbol{j}) \leqslant I_{\rm quad}(\boldsymbol{j}). \tag{44}$$

The quadratic bound on the LDF used in equation (35) has been built to respect the fluctuation theorem [17, 22]. Therefore, at the level of physical observables the quadratic bound obeys the relation

$$I_{\rm quad}(\boldsymbol{j}) - I_{\rm quad}(-\boldsymbol{j}) = -\boldsymbol{j}^{\rm T}\cdot\boldsymbol{F}. \tag{45}$$

Once equation (42) is inserted into this equation, we obtain $\boldsymbol{j}^{\rm T}\cdot\boldsymbol{R}\cdot\boldsymbol{J} = \boldsymbol{j}^{\rm T}\cdot\boldsymbol{F}$ for all $\boldsymbol{j}$, or equivalently $\boldsymbol{R}\cdot\boldsymbol{J} = \boldsymbol{F}$. After comparing with equation (3), we deduce the relation

$$\boldsymbol{G} = \boldsymbol{R}^{-1} = \boldsymbol{\phi}\cdot\tilde{\boldsymbol{R}}^{-1}\cdot\boldsymbol{\phi}^{\rm T}, \tag{46}$$

that provides a consistent definition of the conductance matrix. Also note that we have assumed the matrices $\tilde{\boldsymbol{R}}$, $\boldsymbol{R}$ and $\boldsymbol{G}$ to be invertible, if it is not the case the matrix $\boldsymbol{G}_{\rm min}$ introduced in equation (9) should be used from the beginning. An explicit example of this case is provided for an unicyclic machine in the section 4.1.

In appendix, we derive an alternate route leading to equation (46), which avoids the last step of equation (45) but relies instead on a further change of the level of description from that of cycles to that of physical currents.

To summarize, the property that edge current fluctuations in non-equilibrium stationary states are more likely than those predicted by linear response analysis [21, 22] which is equation (35), carries out to the level of cycles and from there to the level of physical macroscopic currents. This approach leads to a relation between affinities and physical macroscopic currents that defines the non-equilibrium conductance matrix. The construction of this matrix from a large deviation framework represents our second main result.

3. Implications for the thermodynamic efficiency and the output power

In this section, we show how previously obtained bounds on efficiency [24], and power-efficiency trade-offs [25] can be derived from a framework based on the non-equilibrium conductance matrix.

J. Stat. Mech. (2018) 023205

3.1. Inequality involving the non-equilibrium conductance matrix and the covariance matrix of physical currents

We introduce the cumulant generating function (CGF) defined by

$$\lambda(\gamma_1,\gamma_2) \equiv \lim_{t\to\infty} \frac{1}{t} \ln \left\langle \mathrm{e}^{t(\gamma_1 j_1+\gamma_2 j_2)} \right\rangle , \tag{47}$$

which is the Legendre transform of the LDF of the physical currents $\lambda(\gamma_1,\gamma_2) = \max_{j_1,j_2}[\gamma_1 j_1 + \gamma_2 j_2 - I(j_1,j_2)]$. Similarly, the Legendre transform of the quadratic LDF is $\lambda_{\mathrm{quad}}(\gamma_1,\gamma_2) \equiv \max_{j_1,j_2}[\gamma_1 j_1 + \gamma_2 j_2 - I_{\mathrm{quad}}(j_1,j_2)]$. From equation (44), we have

$$\lambda_{\mathrm{quad}}(\gamma_1,\gamma_2) \leqslant \lambda(\gamma_1,\gamma_2), \tag{48}$$

where $\lambda_{\mathrm{quad}}(\gamma_1,\gamma_2)$ can be explicitly determined using equation (42). The maximum with respect to j_1 and j_2 leads to the condition

$$\boldsymbol{\gamma} = \frac{1}{2}\boldsymbol{R}\cdot(\boldsymbol{j}-\boldsymbol{J}), \tag{49}$$

where $\boldsymbol{\gamma}$ is the vector (γ_1,γ_2). Inserting this result into the definition of λ_{quad} and using the property $\boldsymbol{R}^{-1} = \boldsymbol{G}$, we obtain

$$\lambda_{\mathrm{quad}}(\boldsymbol{\gamma}) = \boldsymbol{\gamma}^{\mathrm{T}}\cdot\boldsymbol{G}\cdot\boldsymbol{\gamma} + \boldsymbol{J}\cdot\boldsymbol{\gamma}. \tag{50}$$

This equation holds for any value of the conjugated variables $\boldsymbol{\gamma}$. Then, the functions λ and λ_{quad} have the same value at origin and the same first derivative with respect to $\boldsymbol{\gamma}$ around the origin, therefore the inequality (48) can be carried out to second order derivatives. The result is the following inequality

$$\forall\boldsymbol{\gamma}\in\mathbb{R}^2, \quad \boldsymbol{\gamma}^{\mathrm{T}}\cdot\boldsymbol{G}\cdot\boldsymbol{\gamma} \leqslant \frac{1}{2}\boldsymbol{\gamma}^{\mathrm{T}}\cdot\boldsymbol{C}\cdot\boldsymbol{\gamma}, \tag{51}$$

where we have introduced the covariance matrix as

$$C_{XY} = \mathrm{Cov}(j_X,j_Y) \equiv \lim_{t\to\infty} t\left[\langle j_X j_Y\rangle - \langle j_X\rangle\langle j_Y\rangle\right] = \frac{\partial^2\lambda}{\partial\gamma_X\partial\gamma_Y}(0,0). \tag{52}$$

Now, equation (51) simply reads $\boldsymbol{G}\leqslant\boldsymbol{C}/2$ for the matrix order introduced in equation (10). Choosing $\boldsymbol{\gamma} = (\gamma_1,0)^{\mathrm{T}}$ or $(0,\gamma_2)^{\mathrm{T}}$ in equation (51) leads to the tight bounds derived in [20]:

$$G_{1,1}{F_1}^2 \leqslant \frac{\mathrm{Var}(\sigma_1)}{2}, \tag{53}$$

$$G_{2,2}{F_2}^2 \leqslant \frac{\mathrm{Var}(\sigma_2)}{2}, \tag{54}$$

after multiplying the inequalities by ${F_1}^2$ or ${F_2}^2$ respectively. These inequalities are saturated in the linear regime close to equilibrium, where the non-equilibrium conductance matrix becomes the standard Onsager matrix $\boldsymbol{L}$ and the relation $\boldsymbol{L} = \boldsymbol{C}/2$ is the well-known fluctuation-response relation. When using the above inequalities (53) and (54) into (25) and (26), one obtains

J. Stat. Mech. (2018) 023205

$$-\langle\sigma_2\rangle \leqslant \Pi\eta(1-\eta) \leqslant \frac{\mathrm{Var}(\sigma_1)}{2}\eta(1-\eta), \tag{55}$$

$$-\langle\sigma_2\rangle \leqslant G_{22}(F_2)^2\frac{1-\eta}{\eta} \leqslant \frac{\mathrm{Var}(\sigma_2)}{2}\frac{1-\eta}{\eta}. \tag{56}$$

Thus we retrieve the power-efficiency trade-offs derived by Pietzonka and Seifert [25]

$$-\langle\sigma_2\rangle \leqslant \frac{\mathrm{Var}(\sigma_1)}{2}\eta(1-\eta), \tag{57}$$

$$-\langle\sigma_2\rangle \leqslant \frac{\mathrm{Var}(\sigma_2)}{2}\frac{1-\eta}{\eta}. \tag{58}$$

3.2. From uncertainty relations to bounds on the efficiency

By combining the inequality $\boldsymbol{G} \leqslant \boldsymbol{C}/2$ obtained in the previous section with equation (11), one obtains

$$\boldsymbol{G}_{\min} \leqslant \boldsymbol{G} \leqslant \frac{\boldsymbol{C}}{2}, \tag{59}$$

where the first inequality on the left hand side becomes saturated only if the system has strongly coupled physical currents. Using again the property (10) for the matrix order, the relation $\boldsymbol{G}_{\min} \leqslant \boldsymbol{C}/2$ implies three inequalities by choosing three particular values of the vector $\boldsymbol{x}$, namely $(F_1, 0)^{\mathrm{T}}$, $(0, F_2)^{\mathrm{T}}$ and $(F_1, F_2)^{\mathrm{T}}$. These are the so-called *uncertainty relations* [21, 22]:

$$\frac{\langle\sigma_1\rangle^2}{\langle\sigma\rangle} \leqslant \frac{\mathrm{Var}(\sigma_1)}{2}, \tag{60}$$

$$\frac{\langle\sigma_2\rangle^2}{\langle\sigma\rangle} \leqslant \frac{\mathrm{Var}(\sigma_2)}{2}, \tag{61}$$

$$\langle\sigma\rangle \leqslant \frac{\mathrm{Var}(\sigma)}{2}. \tag{62}$$

Now, we recall the definition of efficiency in terms of average partial and total entropy production rates

$$\eta = 1 - \frac{\langle\sigma\rangle}{\langle\sigma_1\rangle}. \tag{63}$$

Inserting this definition into equations (60)–(62), one recovers two known bounds on efficiency [24]:

$$\eta \leqslant \min\left(1 - 2\frac{\langle\sigma_1\rangle}{\mathrm{Var}(\sigma_1)}, \frac{1}{1-2\frac{\langle\sigma_2\rangle}{\mathrm{Var}(\sigma_2)}}\right), \tag{64}$$

J. Stat. Mech. (2018) 023205

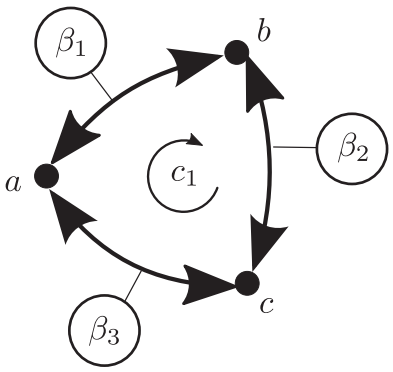

Figure 1. Sketch of the unicyclic heat to heat converter with three states a, b, and c. Transition $a \leftrightarrow b$ is promoted by the heat reservoir at inverse temperature β_1, transition $b \leftrightarrow c$ by the heat reservoir at inverse temperature β_2, and $c \leftrightarrow a$ for β_3.

and

$$\eta \geqslant \max\left(1 - \frac{\mathrm{Var}(\sigma)}{\langle\sigma_1\rangle}, \frac{1}{1 - \frac{\mathrm{Var}(\sigma)}{\langle\sigma_2\rangle}}\right). \tag{65}$$

Among these two inequalities, the first one namely equation (64) is probably the most useful one because it involves only the partial entropy production rates of process 1 or 2, whereas equation (65) requires information on both processes which is often missing.

4. Illustration on small machines

4.1. Unicyclic engine

We start by studying a simple example of heat-to-heat converter. We consider the unicyclic three states model depicted on figure 1. Each state a,b,c has a different energy E_a, E_b, E_c and each transition is connected to a different heat reservoir at inverse temperature $\beta_1, \beta_2, \beta_3$. The transition rates are

$$\begin{aligned} k_{(b,a)} &= \Gamma \mathrm{e}^{-\frac{\beta_1}{2}(E_b - E_a)}, \quad k_{(a,b)} = \Gamma \mathrm{e}^{-\frac{\beta_1}{2}(E_a - E_b)}, \\ k_{(c,b)} &= \Gamma \mathrm{e}^{-\frac{\beta_2}{2}(E_c - E_b)}, \quad k_{(b,c)} = \Gamma \mathrm{e}^{-\frac{\beta_2}{2}(E_b - E_c)}, \\ k_{(a,c)} &= \Gamma \mathrm{e}^{-\frac{\beta_3}{2}(E_a - E_c)}, \quad k_{(c,a)} = \Gamma \mathrm{e}^{-\frac{\beta_3}{2}(E_c - E_a)}, \end{aligned} \tag{66}$$

where Γ is the coupling strength to the reservoirs. The system is coupled to three heat reservoirs, and its total entropy production rate is $\sigma = -\beta_1 J_1 - \beta_2 J_2 - \beta_3 J_3$, where J_i denotes the heat flux from the heat reservoir i to the system. Using the energy conservation $J_1 + J_2 + J_3 = 0$, we obtain the total entropy production rate $\sigma = (\beta_3 - \beta_1)J_1 + (\beta_3 - \beta_2)J_2$. We consider as driving current the heat flow J_1 and output current the heat flow J_2, and we assume that the temperatures of the reservoirs satisfy $\beta_3 > \beta_1$ and $\beta_3 > \beta_2$ and the energies are such that $E_b > E_c > E_a$. Under these conditions, the driving and output currents are such that $J_1 > 0$ and $J_2 < 0$, and the system operates as a machine that transfers heat from a cold to a hot reservoir using the

J. Stat. Mech. (2018) 023205

thermodynamic force generated by the transfer of heat from a hot to a cold reservoir. The partial entropy production rates and physical affinities are then

$$\begin{aligned}\sigma_1 &= (\beta_3-\beta_1)J_1, \quad F_1 = (\beta_3-\beta_1)\\ \sigma_2 &= (\beta_3-\beta_1)J_2, \quad F_2 = (\beta_3-\beta_2).\end{aligned} \tag{67}$$

At the lower level, the system has a single cycle c_1 for which we chose the orientation $a \to b \to c$. Thus, the matrix of fundamental cycles $\boldsymbol{A}$ is actually the vector $\boldsymbol{A} = (1,1,1)^{\mathrm{T}}$. Due to the stationary condition, the current is the same on each edge and is equal to the cycle current

$$J_{(b,a)} = J_{(c,b)} = J_{(a,c)} = J_{c_1} = \frac{\Gamma}{Z}\left(k_{(b,a)}k_{(a,c)}k_{(c,b)} - k_{(a,b)}k_{(b,c)}k_{(c,a)}\right), \tag{68}$$

where we have defined

$$\begin{aligned}Z = {} & k_{(a,b)}k_{(a,c)} + k_{(a,b)}k_{(b,c)} + k_{(a,c)}k_{(c,b)} + k_{(b,a)}k_{(b,c)} + k_{(b,c)}k_{(c,a)}\\ & + k_{(b,a)}k_{(a,c)} + k_{(c,a)}k_{(c,b)} + k_{(c,b)}k_{(b,a)} + k_{(c,a)}k_{(a,b)}.\end{aligned} \tag{69}$$

The corresponding edge affinities are defined in equation (28). From the matrix of fundamental cycles $\boldsymbol{A}$, we derive the cycle affinity

$$F_{c_1} = (\beta_3-\beta_1)(E_b-E_a) + (\beta_3-\beta_2)(E_c-E_b) = \ln\frac{k_{(b,a)}k_{(a,c)}k_{(c,b)}}{k_{(a,b)}k_{(b,c)}k_{(c,a)}}. \tag{70}$$

When comparing with the physical affinities F_1 and F_2 of equation (67), we identify using equation (33) the matrix

$$\boldsymbol{\phi} = \begin{pmatrix} E_b - E_a \\ E_c - E_b \end{pmatrix}. \tag{71}$$

The physical currents follow from equation (30) as $J_1 = J_{c_1}(E_b - E_a)$ and $J_2 = J_{c_1}(E_c - E_b)$, in order that the entropy production rate writes $\sigma = J_{c_1}F_{c_1} = J_1F_1 + J_2F_2$.

We now turn to the conductance and resistance matrices. From the definition of the edge resistance matrix of equation (36), we have $\bar{R}_{(x,y)} = F_{(x,y)}/J_{c_1}$ since all edge probability currents are equal to the cycle current. Equation (38) yields the cycle resistance matrix which is the scalar

$$\tilde{\boldsymbol{R}} = \frac{F_{c_1}}{J_{c_1}}. \tag{72}$$

In the end, equation (46) for the non equilibrium conductance matrix yields

$$\boldsymbol{G} = \frac{J_{c_1}}{F_{c_1}}\begin{pmatrix} (E_b-E_a)^2 & (E_c-E_b)(E_b-E_a) \\ (E_c-E_b)(E_b-E_a) & (E_c-E_a)^2 \end{pmatrix}, \tag{73}$$

which is not invertible as expected for unicyclic machines. In this case, the conductance matrix is equal to the minimum conductance matrix $\boldsymbol{G}_{\min}$ defined in equation (9). In the end, the parameters associated to the non-equilibrium conductance matrix are:

$$\Pi = (E_a-E_b)^2(\beta_1-\beta_3)^2\frac{J_{c_1}}{F_{c_1}} = \frac{J_1^2F_1^2}{\sigma}, \tag{74}$$

J. Stat. Mech. (2018) 023205

$$\varphi = \left|\frac{(\beta_2-\beta_3)(E_b-E_c)}{(\beta_1-\beta_3)(E_a-E_b)}\right| = \frac{-J_2F_2}{J_1F_1} = \eta, \tag{75}$$

$$\xi = -1, \tag{76}$$

confirming that this system operates in the tight coupling regime.

4.2. Molecular motor

Our second example is a discrete model of a molecular motor [26, 27]. The motor has only two internal states and evolves on a linear discrete lattice by consuming adenosine triphosphate (ATP) molecules. The position of the motor is given by two variables the position n on the lattice and y is the number of ATP consumed, as shown in figure 2. The even and odd sites are denoted by a and b, respectively. Note that the lattice of a and b sites extends indefinitely in both directions along the n and y axis; for the spatial direction n, the lattice step defines the unit length. There are two physical forces acting on the motor, a chemical force controlled by the chemical potential difference of the hydrolysis reaction of ATP, $\Delta\mu$ and a mechanical force f applied directly on the motor. The whole system is in contact with a heat bath, and we choose to express all energies in units of k_BT. Equilibrium corresponds to the vanishing of the two currents, namely the mechanical current $\bar{v}$ which is the average velocity of the motor on the lattice, and r the chemical current, which is its average rate of ATP consumption. Since the system operates cyclically, the change of internal energy in a cycle is zero and the first law takes the form $q + r\Delta\mu + f\bar{v} = 0$ where q is the heat flow coming from the heat bath, $r\Delta\mu$ represents the chemical work and $f\bar{v}$ represents the mechanical work; all quantities are evaluated in a cycle. Under these conditions, the second law takes the form $\sigma = -q$, and the entropy production rate takes the following form:

$$\sigma = f\bar{v} + r\Delta\mu. \tag{77}$$

In the normal operation of the motor, chemical energy is converted into mechanical energy, which means that the driving process (1) is the chemical one and the output process (2) the mechanical one in agreement with the choice of convention made in this paper. Thus, the two partial entropy production rates should be $\sigma_1 = r\Delta\mu$, with the chemical affinity $F_1 = \Delta\mu$ and $\sigma_2 = f\bar{v}$, with mechanical affinity $F_2 = f$.

In this model, there are four reactions between the two states, corresponding to four edges, with for each of them a forward or backward direction along each edge as represented in figure 3. Two of these reactions are passive and do not involve ATP while the other two are active and do involve ATP. Together, there are eight rates for these four reactions which are given by

$$\begin{aligned}
\overrightarrow{\omega}_b^{-1} &= \alpha' \mathrm{e}^{\theta_b^+ f}, & \overrightarrow{\omega}_b^{0} &= \omega' \mathrm{e}^{\theta_b^+ f},\\
\overleftarrow{\omega}_a^{1} &= \alpha' \mathrm{e}^{-\epsilon+\Delta\mu-\theta_a^- f}, & \overleftarrow{\omega}_a^{0} &= \omega' \mathrm{e}^{-\epsilon-\theta_a^- f},\\
\overleftarrow{\omega}_b^{-1} &= \alpha \mathrm{e}^{-\theta_b^- f}, & \overleftarrow{\omega}_b^{0} &= \omega \mathrm{e}^{-\theta_b^- f},\\
\overrightarrow{\omega}_a^{1} &= \alpha \mathrm{e}^{-\epsilon+\Delta\mu+\theta_a^+ f}, & \overrightarrow{\omega}_a^{0} &= \omega \mathrm{e}^{-\epsilon+\theta_a^+ f},
\end{aligned} \tag{78}$$

where we have kept the original notation of [26, 27] for the rates. In the above expressions, $\theta_i^{\pm}$ represent load distribution factors which are arbitrary except for the constraint

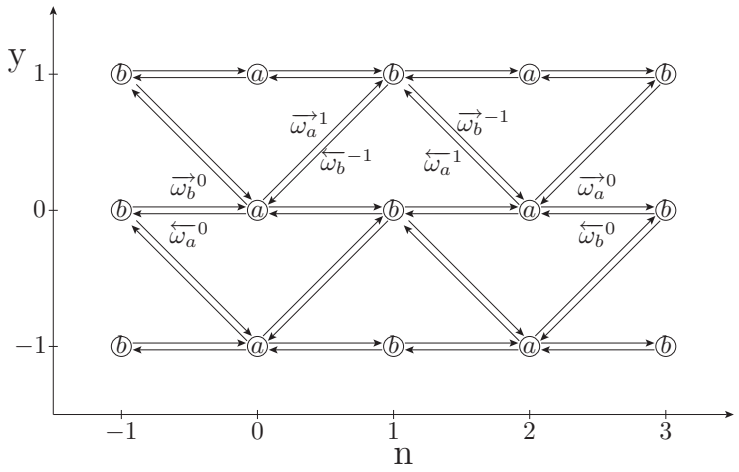

Figure 2. Sketch of the state space for our discrete model of molecular motor specifying the transition rates. The horizontal axis provides the motor position n and the vertical axis the number y of consumed ATP. This figure is reproduced from [27] with permission from authors.

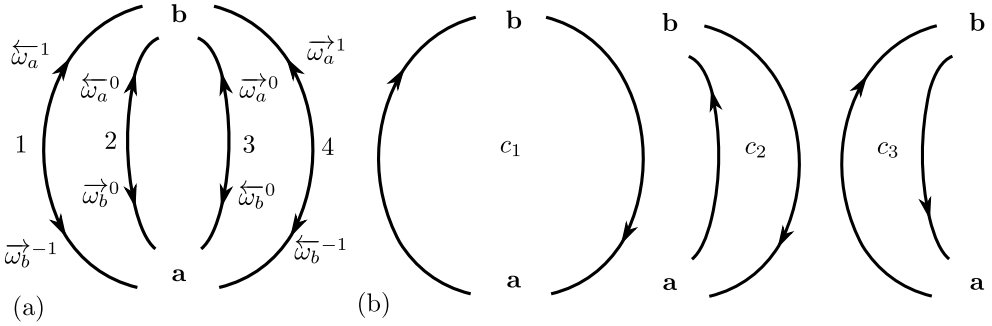

Figure 3. (a) Sketch of the effective two-state system with four edges. Edge orientation is head toward b. (b) Set of fundamental cycles with their orientations.

$\theta_a^+ + \theta_b^- + \theta_a^- + \theta_b^+ = 2$ [27]. Let us choose to orientate all these edges from state a to b. Then, the four edge currents and affinities are

$$J_{(1)} = \pi_a \overleftarrow{\omega}_a^{\,1} - \pi_b \overrightarrow{\omega}_b^{\,-1}, \qquad F_{(1)} = \ln \frac{\overleftarrow{\omega}_a^{\,1} \pi_a}{\overrightarrow{\omega}_b^{\,-1} \pi_b}, \tag{79}$$

$$J_{(2)} = \pi_a \overleftarrow{\omega}_a^{\,0} - \pi_b \overrightarrow{\omega}_b^{\,0}, \qquad F_{(2)} = \ln \frac{\overleftarrow{\omega}_a^{\,0} \pi_a}{\overrightarrow{\omega}_b^{\,0} \pi_b}, \tag{80}$$

$$J_{(3)} = \pi_a \overrightarrow{\omega}_a^{\,0} - \pi_b \overleftarrow{\omega}_b^{\,0}, \qquad F_{(3)} = \ln \frac{\overrightarrow{\omega}_a^{\,0} \pi_a}{\overleftarrow{\omega}_b^{\,0} \pi_b}, \tag{81}$$

$$J_{(4)} = \pi_a \overrightarrow{\omega}_a^{\,1} - \pi_b \overleftarrow{\omega}_b^{\,-1}, \qquad F_{(4)} = \ln \frac{\overrightarrow{\omega}_a^{\,1} \pi_a}{\overleftarrow{\omega}_b^{\,-1} \pi_b}, \tag{82}$$

in terms of the stationary probabilities to be in state a or b, namely π_a and π_b. The explicit expressions of the currents in terms of the transition rates is known [26, 27].

Here, there are three cycles identified in figure 3(c). Given our convention of orientation of the edges, the edge currents and the cycle currents are related in the following way

$$J_{(1)} = J_{c1} + J_{c3}, \tag{83}$$

$$J_{(2)} = -J_{c3}, \tag{84}$$

$$J_{(3)} = J_{c2}, \tag{85}$$

$$J_{(4)} = -J_{c1} - J_{c2}, \tag{86}$$

which means that the matrix $\boldsymbol{A}$ is

$$\boldsymbol{A} = \begin{pmatrix} 1 & 0 & 1 \\ 0 & 0 & -1 \\ 0 & 1 & 0 \\ -1 & -1 & 0 \end{pmatrix}. \tag{87}$$

The physical currents can be expressed in terms of the displacements Δn and the change in the number of ATP molecules Δy along each transition per unit time. For the four edges, these changes are

edge	(1)	(2)	(3)	(4)
Δy	1	0	0	1
Δn	−1	−1	1	1

$$\bar{\boldsymbol{\phi}} = \begin{pmatrix} 1 & 0 & 0 & 1 \\ -1 & -1 & 1 & 1 \end{pmatrix}, \tag{88}$$

which defines a matrix that we denote $\bar{\boldsymbol{\phi}}$. Then, summing the edge contributions over cycles gives the matrix

$$\boldsymbol{\phi} = \bar{\boldsymbol{\phi}} \cdot \boldsymbol{A} = \begin{pmatrix} 0 & -1 & 1 \\ -2 & 0 & 0 \end{pmatrix}. \tag{89}$$

Another approach is to identify the matrix $\boldsymbol{\phi}$ by making the description at the edge and cycle levels matches with the one at the level of physical observables. Precisely the entropy production rate is $\sigma = \sum_{i=1,4} J_{(i)} F_{(i)}$ at the edge level, $\sigma = \sum_{i=1,3} J_{c_i} F_{c_i}$, at cycle level, and $\sigma = f\bar{v} + r\Delta\mu$ at the level of physical currents and affinities. Note that all edge affinities and currents are not independent, with the above choice of transition rates, one finds the constraint on edge currents $\sum_i J_{(i)} = 0$ and similarly for edge affinities $F_{(1)} + F_{(3)} - F_{(2)} - F_{(4)} = 0$. These compatibility relations are essential to relate edge or cycle currents to the two physical currents $(\bar{v}, r)$. The physical currents are $\bar{v} = 2(J_{(3)} + J_{(4)})$ and $r = -J_{(3)} - J_{(2)}$ in terms of the edge currents while the physical affinities are $2f = F_{(4)} - F_{(1)}$ and $\Delta\mu = F_{(1)} - F_{(2)}$ in terms of the edge affinities. In the end, the relations between the cycle affinities and the physical affinities read

$$F_{c_1} = -2f, \tag{90}$$

$$F_{c_2} = -\Delta\mu, \tag{91}$$

$$F_{c_3} = \Delta\mu, \tag{92}$$

J. Stat. Mech. (2018) 023205

in agreement with the matrix $\boldsymbol{\phi}$ given in equation (89).

We now turn to the conductance and resistance matrices. From the definition of the edge resistance matrix below equation (35), we have

$$\bar{\boldsymbol{R}} = \begin{pmatrix} \bar{R}_{(1)} & 0 & 0 & 0 \\ 0 & \bar{R}_{(2)} & 0 & 0 \\ 0 & 0 & \bar{R}_{(3)} & 0 \\ 0 & 0 & 0 & \bar{R}_{(4)} \end{pmatrix}, \tag{93}$$

where using equations (79)–(82), we have $\bar{R}_{(i)} = J_{(i)}/F_{(i)}$ for $i = 1, \ldots, 4$. The cycle resistance matrix is then obtain from (38)

$$\tilde{\boldsymbol{R}} = \begin{pmatrix} \bar{R}_{(1)} + \bar{R}_{(4)} & \bar{R}_{(4)} & \bar{R}_{(1)} \\ \bar{R}_{(4)} & \bar{R}_{(3)} + \bar{R}_{(4)} & 0 \\ \bar{R}_{(1)} & 0 & \bar{R}_{(1)} + \bar{R}_{(2)} \end{pmatrix}. \tag{94}$$

The cycle conductance matrix is the inverse of the cycle resistance matrix (94), then this leads using (43), to the following non-equilibrium conductance matrix

$$\boldsymbol{G} = \frac{1}{Z_G} \begin{pmatrix} (\bar{R}_{(1)} + \bar{R}_{(4)})(\bar{R}_{(3)} + \bar{R}_{(2)}) & 2(\bar{R}_{(4)}\bar{R}_{(2)} - \bar{R}_{(1)}\bar{R}_{(3)}) \\ 2(\bar{R}_{(4)}\bar{R}_{(2)} - \bar{R}_{(1)}\bar{R}_{(3)}) & 4(\bar{R}_{(1)} + \bar{R}_{(2)})(\bar{R}_{(3)} + \bar{R}_{(4)}) \end{pmatrix}, \tag{95}$$

with

$$Z_G = \bar{R}_{(1)}\bar{R}_{(4)}\bar{R}_{(3)} + \bar{R}_{(1)}\bar{R}_{(4)}\bar{R}_{(2)} + \bar{R}_{(1)}\bar{R}_{(3)}\bar{R}_{(2)} + \bar{R}_{(4)}\bar{R}_{(3)}\bar{R}_{(2)}. \tag{96}$$

Using this matrix and the definitions of equation (12), we find the following parameters

$$\Pi = \frac{(\bar{R}_{(1)} + \bar{R}_{(4)})(\bar{R}_{(3)} + \bar{R}_{(2)})}{\bar{R}_{(1)}\bar{R}_{(4)}\bar{R}_{(3)} + \bar{R}_{(1)}\bar{R}_{(4)}\bar{R}_{(2)} + \bar{R}_{(1)}\bar{R}_{(3)}\bar{R}_{(2)} + \bar{R}_{(4)}\bar{R}_{(3)}\bar{R}_{(2)}} (\Delta\mu)^2, \tag{97}$$

$$\varphi = \sqrt{\frac{(\bar{R}_{(1)} + \bar{R}_{(2)})(\bar{R}_{(3)} + \bar{R}_{(4)})}{(\bar{R}_{(1)} + \bar{R}_{(4)})(\bar{R}_{(3)} + \bar{R}_{(2)})}} \frac{2|f|}{|\Delta\mu|}, \tag{98}$$

$$\xi = \frac{-(\bar{R}_{(4)}\bar{R}_{(2)} - \bar{R}_{(1)}\bar{R}_{(3)})}{\sqrt{(\bar{R}_{(1)} + \bar{R}_{(2)})(\bar{R}_{(3)} + \bar{R}_{(4)})(\bar{R}_{(1)} + \bar{R}_{(4)})(\bar{R}_{(3)} + \bar{R}_{(2)})}}, \tag{99}$$

which are used to make the plots of figures 4 and 5.

4.3. Discussion

The maximal efficiency given by equation (19) is shown as function of the degree of coupling in figure 4. This maximal efficiency is compared with the efficiency of the molecular motor model which is analytically solvable. The corresponding comparison for the unicyclic engine is not shown because the degree of coupling is always -1. In order to test this bound, we vary either (i) the thermodynamic forces, namely f and $\Delta\mu$, which together characterize the distance to equilibrium, or (ii) the kinetic parameters of the model (α, α', ϵ, θ_i..). The test (i) is carried out in the main figure in which either the

J. Stat. Mech. (2018) 023205

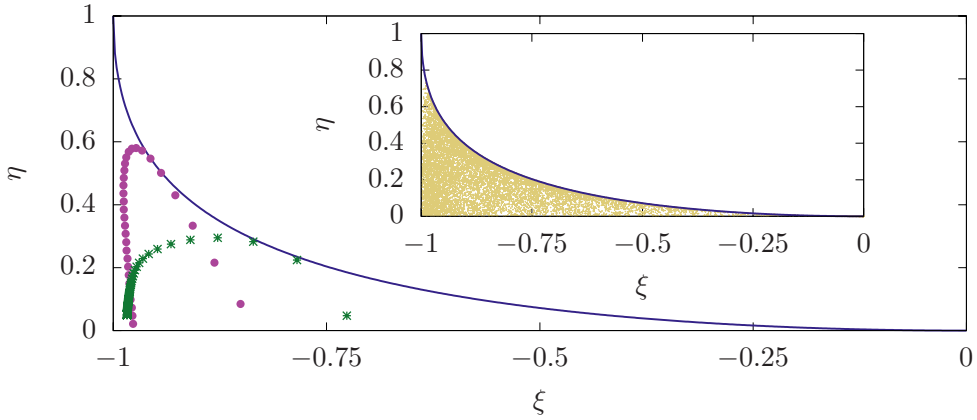

Figure 4. Illustration of the bound of equation (19) (blue solid line) for the molecular motor model. For a given chemical potential difference $\Delta\mu = 15.0$ (purple circles), the force f is varied along the curve. Alternatively, for a given force $f = -1$ (green crosses) the chemical potential difference is varied along the curve. The kinetic parameters are those of [27]: $\alpha = 0.57$, $\alpha' = 1.3.10^{-6}$, $\omega = 3.5$, $\omega' = 108.15$ $\epsilon = 10.81$, $\theta_a^+ = 0.25$, $\theta_a^- = 1.83$, $\theta_b^+ = 0.08$, $\theta_b^- = -0.16$. Inset: Efficiency versus degree of coupling when varying all kinetic parameters at fixed affinities $\Delta\mu = 10.0$ and $f = -1.9$. The kinetic parameters listed above are randomly chosen by multiplying the values used in the main figure by e^x with x drawn uniformly within $[-2, 2]$.

affinity f is varied at fixed $\Delta\mu$ or vice versa, covering a large regime of conditions far from equilibrium. The test (ii) is carried out in the inset, by scanning over a large panel of kinetic parameters. Both figures confirm that the maximum efficiency only depends on the degree of coupling. These figures also show that this maximum efficiency is reached under some accessible conditions.

Figures 5(a) and (b) illustrate the power-efficiency trade-off for the molecular motor and the unicyclic engine respectively, by showing the mean output entropy production rate $-\langle\sigma_2\rangle$ as function of the efficiency η. A striking feature in these plots is that the entropy production rate is bi-valued for the molecular motor as explained in section 1.5 while it is single-valued for the unicyclic engine, because the unicyclic engine is a tight coupled engine. In order to test the inequality of equations (25) and (26), we compare $-\langle\sigma_2\rangle$ (solid line) evaluated using exact expressions of the average currents, with the power-efficiency bounds of equations (25) and (26) (empty symbols). As shown in figure 5(b), these bounds become exact in the tight coupled case.

The figure also shows a comparison with the power-efficiency inequalities derived by Pietzonka and Seifert [25] (full symbols). The variances appearing in these inequalities can be evaluated from the cumulant generating function of the currents that is known exactly for these models [21, 26, 27]. We confirm with this figure that the new bound derived from the present framework is more tight than the bounds derived in [25], in agreement with equations (55). Note that the two bounds derived in this reference collapse with each other in the tight coupled case, but stay above the exact value except at the two extremal values of $\eta = 0$ and $\eta = 1$. Indeed, in these regions, the engine works near equilibrium. One reason for which the bounds of [25] are less

J. Stat. Mech. (2018) 023205

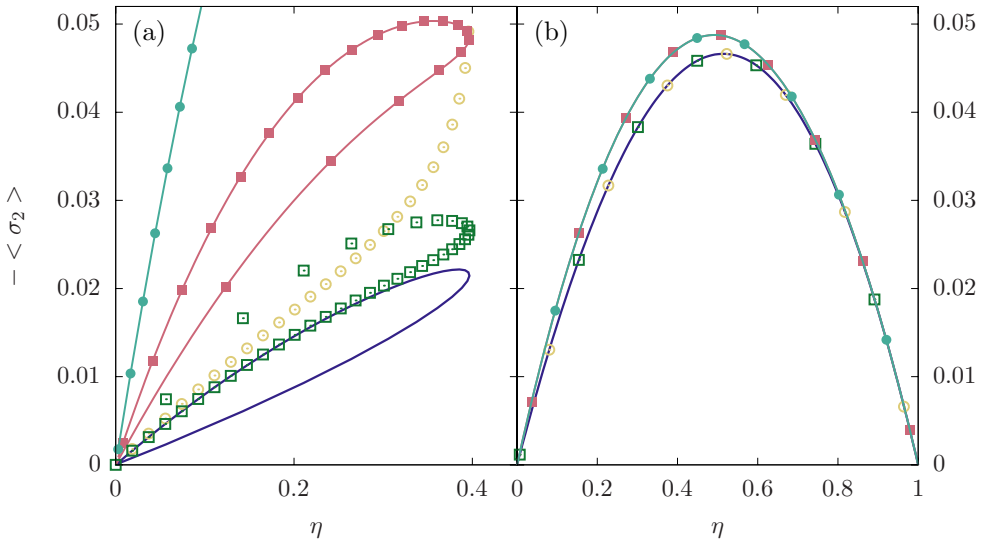

Figure 5. Output entropy production rate as a function of the machine efficiency using exact expression (solid blue line). Power-efficiency bounds of equations (25) (green open squares), (26) (yellow open circles), (57) (magenta full squares) and (58) (blue full circles) for (a) the molecular motor model with $\Delta\mu = 7.0$ and the same kinetic parameters as in figures 4 and (b) the unicyclic engine at $\beta_1 = 0.5$, $\beta_3 = 1$, $\Gamma = 1$, $E_a = 1$, $E_b = 4$ and $E_c = 2$. For both figures, F_1 is held fixed when varying F_2.

tight than ours is that they are a consequence of uncertainty relations, which for this molecular motor model do not yield a particularly sharp prediction of the efficiency, as discussed in [30].

5. Conclusion

In this work, we have developed a framework based on the notion of non-equilibrium conductance matrix to analyze the efficiency and the output power of energy converters operating far from equilibrium. This matrix is initially only partially constrained by the dependence of the physical currents on thermodynamic affinities. Nevertheless it shares many properties with the Onsager matrix, the two matrices are symmetric positive definite and become identical near equilibrium but differ otherwise. These properties are sufficient to exploit a parametrization of the efficiency introduced by Kedem and Kaplan for machines operating near equilibrium [2] and use it for general machines operating far from equilibrium. With this parametrization linked to a specific choice of non-equilibrium conductance matrix, we have shown that the efficiency of machines is generally bounded by an universal expression dependent only on the degree of coupling. The maximum value of this bound is the reversible efficiency which is only accessible to tight coupled machines. This result means practically that a bound on the efficiency of a machine can be deduced from a measurement of its degree of coupling. This observation could have interesting applications for various thermodynamic devices, such as for instance photoelectric cells.

https://doi.org/10.1088/1742-5468/aaa8fe

J. Stat. Mech. (2018) 023205

When a microscopic kinetic model of the machine is known, more insights into the efficiency of the machine can be obtained. In particular, tighter bounds on the output power in terms of the efficiency as compared to [25] follow from our approach. We have explained the relation between the various bounds using properties on the large deviations of the currents.

This work naturally begs the question whether the non-equilibrium conductance matrix can itself be determined experimentally. As mentioned above the dependence of the physical currents on thermodynamic affinities is in general insufficient to define the conductance matrix uniquely. However we have also shown that a unique conductance matrix can be defined from the knowledge of local resistances (which make up the resistance matrix) and of the weights between cycle currents and physical currents (which make up the $\boldsymbol{\phi}$ matrix).

The framework introduced here should be useful to revisit old questions such as the efficiency at maximum power or the role played of time reversal symmetry for the efficiency. In this context, it would be interesting to study extensions of the present framework to systems in which the Onsager reciprocity relations are modified, either due to a magnetic field [31, 32] or because the machine operates under time-periodic driving [33].

Acknowledgments

We acknowledge H-J Hilhorst for his pertinent comments on this paper.

Appendix. Microscopic framework for the non-equilibrium conductance matrix

In the following, we emphasize the physical meaning of $\boldsymbol{G}$ as a conductance matrix. We intend to shown how to switch from the resistance matrix at the edge level to the NE conductance matrix at the level of physical currents.

Starting at the edge level, the resistance matrix $\bar{\boldsymbol{R}}$ is diagonal in the space of edges, with diagonal elements $\bar{R}_{(x,y)}$ as defined in equation (36). The inverse of the edge resistance matrix is the edge conductance matrix $\bar{\boldsymbol{G}} = \bar{\boldsymbol{R}}^{-1}$. We remark that the elements of the resistance matrix depend on the physical affinities through transition rates and stationary probability.

At the level of cycles, the matrix $\tilde{\boldsymbol{R}}$ for cycle resistance introduced in equation (38) connects cycle affinities and currents via

$$F_c = \sum_{c'} \tilde{R}_{c,c'} J_c. \tag{A.1}$$

Indeed, using equation (29) in equation (36), one may express $\tilde{\boldsymbol{R}}$ as a function of $\bar{\boldsymbol{R}}$ since

$$F_{(x,y)} = \sum_{c} \bar{R}_{(x,y)} A_{(x,y),c} J_c, \tag{A.2}$$

$$F_{c'} = \sum_{c} \sum_{(x,y)} (A^{\mathrm{T}})_{c',(x,y)} \bar{R}_{(x,y)} A_{(x,y),c} J_c, \tag{A.3}$$

where we have used equation (32) in the second step. This leads to the cycle resistance matrix defined in the main text

$$\tilde{R}_{c',c} = \sum_{(x,y)} (A^{\mathrm{T}})_{c,(x,y)} \bar{R}_{(x,y)} A_{(x,y),c}. \tag{A.4}$$

Here the analogy with electric circuits holds: electrical resistances add when connected in series. The cycle conductance matrix $\tilde{\boldsymbol{G}}$ is then

$$\tilde{\boldsymbol{G}} \equiv \tilde{\boldsymbol{R}}^{-1} = (\boldsymbol{A}^{\mathrm{T}} \cdot \bar{\boldsymbol{R}} \cdot \boldsymbol{A})^{-1} = \boldsymbol{A}^{+} \cdot \bar{\boldsymbol{G}} \cdot \boldsymbol{A}^{\mathrm{T}+}, \tag{A.5}$$

where $\boldsymbol{A}^{+}$ is the Moore–Penrose pseudo inverse of the matrix of fundamental cycles $\boldsymbol{A}$ [34].

At the level of physical observables, the NE conductance connects currents to affinities via

$$J_Y \equiv \sum_X G_{Y,X} F_X. \tag{A.6}$$

Considering that the amount of physical quantity Y exchanged with the environment during cycle c is $\phi_{Y,c}$ and using equation (A.1), one gets

$$J_Y = \sum_c \phi_{Y,c} J_c = \sum_{c,c'} \phi_{Y,c} \tilde{G}_{c,c'} F_c = \sum_X \sum_{c,c'} \phi_{Y,c} \tilde{G}_{c,c'} \phi^{\mathrm{T}}_{c,X} F_X. \tag{A.7}$$

Therefore, the physical conductance matrix writes

$$\boldsymbol{G} = \boldsymbol{\phi} \cdot \boldsymbol{A}^{+} \cdot \bar{\boldsymbol{G}} \cdot (\boldsymbol{\phi} \cdot \boldsymbol{A}^{+})^{\mathrm{T}}, \tag{A.8}$$

which is the same non-equilibrium matrix as given by equations (43)–(46). The electrical analogy also holds: cycle conductances add when connected in parallel which makes senses when considering that the current flows from one reservoir to another through sequences of cycles.

References

[1] Callen H B 1985 *Thermodynamics and an Introduction to Thermostatistics* 2nd edn (New York: Wiley)
[2] Kedem O and Caplan S R 1965 Degree of coupling and its relation to efficiency of energy conversion *Trans. Faraday Soc.* **61** 1897–11
[3] Esposito M, Lindenberg K and Van den Broeck C 2009 Thermoelectric efficiency at maximum power in a quantum dot *Europhys. Lett.* **85** 60010
[4] Polettini M, Verley G and Esposito M 2015 Efficiency statistics at all times: carnot limit at finite power *Phys. Rev. Lett.* **114** 050601
[5] Polettini M and Esposito M 2017 Carnot efficiency at divergent power output *Europhys. Lett.* **118** 40003
[6] Onsager L 1931 Reciprocal relations in irreversible processes. I *Phys. Rev.* **37** 405–26
[7] Onsager L 1931 Reciprocal relations in irreversible processes. II *Phys. Rev.* **38** 2265–79
[8] Wood C 1988 Materials for thermoelectric energy conversion *Rep. Prog. Phys.* **51** 459
[9] Domenicali C A 1954 Irreversible thermodynamics of thermoelectricity *Rev. Mod. Phys.* **26** 237–75
[10] Caplan S R 1966 The degree of coupling and its relation to efficiency of energy conversion in multiple-flow systems *J. Theor. Biol.* **10** 209–35
[11] Hill T L 1989 *Free Energy Transduction and Biochemical Cycle Kinetics* (New York: Springer)
[12] Van den Broeck C 2005 Thermodynamic efficiency at maximum power *Phys. Rev. Lett.* **95** 190602
[13] Esposito M, Lindenberg K and Van den Broeck C 2009 Universality of efficiency at maximum power *Phys. Rev. Lett.* **102** 130602

J. Stat. Mech. (2018) 023205

[14] Benenti G, Casati G, Saito K and Whitney R S 2017 Fundamental aspects of steady-state conversion of heat to work at the nanoscale *Phys. Rep.* **694** 1–124
[15] Andrieux D and Gaspard P 2004 Fluctuation theorem and Onsager reciprocity relations *J. Chem. Phys.* **121** 6167–74
[16] Andrieux D and Gaspard P 2007 A fluctuation theorem for currents and non-linear response coefficients *J. Stat. Mech.* P02006
[17] Seifert U 2012 Stochastic thermodynamics, fluctuation theorems and molecular machines *Rep. Prog. Phys.* **75** 126001
[18] Verley G, Mallick K and Lacoste D 2011 Modified fluctuation-dissipation theorem for non-equilibrium steady states and applications to molecular motors *Europhys. Lett.* **93** 10002
[19] Polettini M, Bulnes-Cuetara G and Esposito M 2016 Conservation laws and symmetries in stochastic thermodynamics *Phys. Rev.* E **94** 052117
[20] Polettini M, Lazarescu A and Esposito M 2016 Tightening the uncertainty principle for stochastic currents *Phys. Rev.* E **94** 052104
[21] Pietzonka P, Barato A C and Seifert U 2016 Universal bounds on current fluctuations *Phys. Rev.* E **93** 052145
[22] Gingrich T R, Horowitz J M, Perunov N and England J L 2016 Dissipation bounds all steady-state current fluctuations *Phys. Rev. Lett.* **116** 120601
[23] Horn R A and Johnson C R 1985 *Matrix Analysis* (Cambridge: Cambridge University Press)
[24] Pietzonka P, Barato A C and Seifert U 2016 Universal bound on the efficiency of molecular motors *J. Stat. Mech.* 124004
[25] Pietzonka P and Seifert U 2017 Universal trade-off between power, efficiency and constancy in steady-state heat engines (arXiv:1705.05817)
[26] Lau A W C, Lacoste D and Mallick K 2007 Nonequilibrium fluctuations and mechanochemical couplings of a molecular motor *Phys. Rev. Lett.* **99** 158102
[27] Lacoste D, Lau A W C and Mallick K 2008 Fluctuation theorem and large deviation function for a solvable model of a molecular motor *Phys. Rev.* E **78** 011915
[28] Schnakenberg J 1976 Network theory of microscopic and macroscopic behavior of master equation systems *Rev. Mod. Phys.* **48** 571–85
[29] Touchette H 2009 The large deviation approach to statistical mechanics *Phys. Rep.* **478** 1–69
[30] Baiesi M and Maes C 2017 Life efficiency does not always increase with the dissipation rate (arXiv:1707.09614)
[31] Benenti G, Saito K and Casati G 2011 Thermodynamic bounds on efficiency for systems with broken time-reversal symmetry *Phys. Rev. Lett.* **106** 230602
[32] Bonella S, Coretti A, Rondoni L and Ciccotti G 2017 Time-reversal symmetry for systems in a constant external magnetic field *Phys. Rev.* E **96** 012160
[33] Proesmans K and Van den Broeck C 2015 Onsager coefficients in periodically driven systems *Phys. Rev. Lett.* **115** 090601
[34] Greville T N E and Ben-Israel A 2003 *Generalized Inverses: Theory and Applications* (Berlin: Springer)

J. Stat. Mech. (2018) 023205

Circuits of thermodynamic devices in stationary non-equilibrium

Paul Raux,[1,2] Christophe Goupil,[2] and Gatien Verley[1]

[1] *Université Paris-Saclay, CNRS/IN2P3, IJCLab, 91405 Orsay, France*
[2] *Université Paris Cité, CNRS, LIED, F-75013 Paris, France*

(Dated: September 26, 2023)

We introduce a non-linear theory of thermodynamic circuits in non-equilibrium stationary states. The non-equilibrium conductance matrix of a composite device is obtained from the ones of its sub-devices. This generalizes to thermodynamic devices the concept of equivalent impedance defined in electronics. An abstract example and the serial connection of two thermoelectric generators (TEG) with constant thermoelectric coefficients are considered. Interestingly, a current-dependent electrical resistance emerges from this connection.

Introduction— Dividing a problem into several pieces often simplifies its resolution. Combining this approach with a graphical representation produces circuits made of various sub-circuits. Circuits conveniently summarize the conservation of physical quantities such as energy, momentum, charge, or chemical species. Different kinds of circuits or graphs have emerged: bond graphs in engineering science [1], Feynman diagrams in particle physics [2], electric circuits in electrokinetic [3, 4] or hyper-graphs of chemical reactions in chemistry [5]. Electric power and signal processing represent the paramount application of circuit theory, although only one conserved quantity is usually considered. For a single (or multiple but decoupled) potential(s), the problem has long since been solved. Many works were devoted to coupled potentials although without considering arbitrary boundary conditions [6–10]. Neumann (fixed current) or Dirichlet (fixed potential) conditions are often assumed but never mixed boundary conditions where both current and potential achieve non-prescribed stationary values. In this case, real integrated balances at the boundaries, such as entropy balance, are central in determining the stationary state. A non-linear theory dealing with mixed boundary conditions and several conserved quantities coupled through complex circuits is appealing. It will have deep consequences in many scientific fields, such as biology, chemistry, and engineering.

The treatment of conservation laws has been systematized within stochastic thermodynamics in Ref. [11, 12]. This breakthrough allows the foundation of a circuit theory mixing various thermodynamic systems. For instance, in the framework of chemical reaction networks, this approach has led to an effective circuit description of otherwise complex chemical reaction networks [13, 14]. Then, in principle, the current–concentration characteristics of each chemical module yield the stationary currents exchanged with the environment or other modules. However, getting rid of all internal degrees of freedom and going beyond multivariable functions connecting currents and forces within global characteristics call for more operational methods valid for any thermodynamic system.

Non-equilibrium conductance matrices accurately characterize thermodynamic devices while providing the current–force relations [15, 16]. They are the multidimensional generalization of the scalar current–force characteristic of dipoles (e.g. current–tension for an electric dipole). As such, they extend to vectors the concept of impedance defined as the scalar ratio between a force and a current. Conductance matrices generalize to non-equilibrium stationary states Onsager's response matrices of linear irreversible thermodynamics [17–19]. It is possible to compute them when precise modeling is available, as in stochastic thermodynamics, or from integrating a local response, as for our model of TEGs. In this letter, the non-equilibrium conductance matrix of a composite thermodynamic system is determined using those of its two subsystems' non-equilibrium conductance and their conservation laws. We first explain how current conservation at the interface allows to integrate the internal degrees of freedom, i.e. the local potentials at the connection; second, we generalize the law of impedance addition in a way that matches their matrix dimension thanks to conservation laws within each subsystem.

Devices connection and internal degrees of freedom— Fig. 1 shows three devices represented by boxes with sets of pins $\mathscr{P}^{(m)} = \{1, 2, \dots, |\mathscr{P}^{(m)}|\}$ for $m = 1, 2, 3$. We denote $|\mathscr{P}^{(m)}|$ the total number of pins of device m. Without loss of generality, we focus on connecting device 1 to device 2 to create device 3. Connecting more devices follows from a sequence of pairwise connections. We split the pins of each device into left and right disjoint sets $\mathscr{P}^{(m)} = \mathscr{P}_l^{(m)} \cup \mathscr{P}_r^{(m)}$ to connect the right pins of device 1 to the left pins of device 2 as in Fig. 1. For device 3, these connected pins are internal: local potentials there are functions of the external ones. The local potential vector $\boldsymbol{a}^{(m)}$, of component $a_p^{(m)}$ (e.g., temperature, pressure, chemical potential) at pin $p \in \mathscr{P}^{(m)}$ can be set by another device or by reservoirs of various conjugated extensive quantity (e.g. heat, volume, chemical species). By convention, the physical current vector $\boldsymbol{i}^{(m)}$ has a positive p'th component $i_p^{(m)}$ when a positive amount of the corresponding extensive quantity is received by the device m through

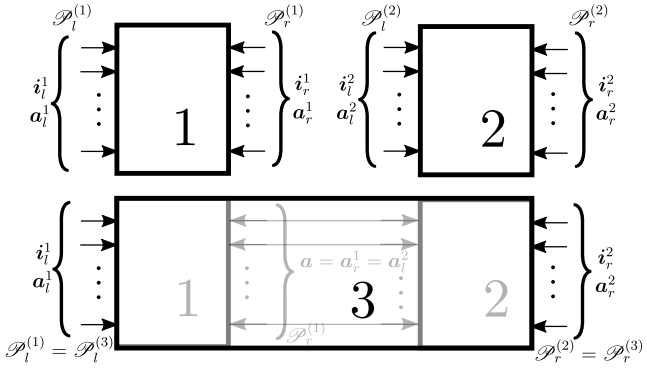

FIG. 1. (Top) Separated devices 1 and 2 with their various pins $\mathscr{P}^{(m)} = \mathscr{P}_l^{(m)} \cup \mathscr{P}_r^{(m)}$ where currents $\boldsymbol{i}^{(m)}$ and conjugated local potentials $\boldsymbol{a}^{(m)}$ takes well defined values. (Bottom) Merged device 3 made out of 1 and 2, with equal local potentials $\boldsymbol{a}$ on the wire connecting 1 and 2. Current conservation at connection implies $\boldsymbol{i}_r^1 + \boldsymbol{i}_l^2 = 0$.

pin p. Given the left/right splitting of pins, the column vector for physical currents and local potentials write $\boldsymbol{i}^{(m)} = (\boldsymbol{i}_l^{(m)}, \boldsymbol{i}_r^{(m)})^T$ and $\boldsymbol{a}^{(m)} = (\boldsymbol{a}_l^{(m)}, \boldsymbol{a}_r^{(m)})^T$ respectively, the sub-vectors with index $\chi = l, r$ including only components on the χ side. The superscript T denotes transposition. We notice that $\boldsymbol{i}^{(3)} = (\boldsymbol{i}_l^{(1)}, \boldsymbol{i}_r^{(2)})^T$ by definition. Given $\boldsymbol{a}^{(m)}$, we assume that device m reaches a unique stationary state with constant physical currents $\boldsymbol{i}^{(m)}$ that are non-linear functions of $\boldsymbol{a}^{(m)}$. The Entropy Production Rate (EPR) for device m in this stationary state reads $\sigma^{(m)} = \boldsymbol{a}^{(m)T}\boldsymbol{i}^{(m)}$. Assuming no dissipation at the interface, the EPR of device 3 is

$$\sigma^{(3)} = \boldsymbol{a}_l^{(1)T}\boldsymbol{i}_l^{(1)} + \boldsymbol{a}_r^{(2)T}\boldsymbol{i}_r^{(2)} = \sigma^{(1)} + \sigma^{(2)}. \tag{1}$$

The last equality requires identical local potentials on the connection pins $\boldsymbol{a}_r^{(1)} = \boldsymbol{a}_l^{(2)} \equiv \boldsymbol{a}$ given the current conservation at the interface

$$\boldsymbol{i}_r^{(1)} + \boldsymbol{i}_l^{(2)} = 0. \tag{2}$$

Eq. (2) is a system of $|\mathscr{P}_r^{(1)}| = |\mathscr{P}_l^{(2)}|$ equations that must be solved to determine the internal local potentials. This provides $\boldsymbol{a}$ as a function of the external potentials $\boldsymbol{a}_l^{(1)}$ and $\boldsymbol{a}_r^{(2)}$ eliminating all internal degrees of freedom.

Non-equilibrium conductance for serial connection— We focus on conductance matrices relating *independent* currents to their conjugated forces. Physical currents $\boldsymbol{i}^{(m)}$ are linearly dependent due to the set $\mathscr{L}^{(m)} = \{\boldsymbol{\ell}_1^{(m)}, \boldsymbol{\ell}_2^{(m)}, \dots\}$ of conservation laws. These linear dependencies read $\boldsymbol{\ell}^{(m)}\boldsymbol{i}^{(m)} = \boldsymbol{0}$ denoting $\boldsymbol{\ell}^{(m)}$ the matrix whose kth line is given by $\boldsymbol{\ell}_k^{(m)}$. The row vectors in $\mathscr{L}^{(m)}$ have $|\mathscr{P}^{(m)}|$ components and are linearly independent. Given the left/right partition of $\mathscr{P}^{(m)}$ for $m = 1, 2$, the matrix of conservation laws splits into two submatrices such that

$$\boldsymbol{\ell}^{(m)}\boldsymbol{i}^{(m)} = \begin{pmatrix}\boldsymbol{\ell}_l^{(m)} & \boldsymbol{\ell}_r^{(m)}\end{pmatrix}\begin{pmatrix}\boldsymbol{i}_l^{(m)} \\ \boldsymbol{i}_r^{(m)}\end{pmatrix} = \boldsymbol{0}. \tag{3}$$

This will be useful in the following to relate internal and external currents. Graphically, each conservation law of devices $m = 1, 2$ can be represented as a tree graph, see Fig. 2 and 3. We assume that after connection, the conservation laws of device 3 are also tree graphs, i.e. with no internal loops. Making loops is possible in the end by equating the local potential of two external pins, effectively connecting them and fixing the gauge freedom with a reservoir. Using the conservation laws, we select a subset of pins $\mathscr{I}^{(m)} \subset \mathscr{P}^{(m)}$ for which currents $i_p^{(m)}$ with $p \in \mathscr{I}^{(m)}$ are independent. This defines the basis of fundamental currents [12]. We denote in capital letters the vector of fundamental currents $\boldsymbol{I}^{(m)} = (i_p^{(m)} | p \in \mathscr{I}^{(m)})^T$ whose dimension is $|\mathscr{I}^{(m)}| = |\mathscr{P}^{(m)}| - |\mathscr{L}^{(m)}|$. The selection matrix $\boldsymbol{S}^{(m)}$ relates the physical and fundamental current vectors and defines the vector of fundamental forces $\boldsymbol{A}^{(m)}$:

$$\boldsymbol{i}^{(m)} = \boldsymbol{S}^{(m)}\boldsymbol{I}^{(m)}, \quad \boldsymbol{A}^{(m)} = \boldsymbol{S}^{(m)T}\boldsymbol{a}^{(m)}, \tag{4}$$

such that the EPR satisfies

$$\sigma^{(m)} = \boldsymbol{a}^{(m)T}\boldsymbol{i}^{(m)} = \boldsymbol{a}^{(m)T}\boldsymbol{S}^{(m)}\boldsymbol{I}^{(m)} = \boldsymbol{A}^{(m)T}\boldsymbol{I}^{(m)}. \tag{5}$$

We remark that by construction $\boldsymbol{\ell}^{(m)}\boldsymbol{S}^{(m)} = 0$ and the $|\mathscr{I}^{(m)}|$ columns of the selection matrix are independent. The non-linear characteristic of each device provides the fundamental currents $\boldsymbol{I}^{(m)}$ as a function of the forces $\boldsymbol{A}^{(m)}$

$$\boldsymbol{I}^{(m)} = \boldsymbol{G}^{(m)}\boldsymbol{A}^{(m)}, \tag{6}$$

where $\boldsymbol{G}^{(m)} = \boldsymbol{G}^{(m)}(\boldsymbol{A}^{(m)})$ is a non-equilibrium conductance matrix. It is symmetric, force-dependent, and positive definite at non-equilibrium stationary state [15]. In this state, the numerical values of the entries of matrices $\boldsymbol{G}^{(1)}$ and $\boldsymbol{G}^{(2)}$ are known for the fundamental forces given by Eq. (4) evaluated at $\boldsymbol{a}^{(1)} = (\boldsymbol{a}_l^{(1)}, \boldsymbol{a})^T$ and $\boldsymbol{a}^{(2)} = (\boldsymbol{a}, \boldsymbol{a}_r^{(2)})^T$ respectively. Then, Eqs. (1) and (5–6) lead to the relation between conductance matrices

$$\boldsymbol{I}^{(3)T}{\boldsymbol{G}^{(3)}}^{-1}\boldsymbol{I}^{(3)} = \sum_{m=1,2}\boldsymbol{I}^{(m)T}{\boldsymbol{G}^{(m)}}^{-1}\boldsymbol{I}^{(m)}. \tag{7}$$

This defines the inverse of the non-equilibrium conductance matrix for device 3 as

$${\boldsymbol{G}^{(3)}}^{-1} = \sum_{m=1}^{2}\boldsymbol{\Pi}^{(m,3)T}{\boldsymbol{G}^{(m)}}^{-1}\boldsymbol{\Pi}^{(m,3)}, \tag{8}$$

provided that a matrix $\boldsymbol{\Pi}^{(m,3)}$ exists for which $\boldsymbol{I}^{(m)} = \boldsymbol{\Pi}^{(m,3)}\boldsymbol{I}^{(3)}$ for $m = 1, 2$. Eq. (8) is our main result: it

generalizes the concept of equivalent impedance for the serial connection of thermodynamic devices.

In the following, we determine $\mathbf{\Pi}^{(m,3)}$ in two steps. We look for $\boldsymbol{\pi}^{(m,3)}$ satisfying $\boldsymbol{i}^{(m)} = \boldsymbol{\pi}^{(m,3)}\boldsymbol{i}^{(3)}$ and related to the former matrix by

$$\mathbf{\Pi}^{(m,3)} = \boldsymbol{S}^{(m)+}\boldsymbol{\pi}^{(m,3)}\boldsymbol{S}^{(3)}. \tag{9}$$

We use $\boldsymbol{S}^{(m)+} = [\boldsymbol{S}^{(m)T}\boldsymbol{S}^{(m)}]^{-1}\boldsymbol{S}^{(m)T}$ as the pseudo inverse of $\boldsymbol{S}^{(m)}$ for $m = 1, 2$. These matrices are known since they determine the fundamental currents in which the conductance matrices $\boldsymbol{G}^{(1)}$ and $\boldsymbol{G}^{(2)}$ are given. As a first step, we combine Eqs. (2–3) into

$$\boldsymbol{L}_i\boldsymbol{i}_r^{(1)} = \boldsymbol{L}_e\boldsymbol{i}^{(3)} \text{ with } \boldsymbol{L}_i \equiv \begin{bmatrix} -\boldsymbol{\ell}_r^{(1)} \\ \boldsymbol{\ell}_l^{(2)} \end{bmatrix}, \ \boldsymbol{L}_e \equiv \begin{bmatrix} \boldsymbol{\ell}_l^{(1)} & \mathbb{0} \\ \mathbb{0} & \boldsymbol{\ell}_r^{(2)} \end{bmatrix}. \tag{10}$$

We remark that $\boldsymbol{L}_i$ is full column rank since it is an incidence matrix of a tree graph whose vertices are the conservation laws and whose edges are the connection pins [20]. Then, we define $\boldsymbol{\pi} = \boldsymbol{L}_i^{+}\boldsymbol{L}_e$ to obtain $\boldsymbol{i}_r^{(1)} = \boldsymbol{\pi}\boldsymbol{i}^{(3)} = -\boldsymbol{i}_l^{(2)}$ and conclude our first step with

$$\boldsymbol{\pi}^{(1,3)} = \begin{bmatrix} \mathbb{1} & \mathbb{0} \\ \hline \boldsymbol{\pi} \end{bmatrix} \text{ and } \boldsymbol{\pi}^{(2,3)} = \begin{bmatrix} -\boldsymbol{\pi} \\ \hline \mathbb{0} & \mathbb{1} \end{bmatrix}, \tag{11}$$

since $\boldsymbol{i}_l^{(1)} = [\mathbb{1}\ \mathbb{0}]\boldsymbol{i}^{(3)}$ and $\boldsymbol{i}_r^{(2)} = [\mathbb{0}\ \mathbb{1}]\boldsymbol{i}^{(3)}$ by definition. Second, the column of $\boldsymbol{S}^{(3)}$ defines a basis of $\ker(\boldsymbol{\ell}^{(3)})$ albeit the conservation laws of the third device remain to determine. This can be done by computing the left null eigenvectors of $\boldsymbol{L}_i$, gathered as lines of a matrix $\boldsymbol{v}$. The rank-nullity theorem gives the number of lines of $\boldsymbol{v}$:

$$\dim\,(\operatorname{coker}\boldsymbol{L}_i) = |\mathscr{L}^{(1)}| + |\mathscr{L}^{(2)}| - |\mathscr{P}_r^{(1)}|, \tag{12}$$

since $\boldsymbol{L}_i$ has $|\mathscr{L}^{(1)}| + |\mathscr{L}^{(2)}|$ lines, $|\mathscr{P}_r^{(1)}|$ columns and rank $|\mathscr{P}_r^{(1)}|$. Given our constraints on the devices' connection, Eq. (12) also gives the cardinal of $\mathscr{L}^{(3)}$. Then, from $\boldsymbol{v}\boldsymbol{L}_i = 0$ and Eq. (10), we find the conservation laws of the third device $\boldsymbol{\ell}^{(3)} = \boldsymbol{v}\boldsymbol{L}_e$. A basis of its kernel leads to $\boldsymbol{S}^{(3)}$ and finally to $\mathbf{\Pi}^{(m,3)}$.

Serial connection of two TEG— We illustrate our general method on the serial association of two TEGs. We chose the fundamental current and force vectors as

$$\boldsymbol{I}^{(m)} = \begin{pmatrix} i_{El}^{(m)} \\ i_{Nl}^{(m)} \end{pmatrix}, \quad \boldsymbol{A}^{(m)} = \begin{pmatrix} \frac{1}{T_r^{(m)}} - \frac{1}{T_l^{(m)}} \\ \frac{\mu_l^{(m)}}{T_l^{(m)}} - \frac{\mu_r^{(m)}}{T_r^{(m)}} \end{pmatrix}, \tag{13}$$

where $i_{El}^{(m)}$ and $i_{Nl}^{(m)}$ are respectively the energy and electric currents entering device m from the left. The magnitude of the electric charge of an electron is denoted $e > 0$. The temperature and electrochemical potential on the $\chi = l, r$ side of device m are denoted $T_\chi^{(m)}$ and $\mu_\chi^{(m)}$ respectively. The current–force characteristic of Eq. (6)

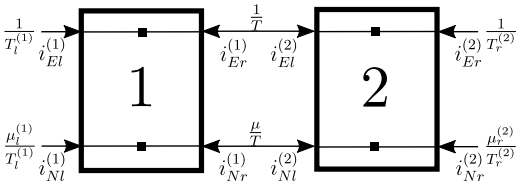

FIG. 2. Serial connection of two TEG. The conservation of energy and matter implies for each device the following relation: $i_{El}^{(m)} + i_{Er}^{(m)} = 0$ and $i_{Nl}^{(m)} + i_{Nr}^{(m)} = 0$. For $m = 1, 2$, $S_N^m, K^{(m)}, R^{(m)}$ are independent of the intensive parameters $\boldsymbol{a}_p^m$.

holds with the conductance matrix [21, 22]

$$\boldsymbol{G}^{(m)} = \frac{T_l^{(m)}T_r^{(m)}}{e^2R^{(m)}\bar{T}^{(m)}} \begin{bmatrix} e^2K^{(m)}R^{(m)}\bar{T}^{(m)} + {H^{(m)}}^2 & H^{(m)} \\ H^{(m)} & 1 \end{bmatrix}. \tag{14}$$

We denote $R^{(m)}$ the electrical resistance, $K^{(m)}$ the thermal conductivity and $S_N^{(m)}$ the Seebeck coefficient of the mth TEG. The later appears in the coupling factor $H^{(m)} = S_N^{(m)}\bar{T}^{(m)} + \bar{\mu}^{(m)}$ involving the average temperature and electrochemical potential

$$\bar{T}^{(m)} = \frac{T_l^{(m)} + T_r^{(m)}}{2}, \quad \bar{\mu}^{(m)} = \frac{\mu_l^{(m)} + \mu_r^{(m)}}{2}. \tag{15}$$

The conservation of the currents at the interface reads $i_{Er}^{(1)} + i_{El}^{(2)} = 0$ and $i_{Nr}^{(1)} + i_{Nl}^{(2)} = 0$. From this we deduce $T_r^{(1)} = T_l^{(2)} \equiv T$ and $\mu_r^{(1)} = \mu_l^{(2)} \equiv \mu$:

$$T = \frac{K^{(1)}T_l^{(1)} + K^{(2)}T_r^{(2)} + \frac{e^2}{2}\left(R^{(1)} + R^{(2)}\right){i_{Nl}^{(2)}}^2}{K^{(1)} + K^{(2)} - \delta_{S_N}i_{Nl}^{(2)}} \tag{16}$$

$$\mu = R_\parallel\left(\frac{\mu_l^{(1)} - S_N^{(1)}\Delta T^{(1)}}{R^{(1)}} + \frac{\mu_r^{(2)} + S_N^{(2)}\Delta T^{(2)}}{R^{(2)}}\right) \tag{17}$$

where $\delta_{S_N} = S_N^{(2)} - S_N^{(1)}$, $1/R_\parallel = 1/R^{(1)} + 1/R^{(2)}$ and $\Delta T^{(m)} = T_r^{(m)} - T_l^{(m)}$. Finally, Eq. (8) becomes ${\boldsymbol{G}^{(3)}}^{-1} = {\boldsymbol{G}^{(1)}}^{-1} + {\boldsymbol{G}^{(2)}}^{-1}$. The outcome of this equation is in fact also given by Eq. (14) for $m = 3$ using the following new parameters

$$\frac{1}{K^{(3)}} = \sum_{m=1}^{2}\frac{1}{K^{(m)}}, \quad \frac{S_N^{(3)}}{K^{(3)}} = \sum_{m=1}^{2}\frac{S_N^{(m)}}{K^{(m)}}, \tag{18}$$

$$\frac{H^{(3)}}{K^{(3)}} = \sum_{m=1}^{2}\frac{H^{(m)}}{K^{(m)}}, \tag{19}$$

and the electrical resistance

$$R^{(3)} = \left[1 - \frac{\delta_{S_N}i_{Nl}^{(2)}}{2(K^{(1)} + K^{(2)})}\right]\sum_{m=1}^{2}R^{(m)} + \frac{\delta_{S_N}^2 T}{e^2(K^{(1)} + K^{(2)})}. \tag{20}$$

The detailed derivation of these results will be published in a forthcoming publication. Interestingly, $R^{(3)}$ depends on the matter current and is not simply the sum of the sub-devices resistances (excepted when $\delta_{S_N}=0$) as already noticed for TEGs under mixed boundary conditions [23, 24].

Example of dimension matching for conductances— We now illustrate the construction of an equivalent non-equilibrium conductance for the devices of Fig. 3. The first and second devices have 4 and 7 pins, 1 and 3 conservation laws leading to 3 and 4 fundamental currents respectively. Their connection via $\boldsymbol{i}_r^{(1)}=(i_3,i_4)^T$ produces a third device with 7 pins, 2 conservation laws and 5 fundamental currents. Contrarily to the serial connection of TEGs, the conductance matrices' dimensions are all different calling for a dimensional matching. We assume that the local potentials at the interface have already been determined and that the conductance matrix $\boldsymbol{G}^{(m)}$ for $m=1,2$ are known for fundamental currents $\boldsymbol{I}^{(1)}=(i_2,i_3,i_4)^T$ and $\boldsymbol{I}^{(2)}=(i_5,i_6,i_7,i_9)^T$ associated to

$$\boldsymbol{S}^{(1)}=\begin{bmatrix}-1&-1&-1\\1&0&0\\0&1&0\\0&0&1\end{bmatrix},\quad \boldsymbol{S}^{(2)}=\begin{bmatrix}-1&-1&0&0\\0&0&-1&0\\1&0&0&0\\0&1&0&0\\0&0&1&0\\0&0&0&-1\\0&0&0&1\end{bmatrix}. \tag{21}$$

Eq. (4) leads to physical currents $\boldsymbol{i}^{(1)}=(i_1,\dots,i_4)^T$ and $\boldsymbol{i}^{(2)}=(i_3,\dots,i_9)^T$ as expected given the matrices

$$\boldsymbol{\ell}^{(1)}=\left[\begin{array}{cc|cc}1&1&1&1\end{array}\right],\quad \boldsymbol{\ell}^{(2)}=\left[\begin{array}{cc|ccccc}1&0&1&1&0&0&0\\0&1&0&0&1&0&0\\0&0&0&0&0&1&1\end{array}\right], \tag{22}$$

for the conservation laws $\boldsymbol{\ell}^{(m)}\boldsymbol{i}^{(m)}=\boldsymbol{0}$ depicted on Fig. 3. Vertical bars emphasize the bloc decomposition

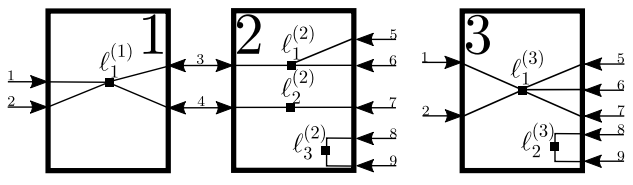

FIG. 3. Example of the serial connection of two devices. For device $m=1$ the pins are divided into $\mathscr{P}_l^{(1)}=\{1,2\}$ and $\mathscr{P}_r^{(1)}=\{3,4\}$. For device $m=2$ the pins are divided into $\mathscr{P}_l^{(2)}=\{3,4\}$ and $\mathscr{P}_r^{(2)}=\{5,6,7,8,9\}$.

of Eq. (3). Applying Eq. (10) to our example, we find

$$\boldsymbol{L}_e=\left[\begin{array}{ccccccc}1&2&5&6&7&8&9\\\hline 1&1&0&0&0&0&0\\\hline 0&0&1&1&0&0&0\\0&0&0&0&1&0&0\\0&0&0&0&0&1&1\end{array}\right],\quad \boldsymbol{L}_i=\left[\begin{array}{cc}3&4\\\hline -1&-1\\\hline 1&0\\0&1\\0&0\end{array}\right], \tag{23}$$

where we indicate the pin index on top of each column. As expected, the matrix $\boldsymbol{L}_i$ is full column rank with pseudo inverse

$$\boldsymbol{L}_i^+=\frac{1}{3}\begin{pmatrix}-1&2&-1&0\\-1&-1&2&0\end{pmatrix}. \tag{24}$$

Matrices $\boldsymbol{\pi}^{(m,3)}$ for $m=1,2$ appearing in Eq. (11) read

$$\boldsymbol{\pi}^{(1,3)}=\left[\begin{array}{ccccccc}\multicolumn{7}{c}{\mathbb{1}_2\quad \mathbb{0}_{2\times5}}\\\hline -\frac{1}{3}&-\frac{1}{3}&\frac{2}{3}&\frac{2}{3}&-\frac{1}{3}&0&0\\-\frac{1}{3}&-\frac{1}{3}&-\frac{1}{3}&-\frac{1}{3}&\frac{2}{3}&0&0\end{array}\right], \tag{25}$$

$$\boldsymbol{\pi}^{(2,3)}=\left[\begin{array}{ccccccc}\frac{1}{3}&\frac{1}{3}&-\frac{2}{3}&-\frac{2}{3}&\frac{1}{3}&0&0\\\frac{1}{3}&\frac{1}{3}&\frac{1}{3}&\frac{1}{3}&-\frac{2}{3}&0&0\\\hline \multicolumn{7}{c}{\mathbb{0}_{5\times2}\quad \mathbb{1}_5}\end{array}\right]. \tag{26}$$

We denote by $\mathbb{1}_n$ the identity square matrix of dimension n and by $\mathbb{0}_{n\times m}$ the null matrix of dimension $n\times m$. Next, the choice of selection matrix $\boldsymbol{S}^{(3)}$ determines the fundamental basis in which $\boldsymbol{G}^{(3)}$ is given. The column vectors of $\boldsymbol{S}^{(3)}$ realize a basis of $\ker(\boldsymbol{\ell}^{(3)})$. Let's first determine $\boldsymbol{\ell}^{(3)}$ by finding the left null eigenvectors of $\boldsymbol{L}_i$ that we gather in the lines of matrix

$$\boldsymbol{v}=\begin{bmatrix}1&1&1&0\\0&0&0&1\end{bmatrix}. \tag{27}$$

Then, the matrix of conservation laws arises from

$$\boldsymbol{\ell}^{(3)}=\boldsymbol{v}\boldsymbol{L}_i=\begin{bmatrix}1&1&1&1&1&0&0\\0&0&0&0&0&1&1\end{bmatrix}. \tag{28}$$

The vector of physical currents $\boldsymbol{i}^{(3)}=(i_1,i_2,i_5,i_6,i_7,i_8,i_9)^T$ is obtained from the product of the selection matrix

$$\boldsymbol{S}^{(3)}=\begin{bmatrix}-1&-1&-1&-1&0\\1&0&0&0&0\\0&1&0&0&0\\0&0&1&0&0\\0&0&0&1&0\\0&0&0&0&-1\\0&0&0&0&1\end{bmatrix} \tag{29}$$

with the vector of fundamental currents $\boldsymbol{I}^{(3)}=(i_2,i_5,i_6,i_7,i_9)^T$. Finally, the matrices $\boldsymbol{\Pi}^{(m,3)}$ for $m=1,2$ and then $\boldsymbol{G}^{(3)}$ follow from Eqs. (8–9).

Conclusion— The connection of thermodynamic devices, converting physical quantities of any kind, opens many possibilities that must be further explored. This

requires theoretical works to extend the notion of non-equilibrium conductance, for instance from stationary states to periodic steady states, or from graphs to hypergraphs. Current fluctuations within composite devices are also of great interest, for instance in relation to relaxation toward stationary non-equilibrium. On a side more inspired by electronics, impedance adaptation could be generalized to allow maximal transmission across the circuits.

[1] Jean U. Thoma, *Introduction to Bond Graphs and their Applications* (Elsevier Science & Techn., 2016).

[2] Matthew Schwartz, *Quantum Field Theory and the Standard Model* (Cambridge University Press, Cambridge, England, 2013).

[3] Paul Horowitz and Winfield Hill, *The Art of Electronics* (Cambridge University Press, 2015).

[4] Éric Bringuier, *Électrocinétique : Transport de l'électricité dans les milieux matériels*, edited by Suzanne Laval (CNRS Édition, 2005).

[5] Martin Feinberg, *Foundations of Chemical Reaction Network Theory* (Springer International Publishing, 2019).

[6] O. Kedem and S. R. Caplan, "Degree of coupling and its relation to efficiency of energy conversion," Trans. Faraday Soc. **61**, 1897–1911 (1965).

[7] Aharon Katchalsky and Peter F. Curran, *Nonequilibrium Thermodynamics in Biophysics* (Harvard University Press, Cambridge, MA and London, England, 1965).

[8] Leonardo Peusner, *Studies in network thermodynamics*, Vol. 5 (Elsevier, Studies in modern thermodynamics., 1986).

[9] Leonardo Peusner, "Network thermostatics," The Journal of Chemical Physics **83**, 1276–1291 (1985).

[10] Jean U. Thoma and Henri Atlan, "Network thermodynamics with entropy stripping," Journal of the Franklin Institute **303**, 319–328 (1977).

[11] Matteo Polettini and Massimiliano Esposito, "Irreversible thermodynamics of open chemical networks. i. emergent cycles and broken conservation laws," J. Chem. Phys. **141**, 024117 (2014), 10.1063/1.4886396.

[12] Matteo Polettini, Gregory Bulnes-Cuetara, and Massimiliano Esposito, "Conservation laws and symmetries in stochastic thermodynamics," Phys. Rev. E **94**, 052117 (2016).

[13] Francesco Avanzini, Nahuel Freitas, and Massimiliano Esposito, "Circuit theory for chemical reaction networks," Phys. Rev. X **13**, 021041 (2023).

[14] Sara Dal Cengio, Vivien Lecomte, and Matteo Polettini, "Geometry of nonequilibrium reaction networks," Phys. Rev. X **13**, 021040 (2023).

[15] Hadrien Vroylandt, David Lacoste, and Gatien Verley, "Degree of coupling and efficiency of energy converters far-from-equilibrium," J. Stat. Mech: Theory Exp. (2018), 10.1088/1742-5468/aaa8fe.

[16] Hadrien Vroylandt, David Lacoste, and Gatien Verley, "An ordered set of power-efficiency trade-offs," J. Stat. Mech: Theory Exp. **2019**, 054002 (2019).

[17] Lars Onsager, "Reciprocal relations in irreversible processes. i." Phys. Rev. **37**, 405–426 (1931).

[18] Lars Onsager, "Reciprocal relations in irreversible processes. ii." Phys. Rev. **38**, 2265–2279 (1931).

[19] Herbert B. Callen, *Thermodynamics and an Introduction to Thermostatistics*, 2nd ed. (Wiley, New York, 1985).

[20] If the uth and vth conservation laws (of respectively devices 1 and 2) are connected via pin p, the components $(\boldsymbol{\ell}_r^{(1)})_{up}$ and $(\boldsymbol{\ell}_l^{(2)})_{vp}$ are non zero and all other components (for $u' \neq u$ and $v' \neq v$ respectively) are zero. Then, $\boldsymbol{L}_i$ is an incidence matrix: its columns have only two non-zero components (e.g., column associated with pin p is an edge relating vertices corresponding to the conservation laws u and v). From our assumption of pairwise connection of conservation laws with no loops, $\boldsymbol{L}_i$ has independent columns.

[21] Christophe Goupil, Wolfgang Seifert, Knud Zabrocki, Eckhart Müller, and G. Jeffrey Snyder, "Thermodynamics of thermoelectric phenomena and applications," Entropy **13**, 1481–1517 (2011).

[22] Christophe Goupil, *Continuum theory and modeling ofthermoelectric elements* (John Wiley & Sons, 2015).

[23] Christophe Goupil Philippe Lecoeur Yann Apertet, Henni Ouerdane, "Efficiency at maximum power of thermally coupled heat engines," Phys. Rev. E **85**, 041144 (2012).

[24] Olga Glavatskaya Christophe Goupil Philippe Lecoeur Yann Apertet, Henni Ouerdane, "Optimal working conditions for thermoelectric generators with realistic thermal coupling," Europhysics Letters **97**, 28001 (2012).

Chapter C

Large deviations theory for non-equilibrium processes

Contents

This chapter is devoted to some applications of Large Deviation Theory (LDT) for studying the fluctuations of nonequilibrium systems. I intend to introduce my research works by discussing them from an alternative point of view, stressing the difficulties, proposing original results when possible, and correcting errors in the literature (mine and of other people). In my publications, I have used LDT to obtain exact CGF for currents in nonequilibrium systems, to unveil new fluctuation relations, and to study efficiency fluctuations. For the latter, I refer to Chapter D and, for the former, directly to my publications.

This chapter focuses on connecting different jump processes. The question of relating stationary equilibrium and non-equilibrium dynamics has drawn a large part of my research effort. I call a non-equilibrium process the one that models the same physical system as the equilibrium one but put under different environmental conditions (e.g., imposed by competing reservoirs). The non-equilibrium process usually differs from the so-called driven process built to produce chosen

typical values of some observables (e.g., physical currents). The latter follows from titling (biasing) the equilibrium process and then using a Dood transformation on the tilted operator. Compared to the non-equilibrium process, the driven process has an additional conservative force that appears in the local detailed balance defined in chapter B. Although this force is apparently not so important for the large time asymptotic of physical currents (it produces a boundary term), it significantly changes the symmetric part of the dynamics and, hence, the current statistics. Then, the non-equilibrium process and driven process belong to different dynamical equivalence classes, except if one adds additional constraints. This is the viewpoint that I explore in Ref. [5].

Alternatively, one can start from given non-equilibrium processes and ask whether they belong to the same equivalence class, i.e., with comparable statistics of physical currents. This is the point of view described in Ref. [18] where I extend the work of D. Andrieux to continuous time processes, see Ref. [87, 110, 111]. It relies on introducing a root process (called equilibrium form in Ref. [18]) from a symmetrization of the rate matrix. Processes with the same root process belongs to the same equivalence class and display comparable current fluctuations. Although going in the opposite direction (from non-equilibrium to equilibrium processes), the conclusion of this work is similar to the one of the previous paragraph. The root process associated with a given non-equilibrium process is not equal to the process under equilibrium conditions, i.e., with reservoirs that are not competing anymore.

In order to extend the notion of equivalence classes from discrete to continuous time processes, I have had to consider the relation between these two kinds of dynamics. This led me to have a fruitful discussion with M. Polettini on Ref. [112] on the study of large deviation in the two cases. The result of which is given in section C.1. Extending the work of A. Budini, R. M. Turner and J. P. Garrahan [113], I compare the spectrum for the discrete and continuous time dynamics, but also the eigenspace in order to determine the connection between the driven processes that can be constructed in the two cases. Section C.2 relates Markov jump processes with Arrhénius dynamics, in- and out-of-equilibrium, via conditioning and Doob transform. The last section comes back on nonlinear conductance matrices from the point of view of LDT for TiPS.

C.1 Large deviation in time or activity

We start by considering an ensemble equivalence for Markov jump processes at large number of jumps in their trajectories or for trajectories of long duration. We show below that one can relate the two ensembles. For conditions of ensemble equivalence and inequivalence, I refer to Ref. [12]. This section introduces my work on dynamical equivalence classes [18] reproduced below in section C.1.4. Indeed, given the dynamical equivalence classes for Markov chain, one can use the results below to define indirectly such equivalence classes for Markov jump process.

C.1.1 Equivalence of LDF for fixed time or activity

We consider a physical system modeled by a continuous-time Markov chain with finite states. This system exchanges energy with χ heat reservoirs labeled by $\nu = 1 \dots \chi$ at inverse temperatures $\beta_\nu = 1/(k_B T_\nu)$, with k_B the Boltzmann constant. For the equilibrium dynamics, $\forall \nu, \nu' \in \{1, \dots, \chi\}$, one has $\beta_\nu = \beta_{\nu'}$. We denote generically the system states by x, y and z. The Markov matrix $\boldsymbol{k} = \sum_\nu \boldsymbol{k}_\nu$ gives the total transition rates. The matrices $\boldsymbol{k}_\nu$ of xy component $k_{(xy,\nu)}$ gives the transition rates for channel ν. When observing this jump process, one can decide

(i) to fix the final observation time t which is then deterministic while the total number of jumps (so-called activity) is a random variable,

(ii) to fix the total number of jumps N which is then deterministic while the time of the last jump is a random variable .

The system's state at time τ is $z(\tau)$. A state trajectory during time interval $[0, t]$ is denoted $[z]$. This trajectory includes the state $z(\tau)$ at all time $\tau \in [0, t]$ and the label $\nu(\tau)$ of the reservoir providing the energy at each change of state in the trajectory. Trajectories with a fixed number of jumps N are denoted $[z]^N$ and include the same information (time and channel of jump) as fixed duration trajectories. They are just of random duration $t[z]^N$, and they all have N jumps. The large deviation of physical observables in these two situations are related. In the following, we consider a change of variable that allows to switch from case (i) to case (ii) and vice versa. Given that observables of interest in physics are functions of the jumps or of the occupancy of the states, we work at the 2.5 large deviation level.

Let us start by defining the observables of level 2.5 LDF: the empirical occupancy of state x writes

$$p_x[z] \doteq \frac{1}{t} \int_0^t \mathrm{d}\tau \delta_{x,z(\tau)}, \tag{C1}$$

along a trajectory $[z]$. We use the Kronecker delta $\delta_{xy} = 1$ if $x = y$ and is null otherwise. Similarly, we define the empirical transition probability from a state y to a different state x, and induced by reservoir ν by

$$\omega^\nu_{xy}[z] \doteq \frac{1}{t} \sum_{\tau \in [0,t]} \delta_{x,z(\tau+d\tau)} \delta_{y,z(\tau)} \delta_{\nu,\nu(\tau)}. \tag{C2}$$

The sum is over all time τ at which the system changes from state $z(\tau)$ to state $z(\tau + d\tau)$, exchanging energy with reservoir $\nu(\tau)$. The LDF in the case (i), derived in the appendix A of Ref. [5] reproduced in C.2.3, writes

$$tI(\boldsymbol{\omega}, \boldsymbol{p}) \doteq \sum_{x,y \neq x,\nu} t \left[k_{(xy,\nu)} p_y - \omega_{(xy,\nu)} + \omega_{(xy,\nu)} \ln \frac{\omega_{(xy,\nu)}}{k_{(xy,\nu)} p_y} \right]. \tag{C3}$$

It is finite whenever $\sum_{y,\nu} (\omega_{xy,\nu} - \omega_{yx,\nu}) = 0$ to ensure probability conservation and when $\sum_x p_x = 1$. This large deviation function informs on the rate at which decays with time t the probability of non-typical empirical occupancies and transition

probabilities

$$\mathrm{Prob}_t\ (\boldsymbol{\omega} = \boldsymbol{\omega}[z], \boldsymbol{p} = \boldsymbol{p}[z]) \asymp e^{-tI(\boldsymbol{\omega},\boldsymbol{p})}. \tag{C4}$$

We denote $\Omega \doteq \Sigma_{xy}\omega_{xy} = N/t$ the jump frequency, i.e. the total number of jumps N divided by the total observation time t. The time between jumps is $\mathcal{T} \doteq \Omega^{-1} = t/N$. In the two cases (i) and (ii), the jump frequency is a random variable since either N or t is fixed. By normalizing the empirical transition probabilities into the jump proportion

$$\mathring{\omega}_{(xy,\nu)} \doteq \omega_{(xy,\nu)}/\Omega, \quad \text{such that} \quad \sum_{x,y,\nu} \mathring{\omega}_{(xy,\nu)} = 1, \tag{C5}$$

we can rewrite the LDF of Eq. (C3) using the change of variable $(\boldsymbol{\omega}, \boldsymbol{p}) \to (\Omega, \mathring{\boldsymbol{\omega}}, \boldsymbol{p})$,

$$tI(\Omega, \mathring{\boldsymbol{\omega}}, \boldsymbol{p}) \quad = \quad -\Omega t + \sum_{x,y\neq x,\nu} t\left[k_{(xy,\nu)}p_y + \Omega\mathring{\omega}_{(xy,\nu)} \ln \frac{\Omega\mathring{\omega}_{(xy,\nu)}}{k_{(xy,\nu)}p_y}\right]. \tag{C6}$$

We define the LDF of time between jumps, of jumps proportion, and of state occupancy by

$$N\mathcal{I}(\mathcal{T}, \mathring{\boldsymbol{\omega}}, \boldsymbol{p}) \quad = \quad -N + \sum_{x,y\neq x,\nu} N\left[\mathcal{T}k_{(xy,\nu)}p_y + \mathring{\omega}_{(xy,\nu)} \ln \frac{\mathring{\omega}_{(xy,\nu)}}{\mathcal{T}k_{(xy,\nu)}p_y}\right]. \tag{C7}$$

It is straightforward to check that

$$tI(\boldsymbol{\omega}, \boldsymbol{p}) = N\mathcal{I}(\mathcal{T}, \mathring{\boldsymbol{\omega}}, \boldsymbol{p}). \tag{C8}$$

A nontrivial step here is the exchange of the role (and random nature) of the final time t and the total number of jumps N. We remark that the process is still in continuous time, even if we use the number of jumps as an extensive parameter in the LDF (usually used for Markov chains, i.e., in discrete time case). In other words, the occupancy

$$p_x[z]^N \doteq \frac{1}{t[z]^N}\int_0^{t[z]^N} \mathrm{d}\tau\delta_{x,z(\tau)}, \tag{C9}$$

and the random time between jumps $\mathcal{T} \doteq t[z]^N/N$ are well defined random variables.

The above LDF $\mathcal{I}(\mathcal{T}, \mathring{\boldsymbol{\omega}}, \boldsymbol{p})$ can be used to study the level 2.5 large deviations of the embedded Markov chain. To see this, and as a justification of our interpretation that $\mathcal{I}$ is a LDF at fixed N, we now contract on time between jumps and on occupancy. The optimization on $\mathcal{T}$ gives

$$0 = \frac{\partial\mathcal{I}}{\partial\mathcal{T}} \quad \Rightarrow \quad 0 = \sum_{x,y\neq x,\nu}\left[k_{(xy,\nu)}p_y - \frac{\mathring{\omega}_{(xy,\nu)}}{\mathcal{T}}\right] = \boldsymbol{\lambda}\cdot\boldsymbol{p} - \frac{1}{\mathcal{T}} \tag{C10}$$

where we define $\lambda_y \doteq \sum_{x\neq y,\nu} k_{(xy,\nu)}$ the escape rate from state y. Given the state occupancy $\boldsymbol{p}$ and the escape rates $\boldsymbol{\lambda}$, it is expected that the optimal time between jumps is $\mathcal{T} = 1/(\boldsymbol{\lambda}\cdot\boldsymbol{p})$. Then, the large deviation of jump proportion and state occupancy becomes

$$\mathcal{I}(\mathring{\boldsymbol{\omega}}, \boldsymbol{p}) = \sum_{x,y\neq x,\nu} \mathring{\omega}_{(xy,\nu)} \ln \frac{\mathring{\omega}_{(xy,\nu)}\boldsymbol{\lambda}\cdot\boldsymbol{p}}{k_{(xy,\nu)}p_y}. \tag{C11}$$

The optimization of this LDF on p_z gives

$$0 = \frac{\partial \mathcal{I}}{\partial p_z} \quad \Rightarrow \quad 0 \;=\; \sum_{x,y\neq x,\nu} \mathring{\omega}_{(xy,\nu)} \left[-\frac{\delta_{yz}}{p_z} + \frac{\lambda_z}{\boldsymbol{\lambda}\cdot\boldsymbol{p}} \right], \tag{C12}$$

allowing to conclude on the connection between the optimal occupancy $\boldsymbol{p}$ and the vector $\boldsymbol{n}$ of components n_z giving the normalized number of visits of state z,

$$n_z \doteq \sum_{x,\nu} \mathring{\omega}_{(xz,\nu)} = \frac{\lambda_z p_z}{\boldsymbol{\lambda}\cdot\boldsymbol{p}}. \tag{C13}$$

This connection is mentioned in appendix A of Ref. [18] reproduced in section C.1.4 below. In the end, using the relation of Eq. (C13), we recover the LDF for the jump proportion of a Markov chain associated to the Markov matrix of components $k_{(xy,\nu)}/\lambda_y$ for transition promoted by reservoir ν

$$\mathcal{I}(\mathring{\boldsymbol{\omega}}) = \sum_{x,y\neq x,\nu} \mathring{\omega}_{(xy,\nu)} \ln \frac{\mathring{\omega}_{(xy,\nu)}\lambda_y}{k_{(xy,\nu)} n_y}. \tag{C14}$$

This LDF of jump proportion can be obtained directly using Sanov theorem for the discrete-time dynamics given by $k_{(xy,\nu)}/\lambda_y$, see example 4.5 of Ref. [114]. We emphasize that a Laplace transform on time t of the path probability for the jump process leads to a path probability for the Markov chain in discrete time involving exactly the rates $k_{(xy,\nu)}/\lambda_y$, see [113]. The later reference studies the ensemble equivalence of case (i) and (ii) for jump-dependent dynamical observables based on spectral arguments. At the level of LDF, Eq. (C8) explicit for the first time this equivalence at the 2.5 level of large deviation, i.e., including level 2 observables depending on $\boldsymbol{p}$. The next section discusses the relation between cases (i) and (ii) in the Legendre conjugated ensembles.

C.1.2 Legendre conjugated ensembles to fixed time and activity

The Legendre transforms of the LDFs of Eqs. (C6) and (C7) are defined by

$$\hat{I}(s,\mathring{\boldsymbol{\omega}},\boldsymbol{p}) \doteq -s\Omega - I(\Omega,\mathring{\boldsymbol{\omega}},\boldsymbol{p}) \quad \Leftrightarrow \quad t\hat{I} = -sN - tI, \tag{C15}$$

$$\hat{\mathcal{I}}(h,\mathring{\boldsymbol{\omega}},\boldsymbol{p}) \doteq -h\mathcal{T} - \mathcal{I}(\mathcal{T},\mathring{\boldsymbol{\omega}},\boldsymbol{p}) \quad \Leftrightarrow \quad N\hat{\mathcal{I}} = -ht - N\mathcal{I}. \tag{C16}$$

They are associated with Laplace transforms of the corresponding probabilities with respect to activity or time. The Legendre transform can be done explicitly:

$$\hat{I}(s,\mathring{\boldsymbol{\omega}},\boldsymbol{p}) \;=\; \exp\left[-s - \sum_{x,y\neq x,\nu} \mathring{\omega}_{(xy,\nu)} \ln \frac{\mathring{\omega}_{(xy,\nu)}}{k_{(xy,\nu)} p_y} \right] - \boldsymbol{\lambda}\cdot\boldsymbol{p}, \tag{C17}$$

$$\hat{\mathcal{I}}(h,\mathring{\boldsymbol{\omega}},\boldsymbol{p}) \;=\; \sum_{x,y\neq x,\nu} \mathring{\omega}_{(xy,\nu)} \ln \left[\frac{\mathring{\omega}_{(xy,\nu)}(\boldsymbol{\lambda}\cdot\boldsymbol{p}+h)}{k_{(xy,\nu)} p_y} \right], \tag{C18}$$

where we have used

$$-s = \frac{\partial I}{\partial \Omega} = \ln \Omega + \sum_{x,y\neq x,\nu} \mathring{\omega}_{(xy,\nu)} \ln \frac{\mathring{\omega}_{(xy,\nu)}}{k_{(xy,\nu)} p_y}, \tag{C19}$$

$$-h = \frac{\partial \mathcal{I}}{\partial \mathcal{T}} = \boldsymbol{\lambda} \cdot \boldsymbol{p} - \frac{1}{\mathcal{T}}, \tag{C20}$$

in the left part of Eqs. (C15–C16). According to Eq. (C8), cases (i) and (ii) are equivalent when

$$sN + t\hat{I} = ht + N\hat{\mathcal{I}} \quad \Leftrightarrow \quad s + \frac{\hat{I}(s, \mathring{\boldsymbol{\omega}}, \boldsymbol{p})}{h + \boldsymbol{\lambda} \cdot \boldsymbol{p}} = \frac{h}{h + \boldsymbol{\lambda} \cdot \boldsymbol{p}} + \hat{\mathcal{I}}(h, \mathring{\boldsymbol{\omega}}, \boldsymbol{p}). \tag{C21}$$

This provides the relation between s and h, making the two ensembles equivalent. This relation is the equivalent of Eq. (44) in the Ref. [113]. Our result is expressed at the level of LDF of jumps and occupancy variables. In contrast, the result of Budini, Turner, and Garrahan is written for the CGF of jump variables only. Therefore, the above relation generalizes (the classical part of) their work to the 2.5 level of large deviation.

C.1.3 Driven processes in discrete and continuous time

In this section, we develop the equivalence of ensemble for given final time or total number of jumps by considering the tilted processes and their Doob transforms. We want to address the question of the commutation of two operations on the Markov generators. The first operation consists of tilting and Doob transforming the generator to obtain the so-called driven generator (also called auxiliary or effective generator). The second is the extraction of the embedded chain. In other words, does the embedded chain of a continuous time-driven process (first approach) coincide with the embedded chain that is later tilted and Dood transformed to obtain a driven chain (second approach)? We show below that the two operations commute, meaning that the ensemble equivalence for the statistics of chosen observables extends to the most likely processes leading to the rare fluctuations.

In the first approach, let us use the generator $\boldsymbol{k}$ of section C.1.1 as our starting point. The tilted generator, when counting the number of jumps (conjugated to s) and the heat currents (conjugated to $\boldsymbol{\alpha}$), writes

$$\boldsymbol{\kappa}(s, \boldsymbol{\alpha}) \doteq \sum_{x,y,\nu} k_{xy,\nu} e^{-s+\alpha_\nu(\varepsilon_x - \varepsilon_y)} |x\rangle\langle y| - \sum_x \lambda_x |x\rangle\langle x| \tag{C22}$$

where Dirac notation $|x\rangle\langle y|$ indicates the x, y component of the matrix $\boldsymbol{\kappa}$. The highest eigenvalue of this matrix is denoted $\Gamma = \Gamma(s, \boldsymbol{\alpha})$ and the associated left eigenvector is $\boldsymbol{\pi} = \boldsymbol{\pi}(s, \boldsymbol{\alpha})$. Then, the Doob transform of the tilted generator reads

$$\boldsymbol{K}(s, \boldsymbol{\alpha}) \doteq \boldsymbol{\pi}\boldsymbol{\kappa}\boldsymbol{\pi}^{-1} - \Gamma \mathbb{1} = \sum_{x,y\neq x} K_{xy} |x\rangle\langle y| - \sum_x \Lambda_x |x\rangle\langle x| \tag{C23}$$

where $\mathbb{1}$ is the identity matrix and we use an abuse of notation considering that the vector $\boldsymbol{\pi}$ is identified with a diagonal matrix, i.e. $\pi_{xy} \simeq \delta_{x,y}\pi_x$. We denote by $\Lambda_x > 0$ the escape rate from state x for the driven generator. The left eigenvector is precisely the vector that allows $\Gamma = \Lambda_x - \lambda_x$ for all x such that the generator $\boldsymbol{K}$ is a Markov matrix (sum of column elements are null), see Ref. C.2.3. The embedded chain associated to the driven generator is

$$\boldsymbol{K}' \doteq \sum_{x,y} \frac{K_{xy}}{\Lambda_y} |x\rangle\langle y| + \mathbb{1} = \boldsymbol{K}\boldsymbol{\Lambda}^{-1} + \mathbb{1} \tag{C24}$$

where in the last equality $\boldsymbol{\Lambda}$ is the diagonal matrix built with the vector of escape rate. The sum of the column elements in $\boldsymbol{K}'$ equals 1, and all diagonal elements are zero, as required for the Markov matrix of a discrete-time process. The extraction of the embedded chain can be reversed by reintroducing an escape time for each state. This procedure could be named "temporizing" a Markov chain and reads $\boldsymbol{K}'\boldsymbol{L} - \boldsymbol{L}$, where $\boldsymbol{L}$ is a diagonal matrix of new escape rates. We remark that temporizing the embedded chain with the escape rate of the original dynamics restores the original Markov jump process with generator $\boldsymbol{K}'\boldsymbol{\Lambda} - \boldsymbol{\Lambda} = \boldsymbol{K}$.

In the second approach, we start by tilting the generator $\boldsymbol{k}$ by counting the final time and the heat currents, with respective counting field $h > 0$ and $\boldsymbol{\alpha}$. This corresponds to a Laplace transform of the path probability on the final time t leading to the tilted generator

$$\boldsymbol{\theta}(h, \boldsymbol{\alpha}) \doteq \sum_{x,y\neq x,\nu} \frac{k_{xy,\nu} e^{\alpha_\nu(\varepsilon_x - \varepsilon_y)}}{h + \lambda_y} |x\rangle\langle y| \tag{C25}$$

This tilted operator is not a Markov matrix. The highest eigenvalue of this operator is denoted e^ζ with $\zeta \doteq \zeta(h, \boldsymbol{\alpha})$ and the corresponding left eigenvector $\boldsymbol{l} = \boldsymbol{l}(h, \boldsymbol{\alpha})$. Then, the Doob transformation of this tilted operator leads to the Markov matrix

$$\boldsymbol{T}(h, \boldsymbol{\alpha}) \doteq \frac{\boldsymbol{l}\boldsymbol{\theta}\boldsymbol{l}^{-1}}{e^\zeta}, \tag{C26}$$

where here, again, we abuse the notation $\boldsymbol{l}$ being a diagonal matrix. We emphasize that the Doob transform of continuous and discrete times processes are different since they must produce different Markov matrices.

Now, let us show that the two approaches yield the same dynamics

$$\boldsymbol{T}(h, \boldsymbol{\alpha}) = \boldsymbol{K}'(s, \boldsymbol{\alpha}) \tag{C27}$$

for $h = \Gamma(s, \boldsymbol{\alpha})$ or alternatively for $s = \zeta(h, \boldsymbol{\alpha})$. We start from the conservation of the escape rate difference, mentioned after Eq. (C23) and leading to

$$\Gamma + \lambda_y = \Lambda_y = \sum_{x\neq y,\nu} \pi_x k_{xy,\nu} e^{-s + \alpha_\nu(\varepsilon_x - \varepsilon_y)} \pi_y^{-1} \tag{C28}$$

which is equivalent to the eigenvalue equation

$$\pi_y e^s = \sum_{x\neq y,\nu} \pi_x \frac{k_{xy,\nu} e^{\alpha_\nu(\varepsilon_x - \varepsilon_y)}}{\Gamma + \lambda_y} = \sum_{x,\nu} \pi_x \theta_{xy,\nu}(\Gamma, \boldsymbol{\alpha}). \tag{C29}$$

Hence, for an exponential bias of the jump process at $s = \zeta(h, \boldsymbol{\alpha})$ and of the Markov chain at $h = \Gamma(s, \boldsymbol{\alpha})$, the above eigenvalue equation shows the identity of the left eigenvectors of the tilted generators $\boldsymbol{\kappa}$ and $\boldsymbol{\theta}$, i.e. $\boldsymbol{\pi} = \boldsymbol{l}$. The fact that these generators have a common eigenstate results from Ref. [113]. From this result, using $\Lambda_y = \Gamma - \lambda_y$ for all y and $s = \zeta$ to compare Eq. (C24) and Eq. (C26), we obtain the result announced in Eq. (C27): We conclude that the trajectories ensembles with a given number of jumps or given final time are equivalent, and the typical events leading to some rare fluctuations are in one to one correspondence under extraction of the embedded chain of the driven process, or alternatively after temporizing the driven chain to obtain the driven process.

We have shown this equivalence at the level of jump observables only (here, heat currents). It seems possible to generalize it at the 2.5 level of large deviations (given our work in section C.1.1). This would use the slightly more general equation of conservation of the escape rate difference $\Gamma = m_y + \Lambda_y - \lambda_y$ involving the so-called escape weight vector $\boldsymbol{m}$ conjugated to occupancy, as defined in Ref. [5] of section C.2.3. However, the quantity corresponding to the Markov chain's escape weight vector is unclear. It could be a counting field conjugated to the number of visits of each state in the Markov chain. This counting field is a refinement s_x of the counting field s based on the initial state of the jump: s_x counts the number of jumps with initial state x whatever the final state. Then, the condition on ensemble equivalence [e.g., $s = \zeta(h, \boldsymbol{\alpha})$] must be generalized to a vectorial equation.

Finally, the discussion of this section on the equivalence of two different ensembles offers a natural comment on the duality of the large deviation theory applied to nonequilibrium dynamics. Duality is ubiquitous in thermodynamics: The maximum entropy principle (for systems with given energy) is dual to the minimum energy principle (for systems with given entropy) [115]. In analytical mechanics, duality arises through the Lagrangian and Hamiltonian formalism. When considering stochastic processes at large volume, the results of this section on the duality between the dynamics with a given number of jumps and the dynamics with a given final time are directly translated to the Lagrangian and Hamiltonian formalism, see Ref. [20]. Indeed, (minus) the Hamiltonian is conjugated to time in analytical mechanics. It is natural that the eigenrate (i.e. the value of the Hamiltonian for given initial conditions) and the Hamiltonian function are equivalent to the eigenvalue Γ and to the associated conserved function $\Gamma = \Lambda_y - \lambda_y$, and play the role of the CGF. The correspondence is done in full generality in our work with L. Chabane and A. Lazarescu, and we refer to Ref.[20] for more details. For instance, an extension of the Perron-Frobenius theorem is conjectured to describe possible solutions to Hamilton–Jacobi equations for a class of Hamiltonian. Then, Doob transformations are written using Canonical transformations based on solutions of the time-independent Hamilton-Jacobi equation, etc.

Journal of Statistical Mechanics: Theory and Experiment
An IOP and SISSA journal

PAPER: Classical statistical mechanics, equilibrium and non-equilibrium

Dynamical equivalence classes for Markov jump processes

Gatien Verley

Université Paris-Saclay, CNRS/IN2P3, IJCLab, 91 405 Orsay, France
E-mail: gatien.verley@universite-paris-saclay.fr

Received 14 October 2021
Accepted for publication 21 December 2021
Published 24 February 2022

Online at stacks.iop.org/JSTAT/2022/023211
https://doi.org/10.1088/1742-5468/ac4981

Abstract. Two different Markov jump processes driven out of equilibrium by constant thermodynamic forces may have identical current fluctuations in the stationary state. The concept of dynamical equivalence classes emerges from this statement as proposed by Andrieux for discrete-time Markov chains on simple graphs. We define dynamical equivalence classes in the context of continuous-time Markov chains on multigraphs using the symmetric part of the rate matrices that define the dynamics. The freedom on the skew-symmetric part is at the core of the freedom inside a dynamical equivalence class. It arises from different splittings of the thermodynamic forces onto the system's transitions.

Keywords: current fluctuations, large deviations in non-equilibrium systems, stationary states, stochastic thermodynamics

Contents

1742-5468/22/023211+17$33.00

1. Introduction

A current is intuitively a flow of a physical quantity, such as energy, matter or charges, that changes sign upon time reversal. Currents exist in different spaces. In an abstract state space on which state probabilities are defined, one may consider probability currents between two states. If the state space is the real space, like in the diffusion of a single colloidal particle, a probability current can be thought of (with an ensemble viewpoint) as a matter current at the microscopic scale. From such local currents between states or given locations in space, one can define more global currents. For instance, across a system–reservoir interface, the sum of local currents for a given physical quantity leads to a macroscopic current through the interface.

Conservation laws strongly constrain currents at all scales, e.g. probability conservation constrains probability currents while conservation of energy, matter or charges constrain physical currents exchanged with the environment. Each conservation law creates a relation between the currents of a system, reducing the number of currents needed to determine all currents in the stationary state by one [1]. For instance, in the framework of electric circuits, the Kirchhoff currents law at each node creates a constraint between currents in each branch of the circuit. Similarly, in the framework of stochastic thermodynamics on a graph, currents along fundamental cycles are enough to determine the currents along any edge of the graph [2]. In the same idea, a subset of physical currents, the so-called fundamental currents [3], are enough to determine all physical currents exchanged with the reservoirs. Hence, there exists a freedom in the choice of the currents to be measured so that any other current can be determined thanks to the conservation laws.

In most applications, such as conversion or transport processes, predictions of physical currents must be done in consistency with conservation laws. Those predictions are made on average, like in hydrodynamic theories [4] or with statistical distribution in stochastic thermodynamics [5, 6]. The most convenient way to determine the statistics of currents is to compute the Laplace conjugate of their probability distribution, namely the moment generating function. However, the aforementioned freedom on the observation of currents translates here in a freedom in the specific form of the stochastic variable whose moments are studied [7]. For instance, one may observe energy exchanges with a heat reservoir for every transition between different states. Alternatively, one may look at specific and well-chosen transitions only and assume that energy is exchanged exclusively during those transitions, but in amounts that compensate the energy that should have been exchanged during other transitions. In short, different splittings of physical currents into local currents are possible, all leading to the same statistics of physical

J. Stat. Mech. (2022) 023211

currents. This freedom in the form of the studied stochastic observable corresponds to a gauge freedom for the dynamics [7, 8]. As long as one observes over a long time a system in its stationary state, such changes of dynamics have no effects on the trajectory ensemble and thus on the statistics of physical currents.

This possibility of different systems sharing the same current statistics raises the question of equivalence between the dynamics of nonequilibrium systems. This question has been explored extensively in the last few decades for Markov processes in steady states. Transition rates including the least possible information on the dynamics, given the measure of some physical currents, have been derived using the maximum entropy principle [9]. For processes conditioned on observables like physical currents, either by filtrating the trajectory ensemble or by exponentially tilting it (with or without Doob rectification), several asymptotically equivalent dynamics have been obtained [10–15]. In these works, the notion of non-equilibrium equivalence may refer to path ensemble equivalence (dynamical equivalence) or to equivalence for the typical value of the observable (concentration equivalence) [16]. The former equivalence implies the latter that is hence less restrictive. As we detail in appendix A, the concentration equivalence can be produced by two kinds of modifications of the rate matrix in the case of jump processes: first, the stationary state probability and the probability currents are not affected by a *symmetric* modification of the jump probability [17], i.e. the same modification for each forward and backward jump probability. Second, the probability currents are not affected as well by a modification of the mean time spent in each of the system states [18]. Nonetheless, the stationary probability has changed in this second case, e.g. it increases for states with longer occupancy times. The dynamical equivalence is physically more relevant, motivating us to find the practical conditions producing it, as Andrieux did for (discrete-time) Markov chains on simple graphs [19, 20]. Indeed, defining nonequilibrium thermodynamic potentials is sometimes possible thanks to dynamical equivalence [21]. In this case, one can connect the rare fluctuations of an equilibrium process with the typical fluctuations of the *same* process put in stationary nonequilibrium by external forces or multiple reservoirs at different intensive parameters.

Although modifying dynamics while keeping comparable statistics of physical currents has been thoroughly studied, a definition of *dynamical equivalence classes* is still missing for Markov jump processes on multigraph, in continuous time, and driven out of equilibrium by stationary forces or competing reservoirs. We aim to provide such an operational definition in this article. In section 2, we review standard techniques to compute cumulant generating functions based on the spectrum of tilted rate matrices. In section 3, we find a similarity transformation connecting a (tilted) rate matrix to its (tilted) symmetrized form called *root matrix*. Based on this result, we define in section 4 a non-equilibrium equivalence class by the ensemble of rate matrices with the same root matrix chosen as the representative of the class. Thanks to the similarity transformation with the root matrix, the identity of the spectrum of the matrices in the equivalence class is guaranteed and so are the fluctuations of physical currents. We end this article by illustrating the equivalence of fundamental currents fluctuations on a solvable model of molecular motor.

Finally, from the concept of equivalence class, we see that thermodynamic forces may appear in many ways in the dynamics with no consequences on the stationary state. In

J. Stat. Mech. (2022) 023211

appendix B, the explicit relation between equivalent dynamics is used to explain the freedom on the specific form of the stochastic variable representing a physical current when computing its cumulants [7].

2. Fluctuations of fundamental currents for systems in non-equilibrium stationary state

We study a system with a finite number of states, modeled by a Markov jump process in continuous time and put out of equilibrium by thermodynamic forces gathered into vector $\boldsymbol{b} = (b_{\mathrm{I}}, b_{\mathrm{II}}, \ldots, b_X, \ldots)$. These forces are generated by several reservoirs assumed to be always in thermodynamic equilibrium (e.g. thermostat, chemostat) with different intensive parameters. To shorten notations, we denote half of the thermodynamic forces by $\boldsymbol{f} = \boldsymbol{b}/2$, and talk of $\boldsymbol{f}$ as a force by abuse of language.

Each reservoir exchanges physical quantities (e.g. energy, matter) with the system enabling its change of state, denoted by x, y or z, via channels labeled by $\nu = 1, 2, 3, \ldots$ Hence, ν labels both a channel and the reservoir involved in the transition via this channel. In the framework of graph theory, a change of system state via a channel is represented by an edge. We label edges by e in general or by (xy, ν) for a specific transition from state y to state x via channel ν. The transition rates $k_e = k_e(\boldsymbol{f})$ along each edge e completely define the dynamics. Using the rates $k_{(xy,\nu)}$, one can define: the total transition rate from y to x denoted as $k_{xy} \doteq \sum_\nu k_{(xy,\nu)}$, the escape rate from state y via channel ν denoted as $\lambda_{(y,\nu)} \doteq \sum_{x\neq y} k_{(xy,\nu)}$, or the total escape rate from state y denoted as $\lambda_y \doteq \sum_{\nu,x\neq y} k_{(xy,\nu)}$. All of these rates are functions of the thermodynamic forces, for instance $\lambda_y = \lambda_y(\boldsymbol{f})$, even though we may omit it in the notation. The rate matrix $\boldsymbol{k} = \boldsymbol{k}(\boldsymbol{f})$ writes

$$\boldsymbol{k} \doteq \sum_\nu \left(\sum_{x,y\neq x} k_{(xy,\nu)} |x\rangle\langle y| - \sum_x \lambda_{(x,\nu)} |x\rangle\langle x| \right) \doteq \sum_\nu \boldsymbol{k}_\nu \tag{1}$$

using bracket notation for the basis of the vector space of system states. We call $\boldsymbol{k}$ the rate matrix of the *reference* dynamics and $\boldsymbol{k}_\nu$ the rate matrix for channel ν. The state probability vector $\boldsymbol{p} = \sum_x p_x |x\rangle$ evolves according to the Markov master equation $\partial_t \boldsymbol{p} = \boldsymbol{k} \cdot \boldsymbol{p}$. If $\boldsymbol{f} \neq \boldsymbol{0}$ the system will eventually relax to a non-equilibrium stationary state. The rate matrix $\boldsymbol{k}$ can be used to generate trajectories of a stochastic jump process. A trajectory $[z]$ of duration t gives the ordered list of visited states, the time interval between jumps, and the channel of each jump (if the transition can be done via different channels). From these trajectories, we define the time-averaged current $j_e[z]$ that counts the number of transitions along the edge e per unit time during the trajectory $[z]$. Many $[z]$ realizations of the stochastic process generate an ensemble of trajectory $\{[z]\}$, from which an ensemble of random edge currents $\{j_e[z]\}$ is produced. With a slight abuse of notation, we denote by $j_X[z]$ the current of physical quantities X exchanged with the environment during a trajectory $[z]$. If $\phi_{X,(xy,\nu)}$ denotes the amount of physical quantity X exchanged with reservoir ν during transition from y to x, then

J. Stat. Mech. (2022) 023211

the physical current along a trajectory is written as

$$j_X[z] = \sum_e j_e[z]\phi_{X,e}. \tag{2}$$

We remark that since $j_e[z] = -j_{-e}[z]$ and $\phi_{X,e} = -\phi_{X,-e}$, an arbitrary orientation of edges used consistently leads to the same physical current.

We call fundamental currents those of the physical currents whose sole knowledge of the average (together with their conjugated thermodynamic forces f_X) is sufficient to compute the total entropy production rate in the stationary state [3, 22]

$$\langle\sigma[z]\rangle_{\boldsymbol{k}} = \sum_X b_X \langle j_X[z]\rangle_{\boldsymbol{k}}, \tag{3}$$

where $\langle\ldots\rangle_{\boldsymbol{k}}$ denotes the mean value on $\{[z]\}$ generated by $\boldsymbol{k}$. Here, $\sigma[z]$ is the logarithm of the path probabilities of $[z]$ divided by the path probabilities of the time reverse trajectory, all divided by the trajectory duration. From now on, the subscript X labels only fundamental currents and their conjugated thermodynamic forces.

The moment generating function for fundamental currents observed on a time t and conditioned on the final state, namely the vector of component

$$g_x(\boldsymbol{\alpha}, \boldsymbol{f}, t) \doteq \left\langle \mathrm{e}^{t\boldsymbol{\alpha}\cdot\boldsymbol{j}[z]}\delta(x - z(t))\right\rangle_{\boldsymbol{k}(\boldsymbol{f})}, \tag{4}$$

evolves according to [6]

$$\partial_t \boldsymbol{g} = \boldsymbol{\kappa}\boldsymbol{g}, \tag{5}$$

where we have introduced the tilted generator

$$\boldsymbol{\kappa}(\boldsymbol{\alpha}, \boldsymbol{f}) \doteq \sum_{\nu,x,y\neq x} k_{(xy,\nu)}(\boldsymbol{f})\mathrm{e}^{\sum_X \alpha_X \hat{\phi}_{X,(xy,\nu)}}|x\rangle\langle y| - \sum_x \lambda_x(\boldsymbol{f})|x\rangle\langle x|, \tag{6}$$

where α_X is the Laplace conjugated variable to physical current j_X. Notice that we have used a freedom for counting fundamental currents that is explained in [23, 24], hence not straightforwardly applying Donsker–Varadhan techniques used to compute large-deviation of currents. The cycle exchange matrix $\hat{\boldsymbol{\phi}}$ gives the exchange of each physical quantity with the environment, i.e. its component $\hat{\phi}_{X,ci}$ is equal to the amount of physical quantity labeled by X that is exchanged during the fundamental cycle ci. This matrix follows from the edge exchange matrix $\boldsymbol{\phi}$ of components $\phi_{X,e}$ appearing in equation (2) and the matrix of fundamental cycles $\boldsymbol{C}$ as

$$\sum_e \phi_{X,e}C_{e,ci} = \hat{\phi}_{X,ci}. \tag{7}$$

The columns of $\boldsymbol{C}$ are the fundamental cycles of the system's graph [2]. A cycle is a vector in the space of (arbitrarily) oriented edges. Entries of a cycle vector are ± 1 (or 0) if the edge belongs to the cycle (or not) with a sign chosen according to the edge orientation; the list of edges of a cycle shall form a loop, i.e. without ending states. Fundamental cycles represent a basis of the cycle vector space. In graph theory, one

J. Stat. Mech. (2022) 023211

can build this basis starting from a spanning tree on the graph, i.e. a list of edges that connect all vertices of the graphs without creating a loop, and adding the remaining edges (called chords) one at a time to create fundamental cycles. In doing so, each chord is uniquely associated to a fundamental cycle [2].

The highest eigenvalue of the tilted matrix $\boldsymbol{\kappa}(\boldsymbol{\alpha}, \boldsymbol{f})$ yields $\Gamma_{\boldsymbol{\kappa}}(\boldsymbol{\alpha}, \boldsymbol{f})$ the scaled cumulant generating function (SCGF) of fundamental currents. This SCGF is connected to the moment generating functions conditioned on final state by

$$\Gamma_{\boldsymbol{\kappa}}(\boldsymbol{\alpha}, \boldsymbol{f}) \underset{t\to\infty}{=} \frac{1}{t} \ln \sum_x g_x(\boldsymbol{\alpha}, \boldsymbol{f}, t). \tag{8}$$

In the next section, we define the so-called root dynamics whose tilted generator $\boldsymbol{\mathcal{R}}$ is related by a similarity transform and a translation on the Laplace variable to $\boldsymbol{\kappa}$. Hence the two tilted generators have identical spectrum. Equivalence classes for non-equilibrium processes are defined next since many dynamics share the same root dynamics.

3. Similarity of root and reference dynamics

We call *root matrix* $\boldsymbol{r} = \boldsymbol{r}(\boldsymbol{f})$ the generator of the root dynamics defined as the sum of the geometric mean between the off-diagonal elements of $\boldsymbol{k}_\nu$ and $\boldsymbol{k}_\nu^T$, i.e.

$$\boldsymbol{r}(\boldsymbol{f}) \doteq \sum_{\nu,x,y\neq x} \sqrt{k_{(xy,\nu)}(\boldsymbol{f}) k_{(yx,\nu)}(\boldsymbol{f})} |x\rangle\langle y| - \sum_x \lambda_x(\boldsymbol{f}) |x\rangle\langle x|, \tag{9}$$

while the diagonal elements are not modified. By definition, the root matrix is symmetric, but it is *not* a Markov matrix. Based on the normalized left eigenvector of $\boldsymbol{r}$ associated to the highest eigenvalue, one can obtain a Markov matrix as the Doob transform of $\boldsymbol{r}$. Such a transformation is essentially a similarity transform of the rate matrix combined with a constant translation on the diagonal [13, 25]. The Doob transform of $\boldsymbol{r}$ will satisfy a detailed balance equation, and therefore has a stationary state that is an equilibrium state.

The tilted root matrix is written as

$$\boldsymbol{\mathcal{R}}(\boldsymbol{a}, \boldsymbol{f}) \doteq \sum_{\nu,x,y\neq x} \sqrt{k_{(xy,\nu)}(\boldsymbol{f}) k_{(yx,\nu)}(\boldsymbol{f})} \mathrm{e}^{\sum_X a_X \hat{\phi}_{X,(xy,\nu)}} |x\rangle\langle y| - \sum_x \lambda_x(\boldsymbol{f}) |x\rangle\langle x|, \tag{10}$$

and we denote with $\Gamma_{\boldsymbol{\mathcal{R}}}(\boldsymbol{a}, \boldsymbol{f})$ its highest eigenvalue. To relate $\boldsymbol{\kappa}$ and $\boldsymbol{\mathcal{R}}$ by similarity transform, we introduce the drift potential $u = u(\boldsymbol{f})$ as

$$\exp\left[\Delta u_e(\boldsymbol{f})\right] \doteq \sqrt{\frac{k_e(\boldsymbol{f})}{k_{-e}(\boldsymbol{f})}} \text{ for any edge } e \text{ that is not a chord}, \tag{11}$$

J. Stat. Mech. (2022) 023211

where $\Delta u_{(xy,\nu)} = u_x - u_y$. This defines $\boldsymbol{u}$ up to an additive constant that we set by choosing a unit norm for $\mathrm{e}^{\boldsymbol{u}}$. More generally, the drift potential satisfies

$$\exp\left[\Delta u_e(\boldsymbol{f})\right] = \sqrt{\frac{k_e(\boldsymbol{f})}{k_{-e}(\boldsymbol{f})}}\,\exp\left(-\sum_X f_X \hat{\phi}_{X,e}\right) \text{ for any edge } e, \tag{12}$$

with a slight abuse of notation to extend the exchange matrix for cycles $\hat{\boldsymbol{\phi}}$ to the full edge space as follows

$$\hat{\phi}_{X,e} \doteq \begin{cases} \hat{\phi}_{X,ci} & \text{if } e \text{ is the chord of cycle c}i, \\ 0 & \text{otherwise.} \end{cases} \tag{13}$$

Indeed, from the generalized detailed balance [2], half cycle affinities $\hat{f}_{ci}$ are defined by

$$\hat{f}_{ci} \doteq \sum_X f_X \hat{\phi}_{X,ci} = \ln\left(\prod_{e\in ci}\sqrt{\frac{k_e}{k_{-e}}}\right), \tag{14}$$

where the product is on all edges belonging to the cycle ci. Using the definition of drift potential in equation (11) and specifying out the chord e' in the product on the edges of cycle ci, we obtain

$$\sum_X f_X \hat{\phi}_{X,e'} = \ln\left(\sqrt{\frac{k_{e'}}{k_{-e'}}}\prod_{e\in ci\setminus e'}\sqrt{\frac{k_e}{k_{-e}}}\right) = \ln\sqrt{\frac{k_{e'}}{k_{-e'}}} - \Delta u_{e'}, \tag{15}$$

which yields equation (12). From this latter equation and the definition of the tilted root matrix of equation (10), one finds

$$\boldsymbol{\kappa}(\boldsymbol{\alpha},\boldsymbol{f}) = \mathrm{D}\left(\mathrm{e}^{\boldsymbol{u}(\boldsymbol{f})}\right)\cdot\boldsymbol{\mathcal{R}}(\boldsymbol{f}+\boldsymbol{\alpha},\boldsymbol{f})\cdot\mathrm{D}\left(\mathrm{e}^{-\boldsymbol{u}(\boldsymbol{f})}\right), \tag{16}$$

where $\mathrm{D}(\boldsymbol{v})$ transforms the vector $\boldsymbol{v}$ into a diagonal matrix. We notice that $\mathrm{e}^{\boldsymbol{u}(\boldsymbol{f})}$ is the left eigenvector of $\boldsymbol{\mathcal{R}}(\boldsymbol{f},\boldsymbol{f})$ associated to the null eigenvalue, since the line vector with all entries equal to one is by definition the left eigenvector of

$$\boldsymbol{k}(\boldsymbol{f}) = \boldsymbol{\kappa}(0,\boldsymbol{f}) = \mathrm{D}\left(\mathrm{e}^{\boldsymbol{u}(\boldsymbol{f})}\right)\cdot\boldsymbol{\mathcal{R}}(\boldsymbol{f},\boldsymbol{f})\cdot\mathrm{D}\left(\mathrm{e}^{-\boldsymbol{u}(\boldsymbol{f})}\right), \tag{17}$$

for the null eigenvalue. Therefore, $\boldsymbol{k}(\boldsymbol{f})$ is the Doob transform of $\boldsymbol{\mathcal{R}}(\boldsymbol{f},\boldsymbol{f})$ based on vector $\mathrm{e}^{\boldsymbol{u}(\boldsymbol{f})}$. From equation (16), we find that the spectra of the reference and root tilted matrices satisfy

$$\Gamma_{\boldsymbol{\kappa}}(\boldsymbol{\alpha},\boldsymbol{f}) = \Gamma_{\boldsymbol{\mathcal{R}}}(\boldsymbol{f}+\boldsymbol{\alpha},\boldsymbol{f}). \tag{18}$$

With words, we interpret equations (16) and (18) as follows: the counting field $\boldsymbol{a} = \boldsymbol{f} + \boldsymbol{\alpha}$ appearing in equation (10) includes a tilting force $\boldsymbol{f}$ that transforms the equilibrium dynamics based on $\boldsymbol{r}$ into the driven dynamics with generator $\boldsymbol{\mathcal{R}}(\boldsymbol{f},\boldsymbol{f})$ (similar to $\boldsymbol{k}$ the generator of the reference dynamics) and a counting field $\boldsymbol{\alpha}$ that explores the current fluctuation of the reference dynamics.

J. Stat. Mech. (2022) 023211

We remark that the exchange $e \to -e$ and $\boldsymbol{a} \to -\boldsymbol{a}$ is a symmetry of equation (10) and hence $\boldsymbol{\mathcal{R}}(\boldsymbol{a}, \boldsymbol{f}) = \boldsymbol{\mathcal{R}}(-\boldsymbol{a}, \boldsymbol{f})$, which encodes the symmetry of current fluctuations at equilibrium. Using $\boldsymbol{a} = \boldsymbol{f} + \boldsymbol{\alpha}$, this translates into $\boldsymbol{\mathcal{R}}(\boldsymbol{f}+\boldsymbol{\alpha}, \boldsymbol{f}) = \boldsymbol{\mathcal{R}}(\boldsymbol{f}-2\boldsymbol{f}-\boldsymbol{\alpha}, \boldsymbol{f})$ and equation (16) produces for the tilted generator of the reference dynamics

$$\boldsymbol{\kappa}(\boldsymbol{\alpha}, \boldsymbol{f}) = \boldsymbol{\kappa}(-2\boldsymbol{f}-\boldsymbol{\alpha}, \boldsymbol{f}) \tag{19}$$

that would follow directly from equations (6) and (14) as well. Therefore, the spectrum of these two matrices are identical and more specifically one gets the asymptotic fluctuation relation for fundamental currents

$$\Gamma_{\boldsymbol{\kappa}}(\boldsymbol{\alpha}, \boldsymbol{f}) = \Gamma_{\boldsymbol{\kappa}}(-2\boldsymbol{f}-\boldsymbol{\alpha}, \boldsymbol{f}). \tag{20}$$

One concludes that the fluctuation relation brings to all elements of a dynamical equivalence class the symmetry of current fluctuations of the equilibrium dynamics in the same dynamical equivalence class, namely the root dynamics. Hence, an alternative and less convenient way of defining the root dynamics is to constrain the reference dynamics on having null entropy production.

4. Dynamical equivalence classes

Since the statistics of fundamental currents is fully determined by the spectrum of the tilted root matrix, two jump processes with the same components of the root matrix on all edges and on the diagonal share the same fluctuations of fundamental currents in the stationary state. This implies that proportionality on each edge and on the diagonal leads to proportional SCGF as well. Accordingly, the following equivalence relation

$$\boldsymbol{k} \equiv \boldsymbol{k}' \quad \text{if } \forall\ e, \sqrt{k_e k_{-e}} = \gamma\sqrt{k'_e k'_{-e}} \ \text{ and if } \ \forall\ y, \sum_{x\neq y,\nu} k_{xy,\nu} = \gamma \sum_{x\neq y,\nu} k'_{xy,\nu}, \tag{21}$$

defines a dynamical equivalence class between two jump processes. We emphasize that a couple of states may be connected by several channels and that the component of the root matrices must be proportional for each channel separately. The above equivalence class extends to jump processes on multigraphs and in continuous time the equivalence class introduced by Andrieux in [19] for Markov chains (discrete time) on simple graphs. As for Markov chains, the spectra of the tilted rate matrices associated to $\boldsymbol{k}$ and $\boldsymbol{k}'$ in the same equivalence class are proportional. We remark that proportionality of the spectra is stronger than that of the SCGF as it is associated to path ensemble equivalence (at finite time) upon a suitable choice of boundary conditions.

The difference between two matrices $\boldsymbol{k}$ and $\boldsymbol{k}'$ in the same equivalence class can arise from the different ways of breaking detailed balance. Generalized detailed balance does so by defining differently the skew symmetric part of these matrices. For instance, forces may appear on every edge

$$\frac{k_e(\boldsymbol{f})}{k_{-e}(\boldsymbol{f})} \propto \mathrm{e}^{\sum_X f_X \phi_{X,e}}, \tag{22}$$

J. Stat. Mech. (2022) 023211

or on chords only

$$\frac{k'_e(\boldsymbol{f})}{k'_{-e}(\boldsymbol{f})} \propto \mathrm{e}^{\sum_X f_X \hat{\phi}_{X,e}}, \tag{23}$$

which means that the forward and backward rates are the same for any other edge (up to a potential contribution). Notices that the cycle forces $\hat{\boldsymbol{f}}$ defined in equation (14) are the same defining them with $\boldsymbol{k}$ or with $\boldsymbol{k}'$. Since these two rate matrices are in the same equivalence class, they are both related by similarity transform to $\boldsymbol{\mathcal{R}}(\boldsymbol{f}, \boldsymbol{f})$, but through two different drift potentials, respectively, the one defined in equation (11) and the one defined by the same equation with $\boldsymbol{k}$ and $\boldsymbol{u}$ replaced by $\boldsymbol{k}'$ and $\boldsymbol{u}'$.

Interestingly, for the equilibrium stationary state, the symmetric part of the rate matrix has no influence on thermodynamic equilibrium and just the detailed balance equation for the skew symmetric part matters. On the opposite, the nonequilibrium stationary state when characterized by the fundamental currents fluctuations is only determined by the symmetric part of the rate matrix (defining the equivalence class), given that the skew symmetric part has the expected fundamental forces. In this sense, when dealing with non-equilibrium stationary jump processes, there is a dynamical freedom in the way of imposing the fundamental forces that has no consequences on the fluctuations of fundamental currents. This dynamical freedom is in fact a gauge freedom since in the framework of path probability the Doob transform relating two elements in an equivalence class is in fact a gauge change [26].

Nonequilibrium systems change equivalence class when modifying the thermodynamic forces since these forces modify at least the diagonal part of the root matrix that is related to the system activity [27]. In most cases, forces also appear in the off-diagonal part of the root matrix. For instance, in photoelectric or thermoelectric devices, transition rates often follow from quantum perturbation analysis producing rates that depend on the Fermi (Bose) statistics of the electrons (bosons or phonons) reservoirs. In these cases, the thermodynamics forces such as the temperature and electrochemical potential differences appear in the symmetric part of the rate matrix and hence in the root matrix. It is a challenge to develop a nonequilibrium thermodynamics of such nontrivial systems by including activity into a coherent thermodynamics structure.

5. Illustration on a discrete model of molecular motor

For clarity, we illustrate our main results on a discrete model of molecular motor described in [28–30]. This isothermal molecular motor has two internal states a and b of energy 0 and ϵ, respectively. The two internal states are connected by four different microreversible transitions: the motor can move one step to the left or to the right with or without consuming adenosine triphosphate (ATP) molecules. We associate as shown in figure 1 a positive edge number $e = 1, 2, 3$ and 4 to each transition from a to b and write k_e the corresponding rate. Edge 1 (resp. 2) corresponds to the motor leaving state a by moving to the *left* while consuming 1 (resp. 0) ATP molecule. Edge 3 (resp. 4) corresponds to the motor leaving state a by moving to the *right* while consuming

J. Stat. Mech. (2022) 023211

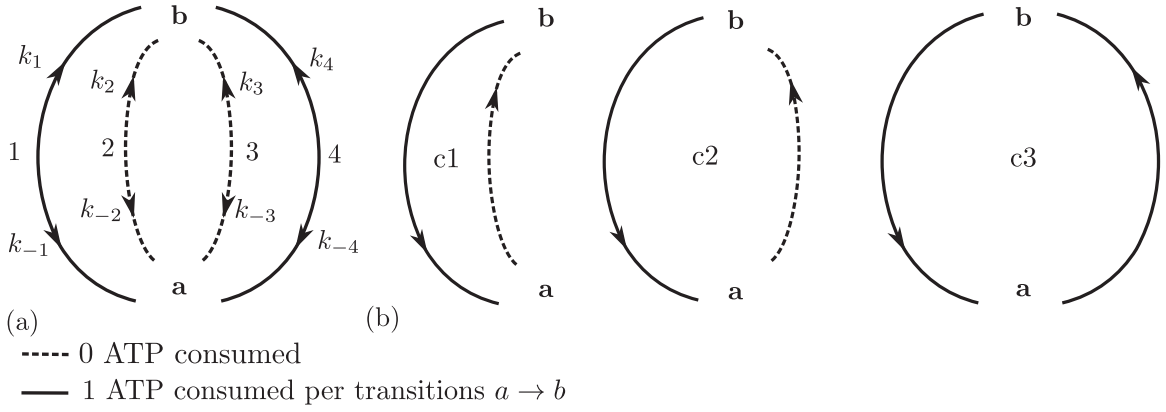

Figure 1. (a) Sketch of the effective two-state system with four edges. Edge orientation is head toward b. (b) Set of fundamental cycles with their orientations given by the orientation of their corresponding chords. The ith column of matrix $\boldsymbol{C}$ in equation (27) is for cycle ci.

0 (resp. 1) ATP molecule. The dimensionless fundamental forces f_X in this model are $f_{\mathrm{I}} = \Delta\mu/(2k_{\mathrm{B}}T)$ that is half the chemical potential difference $\Delta\mu$ of the hydrolysis reaction of ATP and $f_{\mathrm{II}} = fd/(2k_{\mathrm{B}}T)$ that is half the mechanical work fd that the motor performs against force f to make a step of length d. The fundamental currents are the ATP consumption rate j_{I} and the number of step per unit time j_{II}. Hence, the total entropy production rate writes $\sigma = 2j_{\mathrm{I}}f_{\mathrm{I}} + 2j_{\mathrm{II}}f_{\mathrm{II}}$. For simplicity, we write energies in thermal units $k_{\mathrm{B}}T = 1$ where T is the temperature of the motor environment. We take the Boltzmann constant $k_{\mathrm{B}} = 1$: the entropy production rates are homogeneous to an inverse time like fundamental currents.

We completely specify the dynamics using the following transition rates

$$\begin{aligned} k_{-1} &= \tilde{\alpha}\,\mathrm{e}^{2\theta_b^+ f_{\mathrm{II}}}, & k_{-2} &= \tilde{\omega}\,\mathrm{e}^{2\theta_b^+ f_{\mathrm{II}}}, \\ k_1 &= \tilde{\alpha}\,\mathrm{e}^{-\epsilon+2f_{\mathrm{I}}-2\theta_a^- f_{\mathrm{II}}}, & k_2 &= \tilde{\omega}\,\mathrm{e}^{-\epsilon-2\theta_a^- f_{\mathrm{II}}}, \\ k_{-4} &= \alpha\,\mathrm{e}^{-2\theta_b^- f_{\mathrm{II}}}, & k_{-3} &= \omega\,\mathrm{e}^{-2\theta_b^- f_{\mathrm{II}}}, \\ k_4 &= \alpha\,\mathrm{e}^{-\epsilon+2f_{\mathrm{I}}+2\theta_a^+ f_{\mathrm{II}}}, & k_3 &= \omega\,\mathrm{e}^{-\epsilon+2\theta_a^+ f_{\mathrm{II}}}, \end{aligned} \tag{24}$$

where α, $\tilde{\alpha}$, ω and $\tilde{\omega}$ are time scales for the various transitions, and $\theta_x^{\pm}$ are the load distribution factors that encode the left/right asymmetry of the motor (inherited from the modeling in a continuous state space). These factors are arbitrary except for the constraint $\theta_a^+ + \theta_b^- + \theta_a^- + \theta_b^+ = 2$. This constraint ensures the thermodynamic consistency of the model: the entropy production computed using edge currents and forces is equal to the entropy production computed using fundamental current and forces [3, 29]. The root matrix writes

$$\boldsymbol{r}(\boldsymbol{f}) = \left(\sum_{e=1}^{4} r_e\right)|a\rangle\langle b| + \left(\sum_{e=1}^{4} r_e\right)|b\rangle\langle a| - \left(\sum_{e=1}^{4} k_e\right)|a\rangle\langle a| - \left(\sum_{e=1}^{4} k_{-e}\right)|b\rangle\langle b| \tag{25}$$

J. Stat. Mech. (2022) 023211

in terms of the symmetrized rates $r_e = \sqrt{k_e k_{-e}}$ that are explicitly:

$$\begin{aligned} r_1 = r_{-1} &= \tilde{\alpha}\, \mathrm{e}^{-\epsilon/2 + f_{\mathrm{I}} + (\theta_b^+ - \theta_a^-) f_{\mathrm{II}}}, & r_2 = r_{-2} &= \tilde{\omega}\, \mathrm{e}^{-\epsilon/2 + (\theta_b^+ - \theta_a^-) f_{\mathrm{II}}}, \\ r_4 = r_{-4} &= \alpha\, \mathrm{e}^{-\epsilon/2 + f_{\mathrm{I}} + (\theta_a^+ - \theta_b^-) f_{\mathrm{II}}}, & r_3 = r_{-3} &= \omega\, \mathrm{e}^{-\epsilon/2 + (\theta_a^+ - \theta_b^-) f_{\mathrm{II}}}. \end{aligned} \tag{26}$$

We define now the cycle and exchange matrices in order to build the tilted root matrix $\boldsymbol{\mathcal{R}}(\boldsymbol{\alpha}, \boldsymbol{f})$. There are four different spanning trees for the graph of this model of molecular motor since its spanning trees correspond here to just one edge. We chose as the spanning tree edge 1. Adding an edge to this spanning tree creates one cycle. We use the following cycle matrix

$$\boldsymbol{C} = \begin{pmatrix} -1 & -1 & -1 \\ 1 & 0 & 0 \\ 0 & 1 & 0 \\ 0 & 0 & 1 \end{pmatrix}, \tag{27}$$

for cycles c1, c2 and c3 defined in figure 1 and corresponding to the first, second and third column of $\boldsymbol{C}$. Notice that chord orientation determines the orientation of its associated fundamental cycle. Since we assume positive edge orientation for transitions from a to b, chords are oriented in the same way from a to b and hence cycle c1 is made of edges 2 and -1, cycle c2 is made of edges 3 and -1, etc. To convert probability currents in edge space to physical currents, we need to define the edge exchange matrix whose line i (resp. ii) provides the number of consumed ATP molecule (resp. the number of steps to the right done by the motor) when the eth transition occurs, with e being the column index,

$$\boldsymbol{\phi} = \begin{pmatrix} 1 & 0 & 0 & 1 \\ -1 & -1 & 1 & 1 \end{pmatrix}. \tag{28}$$

Then, summing the exchanges along every edges of each fundamental cycle gives the cycle exchange matrix

$$\hat{\boldsymbol{\phi}} = \boldsymbol{\phi} \cdot \boldsymbol{C} = \begin{pmatrix} -1 & -1 & 0 \\ 0 & 2 & 2 \end{pmatrix} \text{ in cycle space.} \tag{29}$$

To define this matrix of components $\hat{\phi}_{X,ci}$ into the space of edges instead of fundamental cycles as done in equation (13), we extend it on the left with one more column filled with zeros since edge 1 is not a chord, while edges 2, 3 and 4 are respectively the chords of cycles c1, c2 and c3:

$$\hat{\boldsymbol{\phi}} = \begin{pmatrix} 0 & -1 & -1 & 0 \\ 0 & 0 & 2 & 2 \end{pmatrix} \text{ in edge space.} \tag{30}$$

J. Stat. Mech. (2022) 023211

The drift potential is defined thanks to edge 1 (the unique edge of our spanning tree) and for all edges $e = 1, 2, 3, 4$ (hence going from a to b) we have

$$\Delta u_e = u_b - u_a = \ln \sqrt{\frac{k_1}{k_{-1}}} = -\epsilon/2 + f_{\mathrm{I}} - (\theta_a^- + \theta_b^+) f_{\mathrm{II}}. \tag{31}$$

We emphasize that the rates of equation (24) satisfy equation (12) since

$$\ln \sqrt{\frac{k_2}{k_{-2}}} = -\epsilon/2 - (\theta_a^- + \theta_b^+) f_{\mathrm{II}} = u_b - u_a - f_{\mathrm{I}}, \tag{32}$$

$$\ln \sqrt{\frac{k_3}{k_{-3}}} = -\epsilon/2 + (2 - \theta_a^- - \theta_b^+) f_{\mathrm{II}} = u_b - u_a - f_{\mathrm{I}} + 2 f_{\mathrm{II}}, \tag{33}$$

$$\ln \sqrt{\frac{k_4}{k_{-4}}} = -\epsilon/2 + f_I + (2 - \theta_a^- - \theta_b^+) f_{\mathrm{II}} = u_b - u_a + 2 f_{\mathrm{II}}, \tag{34}$$

where we used $\theta_a^+ + \theta_b^- + \theta_a^- + \theta_b^+ = 2$ for the last two lines.

First, we illustrate equation (18) relating the spectrum of the tilted rate matrix to the spectrum of the tilted root matrix. With the cycle exchange matrix written in the edge space, the tilted root matrix reads

$$\begin{aligned} \boldsymbol{\mathcal{R}}(\boldsymbol{\alpha}, \boldsymbol{f}) = &\left(\sum_{e=1}^{4} r_e \, \mathrm{e}^{\sum_X \alpha_X \hat{\phi}_{X,e}} \right) |b\rangle\langle a| + \left(\sum_{e=1}^{4} r_e \, \mathrm{e}^{-\sum_X \alpha_X \hat{\phi}_{X,e}} \right) |a\rangle\langle b| \\ &- \left(\sum_{e=1}^{4} k_e \right) |a\rangle\langle a| - \left(\sum_{e=1}^{4} k_{-e} \right) |b\rangle\langle b| \end{aligned} \tag{35}$$

whose highest eigenvalue $\Gamma_{\boldsymbol{\mathcal{R}}} = \Gamma_{\boldsymbol{\mathcal{R}}}(\boldsymbol{\alpha}, \boldsymbol{f})$ writes in terms of its trace and determinant as

$$\Gamma_{\boldsymbol{\mathcal{R}}} = \frac{1}{2} \left(\mathrm{Tr}\, \boldsymbol{\mathcal{R}} + \sqrt{[\mathrm{Tr}\, \boldsymbol{\mathcal{R}}]^2 - 4\, \mathrm{Det}\, \boldsymbol{\mathcal{R}}} \right). \tag{36}$$

Similarly, tilting the rate matrix $\boldsymbol{k}$ gives

$$\begin{aligned} \boldsymbol{\kappa}(\boldsymbol{\alpha}, \boldsymbol{f}) = &\left(\sum_{e=1}^{4} k_e \, \mathrm{e}^{\sum_X \alpha_X \hat{\phi}_{X,e}} \right) |b\rangle\langle a| + \left(\sum_{e=1}^{4} k_{-e} \, \mathrm{e}^{-\sum_X \alpha_X \hat{\phi}_{X,e}} \right) |a\rangle\langle b| \\ &- \left(\sum_{e=1}^{4} k_e \right) |a\rangle\langle a| - \left(\sum_{e=1}^{4} k_{-e} \right) |b\rangle\langle b| \end{aligned} \tag{37}$$

whose trace and determinant are by construction exactly the same as those of $\boldsymbol{\mathcal{R}}(\boldsymbol{\alpha} + \boldsymbol{f}, \boldsymbol{f})$. This can be checked directly using equations (31)–(34) illustrating equation (18) for the identity of the two spectra (when translating the counting field $\boldsymbol{\alpha}$ with the force $\boldsymbol{f}$). Alternatively, we illustrate this relation in figure 2.

Second, we illustrate the notion of dynamical equivalence class by finding two models of molecular motor having the same SCGF for currents j_{I} and j_{II}, up to a multiplicative

J. Stat. Mech. (2022) 023211

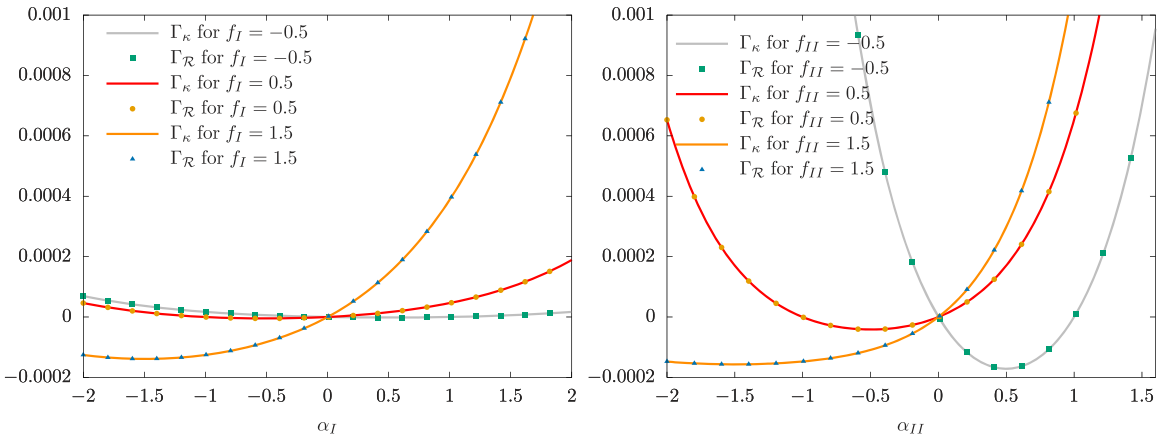

Figure 2. Comparison of the spectra of the tilted root matrix $\mathcal{R}$ with the one of the tilted rate matrix κ. (Left) Spectra $\Gamma_\kappa(\alpha_\mathrm{i}, \alpha_\mathrm{ii} = 0, f_\mathrm{I}, f_\mathrm{II} = 0)$ and $\Gamma_\mathcal{R}(f_\mathrm{I} + \alpha_\mathrm{i}, \alpha_\mathrm{ii} = 0, f_\mathrm{I}, f_\mathrm{II} = 0)$ as a function of α_i for $f_\mathrm{I} = -0.5$, 0.5 and 1.5. (Right) Spectra $\Gamma_\kappa(\alpha_\mathrm{i} = 0, \alpha_\mathrm{ii}, f_\mathrm{i} = 0, f_\mathrm{II})$ and $\Gamma_\mathcal{R}(\alpha_\mathrm{i} = 0, f_\mathrm{II} + \alpha_\mathrm{ii}, f_\mathrm{I} = 0, f_\mathrm{II})$ as a function of α_ii for $f_\mathrm{II} = -0.5$, 0.5 and 1.5. For both figures, we took $\alpha = 0.57$, $\tilde{\alpha} = 1.3 \times 10^{-6}$, $\omega = 3.5$, $\tilde{\omega} = 108.15$, $\epsilon = 10.81$, $\theta_a^+ = 0.25$, $\theta_a^- = 0.75$, $\theta_b^+ = 0.75$, $\theta_b^- = 0.25$.

constant γ relating the time scales of the two models. As we saw in section 4, this is possible if each root rate and escape rate of the two models are proportional with the same proportionality constant γ. For the molecular motor introduced above, a well-chosen modification of the load factors $(\theta_a^\pm, \theta_b^\pm)$ and energy ϵ allows us to change of dynamics, while remaining in the same dynamical equivalence class.

The modification of the load factors must be done in agreement with the thermodynamic consistency $\theta_a^+ + \theta_b^- + \theta_a^- + \theta_b^+ = 2$ and we chose to keep $\theta_b^+ - \theta_a^-$ and $\theta_a^+ - \theta_b^-$ constant. Introducing two parameters θ_a and θ_b used to move inside the dynamical equivalence class, the load factors can be set by

$$\theta_a^\pm = \frac{1 \pm \theta_a}{2}, \qquad \theta_b^\pm = \frac{1 \pm \theta_b}{2} \Rightarrow \theta_b^+ - \theta_a^- = \theta_a^+ - \theta_b^- = \frac{\theta_a + \theta_b}{2}. \tag{38}$$

Then, the escape rates from state a and b read, respectively

$$\sum_{e=1}^{4} k_e = \mathrm{e}^{-\epsilon + (1+\theta_a) f_\mathrm{II}} \left(\tilde{\alpha}\, \mathrm{e}^{2(f_\mathrm{I} - f_\mathrm{II})} + \tilde{\omega}\, \mathrm{e}^{-2 f_\mathrm{II}} + \alpha\, \mathrm{e}^{2 f_\mathrm{I}} + \omega \right), \tag{39}$$

$$\sum_{e=1}^{4} k_{-e} = \mathrm{e}^{(1+\theta_b) f_\mathrm{II}} \left(\tilde{\alpha} + \tilde{\omega} + \alpha\, \mathrm{e}^{-2 f_\mathrm{II}} + \omega\, \mathrm{e}^{-2 f_\mathrm{II}} \right), \tag{40}$$

while any root rate behaves as

$$r_{\pm e} \propto \mathrm{e}^{-\epsilon/2 + f_\mathrm{II}(\theta_b + \theta_a)/2}, \tag{41}$$

J. Stat. Mech. (2022) 023211

where the proportionality constant is independent of the load factors and of the energy. From equations (39)–(41), we notice that the change

$$\theta_a \to \theta_a + \Delta\theta_a \tag{42}$$

$$\theta_b \to \theta_b + \Delta\theta_b \tag{43}$$

$$\epsilon \to \epsilon + f_{\mathrm{II}}(\Delta\theta_a - \Delta\theta_b) \tag{44}$$

produces an edgewise modification of the root dynamics by just a multiplicative factor $\gamma = \mathrm{e}^{\Delta\theta_b f_{\mathrm{II}}}$. Therefore, modifying the dynamics according to equations (42)–(44) is a non-trivial displacement within a dynamical equivalence class. This modification is not trivial in the sense that it does not just multiply the transition rates of equation (24) by a constant factor.

Acknowledgments

I thank Luca Peliti for organizing the workshop 'Random Talks on Stochastic and Non-Equilibrium Thermodynamics' for which most of this work was prepared.

Appendix A. Dynamics with same mean currents

Symmetric freedom—for the sake of completeness, we review in this appendix former works on non-equilibrium equivalence class at the level of mean currents. As mentioned in the introduction, Zia and Schmittmann have shown that an *additive* and symmetric modification of the jump probabilities does not modify the stationary state probability and the probability current [17]. To see it, let us define p_y^{st} the stationary probability of state y such that $\sum_y k_{xy} p_y^{\mathrm{st}} = 0$. Let us define the symmetric matrix $\boldsymbol{h}$ with off-diagonal elements h_{xy} (and diagonal elements $h_{yy} = -\sum_{x\neq y} h_{xy}$), chosen such that the new rate matrix $k'_{xy} = k_{xy} + h_{xy}/p_y^{\mathrm{st}}$ has positive off-diagonal elements. Then, the stationary state probability for matrices $\boldsymbol{k}$ and $\boldsymbol{k}'$ are the same since

$$\sum_y k'_{xy} p_y^{\mathrm{st}} = \sum_y \left(k_{xy} + h_{xy}/p_y^{\mathrm{st}}\right) p_y^{\mathrm{st}}, \tag{A.1}$$

$$= \sum_y k_{xy} p_y^{\mathrm{st}} + \sum_y h_{xy}, \tag{A.2}$$

$$= \sum_y h_{xy} = \sum_x h_{xy} = 0, \tag{A.3}$$

where we used the symmetry of $\boldsymbol{h}$ and the fact that the sums of its column elements are zero. Similarly, the probability currents associated to rate matrices $\boldsymbol{k}$ and $\boldsymbol{k}'$ are the same

$$j_{xy}^{\mathrm{st}'} \doteq k'_{xy} p_y^{\mathrm{st}} - k'_{yx} p_x^{\mathrm{st}}, \tag{A.4}$$

J. Stat. Mech. (2022) 023211

$$= k_{xy}p_y^{\mathrm{st}} + h_{xy} - k_{yx}p_x^{\mathrm{st}} - h_{yx}, \tag{A.5}$$

$$= k_{xy}p_y^{\mathrm{st}} - k_{yx}p_x^{\mathrm{st}} = j_{xy}^{\mathrm{st}}, \tag{A.6}$$

again by the symmetry of matrix $\boldsymbol{h}$. Therefore, if a nonequilibrium stationary state is characterized by the state probability p_x^{st} and all probability currents j_{xy}^{st}, then the symmetric part of the rate matrix (without the diagonal) remains free (given that it is still a well-defined rate matrix). Hence, there is just as much freedom in choosing rates to reach a given nonequilibrium stationary state as for systems to reach a thermal equilibrium state (since detailed balance condition associated to equilibrium state imposes no constraint either on the symmetric part of the rate matrix). Notice that the state probability and the probability currents enable us to compute mean physical currents but no higher moments.

Waiting-times freedom—when characterizing a non-equilibrium stationary state by the probability currents only, we find one additional dynamical degree of freedom for each state in comparison with the situation above. By construction, this freedom in the rate matrix corresponds to the arbitrariness of the stationary probability $\boldsymbol{p}^{\mathrm{st}}$. Indeed, introducing new transition rates $k'_{xy} = k_{xy}\,\mathrm{e}^{\varphi_y}$, with $\boldsymbol{\varphi}$ an arbitrary state vector, leads to the new stationary probability with components $p_x^{\mathrm{st}'} = p_x^{\mathrm{st}}\,\mathrm{e}^{-\varphi_x}$ since

$$\sum_y k'_{xy}p_y^{\mathrm{st}'} = \sum_y \left(k_{xy}\,\mathrm{e}^{\varphi_y}\right)\left(\mathrm{e}^{-\varphi_y}p_y^{\mathrm{st}'}\right) = 0. \tag{A.7}$$

As required, all probability currents are preserved $k'_{xy}p_y^{\mathrm{st}'} - k'_{yx}p_x^{\mathrm{st}'} = k_{xy}p_y^{\mathrm{st}} - k_{yx}p_x^{\mathrm{st}}$. However, the escape rates become $\lambda'_y = \lambda_y\,\mathrm{e}^{\varphi_y}$ and we may interpret the freedom on the stationary probability as a waiting-time freedom. This interpretation is confirmed by the fact that $\forall\, x, p_x^{\mathrm{st}} \propto n_x/\lambda_x$, where n_x is the stationary probability of the embedded Markov chain (for very long trajectories, it is also the number of visit of state x divided by the total number of jumps). From this proportionality relation, we find that the stationary probability of the embedded chain is also preserved when switching from $\boldsymbol{k}$ to $\boldsymbol{k}'$

$$n_x = \frac{p_x^{\mathrm{st}}\lambda_x}{\sum_y p_y^{\mathrm{st}}\lambda_y} = \frac{p_x^{\mathrm{st}'}\lambda'_x}{\sum_y p_y^{\mathrm{st}'}\lambda'_y}. \tag{A.8}$$

Hence, the modification of the stationary probability of the continuous time Markov jump process only comes from the freedom on the escape rates. Interestingly, Polettini has shown that more general transformations such as $k'_{xy} = k_{xy}v_{xy}\,\mathrm{e}^{\varphi_y}$ will not lead to $p_x^{\mathrm{st}'} = p_x^{\mathrm{st}}\,\mathrm{e}^{-\varphi_x}$ excepted if v_{xy} is independent of x and y [18]. In this work, the modification of the stationary probability is referred to as a gauge freedom. However, the terminology 'gauge freedom' should be used for the dynamical changes inside the equivalence classes introduced in the main text.

Appendix B. Equivalence of edge-wise or cycle-wise tilting

In this appendix, we provide another point of view on the edge and cycle freedom in the counting statistics of physical currents developed in [7]. In the stationary state, the

J. Stat. Mech. (2022) 023211

statistics of fundamental currents is the same whether the physical quantity is counted for every transition or for transitions associated with chords only, but with weights determined by the exchanged quantity during the corresponding fundamental cycle. In our framework, this freedom comes from the possibility of relating one tilting procedure to the other one by moving inside the equivalence class.

To show this, we introduce many drift potentials $\boldsymbol{u}^\beta$ defined thanks to the many possibilities for choosing a spanning tree T^β labeled by β:

$$\mathrm{e}^{\Delta u_e^\beta(\boldsymbol{\alpha})} \doteq \sqrt{\frac{k_e(\boldsymbol{\alpha})}{k_{-e}(\boldsymbol{\alpha})}}\,\exp\left(-\sum_X \alpha_X \hat{\phi}^\beta_{X,e}\right) \tag{B.1}$$

with $\hat{\phi}^\beta_{X,e} = \sum_{e'} \phi_{X,e'} C^\beta_{e',ci}$ if $e = ci$ and 0 otherwise, and where $\boldsymbol{C}^\beta$ is the matrix of fundamental cycles associated to the spanning tree T^β. Then, assuming m^β are for now arbitrary real numbers, the off-diagonal components of the tilted matrix when counting on edges can be written

$$k_e(\boldsymbol{f})\mathrm{e}^{\sum_X \alpha_X \phi_{X,e}} = k_e(\boldsymbol{f})\mathrm{e}^{\sum_X \alpha_X \phi_{X,e}} \prod_\beta \left[\sqrt{\frac{k_e(\boldsymbol{\alpha})}{k_{-e}(\boldsymbol{\alpha})}}\,\mathrm{e}^{-\Delta u_e^\beta(\boldsymbol{\alpha}) - \sum_X \alpha_X \hat{\phi}^\beta_{X,e}}\right]^{m^\beta}, \tag{B.2}$$

$$= \underbrace{k_e(\boldsymbol{f})\left[\frac{k_e(\boldsymbol{\alpha})}{k_{-e}(\boldsymbol{\alpha})}\right]^{m^\beta/2} \mathrm{e}^{-\sum_\beta m^\beta \Delta u_e^\beta(\boldsymbol{\alpha})}}_{\text{inside equivalence class of } \boldsymbol{k}(\boldsymbol{f})} \mathrm{e}^{\sum_X \alpha_X \left[\phi_{X,e} - \sum_\beta m^\beta \hat{\phi}^\beta_{X,e}\right]}. \tag{B.3}$$

Hence, finding m^β such that $\sum_X \alpha_X \left[\phi_{X,e} - \sum_\beta m^\beta \hat{\phi}^\beta_{X,e}\right] = \sum_X \alpha_X \hat{\phi}_{X,e}$ would map the edge tilting into a chord tilting of another matrix that belongs to the equivalence class of $\boldsymbol{k}(\boldsymbol{f})$. The problem of finding m^β writes as a linear algebra problem

$$\sum_X \alpha_X \left[\phi_{X,e} - \hat{\phi}_{X,e}\right] = \sum_\beta m^\beta \left(\sum_X \alpha_X \hat{\phi}^\beta_{X,e}\right) \tag{B.4}$$

where one needs to find the inverse of matrix $\hat{\boldsymbol{\Phi}}$ with (β, e) components equal to $\sum_X \alpha_X \hat{\phi}^\beta_{X,e}$. The index β runs on the number of spanning trees. This number is 1 for a tree graph (but switching from edge to cycle counting is meaningless in this case). It is equal to the number of edges on a cycle graph. It will be higher than the number of edges involved in all the cycles for an arbitrary connected graph. Then, there is enough free parameters m^β to find an inverse for all edges that belongs to cycles of the graph. If matrix $\hat{\boldsymbol{\Phi}}$ is singular, then one can reduce the number of free parameter m^β to find its inverse. In the end, using the freedom on the basis of fundamental cycles, on may bias dynamics using the chords in many different ways that, together, can produce the desired bias on each edge.

Let us notice that edges belonging to tree parts of a graph do not contribute to current statistics at all: any physical quantity exchanged while entering into such a tree part will be exchanged back when leaving this tree part. Algebraically, the exponential tilting on edges that are on the tree part of the graph disappears upon symmetrization

J. Stat. Mech. (2022) 023211

of the tilted rate matrix. They just contribute to the skew symmetric part of the rate matrix and just change the particular representative in the class that is being tilted.

References

[1] Polettini M and Esposito M 2014 *J. Chem. Phys.* **141** 024117
[2] Schnakenberg J 1976 *Rev. Mod. Phys.* **48** 571–85
[3] Polettini M, Bulnes-Cuetara G and Esposito M 2016 *Phys. Rev.* E **94** 052117
[4] van Beijeren H 2011 Statistical physics of systems out of equilibrium (http://staff.science.uu.nl/beije101/outofeqseoul.htm)
[5] Van den Broeck C 2013 *Course CLXXXIV Physics of Complex Colloids: Proc. Int. School of Physics 'Enrico Fermi'* ed C Bechinger, F Sciortino and P Ziherl (Italian Physical Society) (http://doi.org/10.3254/978-1-61499-278-3-155)
[6] Sekimoto K 2010 *Stochastic Energetics* (*Lecture Notes in Physics*) vol 799 (Berlin: Springer)
[7] Wachtel A, Vollmer J and Altaner B 2015 *Phys. Rev.* E **92** 042132
[8] Garrahan J P 2016 *J. Stat. Mech.* 073208
[9] Evans R M L 2005 *J. Phys. A: Math. Gen.* **38** 293
[10] Popkov V, Schütz G M and Simon D 2010 *J. Stat. Mech.* P10007
[11] Chétrite R and Touchette H 2013 *Phys. Rev. Lett.* **111** 120601
[12] Budini A A, Turner R M and Garrahan J P 2014 *J. Stat. Mech.* P03012
[13] Chétrite R and Touchette H 2015 *Ann. Henri Poincaré* **16** 2005–57
[14] Chétrite R and Touchette H 2015 *J. Stat. Mech.* P12001
[15] Chabane L, Chétrite R and Verley G 2020 *J. Stat. Mech.* 033208
[16] Touchette H 2017 arXiv:1708.02890
[17] Zia R K P and Schmittmann B 2007 *J. Stat. Mech.* P07012
[18] Polettini M 2012 *Europhys. Lett.* **97** 30003
[19] Andrieux D 2012 arXiv:1208.5699
[20] Andrieux D 2012 arXiv:1212.1807
[21] Verley G 2016 *Phys. Rev.* E **93** 012111
[22] Rao R and Esposito M 2018 *J. Chem. Phys.* **149** 245101
[23] Andrieux D and Gaspard P 2007 *J. Stat. Phys.* **127** 107–31
[24] Altaner B, Wachtel A and Vollmer J 2015 *Phys. Rev.* E **92** 042133
[25] Jack R L and Sollich P 2010 *Prog. Theor. Phys. Suppl.* **184** 304–17
[26] Chabane L, Lazarescu A and Verley G 2022 *J. Stat. Phys.* **187** 1
[27] Maes C 2020 *Phys. Rep.* **850** 1–33
[28] Lau A W C, Lacoste D and Mallick K 2007 *Phys. Rev. Lett.* **99** 158102
[29] Lacoste D, Lau A W and Mallick K 2008 *Phys. Rev.* E **78** 011915
[30] Vroylandt H, Lacoste D and Verley G 2018 *J. Stat. Mech.* 023205

J. Stat. Mech. (2022) 023211

C.2 Mapping equilibrium and non-equilibrium processes

C.2.1 Folding large deviations: Equilibrium case

Below, we illustrate a fundamental difference between equilibrium statistical physics and large deviation theory when applied to far-from-equilibrium systems. We use the LDT for equilibrium systems in a noneducated way to emphasize what happens for nonequilibrium dynamics. The educated way introduces the equilibrium canonical ensemble with its equilibrium free energy F defined by

$$\beta F(\beta) = -\ln \sum_x e^{-\beta \varepsilon_x} \tag{C30}$$

where $\beta = 1/(k_B T)$ is the inverse temperature of the environment, k_B the Boltzmann constant and ε_x the energy of the system in state x. The equilibrium free energy can be exactly computed or approximated, and its derivative provides the energy cumulants of the system in any chosen equilibrium state. The free energy is a function of one variable only, we omit the volume, the number of particles, etc. One uses the same variable β to count the energy fluctuations and to determine the studied equilibrium states: there is no need for an extra counting field. Energy and (inverse) temperature are conjugated variables. The thermodynamic potential includes all the statistical information on the system in any of its equilibrium states with a given inverse temperature.

For a physicist with no statistical physics background, although aware of large deviation theory, it is natural to introduce the CGF of energy

$$\mathcal{F}(\alpha, \beta) = -\ln \left\langle e^{-\alpha \varepsilon} \right\rangle_\beta \tag{C31}$$

where $\langle \dots \rangle_\beta$ is the mean value in the equilibrium state with inverse temperature β. The counting field α is conjugated to energy ε and is used to study energy fluctuations. Then, partial derivatives with respect to α of the CGF at $\alpha = 0$ provide the cumulants of energy in the canonical equilibrium state with inverse temperature β. For the multivariate CGF, the line of constant β stores the statistics of energy for the equilibrium state with this β only. The parameter α is used to explore the CGF's curvature along this line. The parameters α and β have different roles for exploring the level of fluctuations or investigating different equilibrium states.

This is exactly what happens for nonequilibrium steady states. A physical current has two conjugated variables: a counting field generating the cumulants of physical currents and a thermodynamic force defined from a difference of intensive parameters of two reservoirs. For technical reasons, merging thermodynamic forces and counting fields is impossible when studying nonequilibrium systems. Doing so leads to null CGF, which may be related to getting null functions when computing too many Legendre transforms of a thermodynamic potential (they must remain extensive). This is a strong limitation that prevents the definition of non-equilibrium thermodynamic potential (in the equilibrium sense). The LDF or the Legendre conjugated CGF include information on a system's fluctuations, but for a given set of

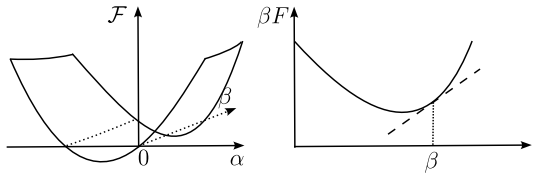

Figure C.1: (Left) CGF $\mathcal{F}(\alpha, \beta)$ whose derivative at $\alpha = 0$ provides the mean energy $\langle \varepsilon \rangle_\beta$. (Right) Concave free energy $\beta F(\beta)$ whose derivative at β provides the mean energy $\langle \varepsilon \rangle_\beta$ in canonical equilibrium.

thermodynamic forces only. In other words, in the far-from-equilibrium case, the effects of a fluctuation are not entirely equivalent to a forcing of the system, as is the case in the close-to-equilibrium regime (regression hypothesis). To obtain the complete information on the statistic of χ currents, the CGF must be a function of 2χ parameters: the thermodynamics forces and the counting fields. Fig. C.1 illustrates for equilibrium states the "folding" of the two-parameter space for the energy CGF to the one dimension space for the free energy.

In the next section, we further explore the "regression hypothesis". We determine a relation between the fluctuations of an equilibrium system and those of the same system put out of equilibrium by competing reservoirs. In addition to restricting the dynamics, the price to pay to allow a mapping is the multiplication of the number of conjugated variables (among which some are non-extensive, such as occupancies).

C.2.2 Folding nonequilibrium fluctuations as in Ref. [5]

In Ref. [5] reproduced in Section C.2.3, the equilibrium fluctuations of a Markov jump process (with Arrhenius rates) are mapped onto those of the same process under nonequilibrium conditions (local detailed balance for competing heat reservoirs). In this section, we summarize the main result of this reference by providing an alternative viewpoint on this equilibrium and nonequilibrium mapping. This illustrates the discussion of the previous section on nonequilibrium systems.

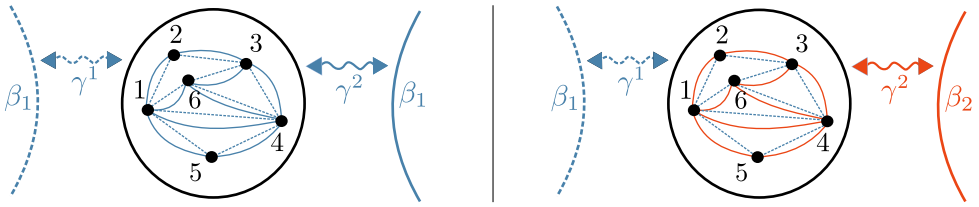

Figure C.2: Multigraphs of a system with six vertices that is in an equilibrium stationary state (Left), or in a nonequilibrium stationary state (Right). In the left equilibrium case, blue dashed and solid lines connecting the same pair of vertices are associated with transition channels for reservoirs all at the same inverse temperature $\beta_1 = 1/(k_B T_1)$. In the right out of equilibrium cases, blue dashed lines represent the channel for reservoirs at β_1, while orange solid lines those at $\beta_2 = 1/(k_B T_2)$.

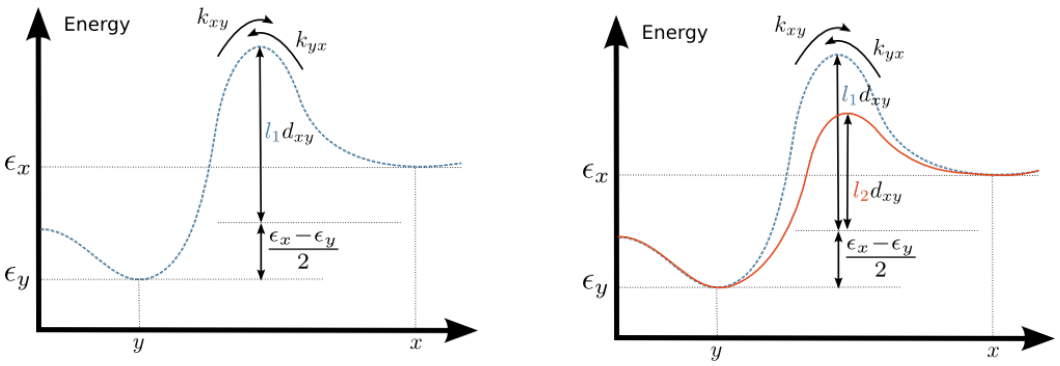

Figure C.3: (Left) Arrhenius rates for the equilibrium dynamics decomposed into a antisymmetric $(\varepsilon_x - \varepsilon_y)/2$ and symmetric parts d_{xy} of the energy barrier. (Right) Arrhenius rates for the non-equilibrium dynamics: one energy barrier per reservoir, with the same antisymmetric part, but different symmetric parts due to different dilatation factors l_ν for $\nu = 1, 2$.

Fig. C.2 shows on the left side an example of an equilibrium system, with a rate Matrix $\boldsymbol{k}$ verifying a detailed balance equation with a heat reservoir at inverse temperature β_1. On the right, the same system is put out-of-equilibrium and described with the rate Matrix $\bar{\boldsymbol{k}} = \sum_\nu \bar{\boldsymbol{k}}_\nu$. Each $\bar{\boldsymbol{k}}_\nu$ verifies a local detailed balance equation with one of the two heat reservoirs at inverse temperature β_ν for $\nu = 1, 2$. Fig. C.3 shows the energy landscape from which are obtained the Arrhenius rates. It shows the half difference $(\varepsilon_x - \varepsilon_y)/2$ between the local minima of energy and the symmetric height of the energy barrier $l_\nu d_{xy} = l_\nu d_{yx}$, with l_ν a dimensionless dilatation factor used to compensate the effect of temperature. The transition rates are exactly

$$k_{xy,\nu} \doteq \gamma_{xy,\nu} e^{-\beta_1(\varepsilon_x - \varepsilon_y)/2 - \beta_1 l_1 d_{xy}} \qquad \text{(Equilibrium)}, \tag{C32}$$

$$\bar{k}_{xy,\nu} \doteq \gamma_{xy,\nu} e^{-(\beta_1/2 - a_\nu)(\varepsilon_x - \varepsilon_y) - (\beta_1 l_1 - b_\nu) d_{xy}} \qquad \text{(Nonequilibrium)}, \tag{C33}$$

with $\gamma_{xy} = \gamma_{xy}$ a symmetric constant matrix (with the physical dimension of inverse time) and where a and b are variables defined in Eqs. (C37–C38) below. The variables of particular interest are $(\boldsymbol{j}, \boldsymbol{f}, \boldsymbol{p})$. The two first have $\nu = 2, \ldots, \chi$ components, and the occupancy is a vector in state space:

$$j_\nu[z] = \frac{1}{t} \sum_{\tau \in [0,t]} \left(\varepsilon_{z(\tau + d\tau)} - \varepsilon_{z(\tau)}\right) \delta_{\nu\nu(\tau)} \qquad \text{(energy currents)}, \tag{C34}$$

$$f_\nu[z] = \frac{1}{t} \sum_{\tau \in [0,t]} d_{z(\tau+d\tau),z(\tau)} \delta_{\nu\nu(\tau)} \qquad \text{(reservoir activities)}, \tag{C35}$$

$$p_x[z] = \frac{1}{t} \int_0^t \mathrm{d}\tau \delta_{x,z(\tau)} \qquad \text{(state occupancy)} \tag{C36}$$

Their conjugated variables $(\boldsymbol{a}, \boldsymbol{b}, \boldsymbol{c})$ are the vectors of components

$$a_\nu = \frac{1}{2}(\beta_1 - \beta_\nu) \qquad \text{(half fundamental force)}, \tag{C37}$$

$$b_\nu = \beta_1 l_1 - \beta_\nu l_\nu \qquad \text{(dynamical bias)}, \tag{C38}$$

$$c_x = \lambda_x - \bar{\lambda}_x \qquad \text{(escape rate change)}. \tag{C39}$$

The escape rates are denoted $\lambda_y \doteq \sum_{x\neq y,\nu} k_{(xy,\nu)}$ and $\bar{\lambda}_y \doteq \sum_{x\neq y,\nu} \bar{k}_{(xy,\nu)}$. We emphasize that the escape rate change is a function of the half fundamental forces and the dynamical bias, $\boldsymbol{c} \doteq \boldsymbol{c}(\boldsymbol{a}, \boldsymbol{b})$. The above variables are conjugated because their pairwise products appear in the following action

$$\ln \frac{\mathcal{P}_{\bar{\boldsymbol{k}}}[z]}{\mathcal{P}_{\boldsymbol{k}}[z]} = t \sum_\nu \left(a_\nu j_\nu[z] + b_\nu f_\nu[z]\right) + t \sum_x c_x p_x[z], \tag{C40}$$

defined as the logarithm of the ratio of the path probabilities of the same trajectory $[z]$ for the non-equilibrium and equilibrium dynamics. Then, the CGF of variables in Eqs. (C34–C36) defined by

$$\Gamma(\boldsymbol{a}, \boldsymbol{b}, \boldsymbol{m}) \underset{t\to\infty}{=} \frac{1}{t} \ln \left\langle e^{t(\boldsymbol{a}\cdot\boldsymbol{j}[z] + \boldsymbol{b}\cdot\boldsymbol{f}[z] + \boldsymbol{m}\cdot\boldsymbol{p}[z])} \right\rangle_{\boldsymbol{k}} \tag{C41}$$

vanishes when the counting field for occupancy is equal to the escape rate change $\boldsymbol{m} = \boldsymbol{c}$,

$$\Gamma(\boldsymbol{a}, \boldsymbol{b}, \boldsymbol{c}) \underset{t\to\infty}{=} \frac{1}{t} \ln \left\langle e^{\ln \frac{\bar{\mathcal{P}}[z]}{\mathcal{P}[z]}} \right\rangle_{\boldsymbol{k}} = \frac{1}{t} \ln \sum_{[z]} \mathcal{P}_{\boldsymbol{k}}[z] \frac{\mathcal{P}_{\bar{\boldsymbol{k}}}[z]}{\mathcal{P}_{\boldsymbol{k}}[z]} = 0. \tag{C42}$$

A difficulty comes from the fact that the escape rate change is a function of $\boldsymbol{a}$ and $\boldsymbol{b}$, which are themselves related in the NESS since then $\boldsymbol{b} = 2\boldsymbol{a}$. This last equation ensures no difference of dilation factor in the NESS with respect to equilibrium value, i.e., $l_1 = l_\nu$. We see that the thermodynamic forces appear in several places in the definition of the CGF and not only in the product with the energy currents with its associated reservoir. In any case, the partial derivatives of the CGF with respect to any variable and taken at $\boldsymbol{a}$, $\boldsymbol{b} = 2\boldsymbol{a}$ and $\boldsymbol{m} = \boldsymbol{c}(\boldsymbol{a}, \boldsymbol{b})$ generates the cumulants of the conjugated variable. This is exactly the structure of equilibrium statistical physics, although many new variables had to be introduced.

In conclusion, we have decomposed the action into several variables, allowing us to consider a non-equilibrium fluctuation as particular cases of an equilibrium fluctuation. However, the relations between the considered variables make the nonequilibrium fluctuations relatively well interlaced. This obliges to study several types of variables in addition to currents so as to separate their contributions in the partial derivatives with respect to a_ν generating the current cumulants. Although the obtained structure is closer to the one of equilibrium statistical physics, the large number of variables and the specific frame of application narrows the interest of the above approach with respect to a LDT focusing on currents and counting fields only (at some value of conjugated thermodynamic forces). The latter case corresponds to choosing $\boldsymbol{m} = \boldsymbol{c}(\boldsymbol{b}/2, \boldsymbol{b})$ in $\boldsymbol{\Gamma}(\boldsymbol{a}, \boldsymbol{b}, \boldsymbol{m})$ where $\boldsymbol{b}$ would be the thermodynamic force vector and $\boldsymbol{a}$ the vector of counting fields conjugated to currents.

Nonequilibrium thermodynamic potentials for continuous-time Markov chains

Gatien Verley
Laboratoire de Physique Théorique (UMR8627), CNRS, Univ. Paris-Sud, Université Paris-Saclay, 91405 Orsay, France
(Received 11 August 2015; revised manuscript received 16 October 2015; published 11 January 2016)

We connect the rare fluctuations of an equilibrium (EQ) process and the typical fluctuations of a nonequilibrium (NE) stationary process. In the framework of large deviation theory, this observation allows us to introduce NE thermodynamic potentials. For continuous-time Markov chains, we identify the relevant pairs of conjugated variables and propose two NE ensembles: one with fixed dynamics and fluctuating time-averaged variables, and another with fixed time-averaged variables, but a fluctuating dynamics. Accordingly, we show that NE processes are equivalent to conditioned EQ processes ensuring that NE potentials are Legendre dual. We find a variational principle satisfied by the NE potentials that reach their maximum in the NE stationary state and whose first derivatives produce the NE equations of state and second derivatives produce the NE Maxwell relations generalizing the Onsager reciprocity relations.

DOI: 10.1103/PhysRevE.93.012111

I. INTRODUCTION

Potentials define a specific concept in physics. They predict the evolution of a system from a variational principle. Such principles span many scientific fields from mechanics, electromagnetism, and optics to control theory, thermodynamics, and statistical physics. A variational principle elegantly summarizes the method used to solve a problem into the extremization of the appropriated cost function, for instance, the action in mechanics [1], the optical path length in optics [2], or the thermodynamic potential in statistical physics [3]. The underlying idea is to explore all possibilities, including nonphysical ones, to find the physical solution from the extremum of the cost function.

In statistical physics, a thermodynamic potential is a state function of the thermodynamic variables. The latter specify a coarse-grained representation of the state of a system including a large number of degrees of freedom. Thermodynamic variables come in conjugated pairs: in each pair, one variable is free and one is constrained according to the environmental conditions. The equilibrium (EQ) thermodynamic potentials proceed from the Legendre transformation of either energy or entropy. This transformation, at the core of the theory's dual structure, allows us to interchange the free and constrained variables. The thermodynamic state is reached at the extremum of the thermodynamic potential. There, the mean free variables are functions of the constrained ones. Beyond the mean description, the potential also predicts the statistics of the free thermodynamic variables, either by generating their cumulants, or from its connection with the asymptotic probability of the free variables.

Statistical physics provides a microscopic foundation to thermodynamics and a method to describe equilibrium systems. In the last decades, the large deviation theory [4,5] has modernized our understanding of statistical physics and accounted for its successes. More recently, it has received a growing interest thanks to its applications to nonequilibrium (NE) systems, for instance, in glasses [6–9], biological systems [10–12], or rare events sampling [13].

Clearly, one step toward understanding NE phenomena starts with the derivation of a NE thermodynamic potential verifying most of the aforementioned properties. With this in mind, many authors have shed light on the structure of statistical physics for NE Markov processes. Oono and Eyink considered that large deviation functions (LDF) could represent NE potentials [4,14,15]. On this basis, Oono and Paniconi proposed a phenomenological framework to study NE steady states [16]. For NE continuous processes, Bertini *et al.* developed the macroscopic fluctuation theory describing the statistics of density and current fluctuations in nonequilibrium stationary states (NESS) [17,18]. Bodineau and Derrida used an additivity principle to predict those fluctuations in diffusive systems [19,20].

For discrete processes, Lecomte, Appert-Rolland, and van Wijland introduced a dynamical partition function and the corresponding topological pressure identified as a LDF [21,22]. Baule and Evans explored these ideas using a path entropy with the aim of finding rules constraining the dynamics of fluids under continuous shear [23–25]. Monthus proposed a similar approach, but involving the maximization of a trajectory-based relative entropy in the presence of constraints [26]. Using large deviation theory, Maes and Netočný [27] found a canonical structure and obtained the LDF of occupation and current probabilities from a variational approach based on the LDF of occupation and transition probabilities. A key step was the introduction of an EQ reference process to highlight that EQ fluctuations naturally appear when studying NE fluctuations. From another perspective, Nemoto and Sasa have shown that a cumulant generating function (CGF) also proceeds from a variational principle, strengthening the dual structure of the theory [28].

More recently, Chetrite and Touchette proposed a general framework for both continuous and discrete processes: they found that a conditioned Markov process is ensemble equivalent to a condition-free process called the driven (or auxiliary) process, but also to an exponentially tilted process called the canonical process [29,30]. This latter process is defined by exponentially weighting the probability of each trajectory with a weight depending on a functional v of the stochastic process. This weighting procedure is analogous to the definition of the canonical ensemble from the superposition of microcanonical ensembles using a Boltzmann weight. On the other hand, the conditioned Markov process assumes that the variable v is constrained to a given value. Finally, the driven

TABLE I. Relationship between the various stochastic processes and NE ensembles. The EQ reference process conditioned on the energy currents j, activities f, and occupations p generates the trajectories of the systems in the NE microcanonical ensemble. The process with mean energy currents, activities, and occupations equal to the constrained values of the conditioned process is the driven process. The path probabilities of the driven process are asymptotically equivalent to the path probability of the NE process and of the canonical reference process. The CGF of j, f, and p for the NE process is exactly the same as the CGF of the EQ reference process (up to a translation), i.e., spontaneous rare fluctuations of the EQ process are associated to typical realizations of the NE process. The NE process generates the trajectories of the systems in the metacanonical ensemble. This ensemble includes the systems that are put out of equilibrium by gradients of temperatures imposed by heat reservoirs. From the equivalence between the conditioned reference process with the driven reference process and the NE process, we conclude that the NE microcanonical and metacanonical ensembles are equivalent.

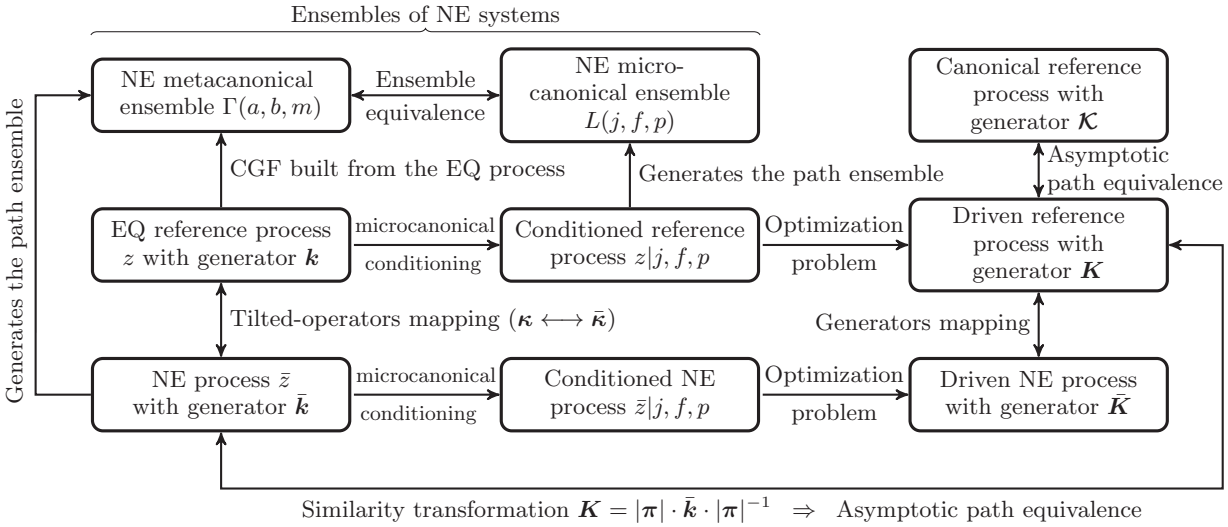

process has a dynamics defined such that the mean value of v is equal to the imposed value in the conditioned process. A systematic method of constructing this driven process from a variational approach was provided in Ref. [31]. A construction of the canonical process was also proposed by Giardiná, Kurchan, and Peliti in Ref. [32] for classical systems and by Garrahan and Lesanovsky in Ref. [33] for dissipative quantum systems. Jack and Sollich constructed a driven process for classical systems in Ref. [34]. The questions of the validity of the path ensemble equivalence has recently been studied in Ref. [35].

Despite all these results, the structure of NE statistical physics is incomplete as regards to EQ statistical physics. For instance, the identification of the relevant coarse-grained degrees of freedom, i.e., the NE thermodynamic variables, is still missing. Accordingly, no general definition exists for stationary NE thermodynamic potentials. To progress in this direction, focusing on continuous-time Markov chains and stationary processes, we consider the following questions: Can we describe the NE fluctuations of a system from the fluctuations of the *same* system at EQ? If yes, can we define meaningful NE thermodynamic potentials using the variables involved in this correspondence? We positively answer these two questions by finding an exact mapping between the statistics of EQ and NE processes. This mapping involves, among others, the affinities of the NE process and some dynamical biases. The latter parameter enables to dilate the energy barriers separating the various states of the system. The variables conjugated to the affinities and the dynamical biases are, respectively, the energy currents and the activities of the exchanges with the environment. The existence of a simple mapping when considering the appropriated couples of conjugated variables suggests that a complete canonical structure for NE statistical physics exists. With respect to previous works on conditioned Markov processes, our main contribution is to identify the constraints that do not modify the system dynamics, apart from changing the temperatures of the heat reservoirs. Accordingly, we define two ensembles of NE systems: the metacanonical ensemble where the constrained variables are the affinities, and the NE microcanonical ensemble where the constrained variables are the energy currents. We prove the equivalence of these ensembles and derive the NE thermodynamic potentials conjugated by Legendre transformation. We also obtain the NE equations of state connecting the conjugated variables.

Our results and the structure of the theory are summarized in Table I. Accordingly, the outline of the paper is as follows. We start by studying the fluctuations of an EQ reference process in Sec. II whose material corresponds to the middle row of Table I. The definition of the EQ reference process and an introduction to large deviation theory are provided in Secs. II A and II B. After these introductory sections, we look for an asymptotic approximation of the probability of the energy currents, activities, and occupations of the systems states. Since we are dealing with an EQ system, no mean energy current exists. However, rare spontaneous fluctuations may produce nonzero energy currents and some arbitrary activities and occupations. We seek the probability of these events from an optimization problem: given that some energy currents j, activities f, and occupations p are observed, defining

the conditioned reference process, which process (called the driven reference process) reproduces these conditioned values j, f, and p as typical values? We construct this driven process in Sec. II C and obtain the LDF of j, f, and p. We use this result to derive the corresponding scaled CGF from a variational approach in Sec. II D.

We switch to the study of the fluctuations of a NE process in Sec. III. This section corresponds to the third row of Table I, which is obtained following exactly the same path as for the EQ reference process, except that we start with a NE process as defined in Sec. III A: we look for the NE driven process that will typically reproduce the arbitrary energy currents j and activities f imposed in the NE conditioned process. Our first main result is to connect, in Sec. III B, the EQ reference process and the NE process and, as a consequence, also to connect their associated driven processes (see the vertical arrows in Table I). Our second main result is to prove, in Sec. III C, the asymptotic equivalence between the path probabilities of the driven reference process with the NE process. This equivalence is at the core of the aforementioned equivalence between the NE microcanonical ensemble and the metacanonical ensemble. In Sec. IV, we comment the structure of the theory starting with a short summary in Sec. IV A. We discuss the symmetries of the NE potentials and the connection with close-to-equilibrium and far-from-equilibrium perturbation theory in Secs. IV B and IV C, respectively. We end by illustrating our work on a two-level model in Sec. V.

For the sake of simplicity, we focus on systems exchanging only energy with heat reservoirs. The generalization of our results to include matter, volume, or other extensive variable exchanges with reservoirs is straightforward [36].

II. EQUILIBRIUM FLUCTUATIONS

A. Definition of the EQ reference process

We consider an *EQ reference process* corresponding to a physical system modeled by a continuous-time Markov chain with a finite number M of discrete states. This system exchanges energy with χ heat reservoirs labeled by $\nu = 1 \dots \chi$ at inverse temperatures $\beta_1 = 1/(k_B T_1)$, with $k_B = 1$ the Boltzmann constant (see Fig. 1). The reference process is at EQ, i.e., all the heat reservoirs share the same inverse temperature β_1. We use several heat reservoirs to allow different mechanisms of energy exchange. As a result, some rare events with net

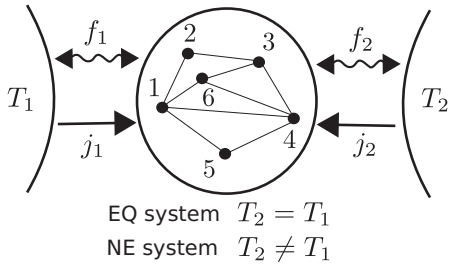

FIG. 1. System with $M = 6$ states connected to $\chi = 2$ heat reservoirs at the same temperature $T_1 = T_2$ for the EQ reference process, or at different temperature $T_1 \neq T_2$ for the NE process.

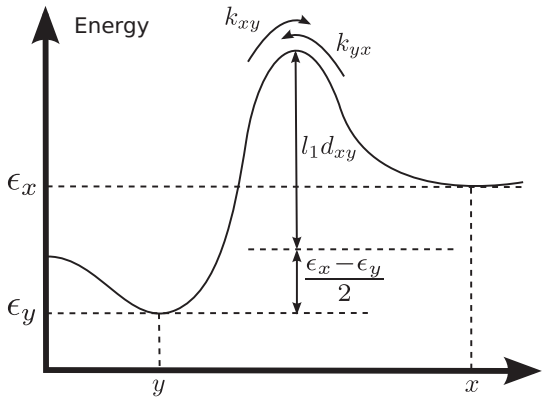

FIG. 2. Energy lanscape for the $x \leftrightarrow y$ transition. The discrete states x and y represent the locations of the minima in the energy landscape. Changing the dilatation factor l_1 modifies the height of all energy barriers for the EQ reference process.

energy flow from one heat reservoir to another may occur. The system states are generically denoted x, y, and z. The state at time τ is $z(\tau)$. A system state trajectory during time interval $[0,t]$ is denoted $[z]$. This trajectory includes the state $z(\tau)$ at all time $\tau \in [0,t]$ and the label $\nu(\tau)$ of the reservoir providing the energy at each change of state in the trajectory.

The energy of state x is ϵ_x. The probability per unit time of switching from state y to state x exchanging the energy $\epsilon_x - \epsilon_y$ with reservoir ν is given by the Arrhenius transition rates

$$k^\nu_{xy} \equiv \gamma^\nu_{xy} e^{-\beta_1(\epsilon_x-\epsilon_y)/2-\beta_1 l_1 d_{xy}}. \tag{1}$$

We have introduced the symmetric matrices $\boldsymbol{\gamma}^\nu$, whose (x,y) element yields the coupling with reservoir ν for a transition from y to x. The (x,y) element of the symmetric matrix $\boldsymbol{d}$ represents the height of the energy barrier that must be crossed when the system switches between states y and x (see Fig. 2). The dimensionless parameter l_1 is a *dilatation factor* that enables to modify the height of the energy barriers ($l_1 = 1$ implies no dilatation). The transition rates defined in Eq. (1) verify for all ν the local detailed balance relation

$$\ln \frac{k^\nu_{xy}}{k^\nu_{yx}} = -\beta_1(\epsilon_x - \epsilon_y), \tag{2}$$

which ensures that the system will reach EQ [37]. The reference probability per unit time of escaping from state y, given that energy is exchanged with reservoir ν, is denoted

$$\lambda^\nu_y \equiv \sum_{x \neq y} k^\nu_{xy} = -k^\nu_{yy}, \tag{3}$$

such that each column of the matrix $\boldsymbol{k}^{(\nu)}$ sums to zero as required for continuous-time Markov chains. The reference transition rate matrix $\boldsymbol{k} \equiv \sum_\nu \boldsymbol{k}^{(\nu)}$ returns the transition probabilities per unit time disregarding the reservoir involved in the energy exchanges. Similarly, $\lambda \equiv \sum_\nu \lambda^{(\nu)}$ is the total escape-rate vector. As a convention, we drop the subscripts of vector or matrix elements to refer to the whole vector or matrix and use boldface letters for matrices. We denote the ensemble average over all trajectories $[z]$

generated with dynamics corresponding to $\boldsymbol{k}$ with the brackets $\langle \dots \rangle_{\boldsymbol{k}}$.

B. Large deviations of empirical time-averaged variables

Throughout the paper, we assume that the long-time statistics of time-extensive variables obey a large deviation principle. For instance, let $z(t)$ be the position at time t of a random walker on a one-dimensional circular lattice and $X[z]$ the number of steps the walker takes during the trajectory $[z]$. We remark that the variable X is a functional of the trajectory $[z]$ that is a realization of a stochastic process. X is not a random variable in itself. When X is not evaluated on a trajectory, it refers either to the physical variable "number of step" or to a numerical value of this variable. The variable $X[z]$ is *time extensive* since $X[z] + X[z'] = X[z,z']$, where $[z,z']$ denote the trajectory made with $[z]$ followed by $[z']$. Then, the number of transitions typically increases with time. Accordingly, $v[z] = X[z]/t$ is the number of steps per unit time and is regarded as a *time-averaged* variable. At long time, it converges to the step frequency of the walker. The probability of $v[z] = v$, i.e., that the time-averaged number of steps $v[z]$ takes the value v at long time t, is $P_t(v) \simeq e^{-tI(v)}$. The function I is called a large deviation function (LDF). It is non-negative and vanishes at $v = \langle v[z] \rangle_{\boldsymbol{k}}$, denoting that the ensemble-average value is the most likely time averaged v. Small (respectively large) deviations correspond to the time-averaged number of steps that are close to (respectively far from) the ensemble-average value. These events become exponentially unlikely with increasing time for ergodic systems. The convexity of the LDF ensures that a large deviation is less likely than a small fluctuation.

Following, we introduce the empirical time-averaged variables used to derive our central results. We name *empirical variables* those that are defined from experimental observations of the system and that usually depend on the observed trajectory $[z]$. First, we define the empirical occupation in x by

$$p_x[z] \equiv \frac{1}{t} \int_0^t d\tau \, \delta_{x,z(\tau)}, \tag{4}$$

where δ is the Kronecker symbol. Given the probability of each state being gathered into the column vector $p = (p_1, \dots, p_M)^\dagger$, the Shannon entropy $s = s(p)$ is

$$s(p) \equiv -\sum_x p_x \ln p_x = -(p^\dagger \cdot \ln p), \tag{5}$$

and the energy $e = e(p)$ is

$$e(p) \equiv \sum_x \epsilon_x p_x = \epsilon^\dagger \cdot p, \tag{6}$$

with the central dot denoting the matrix product and $\dagger$ the transposition. The time-averaged energy along trajectory $[z]$ can be written $e[z] = e(p[z])$, and similarly for the entropy. Second, we define the empirical transition probability from y to x induced by reservoir ν:

$$\omega_{xy}^\nu[z] \equiv \frac{1}{t} \sum_{\tau \in [0,t]} \delta_{x,z(\tau+d\tau)} \delta_{y,z(\tau)} \delta_{\nu,\nu(\tau)}, \tag{7}$$

where the sum is over all time τ at which the system changes from state $z(\tau)$ to state $z(\tau + d\tau)$, exchanging energy with reservoir $\nu(\tau)$. Given a transition probability ω_{xy}^ν for each possible transitions, the current of energy received from reservoir ν by the system is

$$j_\nu(\boldsymbol{\omega}) \equiv \frac{1}{2} \sum_{x,y} \left(\omega_{xy}^\nu - \omega_{yx}^\nu\right)(\epsilon_x - \epsilon_y). \tag{8}$$

Its empirical value during trajectory $[z]$ is written $j_\nu[z] = j_\nu(\boldsymbol{\omega}[z])$. These time-averaged currents describe the antisymmetric part of fluctuations since they change sign upon time reversal of the trajectories. On the contrary, the weighted frequency of interaction with reservoir ν, named *activity* for short and written

$$f_\nu(\boldsymbol{\omega}) \equiv \frac{1}{2} \sum_{x,y \neq x} \left(\omega_{xy}^\nu + \omega_{yx}^\nu\right) d_{xy}, \tag{9}$$

describes the symmetric part of fluctuations. Indeed, $f_\nu[z] = f_\nu(\boldsymbol{\omega}[z])$ does not change sign upon time reversal of the trajectory $[z]$. When the activity is low (high), the system either changes of state less (more) frequently or mostly switches between states with low (high) d_{xy}. The term "activity" was proposed to qualify the symmetric part of the fluctuations in [22,38–41] (see also references therein). Let us finally remark that, in the definitions of the energy currents and activities, the one-half factor is just a symmetry factor since we can sum over transitions disregarding their directions ($\sum_{x,y}$) or for only one direction ($\sum_{x>y}$). Half of the first sum is equivalent to the second sum.

C. LDF of energy currents, activities, and occupation from a variational approach

At long time t, the probability of observing an empirical transition probability $\boldsymbol{\omega}[z] = \boldsymbol{\omega}$ and an empirical occupation $p[z] = p$ is

$$P_t(\boldsymbol{\omega}, p) \underset{t\to\infty}{\simeq} e^{-tI(\boldsymbol{\omega},p)}. \tag{10}$$

From the work of Maes and Netočný [27], Wynants [42], or Bertini *et al.* [43], the LDF $I(\boldsymbol{\omega}, p)$ of the empirical transition probabilities and occupations for the continuous-time Markov chain with generator $\boldsymbol{k}$ is

$$I(\boldsymbol{\omega}, p) = \sum_{x,y\neq x,\nu} \left[k_{xy}^\nu p_y - \omega_{xy}^\nu + \omega_{xy}^\nu \ln \frac{\omega_{xy}^\nu}{k_{xy}^\nu p_y} \right], \tag{11}$$

where the sum is over ν from 1 to χ and all couples (x,y) such that $x \neq y$. The derivation of Eqs. (10) and (11) is reproduced in Appendix A.

In Ref. [27], the LDF of the occupation and probability current was obtained from a constrained optimization problem constructed with $I(\boldsymbol{\omega}, p)$. This procedure, called "contraction" [4], is equivalent at the level of probabilities to marginalize $P_t(\boldsymbol{\omega}, p)$ to obtain the probability of currents and occupations. We now proceed to the contraction of $I(\boldsymbol{\omega}, p)$ to obtain the LDF of energy currents, activities, and occupations denoted $L(j, f, p)$. The long-time asymptotic approximation of the probability $P_t(j, f, p)$ that $j[z] = j$, $f[z] = f$, and $p[z] = p$

at time t will then read as

$$P_t(j,f,p) \underset{t\to\infty}{\simeq} e^{-tL(j,f,p)}. \tag{12}$$

We prove in Appendix B a sharper approximation of this probability that involves a preexponential factor dictating the thermodynamic behavior: it leads to the statistics of the usual EQ thermodynamic variables that only depend on the system state, such as energy for instance. It is the first correction to the exponential decay of nontypical time-extensive variables after a long time. This prefactor was first obtained in Ref. [41], but we provide in Appendix B a logically independent derivation (though restricted to the large time limit) that involves some results of Sec. III.

At long time, the energy current j, activity f, and occupation p mainly appear thanks to the most likely event producing them. The probability of this event is associated with smaller values of $I(\boldsymbol{\omega},p)$ with $\boldsymbol{\omega}$ constrained by the value of the energy currents and activity. For this reason, and in virtue of the contraction principle, we minimize $I(\boldsymbol{\omega},p)$ under the energy currents constraint

$$j_\nu = j_\nu(\boldsymbol{\omega}), \tag{13}$$

for $\nu > 1$, because current conservation imposes $j_1 = -\sum_{\nu\neq 1} j_\nu$. We also impose the activity constraint

$$f_\nu = f_\nu(\boldsymbol{\omega}). \tag{14}$$

In addition, the probability currents should be compatible with the conservation of the norm of the occupation vector, i.e., for all y,

$$\sum_{x,\nu} \left(\omega^\nu_{xy} - \omega^\nu_{yx}\right) = 0. \tag{15}$$

To perform our optimization problem, we use the following cost function:

$$\mathcal{F}(\boldsymbol{\omega},p) = I(\boldsymbol{\omega},p) + \sum_\nu a_\nu[j_\nu - j_\nu(\boldsymbol{\omega})] + \sum_\nu b_\nu[f_\nu - f_\nu(\boldsymbol{\omega})] + \sum_{x,y,\nu} u_y\left(\omega^\nu_{xy} - \omega^\nu_{yx}\right), \tag{16}$$

where a_ν, b_ν, and u_y are Lagrange multipliers that will be chosen to satisfy the constraints of Eqs. (13)–(15). We choose $a_1 = 0$ so as not to constrain the current j_1 that is already set by the current conservation law. We now minimize the function $\mathcal{F}$ with respect to $\boldsymbol{\omega}$, calculating $\partial\mathcal{F}/\partial\omega^\nu_{xy} = 0$ to get

$$0 = \ln\frac{\omega^\nu_{xy}}{k^\nu_{xy}p_y} - a_\nu(\epsilon_x - \epsilon_y) - b_\nu d_{xy} + (u_y - u_x), \tag{17}$$

where we have used Eqs. (11) and (13) and (14). Therefore, the optimal transition probability in terms of the Lagrange multipliers satisfies

$$\omega^\nu_{xy} = K^\nu_{xy}p_y, \tag{18}$$

where we have introduced $\boldsymbol{K}^\nu = \boldsymbol{K}^\nu(a,b,u)$, the transition probability for mechanism ν divided by the empirical occupation of the state before transition. Its off-diagonal elements are

$$K^\nu_{xy} \equiv k^\nu_{xy} e^{a_\nu(\epsilon_x-\epsilon_y)+b_\nu d_{xy}+u_x-u_y}, \tag{19}$$

or, more explicitly, using Eq. (1),

$$K^\nu_{xy} = \gamma^\nu_{xy} e^{-(\beta_1/2-a_\nu)(\epsilon_x-\epsilon_y)-(\beta_1 l_1-b_\nu)d_{xy}+u_x-u_y}, \tag{20}$$

and the diagonal elements are

$$K^\nu_{yy} = -\sum_{x\neq y} K^\nu_{xy} \equiv -\Lambda^\nu_y, \tag{21}$$

such that any column of any matrix $\boldsymbol{K}^\nu$ sums to zero. We remark that the matrices $\boldsymbol{K}^\nu$ satisfy a modified detailed-balance relation

$$\ln\frac{K^\nu_{xy}}{K^\nu_{yx}} = (2a_\nu - \beta_1)(\epsilon_x - \epsilon_y) + 2(u_x - u_y). \tag{22}$$

In this local detailed balance, the Lagrange multiplier a_ν biases the inverse temperatures β_1 to make typical the energy exchanges corresponding to the energy currents constraint. The reservoir ν behaves as if it had the temperature $\beta_\nu \equiv \beta_1 - 2a_\nu$ in order to satisfy the current constraint. Thus, the variable

$$2a_\nu = \beta_1 - \beta_\nu \tag{23}$$

is an *affinity* [44–46], also called *thermodynamic force* [47,48]. Notice that $a_1 = 0$ as required. The similarity between Eqs. (1) and (20) indicates that we can also introduce new dilatation factors l_ν such that the *dynamical bias*

$$b_\nu \equiv \beta_1 l_1 - \beta_\nu l_\nu \tag{24}$$

gives the modification of the dynamics in order to satisfy the activity constraint. Finally, we call the variable u the *drift* because it acts like a force biasing each transition.

The explicit solution $\boldsymbol{\omega}$ of our variational problem $d\mathcal{F} = 0$ is now almost reached. The next step is to use the constraints of Eqs. (13)–(15) to obtain the Lagrange multipliers. More explicitly, the constraint equations are

$$j_\nu = \frac{1}{2}\sum_{x,y}\left(K^\nu_{xy}p_y - K^\nu_{yx}p_x\right)(\epsilon_x - \epsilon_y), \tag{25}$$

$$f_\nu = \frac{1}{2}\sum_{x,y}\left(K^\nu_{xy}p_y + K^\nu_{yx}p_x\right)d_{xy}, \tag{26}$$

$$0 = \boldsymbol{K}\cdot p, \tag{27}$$

where $\boldsymbol{K} = \sum_\nu \boldsymbol{K}^\nu$ is the generator of the *driven reference process* [29,31]. For the third equation, the conservation law of the probability current of Eq. (15) is reformulated as a requirement that the empirical occupation p is the stationary probability of the continuous-time Markov chain with rate matrix $\boldsymbol{K} = \boldsymbol{K}(a,b,u)$. Inverting these three equations gives the vectors a, b, and u as a function of (j,f,p).

The final step to obtain the asymptotic probability of energy currents, activities, and occupations is to write the LDF of Eq. (11) at the optimal transition probability of Eq. (18). This leads to

$$L(j,f,p) = a^\dagger\cdot j + b^\dagger\cdot f + (\lambda - \Lambda)^\dagger\cdot p, \tag{28}$$

where we have used the antisymmetry of $\epsilon_x - \epsilon_y$ or symmetry of d_{xy} in the exchange of x and y to make explicit the

dependence in j and f. We also used Eq. (15) to get rid of the term involving $u_x - u_y$.

D. Scaled CGF of energy currents, activities, and occupations from a variational approach

In the previous section, we have obtained the LDF L from the solution of an optimization problem. From now on, and for the remainder of the paper, we assume the convexity of the LDF. Our aim here is to derive the scaled CGF conjugated to L from a variational approach, using the fact that LDF and scaled CGF are conjugated by Legendre transformation [4,5,31]. On the way, we obtain useful properties associated to the canonical structure.

The scaled CGF of the energy current, activity, and occupation is defined by

$$\Gamma(a',b',m') \equiv \lim_{t\to\infty} \frac{1}{t} \ln \left\langle e^{t(a'^\dagger\cdot j[z]+b'^\dagger\cdot f[z]+m'^\dagger\cdot p[z])} \right\rangle_{\boldsymbol{k}}, \tag{29}$$

and is the Legendre transformation of L

$$\Gamma(a',b',m') = \max_{p,j,f} [a'^\dagger\cdot j + b'^\dagger\cdot f + m'^\dagger\cdot p - L(p,j,f)]. \tag{30}$$

The maximum on j and f is reached for $a' = a$ and $b' = b$, and the scaled CGF becomes

$$\Gamma(a,b,m') = \max_{p|\boldsymbol{K}\cdot p=0} [(m' + \Lambda - \lambda)^\dagger \cdot p], \tag{31}$$

where the maximum is taken over all occupations with the Lagrange multiplier u in the generators of the driven process $\boldsymbol{K}$ tuned such that $\boldsymbol{K}\cdot p = 0$. An alternative expression of the scaled CGF of energy current, activity, and occupation is

$$\Gamma(a,b,m') = \max_{u} [(m' + \Lambda - \lambda)^\dagger \cdot p] \tag{32}$$

with p the stationary probability associated to $\boldsymbol{K}$. From the optimal drift $u = u(a,b,m')$ realizing the maximum in Eq. (32), we introduce the *escape weight* $m \equiv m(a,b,u)$ giving the value of m' for given (a,b,u). In Eq. (G14) of the appendix of Ref. [28], Nemoto and Sasa gave the scaled CGF of energy current from a variational expression analogous to our Eq. (32). We recover their result taking $b = 0$ and $m' = 0$. We further comment Eq. (32) noticing that the maximum is reached for u satisfying

$$\Gamma(a,b,m) = m_y + \Lambda_y - \lambda_y, \tag{33}$$

for all y. This equation allows us to derive the following escape-rate rule

$$m_y + \Lambda_y - \lambda_y = m_x + \Lambda_x - \lambda_x, \tag{34}$$

that can be related to the exit rate constraint of Refs. [24,25,29] taking $m = 0$. To prove Eq. (33), we introduce the *tilted operator* $\boldsymbol{\kappa} = \boldsymbol{\kappa}(a,b,m)$ for the EQ reference process

$$\kappa_{yy} \equiv -\sum_{x\neq y,\nu} k^\nu_{xy} + m_y, \tag{35}$$

$$\kappa_{xy} \equiv \sum_{\nu} k^\nu_{xy} e^{a_\nu(\epsilon_x-\epsilon_y)+b_\nu d_{xy}}. \tag{36}$$

The generator of the driven reference process $\boldsymbol{K}$ is connected to this tilted operator by

$$K_{xy} = e^{u_x}\kappa_{xy}e^{-u_y} - (m_y + \Lambda_y - \lambda_y)\delta_{xy}. \tag{37}$$

Using this equation and $\boldsymbol{K}\cdot p = 0$, we find

$$\sum_y e^{u_x}\kappa_{xy}e^{-u_y}p_y = (m_x + \Lambda_x - \lambda_x)p_x, \tag{38}$$

after summing over x and maximizing over u, it follows from Eq. (32) that the drift giving the maximum satisfies

$$\sum_{x,y} e^{u_x}\kappa_{xy}e^{-u_y}p_y = \Gamma. \tag{39}$$

By definition [49], the scaled CGF $\Gamma(a,b,m)$ is the highest eigenvalue of $\boldsymbol{\kappa}$. Then, $\pi_x \equiv \pm e^{u_x}/Z(u)$ is the normalized left eigenvector of $\boldsymbol{\kappa}$ with $Z(u)$ a normalization constant such that $\sum_x \pi_x = 1$. The vector $r \equiv \boldsymbol{\pi}^{-1}\cdot p$ is a right eigenvector with $\boldsymbol{\pi}_{xy} \equiv \pi_x\delta_{xy}$. Its norm is set by $\sum_x \pi_x r_x = \sum_x p_x = 1$. Notice that we cannot determine from the values of u the sign of each component of the vectors π and r, but their x components share the same sign. Now, summing Eq. (37) over x leads to Eq. (33) since $\sum_x K_{xy} = 0$ and $\sum_x e^{u_x}\kappa_{xy}e^{-u_y} = \Gamma$.

Then, the optimal drift $u = u(a,b,m)$, leading to the maximum in Eq. (32), is simply obtained from the left eigenvector of the tilted operator by $\ln|\pi_x| = u_x - \ln|Z(u)|$ up to a constant that plays no role since only differences of drifts matter. The drift makes the escape-rate rule holds true and, using Eqs. (28) and (33), leads to the Legendre structure that one expects for LDFs and scaled CGFs. Finally, from Eqs. (33) and (37), we recover the results of Refs. [29–31,34] in which the generator $\boldsymbol{K}$ of the driven process corresponds to the Doob's transformation of the tilted operator $\boldsymbol{\kappa}$:

$$K_{xy} = |\pi_x|\kappa_{xy}|\pi_y|^{-1} - \Gamma\delta_{xy}. \tag{40}$$

Notice that in Refs. [29–31], the right eigenvector of the tilted operator is used in the Doob's transformation instead of the left one since the tilted operator in these references is the adjoint of $\boldsymbol{\kappa}$.

III. NONEQUILIBRIUM FLUCTUATIONS

A. Definition of the NE process

The *NE process* is defined by the rate matrices $\bar{\boldsymbol{k}}^\nu = \bar{\boldsymbol{k}}^\nu(a_\nu,b_\nu)$ associated to energy exchanges with each reservoir ν at different temperatures $\beta_\nu = \beta_1 - 2a_\nu$ and with different dilatation factors l_ν related to dynamical bias by $b_\nu = \beta_1 l_1 - \beta_\nu l_\nu$. The elements of the rate matrices are

$$\bar{k}^\nu_{xy} \equiv \gamma^\nu_{xy} e^{-(\beta_1/2-a_\nu)(\epsilon_x-\epsilon_y)-(\beta_1 l_1-b_\nu)d_{xy}}. \tag{41}$$

Accordingly, the escape rate $\bar{\lambda}^\nu_y = \bar{\lambda}^\nu_y(a_\nu,b_\nu)$ from state y is

$$\bar{\lambda}^\nu_y \equiv \sum_{x\neq y} \bar{k}^\nu_{xy} = -\bar{k}^\nu_{yy}. \tag{42}$$

We define a total rate matrix by $\bar{\boldsymbol{k}} \equiv \sum_\nu \bar{\boldsymbol{k}}^\nu$ and a total escape-rate vector by $\bar{\lambda} \equiv \sum_\nu \bar{\lambda}^\nu$. These rates are functions of the affinities and dynamical bias; their analogs for the reference process are recovered at the point of vanishing of a and b, namely, $\boldsymbol{k} = \bar{\boldsymbol{k}}(0,0)$ and $\lambda = \bar{\lambda}(0,0)$. For the NE process, the state at time τ is $\bar{z}(\tau)$. A system state trajectory during time

interval $[0,t]$ is denoted $[\bar{z}]$. The ensemble average over all trajectories $[\bar{z}]$ generated with dynamics corresponding to $\bar{\boldsymbol{k}}$ is $\langle\dots\rangle_{\bar{\boldsymbol{k}}}$.

B. Mapping typical NE fluctuations on rare EQ fluctuations

We now connect the statistics of the energy currents, activities, and occupations for the EQ process with the statistics of the same variables for the stationary NE process. This mapping involves the *escape-rate change* $c = c(a,b)$ defined by

$$c \equiv \lambda - \bar{\lambda}, \tag{43}$$

that is zero at vanishing affinities and dynamical biases. We emphasize that c cannot be adjusted independently of a and b. This means that the affinity and the dynamical bias are the central variables in determining the NESS reached by the system.

To connect EQ and NE fluctuations, one needs to redo all the calculations of Secs. II C and II D, but for the NE process, introducing the NE scaled CGF $\bar{\Gamma} = \bar{\Gamma}(\bar{a},\bar{b},\bar{m})$ and LDF $\bar{L} = \bar{L}(j,f,p)$, the NE tilted operator $\bar{\boldsymbol{\kappa}} = \bar{\boldsymbol{\kappa}}(\bar{a},\bar{b},\bar{m})$, the generator of the NE driven process $\bar{\boldsymbol{K}} = \bar{\boldsymbol{K}}(\bar{a},\bar{b},\bar{u})$, and associated escape rate $\bar{\Lambda} = \bar{\Lambda}(\bar{a},\bar{b},\bar{u})$, the affinity increment $2\bar{a}$, the dynamical bias increment $\bar{b}$, the NE drift $\bar{u}$, and the NE escape weight $\bar{m} = \bar{m}(\bar{a},\bar{b},\bar{u})$, all denoted with a bar to distinguish them from their equivalent for the EQ reference process. One obtains all these objects replacing k by $\bar{k}$ and the Lagrange multipliers (a,b,u) by $(\bar{a},\bar{b},\bar{u})$ in all the definitions. For instance, for the NE tilted operator, we have

$$\bar{\kappa}_{yy} \equiv -\sum_{x\neq y,\nu} \bar{k}^{\nu}_{xy} + \bar{m}_y, \tag{44}$$

$$\bar{\kappa}_{xy} \equiv \sum_{\nu} \bar{k}^{\nu}_{xy} e^{\bar{a}_\nu(\epsilon_x-\epsilon_y)+\bar{b}_\nu d_{xy}}. \tag{45}$$

Notice that we call $2\bar{a}$ an affinity "increment" since we already deal with a NE process: a deviation from the typical current is associated with an "increase" of affinity that will make this fluctuation typical. For the same reason, the dynamical bias $\bar{b}$ is also qualified as an increment.

The mapping between EQ and NE fluctuations now comes from the connection between the EQ and NE tilted operators

$$\bar{\boldsymbol{\kappa}}(\bar{a},\bar{b},\bar{m}) = \boldsymbol{\kappa}(\bar{a}+a,\bar{b}+b,\bar{m}+c), \tag{46}$$

that we obtain by comparing Eqs. (35) and (36) with Eqs. (44) and (45). Hence, the same symmetry exists between the eigenvalues and between the eigenvectors: the *full* spectrum of the two operators is connected. In particular, the scaled CGFs are connected by

$$\bar{\Gamma}(\bar{a},\bar{b},\bar{m}) = \Gamma(\bar{a}+a,\bar{b}+b,\bar{m}+c), \tag{47}$$

and, from the Legendre transformation, the LDFs verify

$$\bar{L}(j,f,p) = L(j,f,p) - a^{\dagger}\cdot j - b^{\dagger}\cdot f - c^{\dagger}\cdot p. \tag{48}$$

The left eigenvectors of the tilted operators satisfy

$$\bar{\pi}(\bar{a},\bar{b},\bar{m}) = \pi(\bar{a}+a,\bar{b}+b,\bar{m}+c) \tag{49}$$

or, equivalently,

$$\bar{u}(\bar{a},\bar{b},\bar{m}) = u(\bar{a}+a,\bar{b}+b,\bar{m}+c). \tag{50}$$

The mapping also holds for the right eigenvectors and this leads to

$$\bar{p}(\bar{a},\bar{b},\bar{m}) = p(\bar{a}+a,\bar{b}+b,\bar{m}+c). \tag{51}$$

Finally, the generators of the driven processes also verify

$$\bar{\boldsymbol{K}}(\bar{a},\bar{b},\bar{u}) = \boldsymbol{K}(\bar{a}+a,\bar{b}+b,u), \tag{52}$$

where $\bar{u}$ and u are, respectively, the left- and right-hand sides of Eq. (50).

Thus, the EQ and NE processes are tightly connected and one can focus on the EQ process' fluctuations only: Eq. (47) shows that the statistics of energy currents, activities, and occupations for any NE process with affinity $2a$ and dynamical bias b is known from the statistics of the same variables computed for the EQ process. Indeed, the derivatives of Eq. (47) with respect to $\bar{a}$, $\bar{b}$, or $\bar{m}$ evaluated in $(\bar{a},\bar{b},\bar{m}) = (0,0,0)$ yields the NE cumulants of the energy currents, activities, and occupations from the scaled CGF for the EQ reference process, e.g., for j_ν we have

$$\langle j_\nu[\bar{z}]\rangle_{\bar{k}} = \frac{\partial\bar{\Gamma}}{\partial\bar{a}_\nu}(0,0,0) = \frac{\partial\Gamma}{\partial a_\nu}(a,b,c). \tag{53}$$

Notice that evaluating Eq. (47) at the point of vanishing of $(\bar{a},\bar{b},\bar{m})$ returns by definition of a scaled CGF

$$0 = \bar{\Gamma}(0,0,0) = \Gamma(a,b,c), \tag{54}$$

for all a and b, with $c = (\lambda - \bar{\lambda})$. Accordingly, the total derivatives of $\Gamma(a,b,c)$ with respect to a or b also vanish exactly such that Γ remains constant and equal to zero in the direction (a,b,c). We call the subspace where Γ vanishes the *physical system subspace*: each point (a,b,c) in this subspace defines a precise physical process with affinity $2a$ and dynamical bias b. The function Γ includes the full thermodynamic information on any system defined with the same energy levels ϵ, coupling matrices $\boldsymbol{\gamma}^{\nu}$, and energy barriers $\boldsymbol{d}$ (up to a reservoir specific dilatation), and so does the LDF L. One simply changes the degree of NE or the type of dynamics, encoded into the dilatation factors, by moving into the physical system subspace.

We end by remarking that the idea of mapping EQ and NE fluctuations was first proposed by Andrieux in Ref. [50], but for the statistics of energy currents only. However, this mapping had no concrete application since the NE statistics of the currents were needed to define the EQ dynamics involved in the mapping. On the contrary, the mapping of Eqs. (47) and (48) is explicit, with the price that, when comparing with Ref. [50], the EQ statistics of activities and occupations must be known in addition to the energy currents statistics.

C. Asymptotic equivalence of the driven reference process and the NE process

We now discuss the asymptotic equivalence of the driven reference process and the NE process. We first prove the equality of their escape rates and on the way give a slightly simplified expression of L. Using this result, we demonstrate the equivalence of the path probabilities of the driven reference process and the NE process.

From Eqs. (33) and (54), we find $c + \Lambda - \lambda = 0$. This leads with Eq. (43) to the equality of the escape rates of the driven

reference process and the NE process

$$\Lambda = \bar{\lambda}, \tag{55}$$

even though these two processes are different in general due to the drift u, i.e., $K_{xy} \neq \bar{k}_{xy}$ if $x \neq y$. As a consequence, the LDF is written as

$$L(j,f,p) = a^\dagger \cdot j + b^\dagger \cdot f + c^\dagger \cdot p. \tag{56}$$

The equality of the escape rates indicates that the driven reference process and NE process look alike. Their generators are connected by the similarity transformation

$$\boldsymbol{K} = |\boldsymbol{\pi}| \cdot \bar{\boldsymbol{k}} \cdot |\boldsymbol{\pi}|^{-1}, \tag{57}$$

that follows from the comparison of Eqs. (20) and (41). We denote $|\boldsymbol{\pi}|$ the positive and diagonal matrix obtained by taking the absolute value of the elements of $\boldsymbol{\pi}$. The equality of the diagonal part of the Markov matrices of the two processes is granted by Eq. (55). From this similarity transformation, one can show the asymptotic equality of the path probabilities associated to each process

$$\mathcal{P}_{\boldsymbol{K}}[y] \underset{t\to\infty}{\simeq} \mathcal{P}_{\bar{\boldsymbol{k}}}[y] \tag{58}$$

for any trajectory $[y]$. We have defined the path probabilities knowing the initial state $y(0)$

$$\mathcal{P}_{\bar{\boldsymbol{k}}}[y] \equiv \exp\left(-\int_0^t d\tau \bar{\lambda}_{y(\tau)}\right) \prod_{\tau\in[0,t]} \bar{k}^{\nu(\tau)}_{y(\tau+d\tau)y(\tau)} \tag{59}$$

for the NE process, and

$$\mathcal{P}_{\boldsymbol{K}}[y] \equiv \exp\left(-\int_0^t d\tau \Lambda_{y(\tau)}\right) \prod_{\tau\in[0,t]} K^{\nu(\tau)}_{y(\tau+d\tau)y(\tau)} \tag{60}$$

for the driven reference process. In these equations, the product applies for all times τ at which the system changes of state during the trajectory $[y]$, with $y(\tau)$ [respectively $y(\tau + d\tau)$] the system state before (respectively after) the transition at time τ. The exponential terms appearing in these two path probabilities are equal. Concerning the product terms, they differ from boundary terms only:

$$\begin{aligned}\prod_\tau K^{\nu(\tau)}_{y(\tau+d\tau)y(\tau)} &= \prod_\tau |\pi_{y(\tau+d\tau)}| \bar{k}^{\nu(\tau)}_{y(\tau+d\tau)y(\tau)} |\pi_{y(\tau)}|^{-1}, \\ &= |\pi_{y(t)}| \left(\prod_\tau \bar{k}^{\nu(\tau)}_{y(\tau+d\tau)y(\tau)}\right) |\pi_{y(0)}|^{-1}. \end{aligned} \tag{61}$$

Then, the path probabilities of the driven reference process and NE process verify

$$\lim_{t\to\infty} \frac{1}{t} \ln \frac{\mathcal{P}_{\bar{\boldsymbol{k}}}[y]}{\mathcal{P}_{\boldsymbol{K}}[y]} = 0, \tag{62}$$

and are asymptotically equivalent [29]. Since the driven reference process is the dynamics that typically reproduces the conditioned reference process, we conclude that there is an ensemble equivalence between the NE process and the conditioned reference process. This central result is similar to the path-ensemble equivalence derived in Refs. [29,30]. In Appendix C, we show that the NE process is asymptotically equivalent to the canonical process that is defined by exponentially weighting each trajectory, even though these two processes are not exactly identical.

IV. DISCUSSION AND GENERAL SUMMARY

In Sec. II, we have studied the fluctuations of an EQ system exchanging energy with several heat reservoirs at the same temperature. We have seen that energy may spontaneously flow from one reservoir to another, even if it does not on average. Each of these current fluctuations has been associated to a temperature difference that would typically reproduce it. Similarly, we have shown that a fluctuation of the activity of the exchanges with each reservoir would be typically reproduced by dilating the appropriated energy barriers. From these observations, we have identified two couples of conjugated variables and provided the corresponding LDF and CGF from a variational approach.

In Sec. III, we have considered the fluctuations of the system defined in Sec. II, but driven out of equilibrium by temperature differences between the heat reservoirs. We have found an exact mapping between the statistics of the energy currents, activities, and occupations for the EQ and NE systems. We have also discussed the asymptotic equivalence of the trajectory ensembles generated by the conditioned EQ process and the NE process. From the existence of the mapping between EQ and NE systems, we have concluded that the study of a NE system amounts to the calculation of the probability of rare fluctuations of the same system at EQ. Now that the distinction between the dynamical fluctuations of EQ and NE systems has been dispelled, we come back to the results of Sec. II and summarize the canonical structure satisfied by the two ensembles of NE systems.

A. Summary of the NE canonical structure

The ensemble of systems in contact with several heat reservoirs at different temperatures is called the *metacanonical ensemble*. The trajectories of the systems in the metacanonical ensemble are generated by the NE process with generator $\bar{\boldsymbol{k}}$. All the systems in this ensemble have the same energy levels ϵ_x, and the same dynamical parameters, i.e., energy barriers d_{xy} and couplings with the heat reservoirs γ^ν_{xy}. By convention, the heat reservoir of smallest temperature is the reference reservoir ($\nu = 1$) such that all the affinities $2a_\nu = \beta_1 - \beta_\nu$ are positive. Notice that the temperature of the reference reservoir sets the energy scale and has no physical relevance. On the opposite, the affinities a_ν are the central variables of the metacanonical ensemble that are set by the environmental constraints. The affinities are naturally conjugated to the energy currents. However, we know from the previous sections that considering (a, j) as the unique couple of conjugated variables does not afford to study all NE systems from the same NE potential. Intuitively, a change of an affinity also impacts the system activity and the occupation of the various states. Hence, we have introduced additional intensive variables to take into account these effects separately: the dynamical biases connected to the dilatation factors of the energy barriers and the escape weights modifying the escape probability of each state. These two intensive variables cannot be adjusted independently of the affinities if we want to avoid a change of the system dynamics: no dilatation should be applied to the energy barriers ($l_\nu = 1$ for all ν) yielding to dynamical biases that are equal to the affinities ($b = 2a$); the dynamics should

TABLE II. EQ and NE thermodynamic potentials.

Ensemble	Microcanonical	Canonical	NE microcanonical	Metacanonical
Potential	$s = -\sum_x p_x \ln p_x$	$\varphi = -\ln \langle \exp(-\beta_1 e[z]) \rangle_{\boldsymbol{k}}$	$L(j,f,p)$	$\Gamma(a,b,m)$
Variational principle	max	min	max	max
Free variables	β_1	e	a, b, m	j, f, p
Constrained variables	e	β_1	j, f, p	a, b, m
Physical system subspace			$m(j,f,p) = c(a(j,f,p),b(j,f,p))$	$m = c(a,b)$
No dilatation space			$b(j,f,p) = 2a(j,f,p)$	$b = 2a$
Legendre structure		$s + \varphi = \beta_1 e$	$L + \Gamma = a^\dagger \cdot j + b^\dagger \cdot f + m^\dagger \cdot p$	

conserve the norm of the occupation vector imposing that an affinity must be associated with an escape weight equal to the escape-rate change $m = c(a,2a)$. Therefore, in the metacanonical ensemble, the environment sets the affinity vector a which in turn constrains the dynamical intensive variables, namely, the dynamical biases and the escape weights. The NE potential of the metacanonical ensemble is the CGF of energy currents, activities, and occupations $\Gamma(a,b,m)$. It vanishes for all a when $b = 2a$ and $m = c(a,2a)$, but its partial derivatives with respect to a, b, and m produce all the NESS cumulants of energy currents, activities, and occupations for any affinity. For instance, the thermodynamic behavior follows from the NE equations of state

$$\left.\frac{\partial \Gamma}{\partial a_\nu}\right|_{a_{\setminus\nu},b,m} = j_\nu, \tag{63}$$

$$\left.\frac{\partial \Gamma}{\partial b_\nu}\right|_{a,b_{\setminus\nu},m} = f_\nu, \tag{64}$$

$$\left.\frac{\partial \Gamma}{\partial m_x}\right|_{a,b,m_{\setminus x}} = p_x, \tag{65}$$

where the subscripts on the vertical bars indicate variables that remain constant when taking the partial derivative. We denote $a_{\setminus\nu}$ the vector a without the νth component. The cumulants of EQ thermodynamic variables are obtained with the NESS occupations defined by $p^* = p(a,2a,c)$ that only depend on $\chi - 1$ affinities. The mean energy in the NESS is $\langle e[\bar{z}] \rangle_{\bar{\boldsymbol{k}}} = e(p^*)$, and the mean entropy is $\langle s[\bar{z}] \rangle_{\bar{\boldsymbol{k}}} = s(p^*)$.

The ensemble of systems conditioned on the energy currents they received from their environment is called the *NE microcanonical ensemble*. The trajectories of the systems in this ensemble are generated by the EQ reference process with generator $\boldsymbol{k}$ filtrated to achieve the condition on the energy currents. The physical implementation of systems in the NE microcanonical ensemble would require the existence of energy sources with no fluctuations. These sources will very likely not exist in practice [51], even though this problem is not specific to NE ensembles (see for instance p. 83 of Ref. [3] for an example in EQ thermodynamic theory). If we assume that an energy current can be imposed from the outside, the activities and the occupations must take precise values so that the system can sustain the energy current. On the opposite, the conjugated intensive variables become free to fluctuate. The relationship between currents, activities, and occupations is obtained from the correspondence between the conjugated variables (j,f,p) and (a,b,m), as summarized in Table II. The NE microcanonical potential is the LDF $L(j,f,p)$ and the statistics of the intensive variables (a,b,m) follows from its partial derivative

$$\left.\frac{\partial L}{\partial j_\nu}\right|_{j_{\setminus\nu},f,p} = a_\nu, \tag{66}$$

$$\left.\frac{\partial L}{\partial f_\nu}\right|_{j,f_{\setminus\nu},p} = b_\nu, \tag{67}$$

$$\left.\frac{\partial L}{\partial p_x}\right|_{j,f,p_{\setminus x}} = m_x. \tag{68}$$

We proved in Secs. II and III C the equivalence of the ensembles of trajectories generated by the NE process and the conditioned EQ reference process assuming that the NE potentials are convex. Accordingly, the metacanonical ensemble and NE microcanonical ensembles are ensemble equivalent. In other words, systems submitted to temperature gradients are equivalent, at the thermodynamic level, to systems subjected to stationary energy injection (and extraction). By construction, the NE potentials are conjugated by Legendre transformation

$$L(j,f,p) + \Gamma(a,b,m) = a^\dagger \cdot j + b^\dagger \cdot f + m^\dagger \cdot p, \tag{69}$$

and the NE stationary state can be obtained from a variational approach. If we consider $a^\dagger \cdot j + b^\dagger \cdot f + m^\dagger \cdot p - \Gamma(a,b,m)$ as the potential L that would be obtained from Eq. (69) by assuming the independence of the conjugated variables, then the NESS affinity, dynamical bias, and escape weight reached by the system at constant imposed energy current j, activity f, and occupation p maximize this potential in the subspace of constant (j,f,p):

$$(a,b,m) = \underset{a,b,m|j,f,p}{\operatorname{argmax}} \left[a^\dagger \cdot j + b^\dagger \cdot f + m^\dagger \cdot p - \Gamma(a,b,m)\right], \tag{70}$$

which are exactly Eqs. (63)–(65). The same argument holds the other way around. If we consider $a^\dagger \cdot j + b^\dagger \cdot f + m^\dagger \cdot p - L(j,f,p)$ as the potential Γ that would be obtained from Eq. (69) assuming the independence of the conjugated variables, then the NESS energy currents, activities, and occupations reached by the system at constant imposed affinity a, dynamical bias b, and escape weight m maximize this potential in the subspace of constant (a,b,m):

$$(j,f,p) = \underset{j,f,p|a,b,m}{\operatorname{argmax}} \left[a^\dagger \cdot j + b^\dagger \cdot f + m^\dagger \cdot p - L(j,f,p)\right], \tag{71}$$

which are exactly Eqs. (66)–(68).

B. Symmetries of the NE potentials

The metacanonical potential is even under the sign change of all affinities. We prove in Appendix D that this symmetry leads to the fluctuation theorem (FT), a fundamental result regarding the asymptotic statistics of entropy production first studied in Refs. [52–54]. Another fundamental symmetry is obtained from the equality of second derivatives of the NE potentials. This symmetry is the NE equivalent of the Maxwell relations and reads as

$$\frac{\partial^2\Gamma}{\partial h_\alpha \partial h'_{\alpha'}} = \frac{\partial^2\Gamma}{\partial h'_{\alpha'} \partial h_\alpha} \quad \text{and} \quad \frac{\partial^2 L}{\partial v_\alpha \partial v'_{\alpha'}} = \frac{\partial^2 L}{\partial v'_{\alpha'} \partial v_\alpha}, \tag{72}$$

where h and h' are two vectors in (a,b,m) and similarly v and v' in (j,f,p). The subscripts α and α' indicate two arbitrary components of these vectors. At EQ, Maxwell's relations deeply constrain the number of EQ response coefficients that should be introduced to completely describe a system. Here, they constrain the derivatives of the nonlinear functions giving, for instance, the currents in terms of the affinities. In the close-to-EQ limit, Eq. (72) implies that the linear response matrix is symmetric or, in other words, it implies the Onsager reciprocity relations [55,56], as we will see in the next section.

C. NE linear response theory

We study the linear response of a system in an arbitrary NESS and further perturbed by a change of temperature $\beta_\nu \to \beta'_\nu = \beta_\nu + \Delta\beta_\nu$ or of dilatation factor $l_\nu \to l'_\nu = l_\nu + \Delta l_\nu$. More precisely, we want to determine the change of the energy currents and activities when the half affinities $a_\nu = (\beta_1 - \beta_\nu)/2$ and dynamical biases $b_\nu = (\beta_1 l_1 - \beta_\nu l_\nu)$ are slightly changed to the new values $a_\nu + \Delta a_\nu$ and $b_\nu + \Delta b_\nu$. We assume that l_1 and β_1 do not change during the perturbation. Then, the perturbations are written as

$$\Delta a_\nu = -\Delta\beta_\nu/2, \tag{73}$$

$$\begin{aligned}\Delta b_\nu &= (-\beta_\nu + 2\Delta a_\nu)\Delta l_\nu + 2 l_\nu \Delta a_\nu \\ &\simeq -\beta_\nu \Delta l_\nu + 2 l_\nu \Delta a_\nu\end{aligned} \tag{74}$$

at linear order. We remark that the dynamical biases change when perturbing the affinities, but the converse is not true.

A Taylor expansion of the metacanonical potential Γ gives the following quadratic function:

$$\begin{aligned}&\Gamma(a+\Delta a, b+\Delta b, m+\Delta m) \\ &\quad = \Gamma(a,b,m) + \sum_{h=a,b,m} \Delta h^\dagger \cdot \nabla_h \Gamma \\ &\qquad + \frac{1}{2} \sum_{\substack{h=a,b,m \\ h'=a,b,m}} \Delta h^\dagger \cdot \nabla_{hh'}\Gamma \cdot \Delta h',\end{aligned} \tag{75}$$

where Δm is not yet specified. We have used the short notations for the derivatives of the metacanonical potential

$$(\nabla_h \Gamma)_\alpha \equiv \frac{\partial \Gamma}{\partial h_\alpha}(a,b,m), \tag{76}$$

$$(\nabla_{hh'}\Gamma)_{\alpha\alpha'} \equiv \frac{\partial^2 \Gamma}{\partial h_\alpha \partial h'_{\alpha'}}(a,b,m). \tag{77}$$

The perturbation induces a variation Δj of the energy currents, Δf of the activities or Δp of the occupation. Taking the partial derivative of Eq. (75) with respect to Δa, Δb, or Δm and evaluated in $\Delta m = \Delta c$, with Δc the variation of the escape-rate change due to the perturbation, leads to the linear response equation

$$\begin{pmatrix}\Delta j \\ \Delta f \\ \Delta p\end{pmatrix} \simeq \begin{bmatrix}\nabla_{aa}\Gamma & \nabla_{ab}\Gamma & \nabla_{am}\Gamma \\ \nabla_{ba}\Gamma & \nabla_{bb}\Gamma & \nabla_{bm}\Gamma \\ \nabla_{ma}\Gamma & \nabla_{mb}\Gamma & \nabla_{mm}\Gamma\end{bmatrix} \cdot \begin{pmatrix}\Delta a \\ \Delta b \\ \Delta c\end{pmatrix}. \tag{78}$$

From Eq. (72), the response matrix above is symmetric even close to an arbitrary NESS. However, the chain rule yields

$$\Delta c = \nabla_a c \cdot \Delta a + \nabla_b c \cdot \Delta b, \tag{79}$$

and the variation of the currents and activities becomes

$$\begin{aligned}\Delta j =& (\nabla_{aa}\Gamma + \nabla_{am}\Gamma \cdot \nabla_a c) \cdot \Delta a \\ &+ (\nabla_{ab}\Gamma + \nabla_{am}\Gamma \cdot \nabla_b c) \cdot \Delta b,\end{aligned} \tag{80}$$

$$\begin{aligned}\Delta f =& (\nabla_{ab}\Gamma + \nabla_{bm}\Gamma \cdot \nabla_a c) \cdot \Delta a \\ &+ (\nabla_{bb}\Gamma + \nabla_{bm}\Gamma \cdot \nabla_b c) \cdot \Delta b.\end{aligned} \tag{81}$$

The response matrix defined from Eqs. (80) and (81) is no longer symmetric in general as already emphasized in former works on NE linear response theory [38,39,57–62]. The second derivatives of the metacanonical potential appearing in Eq. (80) are

$$\begin{aligned}(\nabla_{aa}\Gamma)_{\nu\nu'} &= \lim_{t\to\infty} t\big\{\langle j_\nu[\bar z] j_{\nu'}[\bar z]\rangle_{\bar k} - \langle j_\nu[\bar z]\rangle_{\bar k}\langle j_{\nu'}[\bar z]\rangle_{\bar k}\big\}, \\ (\nabla_{ab}\Gamma)_{\nu\nu'} &= \lim_{t\to\infty} t\big\{\langle j_\nu[\bar z] f_{\nu'}[\bar z]\rangle_{\bar k} - \langle j_\nu[\bar z]\rangle_{\bar k}\langle f_{\nu'}[\bar z]\rangle_{\bar k}\big\}, \\ (\nabla_{am}\Gamma)_{\nu x} &= \lim_{t\to\infty} t\big\{\langle j_\nu[\bar z] p_x[\bar z]\rangle_{\bar k} - \langle j_\nu[\bar z]\rangle_{\bar k}\langle p_x[\bar z]\rangle_{\bar k}\big\},\end{aligned} \tag{82}$$

and correspond, respectively, to the current-current, the current-activity, and the current-occupation covariances in the unperturbed NESS [63]. In addition to the above covariances, the response functions include another contribution involving the derivatives of the escape-rate change c. Since the escape-rate change satisfies

$$-\frac{\partial c_x}{\partial a_\nu} = \sum_y \bar k^\nu_{yx}(\epsilon_y - \epsilon_x), \tag{83}$$

the unperturbed mean occupation multiplied by this derivative returns the unperturbed mean energy current

$$-\sum_x \frac{\partial c_x}{\partial a_\nu}\langle p_x[\bar z]\rangle_{\bar k} = \sum_{x,y} \bar k^\nu_{yx}\langle p_x[\bar z]\rangle_{\bar k}(\epsilon_y - \epsilon_x) = \langle j_\nu[\bar z]\rangle_{\bar k}. \tag{84}$$

Therefore, the response to the affinity perturbation is

$$\begin{aligned}&(\nabla_{aa}\Gamma + \nabla_{am}\Gamma \cdot \nabla_a c)_{\nu\nu'} \\ &\quad = \lim_{t\to\infty} t\left\{\langle j_\nu[\bar z] j_{\nu'}[\bar z]\rangle_{\bar k} - \left\langle j_\nu[\bar z]\frac{\partial}{\partial a_{\nu'}}(p^\dagger[\bar z]\cdot\bar\lambda)\right\rangle_{\bar k}\right\}.\end{aligned} \tag{85}$$

As expected, the response has an additive structure with an equilibriumlike part given by a currents correlation function, and a NE part corresponding to a current and traffic-excess

correlation function. We call traffic excess the derivative of the empirical escape rate $p^\dagger[\bar{z}]\cdot\bar{\lambda}$ with respect to the perturbed variable [38,39]. Similarly, the response of the energy current to a perturbation of the dynamical bias in the second line of Eq. (80) has two parts with an activity-current correlation function and a current-traffic excess correlation function.

As regards the perturbation of an EQ system, i.e., all β'_ν are close to the reference inverse temperature β_1, one recovers the Yamamoto-Zwanzig formula expressing the response coefficients to a temperature perturbation from the covariances of energy currents [64,65]. In order to see this, let us first consider a reference system at EQ only perturbed by a change of the dilatation factors, i.e., $\Delta a = 0$ and $\Delta b = -\beta_1 \Delta l$. Thanks to Eq. (80), the variation of the energy currents is written as

$$\Delta j = (\nabla_{ab}\Gamma + \nabla_{am}\Gamma\cdot\nabla_b c)\cdot\Delta b = 0. \tag{86}$$

It vanishes for any perturbations Δb since no mean energy current exists at EQ. Thus, we find

$$\nabla_{ab}\Gamma + \nabla_{am}\Gamma\cdot\nabla_b c = 0, \tag{87}$$

if the derivatives are taken in $a = 0$. This removes the contribution due to the dynamical bias from the EQ response. Another contribution disappears in the close-to-equilibrium limit due to the decoupling between occupations and energy currents [42]. Indeed, from the symmetry of the metacanonical potential with sign change of the affinities, namely $\Gamma(a,b,m) = \Gamma(-a,b,m)$, we have

$$\frac{\partial^2\Gamma}{\partial a_\nu \partial m_x}(a,b,m) = -\frac{\partial^2\Gamma}{\partial a_\nu \partial m_x}(-a,b,m). \tag{88}$$

Accordingly, $\nabla_{am}\Gamma = 0$ if the derivatives are taken in $a = 0$. From the third line of Eq. (82), we can conclude that the energy currents and occupations are decoupled. The Yamamoto-Zwanzig formula follows from Eq. (80):

$$\Delta j = \frac{\nabla_{aa}\Gamma}{2}\cdot(\beta_1 - \beta'), \tag{89}$$

where $\nabla_{aa}\Gamma$ is given in the first line of Eq. (82) with EQ averages $\langle\dots\rangle_{\boldsymbol{k}}$ instead of the NE averages $\langle\dots\rangle_{\bar{\boldsymbol{k}}}$. Therefore, we recover the Onsager reciprocity relations from the NE Maxwell relations.

V. ILLUSTRATIVE EXAMPLE: A TWO-LEVEL SYSTEM

We now illustrate our results on a two-level system with states $z = 1,2$ and mechanisms $\nu = 1,2,\dots,\chi$ enabling energy exchanges with χ different heat reservoirs. The coupling strength with reservoir ν is denoted γ_ν in this section since it is not a matrix but a vector when there are only two states. The energy states are ϵ_1 and ϵ_2. Let $\epsilon_\pm = \epsilon_1 \pm \epsilon_2$ to shorten notations. The transition rate matrix of the EQ reference process for each mechanism ν is

$$\boldsymbol{k}^\nu = \begin{bmatrix} -\gamma_\nu e^{\frac{\beta_1\epsilon_-}{2}} & \gamma_\nu e^{-\frac{\beta_1\epsilon_-}{2}} \\ \gamma_\nu e^{\frac{\beta_1\epsilon_-}{2}} & -\gamma_\nu e^{-\frac{\beta_1\epsilon_-}{2}} \end{bmatrix}, \tag{90}$$

where we assume vanishing dilatation factors l_1 [see Eq. (1)]. The rate matrices for the NE system are

$$\bar{\boldsymbol{k}}^\nu = \begin{bmatrix} -\gamma_\nu e^{(\beta_1/2-a_\nu)\epsilon_- + b_\nu\epsilon_+} & \gamma_\nu e^{-(\beta_1/2-a_\nu)\epsilon_- + b_\nu\epsilon_+} \\ \gamma_\nu e^{(\beta_1/2-a_\nu)\epsilon_- + b_\nu\epsilon_+} & -\gamma_\nu e^{-(\beta_1/2-a_\nu)\epsilon_- + b_\nu\epsilon_+} \end{bmatrix}, \tag{91}$$

if we choose $d_{12} = \epsilon_+$. The escape-rate changes for this model are

$$c_1 = \sum_\nu \gamma_\nu e^{\beta_1\epsilon_-/2}(1 - e^{-a_\nu\epsilon_- + b_\nu\epsilon_+}), \tag{92}$$

$$c_2 = \sum_\nu \gamma_\nu e^{-\beta_1\epsilon_-/2}(1 - e^{a_\nu\epsilon_- + b_\nu\epsilon_+}). \tag{93}$$

The tilted operator $\boldsymbol{\kappa} = \boldsymbol{\kappa}(a,b,m)$ for the EQ reference system is

$$\boldsymbol{\kappa} = \begin{bmatrix} -\sum_\nu \gamma_\nu e^{\frac{\beta_1\epsilon_-}{2}} + m_1 & \sum_\nu \gamma_\nu \epsilon^{-(\beta_1/2-a_\nu)\epsilon_- + b_\nu\epsilon_+} \\ \sum_\nu \gamma_\nu e^{(\beta_1/2-a_\nu)\epsilon_- + b_\nu\epsilon_+} & -\sum_\nu \gamma_\nu \epsilon^{-\frac{\beta_1\epsilon_-}{2}} + m_2 \end{bmatrix}. \tag{94}$$

The highest eigenvalue of this matrix is the metacanonical potential

$$\Gamma = -\sum_\nu \gamma_\nu \cosh(\beta_1\epsilon_-/2) + \frac{m_1+m_2}{2} + \sqrt{\hat{\gamma}^2 + \sum_{\nu,\nu'}\gamma_\nu\gamma_{\nu'}e^{(a_\nu - a_{\nu'})\epsilon_- + (b_\nu + b_{\nu'})\epsilon_+}}, \tag{95}$$

where we have introduced

$$\hat{\gamma} \equiv -\sum_\nu \gamma_\nu \sinh\left(\frac{\beta_1\epsilon_-}{2}\right) + \frac{m_1 - m_2}{2}. \tag{96}$$

The metacanonical potential Γ provides the statistics of j_α the energy current flowing from the αth reservoir toward the system and of f_α the activity induced by the αth mechanism. From direct derivation of Γ with respect to a_α, b_α, or m_z, the energy current coming from reservoir $\alpha > 1$ is

$$j_\alpha = \frac{\sum_\nu \epsilon_-\gamma_\alpha\gamma_\nu e^{(b_\nu + b_\alpha)\epsilon_+}\sinh[(a_\alpha - a_\nu)\epsilon_-]}{\sqrt{\hat{\gamma}^2 + \sum_{\nu,\nu'}\gamma_\nu\gamma_{\nu'}e^{(a_\nu - a_{\nu'})\epsilon_- + (b_\nu + b_{\nu'})\epsilon_+}}}, \tag{97}$$

the activity for the transitions induced by mechanism α is

$$f_\alpha = \frac{\sum_\nu \epsilon_+\gamma_\alpha\gamma_\nu e^{(b_\nu + b_\alpha)\epsilon_+}\cosh[(a_\alpha - a_\nu)\epsilon_-]}{\sqrt{\hat{\gamma}^2 + \sum_{\nu,\nu'}\gamma_\nu\gamma_{\nu'}e^{(a_\nu - a_{\nu'})\epsilon_- + (b_\nu + b_{\nu'})\epsilon_+}}}, \tag{98}$$

and the occupation of state z is

$$p_z = \frac{1}{2} + \frac{(\delta_{z,1} - \delta_{z,2})\hat{\gamma}/2}{\sqrt{\hat{\gamma}^2 + \sum_{\nu,\nu'}\gamma_\nu\gamma_{\nu'}e^{(a_\nu - a_{\nu'})\epsilon_- + (b_\nu + b_{\nu'})\epsilon_+}}}, \tag{99}$$

where $\hat{\gamma}$ of Eq. (96) is evaluated in $m = c(a,2a)$, and taking $b = 2a$ to obtain the mean values of j, f, and p in the NESS with affinity $2a$. Deriving once more with respect to $a_{\alpha'}$, $b_{\alpha'}$, or $m_{z'}$ leads to the symmetric response matrix [see Eq. (78)]. The left and right eigenvectors of $\boldsymbol{\kappa}$ associated to the eigenvalue Γ are, respectively, π and $r = \boldsymbol{\pi}^{-1}\cdot p$. We find for the two-level

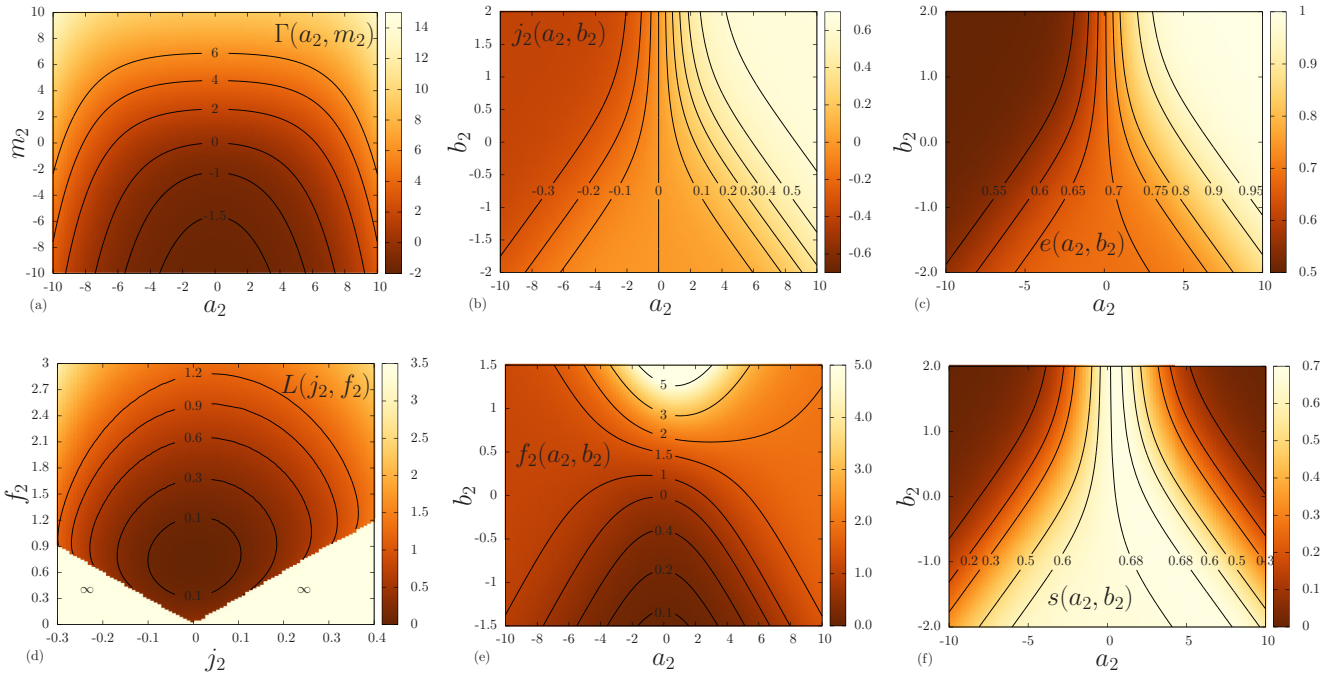

FIG. 3. (a) Metacanonical potential for various (a_2,m_2) with $b = 0$, (b) energy current, (c) energy, (e) activity, and (f) entropy as a function of the affinity a_2 and the dynamical bias b_2. (d) NE microcanonical potential for the energy current j_2 and the activity f_2 after a contraction on f_1, p_1, and p_2. Other parameters are $b_1 = 0$, $\beta_2 = \beta_1 - 2a_2$, $\gamma_2 = 0.5$, $\epsilon_1 = 1$, and $\epsilon_2 = 0.5$. For all figures, $\beta_1 = 1$ set the energy scale and $\gamma_1 = 1$ the time scale. The variables a and b are in unit of $1/\beta_1$, the variables j and f are in unit of γ_1/β_1, and L, Γ, and m are in unit of γ_1.

model

$$\pi_1 = \frac{\sum_\nu \gamma_\nu e^{(\beta_1/2-a_\nu)\epsilon_- + b_\nu \epsilon_+}}{\sum_\nu \gamma_\nu e^{(\beta_1/2-a_\nu)\epsilon_- + b_\nu \epsilon_+} + \sum_\nu \gamma_\nu e^{\beta_1 \epsilon_-/2} - m_1 + \Gamma}, \tag{100}$$

$$\pi_2 = \frac{\sum_\nu \gamma_\nu e^{\beta_1 \epsilon_-/2} - m_1 + \Gamma}{\sum_\nu \gamma_\nu e^{(\beta_1/2-a_\nu)\epsilon_- + b_\nu \epsilon_+} + \sum_\nu \gamma_\nu e^{\beta_1 \epsilon_-/2} - m_1 + \Gamma}, \tag{101}$$

$$r_1 = \frac{\left(\sum_\nu \gamma_\nu e^{-(\beta_1/2-a_\nu)\epsilon_- + b_\nu \epsilon_+}\right)\left(\sum_\nu \gamma_\nu e^{(\beta_1/2-a_\nu)\epsilon_- + b_\nu \epsilon_+} + \sum_\nu \gamma_\nu e^{\beta_1 \epsilon_-/2} - m_1 + \Gamma\right)}{\sum_{\nu,\nu'} \gamma_\nu \gamma_{\nu'} e^{(a_\nu - a_{\nu'})\epsilon_- + (b_\nu + b_{\nu'})\epsilon_+} + \left(\sum_\nu \gamma_\nu e^{\beta_1 \epsilon_-/2} - m_1 + \Gamma\right)^2}, \tag{102}$$

$$r_2 = \frac{\left(\sum_\nu \gamma_\nu e^{\beta_1 \epsilon_-/2} - m_1 + \Gamma\right)\left(\sum_\nu \gamma_\nu e^{(\beta_1/2-a_\nu)\epsilon_- + b_\nu \epsilon_+} + \sum_\nu \gamma_\nu e^{\beta_1 \epsilon_-/2} - m_1 + \Gamma\right)}{\sum_{\nu,\nu'} \gamma_\nu \gamma_{\nu'} e^{(a_\nu - a_{\nu'})\epsilon_- + (b_\nu + b_{\nu'})\epsilon_+} + \left(\sum_\nu \gamma_\nu e^{\beta_1 \epsilon_-/2} - m_1 + \Gamma\right)^2}. \tag{103}$$

We can now illustrate the consistency of the theory: from Eqs. (100)–(103) and the product $\boldsymbol{\pi} \cdot r$, we recover the NESS probability of Eq. (99) obtained from derivation of the metacanonical potential; Eqs. (100) and (101) allow us to compute the drift u to get the current and activity of Eqs. (97) and (98) from Eqs. (25) and (26) knowing the NESS probability.

We turn to the discussion of the properties of the two-level system with $\chi = 2$ heat reservoirs in light of Fig. 3 obtained from our analytic results. For simplicity, we choose $b_1 = 0$. We set the energy scale and the time scale taking, respectively, $\beta_1 = 1$ and $\gamma_1 = 1$. Figure 3(a) shows that the metacanonical potential is a symmetric function of the affinity a_2 and is strictly convex. From this symmetry, one should not conclude that the energy current j_2 is an antisymmetric function of a_2. Indeed, the energy current comes from the derivative of the metacanonical potential with respect to a_2 evaluated in $m = c$ that has no particular symmetry when changing the sign of a_2.

The absolute value of the energy current $|j_2|$ and the activity f_2 always increases with the absolute value of the affinity $|a_2|$ at given dynamical bias b_2 [see Figs. 3(b) and 3(e)]. A decrease of $|j_2|$ with increasing $|a_2|$ would mean that the system has negative response for some affinities. Such a behavior is not expected for a simple two-level model. Another general trend is that $|j_2|$ and f_2 increase with b_2. Indeed, a higher dynamical bias increases the value of the transition rates corresponding to $\nu = 2$, if one has $\epsilon_+ > 0$ [see Eq. (91)]. Then, a high dynamical bias accelerates the dynamics associated to reservoir $\nu = 2$, whereas a small one slows it down, letting the reference dynamics associated to reservoir $\nu = 1$ dominates in the transition rate matrix. Therefore, in the limit of low dynamical bias with respect to the affinity, the system approaches the

EQ state at temperature β_1, with current j_2 and activity f_2 decreasing to zero.

To represent the NE microcanonical potential L, one has to focus on the statistics of some specific variables by contraction: this step consists in evaluating the NE microcanonical potential at the mean value of the disregarded variables, for instance, f_1, p_1, and p_2 in the case of Fig. 3(d). However, it is much more convenient to obtain $L(j_2, f_2)$ directly from a parametric plot of (j_2, f_2, L) with (a_2, b_2) being the parameters and taking $b_1 = 0$. In this way, we have obtained Fig. 3(d) showing the NE microcanonical potential as a convex function of (j_2, f_2). This function is undefined in the regions corresponding to low activities in comparison to the energy current. The explanation is that a current can only flow if some minimal activity holds, i.e., if the system changes state regularly enough.

Finally, the system energy e and Shannon entropy s are, in our framework, functions of the affinity and dynamical bias. We see in Figs. 3(c) and 3(f) that these functions have a very similar shape in a large area corresponding to the EQ limit. The dimensionless free energy of the reference system at temperature β_1 is $\varphi = \beta_1 e - s$ and should reach its minimum value for low affinity $|a_2|$ or low dynamical bias b_2. There, since $\beta_1 = 1$, the system energy and entropy differ only in the value of the dimensionless free energy of the EQ reference system. On the contrary, at high affinity $|a_2|$, most of the time the system is either in energy state $\epsilon_1 = 1$ for positive a_2 or $\epsilon_2 = 0.5$ for negative a_2. The system is driven to a state where the entropy is lower than at EQ and the NE mean energy is moved away from the EQ mean value for the reference process.

VI. CONCLUSION

In this paper, we have established that the asymptotic probability of the energy currents, the activities, and the occupations in a NE process proceeds from the long-time statistics of the same variables at EQ. We have connected the affinities of the NE process, the dynamical biases, and the escape-rate changes to constraints imposed on the EQ reference process, respectively, on the energy currents, on the activities, and on the occupations of each state. This connection is the analog of the ensemble equivalence between the canonical and microcanonical ensembles of EQ statistical physics for which the temperature of the heat reservoir is associated to an energy constraint. We have argued that the mapping between EQ and NE fluctuations allows us to distinguish the reduced set of variables which play a key role in the description of NESSs.

Beyond the understanding of the structure of NE statistical physics, phenomenological and/or operational methods must be developed to compute the NE potentials of real complex systems. In this regard, it was shown that efficient algorithms exist to compute the scaled cumulants of currents [66] or to simulate samples of rare trajectories [13]. A promising technique for macroscopic systems relies on the saddle point approximation of a path integral producing the cumulant generating function [67]. This calculation leads to a dynamical problem with a small number of degrees of freedom compared to the original problem. Solving this dynamical problem seems easier than finding the highest eigenvalue of a large tilted operator.

ACKNOWLEDGMENTS

I thank M. Polettini and D. Lacoste for their useful comments on the manuscript and U. Dimitrijević for her careful rereading. I also thank A. Engel and A. Rançon for the enlightening discussions concerning, respectively, the large deviation theory (Appendix A) and the calculation of asymptotic probabilities (Appendix B).

APPENDIX A: LDF OF EMPIRICAL OCCUPATION AND TRANSITION PROBABILITY

We derive in this appendix the LDF of transition probability and occupation $I(\boldsymbol{\omega}, p)$ for the EQ process. By definition, the probability that $\boldsymbol{\omega}[z] = \boldsymbol{\omega}$ and $p[z] = p$ when the system trajectories are generated by the EQ reference process is

$$P_t(\boldsymbol{\omega}, p) = \sum_{[z]} \mathcal{P}_{\boldsymbol{k}}[z] \delta_{p,p[z]} \delta_{\boldsymbol{\omega},\boldsymbol{\omega}[z]} \tag{A1}$$

$$= \sum_{[z]} \mathcal{P}_{\boldsymbol{\omega}/p}[z] e^{-\mathcal{A}[z]} \delta_{p,p[z]} \delta_{\boldsymbol{\omega},\boldsymbol{\omega}[z]}, \tag{A2}$$

where $\sum_{[z]}$ is the sum over all path $[z]$. We have introduced the action

$$\mathcal{A}[z] = \ln \frac{\mathcal{P}_{\boldsymbol{\omega}/p}[z]}{\mathcal{P}_{\boldsymbol{k}}[z]}, \tag{A3}$$

and the path probabilities with given initial state $z(0)$:

$$\mathcal{P}_{\boldsymbol{k}}[z] = \exp\left(- \int_0^t d\tau \sum_{x \neq z(\tau), \nu} k^{\nu}_{xz(\tau)} \right) \prod_{\tau \in [0,t]} k^{\nu(\tau)}_{z(\tau+d\tau)z(\tau)},$$

$$\mathcal{P}_{\boldsymbol{\omega}/p}[z] = \exp\left(- \int_0^t d\tau \sum_{x \neq z(\tau), \nu} \frac{\omega^{\nu}_{xz(\tau)}}{p_{z(\tau)}} \right) \prod_{\tau \in [0,t]} \frac{\omega^{\nu(\tau)}_{z(\tau+d\tau)z(\tau)}}{p_{z(\tau)}}.$$

Notice that the second line is identical to the first line where the empirical transition rate matrices $\boldsymbol{\omega}^{\nu}[z]/p[z]$ replace the real EQ rate matrices $\boldsymbol{k}^{\nu}$. From these path probabilities, the action becomes

$$\mathcal{A}[z] = \int_0^t d\tau \sum_{x \neq z(\tau), \nu} \left(k^{\nu}_{xz(\tau)} - \frac{\omega^{\nu}_{xz(\tau)}}{p_{z(\tau)}} \right) + \sum_{\tau \in [0,t]} \ln \frac{\omega^{\nu(\tau)}_{z(\tau+d\tau)z(\tau)}}{k^{\nu(\tau)}_{z(\tau+d\tau)z(\tau)} p_{z(\tau)}} \tag{A4}$$

or, equivalently, when introducing the empirical transition probabilities and occupations

$$\mathcal{A}[z] = \int_0^t d\tau \sum_{y, x \neq y, \nu} \delta_{y,z(\tau)} \left(k^{\nu}_{xy} - \frac{\omega^{\nu}_{xy}}{p_y} \right) + \sum_{\tau \in [0,t]} \sum_{y, x \neq y, \nu} \delta_{x,z(\tau+d\tau)} \delta_{y,z(\tau)} \delta_{\nu,\nu(\tau)} \ln \frac{\omega^{\nu}_{xy}}{k^{\nu}_{xy} p_y}$$

$$= t \sum_{x, y \neq x, \nu} \left[p_y[z] \left(k^{\nu}_{xy} - \frac{\omega^{\nu}_{xy}}{p_y} \right) + \omega_{xy}[z] \ln \frac{\omega^{\nu}_{xy}}{k^{\nu}_{xy} p_y} \right]. \tag{A5}$$

Then, using the Kronecker symbols in Eq. (A2) one can take $p[z] = p$ and $\boldsymbol{\omega}[z] = \boldsymbol{\omega}$ to move the action out of the sum and write

$$P_t(\boldsymbol{\omega}, p) = e^{-tI(\boldsymbol{\omega},p)} \sum_{[z]} \mathcal{P}_{\boldsymbol{\omega}/p}[z] \delta_{p,p[z]} \delta_{\boldsymbol{\omega},\boldsymbol{\omega}[z]}. \tag{A6}$$

The remaining sum over all paths $[z]$ is the probability that $p[z]$ and $\boldsymbol{\omega}[z]$ take their typical value since the path probability is generated by $\boldsymbol{\omega}/p$. We expect this probability to converge to 1 in the long-time limit. Then, we get the asymptotic probability of transitions and occupations of Eqs. (10) and (11) in the main text.

APPENDIX B: PREEXPONENTIAL FACTOR FOR THE ASYMPTOTIC PROBABILITY OF ENERGY CURRENTS, ACTIVITIES, AND OCCUPATIONS

Following, we provide an asymptotic approximation of the long-time probability of the energy currents, activities, and occupations when the final state is known. The variables are defined by

$$j_\nu[z] = \frac{1}{t} \sum_{\tau\in[0,t]} [\epsilon_{z(\tau+d\tau)} - \epsilon_{z(\tau)}] \delta_{\nu,\nu(\tau)}, \tag{B1}$$

$$f_\nu[z] = \frac{1}{t} \sum_{\tau\in[0,t]} d_{z(\tau+d\tau)z(\tau)} \delta_{\nu,\nu(\tau)}, \tag{B2}$$

$$p_x[z] = \frac{1}{t} \int_0^t d\tau\, \delta_{x,z(\tau)}. \tag{B3}$$

The corresponding generating function with given final state x is by definition

$$g_x(a,b,m) \equiv \left\langle \delta_{xz(t)} e^{t(a^\dagger\cdot j[z] + b^\dagger \cdot f[z] + m^\dagger \cdot p[z])} \right\rangle_{\boldsymbol{k}}. \tag{B4}$$

It satisfies the linear equation $\partial g/\partial t = \boldsymbol{\kappa} \cdot g$ with $\boldsymbol{\kappa}$ the tilted operator defined in the main text in Eqs. (35) and (36). We now look for a long-time asymptotic approximation of g:

$$g_x(a,b,m) = \left(e^{\boldsymbol{\kappa}(a,b,m)t} \cdot p^0\right)_x \tag{B5}$$

$$\underset{t\to\infty}{\simeq} \sum_y e^{\Gamma(a,b,m)t} (r\cdot\pi^\dagger)_{xy} p^0_y \tag{B6}$$

$$\underset{t\to\infty}{\simeq} e^{\Gamma(a,b,m)t} r_x(a,b,m)(\pi^\dagger \cdot p^0), \tag{B7}$$

where p^0 is the initial state probability. We remind that π and r are, respectively, the left and right eigenvectors of $\boldsymbol{\kappa}$ for the highest eigenvalue Γ. Using an asymptotic approximation to compute the inverse Laplace transformation of $g_x(a,b,m)$, one recovers the exponent appearing in Eq. (12).

Then, the preexponential factor in Eq. (B7) must be evaluated in $a = a(j,f,p)$, $b = b(j,f,p)$, and $m = m(j,f,p)$. We now assume that j, f, and p are related to each other via the physical system subspace constraint (see Table II). From Eq. (49), we find $\pi_x(a,b,c) = \bar{\pi}_x(0,0,0) = 1$ for all x, where the second equality stands from the fact that the left eigenvector of a Markov matrix has all its components equal to one. Then, $\pi^\dagger \cdot p^0 = 1$ by normalization of p^0 and the right eigenvector of κ in the physical system subspace is the NESS probability $r(a,b,c) = p^*$ for the dynamics with energy current j and activity f. This leads to the asymptotic probability of energy currents, activities, and occupations when the final state at time t is x:

$$P_t(j,f,p^*,x) \underset{t\to\infty}{\simeq} e^{-tL(j,f,p^*)} p^*_x. \tag{B8}$$

APPENDIX C: ASYMPTOTIC EQUIVALENCE OF THE NE PROCESS AND THE CANONICAL PROCESS

The path probability of the canonical process, with generator $\mathcal{K}$, is defined by exponentially weighting the path probability of the EQ reference process:

$$\mathcal{P}_{\mathcal{K}}[y] \equiv \frac{\mathcal{P}_{\boldsymbol{k}}[y] e^{t(a^\dagger\cdot j[y] + b^\dagger\cdot f[y] + m^\dagger\cdot p[y])}}{\langle e^{t(a^\dagger\cdot j[z] + b^\dagger\cdot f[z] + m^\dagger\cdot p[z])}\rangle_{\boldsymbol{k}}}. \tag{C1}$$

This tilting procedure is sometimes referred to as canonical conditioning. We show in this appendix that the above canonical process is asymptotically equivalent to the NE process defined in Sec. III A. From Sec. III C, it is also equivalent to the driven process. The connection between the driven process and the canonical process was first obtained in Refs. [33,34] and studied in depth in Refs. [29,31].

From the definition of the CGF in Eq. (29), we have

$$\mathcal{P}_{\mathcal{K}}[y] \underset{t\to\infty}{\simeq} \mathcal{P}_{\boldsymbol{k}}[y] e^{t(a^\dagger\cdot j[y] + b^\dagger\cdot f[y] + m^\dagger\cdot p[y]) - t\Gamma}. \tag{C2}$$

Since Eq. (33) is satisfied for all y, we can write it for any state $y(\tau)$ along the trajectory $[y]$:

$$\Gamma = m_{y(\tau)} + \Lambda_{y(\tau)} - \lambda_{y(\tau)}, \tag{C3}$$

and upon integration over the time τ, one finds

$$t\Gamma = tm^\dagger \cdot p[y] + \int_0^t d\tau (\bar{\lambda}_{y(\tau)} - \lambda_{y(\tau)}) \tag{C4}$$

since $\Lambda = \bar{\lambda}$ from Eq. (55). Finally, Eqs. (C2)–(C4) lead to the asymptotic equivalence of the path probabilities

$$\mathcal{P}_{\mathcal{K}}[y] \underset{t\to\infty}{\simeq} e^{-\int_0^t d\tau \bar{\lambda}_{y(\tau)} + t(a^\dagger\cdot j[y] + b^\dagger\cdot f[y])} \prod_{\tau\in[0,t]} k^{\nu(\tau)}_{y(\tau+d\tau)y(\tau)}$$

$$\underset{t\to\infty}{\simeq} e^{-\int_0^t d\tau \bar{\lambda}_{y(\tau)}} \prod_{\tau\in[0,t]} \bar{k}^{\nu(\tau)}_{y(\tau+d\tau)y(\tau)} \tag{C5}$$

$$\underset{t\to\infty}{\simeq} \mathcal{P}_{\bar{\boldsymbol{k}}}[y]. \tag{C6}$$

Hence, we have proved that the canonical process corresponds at long time to a NE process that can be realized experimentally changing the temperatures of the heat reservoirs and the dynamical biases.

APPENDIX D: FLUCTUATION THEOREM

The fluctuation theorem (FT) is an essential property of the stochastic entropy production [36,68]. According to this theorem, a stochastic positive entropy production is exponentially more likely than the opposite entropy production, i.e., an entropy destruction. On average, this implies a positive entropy production in agreement with the second law. Therefore, the FT is a probabilistic statement of the second law, and as such it is a very fundamental property of NE phenomena. It was first derived with a long-time approximation, but since the mean entropy production always increases, a FT should hold at all time [69,70]. Because the entropy production may be

appropriately defined using different NE variables such as work, heat, or particle currents, depending on the experimental setup, the FT has many faces [56,71–78]. Generally, the joint probability distribution of a set of time antisymmetric variables summing to entropy production will satisfy a FT [79]. In our case, a linear combination of the currents gives the entropy production rate

$$\sigma = 2a^\dagger \cdot j. \tag{D1}$$

Accordingly, the LDF and scaled CGF for the NE process have a FT symmetry. This symmetry strongly relies on local detailed balance, in other words, on the symmetry of transition rates. We already used the local detailed balance to show the equivalence of EQ and NE fluctuations. We show in this appendix that the fluctuation theorem is a consequence of the mapping between EQ and NE fluctuations associated to the symmetric nature of energy-currents fluctuations at EQ. Using Eq. (47), we find

$$\begin{aligned}\bar{\Gamma}(-2a-\bar{a},\bar{b},\bar{m}) &= \Gamma(-2a-\bar{a}+a,\bar{b}+b,\bar{m}+c)\\ &= \Gamma(\bar{a}+a,\bar{b}+b,\bar{m}+c\bar{b}+b,\bar{m}+c)\\ &= \bar{\Gamma}(\bar{a},\bar{b},\bar{m}),\end{aligned} \tag{D2}$$

where we have used the fact that EQ fluctuations are symmetric in the reversal of affinities $\Gamma(a,b,m) = \Gamma(-a,b,m)$. Similarly, from Eq. (48), it is straightforward to see that

$$\bar{L}(j,f,p) - \bar{L}(-j,f,p) = -2a^\dagger \cdot j = -\sigma \tag{D3}$$

since we have $L(j,f,p) = L(-j,f,p)$.

[1] L. D. Landau and E. Lifshitz, *Mechanics, Course of Theoretical Physics*, 3rd ed. (Butterworth-Heinemann, London, 1976).
[2] M. Born and E. Wolf, *Principles of Optics*, 6th ed. (Cambridge University Press, Cambridge, UK, 1999).
[3] H. B. Callen, *Thermodynamics and an Introduction to Thermostatistics*, 2nd ed. (Wiley, New York, 1985).
[4] Y. Oono, Prog. Theor. Phys. Suppl. **99**, 165 (1989).
[5] H. Touchette, Phys. Rep. **478**, 1 (2009).
[6] J. P. Garrahan, R. L. Jack, V. Lecomte, E. Pitard, K. van Duijvendijk, and F. van Wijland, J. Phys. A: Math. Theor. **42**, 075007 (2009).
[7] F. Turci and E. Pitard, Europhys. Lett. **94**, 10003 (2011).
[8] T. Speck, A. Malins, and C. P. Royall, Phys. Rev. Lett. **109**, 195703 (2012).
[9] T. Nemoto, V. Lecomte, S. I. Sasa, and F. van Wijland, J. Stat. Mech. (2014) P10001.
[10] G. Z. Hertz and G. D. Stormo, Bioinformatics **15**, 563 (1999).
[11] D. Lacoste, A. W. C. Lau, and K. Mallick, Phys. Rev. E **78**, 011915 (2008).
[12] F. Ritort, Adv. Chem. Phys. **137**, 31 (2008).
[13] C. Giardina, J. Kurchan, V. Lecomte, and J. Tailleur, J. Stat. Phys. **145**, 787 (2011).
[14] G. L. Eyink, Phys. Rev. E **54**, 3419 (1996).
[15] G. L. Eyink, Prog. Theor. Phys. Suppl. **130**, 77 (1998).
[16] Y. Oono and M. Paniconi, Prog. Theor. Phys. Suppl. **130**, 29 (1998).
[17] L. Bertini, A. De Sole, D. Gabrielli, G. Jona-Lasinio, and C. Landim, J. Stat. Phys. **107**, 635 (2002).
[18] L. Bertini, A. De Sole, D. Gabrielli, G. Jona-Lasinio, and C. Landim, Rev. Mod. Phys. **87**, 593 (2015).
[19] T. Bodineau and B. Derrida, Phys. Rev. Lett. **92**, 180601 (2004).
[20] B. Derrida, J. Stat. Mech. (2007) P07023.
[21] V. Lecomte, C. Appert-Rolland, and F. van Wijland, Phys. Rev. Lett. **95**, 010601 (2005).
[22] V. Lecomte, C. Appert-Rolland, and F. van Wijland, J. Stat. Phys. **127**, 51 (2007).
[23] R. M. Evans, Contemp. Phys. **51**, 413 (2010).
[24] A. Baule and R. M. L. Evans, Phys. Rev. Lett. **101**, 240601 (2008).
[25] A. Baule and R. M. L. Evans, J. Stat. Mech. (2010) P03030.
[26] C. Monthus, J. Stat. Mech. (2011) P03008.
[27] C. Maes and K. Netočný, Europhys. Lett. **82**, 30003 (2008).
[28] T. Nemoto and S. I. Sasa, Phys. Rev. E **84**, 061113 (2011).
[29] R. Chétrite and H. Touchette, Annales Henri Poincaré **16**, 2005 (2015).
[30] R. Chétrite and H. Touchette, Phys. Rev. Lett. **111**, 120601 (2013).
[31] R. Chétrite and H. Touchette, J. Stat. Mech. (2015) P12001.
[32] C. Giardinà, J. Kurchan, and L. Peliti, Phys. Rev. Lett. **96**, 120603 (2006).
[33] J. P. Garrahan and I. Lesanovsky, Phys. Rev. Lett. **104**, 160601 (2010).
[34] R. L. Jack and P. Sollich, Prog. Theor. Phys. Suppl. **184**, 304 (2010).
[35] J. Szavits-Nossan and M. R. Evans, J. Stat. Mech. (2015) P12008.
[36] C. Van den Broeck and M. Esposito, Physica A (Amsterdam) **418**, 6 (2015).
[37] N. Van Kampen, *Stochastic Processes in Physics and Chemistry*, 3rd ed. (North-Holland, Amsterdam, 2007).
[38] M. Baiesi, C. Maes, and B. Wynants, Phys. Rev. Lett. **103**, 010602 (2009).
[39] M. Baiesi, C. Maes, and B. Wynants, J. Stat. Phys. **137**, 1094 (2009).
[40] P. Baerts, U. Basu, C. Maes, and S. Safaverdi, Phys. Rev. E **88**, 052109 (2013).
[41] M. Polettini, J. Phys. A: Math. Theor. **48**, 365005 (2015).
[42] B. Wynants, Ph.D. thesis, Universiteit K.U. Leuven, 2010, arXiv:1011.4210.
[43] L. Bertini, A. Faggionato, and D. Gabrielli, Ann. Henri Poincaré **51**, 867 (2015).
[44] I. Prigogine, *Introduction to Thermodynamics of Irreversible Processes*, 2nd ed. (Wiley, New York, 1955).
[45] T. D. Donder, *L'Affinité* (Lamertin, Bruxelles, 1927).
[46] T. Tomé and M. J. de Oliveira, Phys. Rev. E **91**, 042140 (2015).
[47] D. Andrieux and P. Gaspard, J. Stat. Phys. **127**, 107 (2007).
[48] D. Andrieux and P. Gaspard, J. Stat. Mech. (2007) P02006.
[49] J. L. Lebowitz and H. Spohn, J. Stat. Phys. **95**, 333 (1999).
[50] D. Andrieux, arXiv:1208.5699; arXiv:1212.1807.
[51] Beyond the case of energy sources, one can imagine an experimental setup where a matter flux or a rate of volume increase can be controlled exactly.

[52] G. Bochkov and Y. Kuzovlev, Physica A (Amsterdam) **106**, 443 (1981).
[53] D. J. Evans and D. J. Searles, Phys. Rev. E **50**, 1645 (1994).
[54] G. Gallavotti and E. G. D. Cohen, Phys. Rev. Lett. **74**, 2694 (1995).
[55] L. Onsager, Phys. Rev. **37**, 405 (1931).
[56] D. Andrieux and P. Gaspard, J. Chem. Phys. **121**, 6167 (2004).
[57] G. Verley, K. Mallick, and D. Lacoste, Europhys. Lett. **93**, 10002 (2011).
[58] G. Verley, R. Chétrite, and D. Lacoste, J. Stat. Mech. (2011) P10025.
[59] T. Speck and U. Seifert, Europhys. Lett. **74**, 391 (2006).
[60] R. Chétrite, G. Falkovich, and K. Gawedzki, J. Stat. Mech. (2008) P08005.
[61] R. Chétrite and K. Gawedzki, J. Stat. Phys. **137**, 890 (2009).
[62] U. Seifert and T. Speck, Europhys. Lett. **89**, 10007 (2010).
[63] We have multiplied the covariances by a factor t since we consider time-averaged variables; we would have divided by t if we were considering the time-integrated variables.
[64] T. Yamamoto, J. Chem. Phys. **33**, 281 (1960).
[65] R. Zwanzig, Annu. Rev. Phys. Chem. **16**, 67 (1965).
[66] A. Wachtel, J. Vollmer, and B. Altaner, Phys. Rev. E **92**, 042132 (2015).
[67] J. Ross, *Thermodynamics and Fluctuations Far from Equilibrium* (Springer, Berlin, 2008).
[68] U. Seifert, Rep. Prog. Phys. **75**, 126001 (2012).
[69] G. Bulnes Cuetara, M. Esposito, and A. Imparato, Phys. Rev. E **89**, 052119 (2014).
[70] M. Polettini and M. Esposito, J. Stat. Mech. (2014) P10033.
[71] C. Jarzynski, Phys. Rev. Lett. **78**, 2690 (1997).
[72] K. Kurchan, J. Phys. A: Math. Gen. **31**, 3719 (1998).
[73] G. E. Crooks, Phys. Rev. E **61**, 2361 (2000).
[74] U. Seifert, Phys. Rev. Lett. **95**, 040602 (2005).
[75] T. Sagawa and M. Ueda, Phys. Rev. Lett. **104**, 090602 (2010).
[76] M. Esposito and C. Van den Broeck, Phys. Rev. Lett. **104**, 090601 (2010).
[77] G. Verley, R. Chétrite, and D. Lacoste, Phys. Rev. Lett. **108**, 120601 (2012).
[78] A. Crisanti, M. Picco, and F. Ritort, Phys. Rev. Lett. **110**, 080601 (2013).
[79] R. García-García, D. Domínguez, V. Lecomte, and A. B. Kolton, Phys. Rev. E **82**, 030104 (2010).

C.2.4 Erratum for section III.C of Ref. [5] in C.2.3

In section III.C of Ref. [5], I discuss the equivalence of two processes introduced in the article: The nonequilibrium process and the driven process. The latter is built from the Doob transform of the equilibrium process biased on occupancy, energy currents, and the activity of the exchanges with the heat reservoirs. Actually, the two processes are only equivalent when they are identical. Therefore, the section should not discuss the equivalence of these processes, but their identity. We explain this in the following, using equation numbers of Ref. [5].

The drift potential $u(a, b, m)$ is used in a Doob transform of the transition rates to transform the tilted operator of Eqs. (35–36) into the driven generator of Eqs. (19–21). This potential guaranties that $m_y + \Lambda_x - \lambda_x = \Gamma$ is constant for all x as shown in Eq. (33). If the escape weight is $m_x = c_x = \lambda_x - \bar{\lambda}_x$, then the drift potential is chosen such that $\Lambda_x - \bar{\lambda}_x = 0$ is a null constant when using Eq. (54). But the only difference between the escape rate Λ and $\bar{\lambda}$ is just due to the drift potential u_x, when comparing Eqs. (19–21) and Eqs. (41–42). Therefore, $u_x = 0$ is the solution to $\Lambda_x - \bar{\lambda}_x = 0$: the NE and driven processes are identical. Now, the drift potential is non-zero for an escape weight that is not the escape rate change, i.e., when $m \neq c$. For time asymptotic equivalence of processes, the similarity transformation on the transition rates is unimportant: it leads to boundary terms. However, it is important for the exponential part of the path probabilities of Eqs. (59–60) that are not asymptotically equivalent in this case. To conclude and contrarily to what I thought at the time of publishing Ref. [5], there is no driven process that is different, but equivalent, at the path level with respect to the nonequilibrium process.

C.3 Conductance matrix for TiPS

Bertini et *al* derived the LDF of state occupancy and empirical transition probability for Markov jump processes in TiPS [97]. Building on their results with Lydia Chabane and Raphaël Chétrite, we studied the Doob transformation of biased Markov generators for systems under time-periodic drivings [19]. We obtained the generator of the driven process whose typical trajectories produce rare events of the unbiased original process. As already argued in Chapter A, and also extensively done in my Ph.D. thesis, we can extend to TiPS many results obtained for systems in stationary states, for instance quadratic bounds of LDF [116]. The tightest quadratic bound for the LDF of physical currents has not been reported for TiPS yet. Based on joint work with Hadrien Vroylandt and Lydia Chabane, I quickly derive this bound below. In this section, I follow the steps of the stationary case; see Ref. [9] reproduced in section B.3.4 and Ref. [10]. The main idea is to use an occupancy and empirical probability current ansatz based on the mean probability and current in the TiPS. The probability current ansatz includes a phase-dependent term that satisfies current conservation at each graph vertex and for any phase. This term allows us to describe rather accurately the fluctuations of physical currents in the neighborhood of their mean values.

We start by reviewing the works on the LDF of occupancy and empirical probability current at phase φ of the periods for a Markov jump process. We also review the derivation of a quadratic bound of this LDF. In the last section, I provide a surprisingly simple and quadratic bound for the LDF of physical currents related to our result in the stationary state.

C.3.1 LDF of currents and occupancy for TiPS

Let us consider that the transition rate matrix $\boldsymbol{k}^\varphi$ is time-periodic with period $\mathscr{T}$. The corresponding TiPS probability, denoted $\boldsymbol{\pi}^\varphi$, satisfies

$$\partial_\varphi \boldsymbol{\pi}^\varphi = \boldsymbol{k}^\varphi \boldsymbol{\pi}^\varphi, \tag{C43}$$

where $\varphi \in [0, \mathscr{T}]$ is the phase. The state occupancy vector at phase φ is denoted $\boldsymbol{p}^\varphi$. The empirical transition probability at phase φ is denoted $\boldsymbol{\omega}^\varphi$. After n periods, they are defined by

$$p_x^\varphi[z] \doteq \frac{1}{n}\sum_{m=0}^{n-1} \delta_{x,z(\varphi+mT)} \tag{C44}$$

$$\omega_{xy}^\varphi[z] \doteq \frac{1}{n}\sum_{m=0}^{n-1} \delta_{x,z(\varphi^+ +mT)}\delta_{y,z(\varphi^- +mT)} \tag{C45}$$

where $[z]$ is as before a trajectory in state space and $\varphi^\pm$ denotes a phase infinitesimally close to φ (higher or lower). Then, the LDF of occupancy and empirical transition probability writes

$$\mathscr{I}(\boldsymbol{\omega}, \boldsymbol{p}) = \frac{1}{\mathscr{T}}\int_0^{\mathscr{T}} \mathrm{d}\varphi \sum_{x,y\neq x,\nu} \left[k_{xy,\nu}^\varphi p_y^\varphi - \omega_{xy,\nu}^\varphi + \omega_{xy,\nu}^\varphi \ln \frac{\omega_{xy,\nu}^\varphi}{k_{xy,\nu}^\varphi p_y^\varphi} \right], \tag{C46}$$

$$= \frac{1}{\mathscr{T}}\int_0^{\mathscr{T}} \mathrm{d}\varphi\, I^\varphi(\boldsymbol{\omega}^\varphi, \boldsymbol{p}^\varphi), \tag{C47}$$

where $I^\varphi(\boldsymbol{\omega}^\varphi, \boldsymbol{p}^\varphi)$ is identical to $I(\boldsymbol{\omega}, \boldsymbol{p})$ of Eq. (C3) if we omit all the phase dependencies (we may do so by abuse of notation, on boldface letters mainly). The above LDF is finite when

$$\partial_\varphi p_x^\varphi = \sum_{y,\nu} (\omega_{xy,\nu}^\varphi - \omega_{yx,\nu}^\varphi), \qquad \text{(current conservation)} \tag{C48}$$

$$\sum_x p_x^\varphi = 1, \qquad \text{(normalization)} \tag{C49}$$

$$\boldsymbol{p}^0 = \boldsymbol{p}^{\mathscr{T}} \quad \text{and} \quad \boldsymbol{\omega}^0 = \boldsymbol{\omega}^{\mathscr{T}}. \qquad \text{(periodicity)} \tag{C50}$$

The (xy,ν) edge component of the empirical current $\boldsymbol{j}^\varphi$ at phase φ and its (conditioned) mean value write:

$$j_{xy,\nu}^\varphi = \omega_{xy,\nu}^\varphi - \omega_{yx,\nu}^\varphi, \tag{C51}$$

$$\langle j_{xy,\nu}^\varphi \rangle_{\boldsymbol{\pi}} \doteq \langle \omega_{xy,\nu}^\varphi \rangle_{\boldsymbol{\pi}} - \langle \omega_{yx,\nu}^\varphi \rangle_{\boldsymbol{\pi}} = k_{xy,\nu}^\varphi \pi_y^\varphi - k_{yx,\nu}^\varphi \pi_x^\varphi, \tag{C52}$$

$$\langle j_{xy,\nu}^\varphi \rangle_{\boldsymbol{p}} \doteq \langle \omega_{xy,\nu}^\varphi \rangle_{\boldsymbol{p}} - \langle \omega_{yx,\nu}^\varphi \rangle_{\boldsymbol{p}} = k_{xy,\nu}^\varphi p_y^\varphi - k_{yx,\nu}^\varphi p_x^\varphi, \tag{C53}$$

where $\langle \dots \rangle_{\boldsymbol{\pi}}$ is mean value in TiPS and $\langle \dots \rangle_{\boldsymbol{p}}$ is mean value in TiPS conditioned on observing an occupancy $\boldsymbol{p}^\varphi$ at any phase $\varphi \in [0, \mathscr{T}]$. With those notations, we write the LDF of occupancy and empirical transition probability, ignoring half (reverse) transition as

$$I^\varphi_{\langle \boldsymbol{\omega} \rangle_{\boldsymbol{p}}}(\boldsymbol{\omega}, \boldsymbol{p}) \doteq \sum_{x,y>x,\nu} \left[\langle \omega^\varphi_{xy,\nu} \rangle_{\boldsymbol{p}} - \omega^\varphi_{(xy,\nu)} + \omega^\varphi_{(xy,\nu)} \ln \frac{\omega^\varphi_{(xy,\nu)}}{\langle \omega^\varphi_{xy,\nu} \rangle_{\boldsymbol{p}}} \right]. \tag{C54}$$

where the sum runs over unidirectional transitions [i.e., on all oriented edges $e = (xy, \nu)$ without the opposite edge $-e = (yx, \nu)$]. Then, $I^\varphi(\boldsymbol{\omega}, \boldsymbol{p})$ is such that

$$I^\varphi(\boldsymbol{\omega}, \boldsymbol{p}) = I^\varphi_{\langle \boldsymbol{\omega} \rangle_{\boldsymbol{p}}}(\boldsymbol{\omega}, \boldsymbol{p}) + I^\varphi_{\langle \boldsymbol{\omega} - \boldsymbol{j} \rangle_{\boldsymbol{p}}}(\boldsymbol{\omega} - \boldsymbol{j}, \boldsymbol{p}) \tag{C55}$$

because $\omega_{-e} = \omega_e - j_e$. We look for the optimum $\boldsymbol{\omega}$ that minimizes $I^\varphi(\boldsymbol{\omega}, \boldsymbol{p})$ and is compatible with a given empirical transition current $\boldsymbol{j}^\varphi$ as defined in Eq. (C51). The optimization with respect to $\boldsymbol{\omega}$ of Eq. (C55) leads to

$$\ln \frac{\omega_e(\omega_e - j_e)}{\langle \omega_e \rangle_{\boldsymbol{p}} \langle \omega_e - j_e \rangle_{\boldsymbol{p}}} = 0 \quad \Leftrightarrow \quad \ln \frac{\omega_e \omega_{-e}}{\langle \omega_e \rangle_{\boldsymbol{p}} \langle \omega_{-e} \rangle_{\boldsymbol{p}}} = 0. \tag{C56}$$

If we introduce $(a_e^{\varphi,\boldsymbol{p}})^2 \doteq 4 \langle \omega_e \rangle_{\boldsymbol{p}} \langle \omega_{-e} \rangle_{\boldsymbol{p}}$ that will be useful later, the optimization leading to Eq. (C56) writes explicitly as

$$\omega_e^2 - \omega_e j_e - (a_e^{\varphi,\boldsymbol{p}})^2/4 = 0 \quad \Leftrightarrow \quad 4\omega_e \omega_{-e} = (a_e^{\varphi,\boldsymbol{p}})^2. \tag{C57}$$

We remark that by definition $(a_e^{\varphi,\boldsymbol{p}})^2 = 4 \langle \omega_e \rangle_{\boldsymbol{p}} \langle \omega_e - j_e \rangle_{\boldsymbol{p}}$ which leads to almost the same equation

$$\langle \omega_e \rangle_{\boldsymbol{p}}^2 - \langle \omega_e \rangle_{\boldsymbol{p}} \langle j_e \rangle_{\boldsymbol{p}} - (a_e^{\varphi,\boldsymbol{p}})^2/4 = 0 \quad \Leftrightarrow \quad 4 \langle \omega_e \rangle_{\boldsymbol{p}} \langle \omega_{-e} \rangle_{\boldsymbol{p}} = (a_e^{\varphi,\boldsymbol{p}})^2. \tag{C58}$$

The solutions of Eqs. (C56–C58) read

$$\omega^\varphi_{\pm e} = \frac{1}{2} \left[\pm j_e^\varphi + \sqrt{(j_e^\varphi)^2 + (a_e^{\varphi,\boldsymbol{p}})^2} \right] \qquad \text{(at the optimum)}, \tag{C59}$$

$$\langle \omega^\varphi_{\pm e} \rangle_{\boldsymbol{p}} = \frac{1}{2} \left[\pm \langle j_e^\varphi \rangle_{\boldsymbol{p}} + \sqrt{\langle j_e^\varphi \rangle_{\boldsymbol{p}}^2 + (a_e^{\varphi,\boldsymbol{p}})^2} \right], \tag{C60}$$

since the empirical transition probabilities are nonnegative. The phase-dependent LDF of Eq. (C55)

$$I^\varphi(\boldsymbol{\omega}, \boldsymbol{p}) = \sum_{e>0} \left(\langle \omega_e^\varphi \rangle_{\boldsymbol{p}} - \omega_e^\varphi + \langle \omega_{-e}^\varphi \rangle_{\boldsymbol{p}} - \omega_{-e}^\varphi + \omega_e^\varphi \ln \frac{\omega_e^\varphi}{\langle \omega_e^\varphi \rangle_{\boldsymbol{p}}} + \omega_{-e}^\varphi \ln \frac{\omega_{-e}^\varphi}{\langle \omega_{-e}^\varphi \rangle_{\boldsymbol{p}}} \right) \tag{C61}$$

becomes when using $\boldsymbol{\omega}^\varphi$ obtained at the optimum [117]

$$I^\varphi(\boldsymbol{j}, \boldsymbol{p}) = \sum_{e>0} \left[\sqrt{\langle j_e^\varphi \rangle_{\boldsymbol{p}}^2 + (a_e^{\varphi,\boldsymbol{p}})^2} - \sqrt{(j_e^\varphi)^2 + (a_e^{\varphi,\boldsymbol{p}})^2} + j_e^\varphi \left(\operatorname{asinh} \frac{j_e^\varphi}{a_e^{\varphi,\boldsymbol{p}}} - \operatorname{asinh} \frac{\langle j_e^\varphi \rangle_{\boldsymbol{p}}}{a_e^{\varphi,\boldsymbol{p}}} \right) \right]. \tag{C62}$$

The sum on $e > 0$ is over unidirectional transitions again. To reach this form, we have used

$$\omega^{\varphi}_{\pm e} = \pm\frac{j^{\varphi}_e}{2} + \frac{\omega^{\varphi}_e + \omega^{\varphi}_{-e}}{2} \tag{C63}$$

to evaluate

$$\omega^{\varphi}_e \ln\frac{\omega^{\varphi}_e}{\langle\omega^{\varphi}_e\rangle_{\boldsymbol{p}}} + \omega^{\varphi}_{-e}\ln\frac{\omega^{\varphi}_{-e}}{\langle\omega^{\varphi}_{-e}\rangle_{\boldsymbol{p}}} = \frac{j^{\varphi}_e}{2}\ln\frac{\omega^{\varphi}_e}{\omega^{\varphi}_{-e}} + \frac{j^{\varphi}_e}{2}\ln\frac{\langle\omega^{\varphi}_{-e}\rangle_{\boldsymbol{p}}}{\langle\omega^{\varphi}_e\rangle_{\boldsymbol{p}}}. \tag{C64}$$

We remark that the additional term that should appear in the above equation

$$\frac{\omega^{\varphi}_e + \omega^{\varphi}_{-e}}{2}\ln\frac{\omega^{\varphi}_e\omega^{\varphi}_{-e}}{\langle\omega^{\varphi}_e\rangle_{\boldsymbol{p}}\langle\omega^{\varphi}_{-e}\rangle_{\boldsymbol{p}}} = 0 \tag{C65}$$

has been removed at the optimum due to Eq. (C56). Finally, using $\operatorname{asinh} X = \ln(X + \sqrt{1+X^2}) = -\operatorname{asinh}(-X)$, we finds

$$\pm\frac{j^{\varphi}_e}{2}\ln\omega^{\varphi}_{\pm e} = \pm\frac{j^{\varphi}_e}{2}\ln\frac{a^{\varphi,\boldsymbol{p}}_e}{2}\left[\frac{\pm j^{\varphi}_e}{a^{\varphi,\boldsymbol{p}}_e} + \sqrt{1+(\frac{j^{\varphi}_e}{a^{\varphi,\boldsymbol{p}}_e})^2}\right], \tag{C66}$$

$$= \pm\frac{j^{\varphi}_e}{2}\ln\frac{a^{\varphi,\boldsymbol{p}}_e}{2} + \frac{j^{\varphi}_e}{2}\operatorname{asinh}\frac{j^{\varphi}_e}{a^{\varphi,\boldsymbol{p}}_e}, \tag{C67}$$

and then

$$\frac{j^{\varphi}_e}{2}\ln\frac{\omega^{\varphi}_e}{\omega^{\varphi}_{-e}} = j^{\varphi}_e\operatorname{asinh}\frac{j^{\varphi}_e}{a^{\varphi,\boldsymbol{p}}_e}, \tag{C68}$$

$$\frac{j^{\varphi}_e}{2}\ln\frac{\langle\omega^{\varphi}_{-e}\rangle_{\boldsymbol{p}}}{\langle\omega^{\varphi}_e\rangle_{\boldsymbol{p}}} = j^{\varphi}_e\operatorname{asinh}\frac{\langle j^{\varphi}_e\rangle_{\boldsymbol{p}}}{a^{\varphi,\boldsymbol{p}}_e}, \tag{C69}$$

allowing to conclude on the contracted LDF of Eq. (C62). We remark that we use an abuse of notation when taking the same letter for the contracted LDF and the original one, the variables indicating which function to use.

C.3.2 Quadratic upper bound for current and occupancy LDF in TiPS

The phase-dependent LDF of Eq. (C62) has a quadratic upper bound [116, 118]. This can be seen directly by introducing the two functions

$$\psi(X) \doteq \sqrt{1+X^2} - \sqrt{1+\langle X\rangle_{\boldsymbol{p}}} + X(\operatorname{asinh} X - \operatorname{asinh}\langle X\rangle_{\boldsymbol{p}}), \tag{C70}$$

$$\psi_{\text{quad}}(X) \doteq \frac{\operatorname{asinh}(\langle X\rangle_{\boldsymbol{p}})}{2\langle X\rangle_{\boldsymbol{p}}}(X - \langle X\rangle_{\boldsymbol{p}})^2 \geq \psi(X), \tag{C71}$$

where the last inequality holds for all $\langle X\rangle_{\boldsymbol{p}}$ as illustrated on Fig. C.4. The above functions are used to write the LDF and define its quadratic upper bound as

$$I^{\varphi}(\boldsymbol{j},\boldsymbol{p}) = \sum_{e>0} a^{\varphi,\boldsymbol{p}}_e\,\psi\left(\frac{j^{\varphi}_e}{a^{\varphi,\boldsymbol{p}}_e}\right), \tag{C72}$$

$$I^{\varphi}_{\text{quad}}(\boldsymbol{j},\boldsymbol{p}) \doteq \sum_{e>0} a^{\varphi,\boldsymbol{p}}_e\,\psi_{\text{quad}}\left(\frac{j^{\varphi}_e}{a^{\varphi,\boldsymbol{p}}_e}\right). \tag{C73}$$

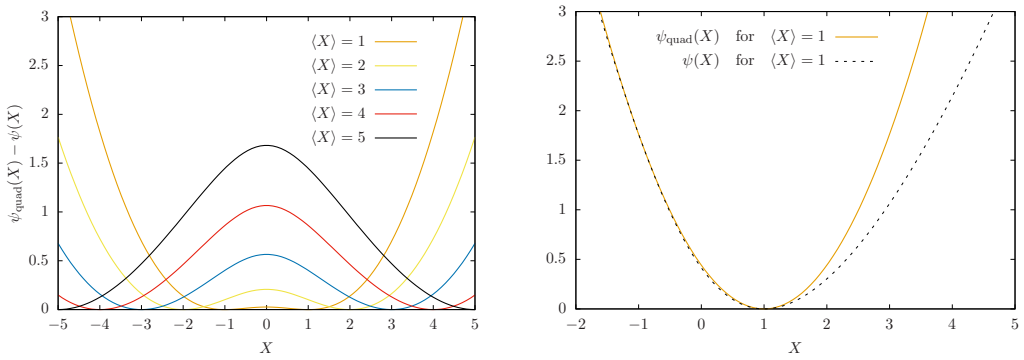

Figure C.4: (Left) Quadratic upper bound for the edge contribution into the LDF of current and occupancy minus the exact edge contribution. (Right) The function $\psi(X)$ is the black dashed line, and its quadratic upper bound $\psi_{\mathrm{quad}}(X)$ is the orange solid line. The bound is rather tight on a large interval.

Then, since the inequality of Eq. (C71) holds for any edge, it holds for the LDF:

$$I^{\varphi}(\boldsymbol{j},\boldsymbol{p}) \leq I^{\varphi}_{\mathrm{quad}}(\boldsymbol{j},\boldsymbol{p}). \tag{C74}$$

Explicitly, the quadratic bound of the LDF writes

$$I^{\varphi}_{\mathrm{quad}}(\boldsymbol{j},\boldsymbol{p}) = \sum_{e>0} \frac{\operatorname{asinh}(\langle j^{\varphi}_e\rangle_{\boldsymbol{p}}/a^{\varphi,\boldsymbol{p}}_e)}{2\langle j^{\varphi}_e\rangle_{\boldsymbol{p}}}(j^{\varphi}_e - \langle j^{\varphi}_e\rangle_{\boldsymbol{p}})^2 \doteq \sum_{e>0}\frac{1}{4}r^{\varphi,\boldsymbol{p}}_e(j^{\varphi}_e - \langle j^{\varphi}_e\rangle_{\boldsymbol{p}})^2, \tag{C75}$$

where we have introduce the phase-dependent quantities $r^{\varphi,\boldsymbol{p}}_e \doteq f^{\varphi,\boldsymbol{p}}_e/\langle j^{\varphi}_e\rangle_{\boldsymbol{p}}$ as the edge resistance, and

$$f^{\varphi,\boldsymbol{p}}_e \doteq \ln\frac{\langle\omega^{\varphi}_e\rangle_{\boldsymbol{p}}}{\langle\omega^{\varphi}_{-e}\rangle_{\boldsymbol{p}}} = 2\operatorname{asinh}\left(\frac{\langle j^{\varphi}_e\rangle_{\boldsymbol{p}}}{a^{\varphi,\boldsymbol{p}}_e}\right), \tag{C76}$$

as the thermodynamic force conjugated to probability current j^{φ}_e. In the end, the occupancy and current LDF for TiPS has an upper bound that is very similar to the one of nonequilibrium stationary states:

$$\mathscr{I}(\boldsymbol{j},\boldsymbol{p}) \leq \mathscr{I}_{\mathrm{quad}}(\boldsymbol{j},\boldsymbol{p}) \doteq \frac{1}{\mathscr{T}}\int_0^{\mathscr{T}} \mathrm{d}\varphi\,\frac{1}{4}\,(\boldsymbol{j}^{\varphi} - \langle\boldsymbol{j}^{\varphi}\rangle_{\boldsymbol{p}})^T\,\boldsymbol{r}^{\varphi,\boldsymbol{p}}(\boldsymbol{j}^{\varphi} - \langle\boldsymbol{j}^{\varphi}\rangle_{\boldsymbol{p}}) \tag{C77}$$

with $\boldsymbol{r}^{\varphi,\boldsymbol{p}}$ the diagonal resistance matrix in edge space whose eth component is $r^{\varphi,\boldsymbol{p}}_e$.

C.3.3 Conductance matrix for TiPS from optimizing the quadratic LDF bound

Using the quadratic upper bound of a LDF greatly simplifies the constraint optimization problem arising from the contraction principle. Using this principle on both sides of the inequality of Eq. (C77) automatically leads to an upper bound

for the contracted LDF. Hence, our goal in the following is to derive the quadratic bound for the (time-averaged) physical current vector $\boldsymbol{i}$ of x component i_X

$$\boldsymbol{i} \doteq \frac{1}{\mathscr{T}} \int_0^{\mathscr{T}} \mathrm{d}\varphi\, \boldsymbol{\phi}^\varphi \boldsymbol{j}^\varphi \quad \Leftrightarrow \quad i_X \doteq \frac{1}{\mathscr{T}} \int_0^{\mathscr{T}} \mathrm{d}\varphi\, \phi^\varphi_{X,e} j^\varphi_e \tag{C78}$$

where the matrix $\boldsymbol{\phi}^\varphi$ of components $\phi^\varphi_{X,e}$ is the amount of physical quantity labeled by x received by the system when transition e occurs at phase φ. For later use, we can also introduce $\boldsymbol{\Phi}^\varphi$ of components $\Phi^\varphi_{X,c} \doteq \sum_e \phi^\varphi_{X,e}\mathcal{C}_{e,c} = (\boldsymbol{\phi}^\varphi\boldsymbol{\mathcal{C}})_{X,c}$ that corresponds to the amount of physical quantity labeled by x received by the system when all the transitions in cycle c have been achieved, although in successive periods such that each transition only occurs at phase φ. We recall that $\boldsymbol{\mathcal{C}}$ is the cycle matrix defined in section B.3.2. In the TiPS, the physical current time averages to

$$\langle \boldsymbol{i} \rangle_{\boldsymbol{\pi}} \doteq \frac{1}{\mathscr{T}} \int_0^{\mathscr{T}} \mathrm{d}\varphi\, \boldsymbol{\phi}^\varphi \langle \boldsymbol{j}^\varphi \rangle_{\boldsymbol{\pi}}. \tag{C79}$$

We report below the result of the above constraint optimization problem fixing a physical current vector $\boldsymbol{i}$, and when $\boldsymbol{p} = \boldsymbol{\pi}$. To deal with the choice of occupancy, we use that $\inf_{\boldsymbol{p}} \mathscr{I}(\boldsymbol{j}, \boldsymbol{p}) \leq \mathscr{I}(\boldsymbol{j}, \boldsymbol{\pi})$. The optimal edge probability current reads

$$\boldsymbol{j}^\varphi = \langle \boldsymbol{j}^\varphi \rangle_{\boldsymbol{\pi}} + \boldsymbol{\mathcal{C}} (\boldsymbol{R}^\varphi)^{-1} (\boldsymbol{\Phi}^\varphi)^T \boldsymbol{g}^{-1} (\boldsymbol{i} - \langle \boldsymbol{i} \rangle_{\boldsymbol{\pi}}) \tag{C80}$$

$$\boldsymbol{g} \doteq \frac{1}{\mathscr{T}} \int_0^{\mathscr{T}} \mathrm{d}\varphi\, \boldsymbol{\Phi}^\varphi (\boldsymbol{R}^\varphi)^{-1} (\boldsymbol{\Phi}^\varphi)^T \tag{C81}$$

where $\boldsymbol{R}^\varphi \doteq \boldsymbol{\mathcal{C}}^T \boldsymbol{r}^\varphi \boldsymbol{\mathcal{C}}$ is a phase dependent resistance matrix in cycle space. We defined the matrix $\boldsymbol{g}$, which is the time average of the nonlinear conductance matrix of the stationary case, see section B.3.3. We take the same notation in the TiPS and stationary case because we recover the latter for the time-independent case. The above probability current satisfies the probability conservation for our choice of occupancy since

$$\partial_\varphi \boldsymbol{p}^\varphi = \partial_\varphi \boldsymbol{\pi}^\varphi = \boldsymbol{D} \langle \boldsymbol{j}^\varphi \rangle_{\boldsymbol{\pi}} = \boldsymbol{D} \boldsymbol{j}^\varphi \tag{C82}$$

given that $\boldsymbol{D}\boldsymbol{\mathcal{C}} = 0$, i.e., the cycle matrix $\boldsymbol{\mathcal{C}}$ is in the kernel of the incidence matrix of the graph $\boldsymbol{D}$, defined in section B.1.2, and playing the role of divergence in graph theory. The probability current of Eq. (C80) is also compatible with our choice $\boldsymbol{i}$ of the physical current vector. To see this, we use Eq. (C78) with the current of Eq. (C80)

$$\boldsymbol{i} = \langle \boldsymbol{i} \rangle_{\boldsymbol{\pi}} + \left[\frac{1}{\mathscr{T}} \int_0^{\mathscr{T}} \mathrm{d}\varphi\, \boldsymbol{\phi}^\varphi \boldsymbol{\mathcal{C}} (\boldsymbol{R}^\varphi)^{-1} (\boldsymbol{\Phi}^\varphi)^T \right] \boldsymbol{g}^{-1} (\boldsymbol{i} - \langle \boldsymbol{i} \rangle_{\boldsymbol{\pi}}), \tag{C83}$$

that is a trivial identity when using $\boldsymbol{\Phi}^\varphi = \boldsymbol{\phi}^\varphi \boldsymbol{\mathcal{C}}$ and the definition of $\boldsymbol{g}$. Finally, using $\boldsymbol{p} = \boldsymbol{\pi}$ and the current of Eq. (C80) in the quadratic upper bound yields our final result

$$\mathscr{I}_{\mathrm{quad}}(\boldsymbol{i}, \boldsymbol{\pi}) = \frac{1}{4} (\boldsymbol{i} - \langle \boldsymbol{i} \rangle_{\boldsymbol{\pi}})^T \boldsymbol{g}^{-1} (\boldsymbol{i} - \langle \boldsymbol{i} \rangle_{\boldsymbol{\pi}}) \tag{C84}$$

that bounds from above the LDF of time-averaged physical currents that would be obtained from the exact contraction of the LDF for occupancy and empirical probability current. Studying this bound on a specific model could be the topic of a M1 internship.

We conclude this section by remarking on the striking parallel between the theory of nonlinear conductance in the stationary state and TiPS after time averaging. Compared to Ref. [118], we have used the cycle decomposition of currents to introduce an increment of current, with respect to the mean periodic one, that satisfies probability conservation. This removes the difficulty of finding a time-dependent occupancy Ansatz compatible with the empirical probability current, a problem that is almost as complex as the exact contraction [19]. Since our final result is identical to the stationary case, we refer to section B.3.3 to switch to a fundamental set of physical currents. However, if some reservoirs are periodically connected and disconnected, the conservation laws and the selection matrix evolve in time, and the situation must be studied in more detail. We also point out that some connections could exist between our framework and Onsager's response theory, as revisited in the last decade by Karel Proesmans and Christian Van den Broeck [119].

Chapter D

Efficiency fluctuations

Contents

D.1 Introduction to selected articles

Converters start to be influenced by fluctuations when the machine's size goes below the micron scale (10^{-6} m). For instance, the pollen grain in the experiments of biologist Robert Brown, who gave his name to the "Brownian motion", undergoes an equilibrium of dynamical nature: This equilibrium is very different from a mechanical equilibrium (characterized by absolutely no motion) in the sense that there is no net motion *on average*, with many back and forth fluctuations [67]. Indeed, in his experiment, Brown showed that collisions of a grain (organic or not) with the molecules of a fluid generate an erratic motion of the grain moving across the surface of the fluid observed under the microscope. This erratic motion is linked to diffusion, although it is more the probability density function of the grain's location that diffuses in this precise case. Diffusion tends to make uniform the distribution of matter, e.g., to reduce chemical potential differences, but diffusion is also influenced by temperature that enhances the molecular agitation [120]. Indeed, temperature can be defined using the equipartition theorem and velocity variance. In general, any coupling with an environment (heat reservoir in the case of the grain, volume reservoir, particle reservoir, etc.) introduces fluctuations (of energy, volume, or particle number) if the considered system is sufficiently small. Converters are intrinsically operating by exchanging with different environments and are hence influenced by them when operating at the micro-scale. Cellular machinery typically operates far from equilibrium and under high fluctuations. Many works in stochastic thermodynamics are devoted to the understanding of biological converters [121, 103, 122], such as kinesin on microtubules, myosin on actin filaments, RNA polymerase, or F_0/F_1 rotating motor, etc. Those converters generate mechanical work [123, 124], maintain gradients accross membranes [125, 126, 127, 128], or collect information for

sensing [129]. The modeling of all these processes is still an active field of research nowadays. Experimental data fit is often challenging due to the many parameters in the most elementary models. A better understanding of the structure of nonequilibrium fluctuations can help in this view. For instance, we realized in Ref. [18] that only a subset of the load factors (that encodes the asymmetry of the potential energy landscape generated by the microtubule) was pertinent [103]. In other words, changing them in some way was not modifying the current fluctuations since this produces a change within a dynamical equivalence class. Characterizing energy converters at the fluctuating scale can help with modeling and parameter inference. The work presented in this chapter contributes to this line of research, although many more works are needed to make a connection with experiments on biological systems, beyond the excellent works on artificial devices [130, 131].

In chapter B, we considered the physics of conversion processes at the mean level, with linear or non-linear characteristics. Many developments are possible while remaining at the macroscopic or mean level, among which the theory of thermodynamic circuits is promising. In chapter C, we studied systems with the perspective of large deviation theory, with the (not necessarily valid) idea of connecting rare events and typical events of far-from-equilibrium and non-linear systems. In the present (and relatively small) chapter, we return to the physics of conversion processes from the large deviation theory perspective to characterize fluctuations' effects on engines' performances.

Our first work on the topic [13] presents the calculation of a large deviation function for a rational observable using the contraction principle. The (type I) stochastic efficiency η of a stationary converter is defined as the ratio of the stochastic (rate of) work delivered by the small converter with the stochastic (rate of) heat it receives from a heat reservoir. This is the first time such a rational observable is considered within LDT. Consequently, the shape of the obtained LDF is unconventional: it converges to a constant value for $\eta \to \pm\infty$ because the probability of small incoming heat solely determines large values of efficiencies. In between this plateau for large (absolute values of the) efficiency, the efficiency LDF decreases to a minimum and then increases to reach a maximum and goes back to the plateau. As expected, the minimum is associated with the most likely efficiency equal to the thermodynamic efficiency, which is defined as the ratio of the mean delivered work with the mean incoming heat. We remark that stochastic efficiency has no finite moment. The maximum is characterized by a more striking property: the reversible efficiency of the device lies at the maximum value of the efficiency LDF, meaning that the reversible efficiency is the least likely to be observed after a long time of operation of the converter. This property, observed for stationary converters, is due to the fluctuations relations satisfied by the LDF of work and heat rates. Indeed, the latter are sufficient to determine the total entropy production rate of the converter and therefore satisfy a joint FR. This maximum value of the LDF for the reversible efficiency explains the title "The unlikely Carnot efficiency" chosen for this letter. The fact that the fluctuations allow higher efficiencies than the reversible efficiency does not contradict the second law of thermodynamics. These fluctuations are not

transient violations either. They correspond to a reverse operating mode for which signs of the numerator and the denominator (in the definition of efficiency) have changed. In this reverse mode (e.g., heat pump mode), the second law provides an upper bound for $1/\eta$, which is the correct efficiency definition in this reverse mode. Finally, we have shown in this work that the shape of efficiency fluctuations observed far from equilibrium is similar to the exact shape obtained close to equilibrium and based on Onsager's response matrix only.

In the following works on efficiency fluctuations, we considered several generalizations. Our first extension concerns converters in TiPS [14]. For time-dependent driving forces enabling the exchange of work (i.e., with no symmetry under time reversal as noticed in [67]), the reversible efficiency is not the most likely in the limit of long conversion time. However, when driving the converter forward and backward in time (time reversed TiPSs), one finds that the LDF of efficiency achieves the same value precisely at the reversible efficiency. This comes again from the FR. Interestingly, this work shows that close-to-equilibrium heat and work fluctuations in the forward and backward cases are identical. Previously introduced models [21, 22], with exact heat and work statistics in TiPS, were here very useful to illustrate the properties of efficiency fluctuations of converters driven by time-dependent forces.

A second extension concerns converters operating in finite time [15]. In the case of Gaussian fluctuations of two coupled currents involved in a time-independent conversion process, it is possible to marginalize exactly the efficiency statistics at a finite time. Instead of plateaus in the large deviation function of efficiency, the Probability Density Function (PDF) displays power law tails. This agrees with the absence of first moments predicted by large deviation theory (no Legendre transform of the efficiency LDF). The PDF of efficiency is bimodal in connection with the existence of two opposite operating modes. A minimum of the PDF develops at the reversible efficiency with the time evolution of the converter. Interestingly, the study of efficiency fluctuations has drawn our attention to two complementary and opposite situations, namely the strong and singular couplings. The strong coupling is associated with a null determinant of the Onsager response matrix (conductance matrix). In contrast, singular coupling is associated with a divergent determinant (or null determinant of the resistance matrix, giving thermodynamics forces as a function of currents). Strong or singular couplings are needed in principle to reach the reversible efficiency for a stationary converter. We observed in this work that the evolution with time of the PDF was as expected from our LDT approach. However, singular coupling leads to qualitatively different distribution (PDF is insensitive to the value of typical efficiency at finite time and accumulates close to the reversible value).

Our third extension on the theory of efficiency fluctuations investigated the case of $n > 2$ independent currents [16]. In this case, we introduced a vector of $n-1$ efficiencies, and all our conclusions can be extended without surprises. For instance, when $n = 3$, the reversible efficiency is replaced by a line in the efficiency plane (corresponding to null entropy production). When considering the fluctuations of the efficiency vector, this line is asymptotically least likely. Still, in the efficiency plane,

a minimum point of the LDF exists for the most likely efficiency vector. Plateaus also exist with asymptotic values depending on the direction in the efficiency plane, etc.

In our initial work, the convexity of the currents' LDF is needed to determine the least likely nature of the reversible efficiency of the stationary converter. Therefore, we ended this series on efficiency fluctuations by considering non-convex current fluctuations. This required several preliminary works. First, we considered the "Brownian donkey model" [73] that is an infinite range Ising model of energy conversion for which the mean-field treatment is exact [8]. We noticed that the mean-field total EPR (that can be calculated using the magnetization only) coincides with the exact EPR. In other words, the EPR can be coarse-grained exactly, and similarly for the partial EPRs associated with heat and work exchanges. Second, we extended to dynamical ensembles the framework of Ref. [72] for calculating non-concave entropies in equilibrium statistical mechanics using LDT. This gave us the possibility to determine currents LDF for models with ergodicity breaking, i.e., for models with LDF defined through different branches according to the initial condition [12]. In a sense, the long time statistics are influenced by the random initial condition determining the branch in which the system will fluctuate after a long time. Third, we calculated efficiency fluctuations in the "Brownian donkey model" of many interacting two-state converters [17]. In this model, the interaction is attractive (ferromagnetic interaction between spins): two individual converters in the same state contribute lower to total energy than in different states. This model undergoes a pitchfork bifurcation when the interaction energy increases. For this model, we obtained the LDF of efficiency in the ergodic (time greater than the typical time-scale allowing transition between the metastable mean-field states) and in the non-ergodic cases (number of converters too high to observe any transition between metastable states in a physically reasonable amount of time). The ergodic case corresponds to typical LDF of currents and hence of efficiency, but the emergence of strong coupling was an interesting new feature of the model. Indeed, each converter was operating with strongly coupled currents. The interaction between the converters destroyed this strong coupling, which reappeared in the macroscopic limit because the collective converter was effectively unicyclic (the macroscopic limit allows the exploration of cycles with the mean-field state only). Due to this emergent strong coupling, the efficiency LDF converges to a constant function except at the typical efficiency, where it vanishes. In the non-ergodic case and after the bifurcation, the efficiency fluctuations were more complex, with a plateau for large $|\eta|$ and several minima corresponding to the output and input currents ratio in the mean-field states. We could extend our conclusion on the least likely nature of the reversible efficiency for stationary converters undergoing a spontaneous phase transition. However, the degeneracy of the CGF for currents due to emergent strong coupling (an indirect consequence of the phase transition) led to a degenerate maximum of the efficiency LDF. This work on current fluctuations at large volume was the precursor of other works focused on the large deviation techniques applied in the macroscopic limit [20].

nature COMMUNICATIONS

ARTICLE

Received 6 May 2014 | Accepted 16 Jul 2014 | Published 15 Sep 2014

DOI: 10.1038/ncomms5721

The unlikely Carnot efficiency

Gatien Verley[1], Massimiliano Esposito[1], Tim Willaert[2] & Christian Van den Broeck[2]

The efficiency of an heat engine is traditionally defined as the ratio of its average output work over its average input heat. Its highest possible value was discovered by Carnot in 1824 and is a cornerstone concept in thermodynamics. It led to the discovery of the second law and to the definition of the Kelvin temperature scale. Small-scale engines operate in the presence of highly fluctuating input and output energy fluxes. They are therefore much better characterized by fluctuating efficiencies. In this study, using the fluctuation theorem, we identify universal features of efficiency fluctuations. While the standard thermodynamic efficiency is, as expected, the most likely value, we find that the Carnot efficiency is, surprisingly, the least likely in the long time limit. Furthermore, the probability distribution for the efficiency assumes a universal scaling form when operating close-to-equilibrium. We illustrate our results analytically and numerically on two model systems.

[1] Complex Systems and Statistical Mechanics, University of Luxembourg, L-1511, Luxembourg, Luxembourg. [2] Theoretical physics, Hasselt University, B-3590, Diepenbeek, Belgium. Correspondence and requests for materials should be addressed to G.V. (email: gatien.verley@gmail.com).

The efficiency of an heat engine operating between a hot and cold reservoir is defined by $\eta = -W/Q_h$, where Q_h is the heat extracted from the hot reservoir, $-W$ is the work produced by the engine and $-Q_c$ is the remaining heat dumped into the cold reservoir. Throughout the study, energy fluxes such as work or heat are positive when flowing into the engine. The Carnot efficiency $\eta_C = 1 - T_c/T_h$ is easily found to be the upper bound of the engine efficiency, $\eta \leq \eta_C$, by combining the first and second law of thermodynamics:

$$\Delta E = W + Q_h + Q_c, \quad (1)$$

$$\Delta S_{tot} = \Delta S - Q_h/T_h - Q_c/T_c \geq 0, \quad (2)$$

in which the engine energy change ΔE and entropy change ΔS have to be set equal to zero, as the engine returns to its original state after each cycle.

Early on, Maxwell raised questions concerning the validity of the second law at small scales[1]. Szilard discussed similar issues in the context of information processing[2]. The theoretical breakthroughs in fluctuation theorems and stochastic thermodynamics have fully clarified these points and enable a consistent thermodynamic description of small-scale systems operating arbitrarily far-from-equilibrium[3–11]. These developments are of crucial practical relevance nowadays, as we are able to design machines operating at the nanoscale as well as to study in great detail biological machines transducing energy and processing information at the sub-micron scale[12–24]. For such engines, fluctuations are ubiquitous and quantities such as work w, heat q, energy change Δe, entropy change Δs and entropy production Δs_{tot} are stochastic and contain a much richer information than their ensemble average values work $W = \langle w \rangle$, heat $Q = \langle q \rangle$, energy change $\Delta E = \langle \Delta e \rangle$, and so on. At the stochastic level, the first law is essentially the same as at the average level, while the second law of thermodynamics is replaced by a universal symmetry in the probability distribution for the total entropy called fluctuation theorem[3–8]:

$$\Delta e = w + q_h + q_c, \;\; \Delta s_{tot} = \Delta s - q_h/T_h - q_c/T_c, \quad (3)$$

$$\frac{P(\Delta s_{tot})}{P(-\Delta s_{tot})} = \exp(\Delta s_{tot}), \quad (4)$$

where the Boltzmann constant is set to unity ($k_B = 1$). In words, the probability for observing a trajectory with entropy increase Δs_{tot} is exponentially more likely than the probability to observe the corresponding entropy decrease. The second law follows by Jensen's inequality, more precisely by taking the logarithm of the following inequality $1 = \langle e^{-\Delta s_{tot}} \rangle \geq e^{-\langle \Delta s_{tot} \rangle}$. The fluctuation theorem equation (4) is a probabilistic statement connecting the energy fluxes in the engine, since the entropy production can be expressed with them. It is surprising that, in view of this dramatic reformulation of the second law, and despite its founding role in thermodynamics, the properties of the resulting stochastic efficiency $\eta \equiv -w/q_h$ have not yet been explored. We will do so in this study and identify universal features of the corresponding probability distribution $P_t(\eta)$. Note that at equilibrium, all realizations are reversible, that is, $\Delta s_{tot} = 0$, leading to a stochastic efficiency equal to the Carnot efficiency $\eta = \eta_C$. When operating irreversibly, it follows from the fluctuation theorem equation (4) that realizations with both $\Delta s_{tot} > 0$ and $\Delta s_{tot} < 0$ appear, the latter albeit with a probability which is exponentially smaller. Hence efficiencies lower but also higher than Carnot will be observed.

Results

Properties of efficiency fluctuations. Our most striking result is the following: the Carnot efficiency η_C becomes the least likely efficiency for long times as a direct consequence of the fluctuation theorem equation (4). This result holds for engines with finite state space and therefore with bounded energy so that the energy and entropy contributions Δe and Δs can be neglected in the first and second law in the long time limit as compared with the work and heat. Hence, the heat dumped in the cold reservoir is just $-q_c = w + q_h$ and we can focus on the work and heat variables, w and $q = q_h$, and their corresponding output and input powers, $-\dot{w} \equiv -w/t$ and $\dot{q} \equiv q/t$. For systems that harbour no long-time correlations, work $\dot{w}$, heat $\dot{q}$ and their ratio $\eta = -w/q = -\dot{w}/\dot{q}$ are expected to converge in the infinite time limit to their most probable values $\langle w \rangle/t$, $\langle q \rangle/t$ and $\bar{\eta} \equiv -\langle w \rangle/\langle q \rangle$. The latter efficiency is the one predicted by standard thermodynamics, with the Carnot efficiency as upper bound: $\bar{\eta} \leq \eta_C$. When considering long trajectories, the probability distribution at time t for w and q as well as for η are described by the theory of large deviations[25] and assume the following asymptotic form:

$$P_t(\dot{w}, \dot{q}) \sim e^{-tI(\dot{w}, \dot{q})}, \quad P_t(\eta) \sim e^{-tJ(\eta)}. \quad (5)$$

The so-called large deviation functions $I(\dot{w}, \dot{q})$ and $J(\eta)$ describe the exponentially unlikely deviations of $\dot{w}$, $\dot{q}$ and η from their most probable values. These functions vanish at the most likely value of the probability distribution. They are otherwise strictly positive. In particular, we have $J(\bar{\eta}) = 0$.

The large deviation function $J(\eta)$, being the ratio of $-\dot{w}$ over $\dot{q}$, is obtained from I by the following so-called contraction:

$$J(\eta) = \min_{\dot{q}} I(-\eta\dot{q}, \dot{q}). \quad (6)$$

Intuitively, the decay rate J for a given efficiency is the smallest among all the decays rates I for the input and output powers which reproduce this efficiency. Note that since the minimization over $\dot{q}$ in equation (6) includes $\dot{q} = 0$, we find that $J(\eta) \leq I(0, 0)$.

Expressing the entropy production as $\Delta s_{tot} = q(1/T_c - 1/T_h) + w/T_c$, the fluctuation theorem equation (4) can be shown to assume the more detailed form[26,27]:

$$\frac{P(w, q)}{P(-w, -q)} = \exp(\Delta s_{tot}). \quad (7)$$

Reversible realizations are characterized by $\Delta s_{tot} = 0$ and thus by an efficiency equal to Carnot efficiency $\eta = -\dot{w}/\dot{q} = \eta_C$. In this case, $P(w, q) = P(-w, -q)$ implying $I(\dot{w}, \dot{q}) = I(-\dot{w}, -\dot{q})$. Hence $I(-\eta_C\dot{q}, \dot{q})$ is a symmetric function of the input power $\dot{q}$. Since I is generically a convex function (assuming no phase transitions), the minimum in equation (6) is, for $\eta = \eta_C$, reached in $\dot{q} = 0$ and thus $J(\eta_c) = I(0, 0)$. Since $J(\eta) \leq I(0, 0)$, this proves our main result, namely that the Carnot efficiency becomes the least likely when $t \to \infty$: $J(\eta) \leq J(\eta_C)$ or $P_t(\eta) \geq P_t(\eta_C)$.

Summarizing so far, all values of the efficiency are possible in a small-scale engine running for a large but finite time, including those forbidden by the second law at the average level. The probability for an efficiency different from the standard thermodynamic value $\bar{\eta}$ decreases exponentially with time with the strongest decrease observed for the Carnot efficiency. Therefore, the probability distribution for the efficiency will develop an exponentially pronounced minimum at the Carnot efficiency as one monitors longer operation times. This observation provides a novel way to define the temperature scale. In standard thermodynamics, the Kelvin temperature scale is introduced by the measurement of the Carnot efficiency of a reversible engine, measurement which is in principle unattainable in a finite time. The identification of the least likely efficiency in a system operating away from reversibility provides an alternative measurement of the Kelvin temperature, which does not suffer from this predicament. For a machine designed to operate like an heat engine ('on average'), the rare events leading to stochastic

efficiencies larger than the Carnot efficiency correspond to realizations along which the machine functions as a heat pump, while those with efficiency lower than zero correspond to a dud engine dissipating heat while absorbing work. The above derivation has been illustrated on an heat engine operating in continuous time, but the results remain valid for all other types of machines, such as isothermal energy transducers, heat engines, refrigerators or heat pumps, operating in non-equilibrium steady states or cyclically as long as the driving cycle is invariant under time reversal. The only difference is that the Carnot efficiency has to be replaced by the reversible efficiency. Below, we give an example of an isothermal work-to-work conversion where the reversible efficiency is equal to 1 and thus corresponds to the least likely efficiency.

Beyond these striking general conclusions about the least and most likely efficiency, we proceed to show that the efficiency fluctuations in the close-to-equilibrium regime have a universal scaling form. Our starting point is that close-to-equilibrium, the relevant work w and heat q fluctuations are generically Gaussian. The resulting large deviation function for the efficiency, being the ratio of two correlated Gaussian variables, is found to be:

$$J(\eta)=\frac{1}{2}\frac{(\eta\langle\dot{q}\rangle+\langle\dot{w}\rangle)^2}{\eta^2C_{qq}+2\eta C_{wq}+C_{ww}}, \qquad (8)$$

where $C_{wq}\equiv(\langle wq\rangle-\langle w\rangle\langle q\rangle)/t$, C_{ww} and C_{qq} are the elements of the symmetric covariance matrix. The crucial thermodynamic ingredient is obtained by combining the Gaussian statistics for $\dot{w}$ and $\dot{q}$ with the fluctuation theorem. More precisely, noting that equation (7) has to be valid for all values of $w=t\dot{w}$ and $q=t\dot{q}$, one finds (cf. methods section):

$$\langle\dot{q}\rangle=\frac{\eta_C C_{qq}+C_{wq}}{2T_c}, \quad \langle\dot{w}\rangle=\frac{\eta_C C_{wq}+C_{ww}}{2T_c}. \qquad (9)$$

The large deviation function J can therefore be solely expressed in terms of the covariance matrix:

$$J(\eta)=\frac{1}{8T_c^2}\frac{[\eta\eta_C C_{qq}+(\eta+\eta_C)C_{wq}+C_{ww}]^2}{\eta^2C_{qq}+2\eta C_{wq}+C_{ww}}. \qquad (10)$$

The above explicit expression for $J(\eta)$ is in agreement with the general properties pointed out above, namely its minimum and maximum are reached for $\eta=\bar{\eta}$ and $\eta=\eta_C$, respectively. These are also the two only extrema of the function. Remarkably, the least likely decay rate, that is, the rate at Carnot efficiency, can be rewritten from equations (9,10) solely in terms of the average heat and work: $J(\eta_C)=(\eta_C\langle\dot{q}\rangle+\langle\dot{w}\rangle)/(4T_c)$. This relation, which ultimately derives from the fluctuation theorem, should be easy to test experimentally. We also note that the two asymptotic values of $J(\eta)$ at $\eta\to\pm\infty$ coincide, namely $J(\infty)=(\eta_C C_{qq}+C_{wq})^2/(8T_c^2C_{qq})=\langle\dot{q}\rangle^2/(2C_{qq})$. We used equation (9) for the second equality. Since the covariance matrix is directly related to the Onsager matrix (cf. methods section), this latter can be obtained from measurements of efficiency fluctuations close to equilibrium. In fact, the covariance matrix C_{ww}, C_{wq} and C_{qq} is uniquely specified by the most probable efficiency $\bar{\eta}$, the value of large deviation function at the Carnot efficiency $J(\eta_C)$, and the asymptotic value of the large deviation function $J(\infty)$ (cf. methods section), so that equation (10) can be rewritten as:

$$\frac{J(\eta)}{J(\eta_C)}=\frac{(\bar{\eta}-\eta)^2}{(\bar{\eta}-2\eta+\eta_C)(\bar{\eta}-\eta_C)+\frac{J(\eta_C)}{J(\infty)}(\eta-\eta_C)^2}. \qquad (11)$$

Brownian work-to-work converter. As a first illustration of our main results, we consider the simplest possible model for work-to-work conversion[28]. An overdamped Brownian particle subjected to two constant forces $\mathbf{F}_1$ and $\mathbf{F}_2$ diffuses on a plane, as illustrated in Fig. 1. $\mathbf{F}_2$ is the driving force, allowing the particle to move against an opposing force $\mathbf{F}_1$. For a given displacement $\mathbf{x}=\mathbf{x}(t)$ of the particle (assuming $\mathbf{x}(0)=\mathbf{0}$), the work performed by each force is given by $w_1=\mathbf{F}_1\cdot\mathbf{x}$ and $w_2=\mathbf{F}_2\cdot\mathbf{x}$. The corresponding stochastic efficiency is $\eta=-w_1/w_2$. The displacement $\mathbf{x}(t)$ is a Gaussian random variable with average $\langle\mathbf{x}(t)\rangle=\mu\mathbf{F}t$, where $\mathbf{F}=\mathbf{F}_1+\mathbf{F}_2$, μ is the mobility and $2Dt$ is the dispersion in any direction of motion: $\langle x_i(t)x_i(t)\rangle=2Dt$ with D the diffusion coefficient. The aforementioned Gaussian scenario is thus exact in this model with the role of $\dot{w}$ and $\dot{q}$ played by $\dot{w}_1=\mathbf{F}_1\cdot\mathbf{x}/t$ and $\dot{w}_2=\mathbf{F}_2\cdot\mathbf{x}/t$. One obviously has $\langle\dot{w}_1\rangle=\mu\mathbf{F}_1\cdot\mathbf{F}$, and $\langle\dot{w}_2\rangle=\mu\mathbf{F}_2\cdot\mathbf{F}$. The corresponding correlation functions read $C_{11}=2D||\mathbf{F}_1||^2$, $C_{22}=2D||\mathbf{F}_2||^2$ and $C_{12}=2D\mathbf{F}_1\cdot\mathbf{F}_2$. The large deviation of efficiency is given by

$$J(\eta)=\frac{1}{2}\frac{(\eta\langle\dot{w}_2\rangle+\langle\dot{w}_1\rangle)^2}{\eta^2C_{22}+2\eta C_{12}+C_{11}}=\frac{\mu^2[(\eta\mathbf{F}_2+\mathbf{F}_1)\cdot\mathbf{F}]^2}{4D(\eta\mathbf{F}_2+\mathbf{F}_1)^2}. \qquad (12)$$

One immediately verifies that $J(\eta)$ takes its maximum value $J(1)=\mu^2||\mathbf{F}_2||^2/4D$ in $\eta=1$ which is the predicted reversible efficiency for work-to-work conversion. Furthermore, the above mentioned averages and correlations functions obey the relations equation (9) on setting $\eta_C=1$ and $D=\mu T$ from the Einstein relation. One can thus also rewrite the $J(\eta)$ as in equation (10) or equation (11) (with $\eta_C=1$).

Photoelectric device. Our second model is a nano-sized photoelectric device powered by black-body radiation at temperature T_h (ref. 29). The device is composed of two quantum dots, each with a single-energy level E_l and E_r ($E_r>E_l$), respectively, cf. Fig. 2. Coulomb repulsion prevents simultaneous occupation by electrons of both quantum dots. Each dot can exchange electrons with its neighbouring electronic lead. Both leads are at the same temperature T_c, but at different voltages and therefore at different chemical potentials $\mu_r>\mu_l$. Electron transfers between the two quantum dots are induced either by hot black-body radiation at T_h or by cold thermal phonons at T_c. This device operates as an heat engine fuelled by the heat $q=n_p(E_r-E_l)$, where n_p is the number of photons absorbed from the hot black body, and producing a positive work output $-w=n_e\Delta\mu$, where n_e is the number of electrons transferred from left to right lead against the chemical potential gradient $\Delta\mu=\mu_r-\mu_l>0$. The stochastic efficiency is thus $\eta=-w/q$. The rates describing the Markovian dynamics of the device as well as the large deviation function for the work and heat statistics are discussed in the methods section. The resulting large deviation function for efficiency is plotted in Fig. 3. All the predicted features—the least

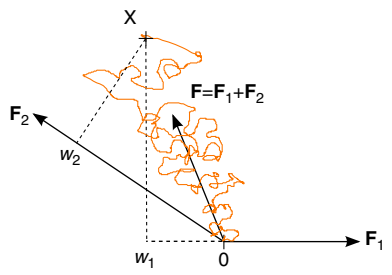

Figure 1 | Work-to-work converter for an overdamped Brownian particle diffusing in a plane. The particle is driven by the two forces $\mathbf{F}_1$ and $\mathbf{F}_2$. The orange line is a specific trajectory ending at position $\mathbf{x}$. The stochastic work w_1 and w_2 are obtained from the scalar products (dashed lines) projecting $\mathbf{x}$ on $\mathbf{F}_1$ and $\mathbf{F}_2$, respectively. The ratio of the lengths obtained from these projections gives the stochastic efficiency for this specific trajectory.

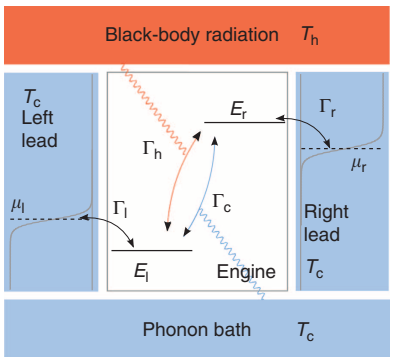

Figure 2 | Sketch of a photoelectric device. The device consists of two single-level quantum dots (in white) connected to two leads (in blue) at temperature T_c and at different chemical potentials μ_l and μ_r. The electron transitions between left and right quantum dots are induced either by photons from the black-body radiation at temperature T_h (in red) or by phonons at temperature T_c (in blue). The arrows indicate possible electronic transitions between different energy levels and the Γ's represent the coupling strengths with the reservoirs.

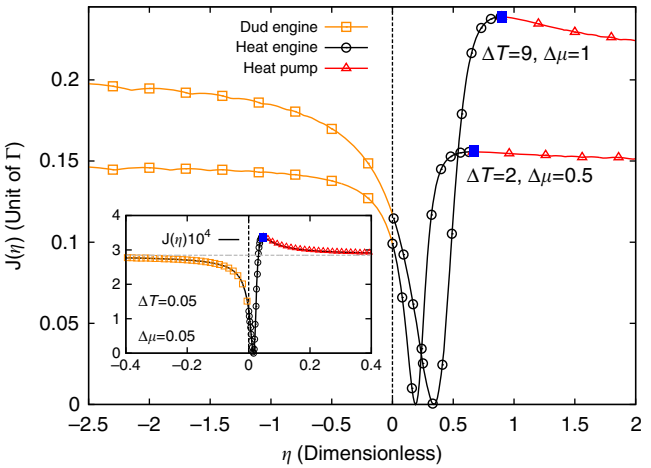

Figure 3 | Large deviation functions of efficiency $J(\eta)$. The curves are obtained from equation (6) for the photoelectric device of Fig. 2 operating on average as an heat engine. Each curve corresponds to a given temperature and chemical potential differences, black circles denote heat engine realizations, red triangles (resp. gold squares) denote heat pump (resp. a dud engine) realizations. The blue-filled squares denote the least likely Carnot efficiency, while the zeros correspond to the most likely one. The left and right horizontal asymptotes coincide and correspond to realizations with low-heat exchange. Inset: the close-to-equilibrium approximation (symbols) fits very well with the exact result equation (10) (black solid line). Parameters for the curves are $E_l=0.5$, $E_r=2.5$, $\mu_l=1$, $T_c=1$, $\Delta T=T_h-T_c$, $\Gamma_h=\Gamma_l=\Gamma_r=10$ and $\Gamma_c=1$.

likely value at Carnot efficiency and the universal shape of the large deviation function close-to-equilibrium—are perfectly reproduced.

Discussion

The efficiency of macroscopic thermal machines is the ratio between two averaged quantities, the extracted work and the heat coming from the hot source. One of the momentous discoveries in science, which lead to the formulation of the second law of thermodynamics, is the observation by Carnot that this efficiency has a maximum called Carnot efficiency. Contrary to macroscopic machines, the behaviour of small machines is subjected to strong fluctuations. Their average behaviour thus provides an incomplete description except in the macroscopic limit where fluctuations are typically strongly peaked around the average. In the present study, we introduce the concept of fluctuating efficiency to accurately characterize the performance of small machines and find universal features in its fluctuations. Using the fluctuation theorem, which generalizes the second law at the fluctuating level, we provide an analogue of the Carnot analysis by proving that the Carnot efficiency becomes the least likely efficiency when long measurement times are considered, independently of any details of the machine or of its mode of operation. Furthermore, we show that close-to-equilibrium, the large deviation function of the efficiency fluctuations obeys a universal form parametrized by the Onsager matrix of the engine. Our study suggests a new direct application of the fluctuation theorem, which was previously mostly invoked to measure free energy differences[18,30,31]. Since heat and work fluctuations are nowadays measured in a wide variety of systems[12–18,20,24], we expect that experimental measurements of the fluctuating efficiency will become a valuable tool to characterize the performance of small engines.

Methods

Linear response and fluctuation theorem. For the photoelectric device, the average photon and electron currents, $\dot{N}_p \equiv \langle n_p\rangle/t$ and $\dot{N}_e \equiv \langle n_e\rangle/t$, read in the linear regime

$$\dot{N}_e = L_{ee}\Delta\mu/T_c + L_{ep}\Delta E\Delta\beta, \tag{13}$$

$$\dot{N}_p = L_{ep}\Delta\mu/T_c + L_{pp}\Delta E\Delta\beta, \tag{14}$$

where $\Delta\beta = 1/T_c - 1/T_h > 0$, $\Delta E = E_r - E_l > 0$ and L is the symmetric Onsager matrix with $L_{pp}\geq 0$, $L_{ee}\geq 0$ and $\det L \geq 0$. The average work and heat per unit time can thus be written as

$$\dot{W} = \Delta\mu\dot{N}_e = \frac{1}{T_c}\left(L_{ee}\Delta\mu^2 + \eta_C L_{ep}\Delta\mu\Delta E\right), \tag{15}$$

$$\dot{Q} = \Delta E\dot{N}_p = \frac{1}{T_c}\left(L_{ep}\Delta\mu\Delta E + \eta_C L_{pp}\Delta E^2\right). \tag{16}$$

From Green–Kubo relation, the linear response coefficients are related to equilibrium fluctuations by

$$L_{ep} = \lim_{t\to\infty}\frac{1}{2t}\langle[n_e(t) - \langle n_e\rangle_{eq}][n_p(0) - \langle n_p\rangle_{eq}]\rangle_{eq}. \tag{17}$$

This implies that in the long time limit, $C_{wq}/2 \to \Delta\mu\Delta E L_{ep}$. Proceeding similarly for the other response coefficients, we find $C_{ww}/2 \to \Delta\mu^2 L_{ee}$ and $C_{qq}/2 \to \Delta E^2 L_{pp}$. Equations (15–16) thus lead to equation (9) of the results section. These equalities may also be derived using the fluctuation theorem for work and heat in the Gaussian limit. Indeed, using

$$I(\dot{w},\dot{q}) - I(-\dot{w},-\dot{q}) = -(\eta_C\dot{q} + \dot{w})\frac{1}{T_c}, \tag{18}$$

and the quadratic large deviation function

$$I(\dot{w},\dot{q}) = \frac{\begin{pmatrix}\dot{w}-\dot{W}\\ \dot{q}-\dot{Q}\end{pmatrix}^T\begin{bmatrix}C_{qq} & -C_{wq}\\ -C_{wq} & C_{ww}\end{bmatrix}\begin{pmatrix}\dot{w}-\dot{W}\\ \dot{q}-\dot{Q}\end{pmatrix}}{2\det C}, \tag{19}$$

we get

$$\frac{\det C}{2T_c}(\eta_C\dot{q} + \dot{w}) = \dot{w}\dot{W}C_{qq} + \dot{q}\dot{Q}C_{ww} - C_{wq}(\dot{w}\dot{Q} + \dot{q}\dot{W}). \tag{20}$$

Since this relation must hold true for any values of $\dot{w}$ and $\dot{q}$, we obtain

$$\frac{1}{\det C}\begin{bmatrix}C_{qq} & -C_{wq}\\ -C_{wq} & C_{ww}\end{bmatrix}\begin{pmatrix}\dot{W}\\ \dot{Q}\end{pmatrix} = \begin{pmatrix}1/2T_c\\ \eta_C/(2T_c)\end{pmatrix} \tag{21}$$

which reproduces the expected result when solved for $\dot{W}$ and $\dot{Q}$.

Photoelectric device: heat and work statistics. The work w and heat q statistics in the photoelectric device is obtained by considering the generating function $g_t(j,\gamma,\lambda) = \langle e^{i\gamma w + \lambda q}\rangle_j$ where the subscript j denotes that the trajectory average is conditioned on the final state j of the device at time t. The three different states of the device are denoted $j=0$, l, r for respectively no electrons in the device, one electron in the energy level E_l connected to the left lead or one electron in the energy level E_r connected to the right lead. The generating function evolves

according to

$$\begin{pmatrix} \dot{g}_t(0,\gamma,\lambda) \\ \dot{g}_t(l,\gamma,\lambda) \\ \dot{g}_t(r,\gamma,\lambda) \end{pmatrix} = \begin{bmatrix} -k_{l0}-k_{r0} & k_{0l} & k_{0r}e^{-\gamma\Delta\mu} \\ k_{l0} & -k_{0l}-k_{rl} & k_{lr}^{c}+k_{lr}^{h}e^{-\lambda(E_r-E_l)} \\ k_{r0}e^{\gamma\Delta\mu} & k_{rl}^{c}+k_{rl}^{h}e^{\lambda(E_r-E_l)} & -k_{0r}-k_{lr} \end{bmatrix} \begin{pmatrix} g_t(0,\gamma,\lambda) \\ g_t(l,\gamma,\lambda) \\ g_t(r,\gamma,\lambda) \end{pmatrix}. \tag{22}$$

When $\lambda=\gamma=0$, equation (22) becomes a Markovian master equation for the probability $P_j=g_t(j,0,0)$ to find the device in state j at time t. The rates k_{ij} denote the probability per unit time to jump from state j to i. Introducing the Fermi–Dirac distribution $f(x)\equiv 1/(e^x+1)$ and the Bose–Einstein distribution $b(x)\equiv 1/(e^x-1)$, they are defined by

$$\begin{aligned} k_{l0} &\equiv \Gamma_l f\left(\frac{E_l-\mu_l}{T_c}\right),\ k_{0l} \equiv \Gamma_l\left[1-f\left(\frac{E_l-\mu_l}{T_c}\right)\right], \\ k_{r0} &\equiv \Gamma_r f\left(\frac{E_r-\mu_r}{T_c}\right),\ k_{0r} \equiv \Gamma_r\left[1-f\left(\frac{E_r-\mu_r}{T_c}\right)\right], \\ k_{rl}^{v} &\equiv \Gamma_v b\left(\frac{E_r-E_l}{T_v}\right),\ k_{lr}^{v} \equiv \Gamma_v\left[1+b\left(\frac{E_r-E_l}{T_v}\right)\right], \end{aligned} \tag{23}$$

and $k_{ij}\equiv k_{ij}^{c}+k_{ij}^{h}$, where $v=$ c, h denotes the cold and hot reservoir and the Γ's the coupling strength with the various reservoirs[29] as illustrated in Fig. 2 of the result section. For long times t, the work and heat-generating function is dominated by the highest eigenvalue $\phi(\gamma,\lambda)$ of the rate matrix in equation (22)

$$\left\langle e^{\gamma w+\lambda q}\right\rangle = \sum_{j=0,l,r} g_t(j,\gamma,\lambda) \underset{t\to\infty}{\sim} e^{t\phi(\gamma,\lambda)}. \tag{24}$$

The latter can be calculated analytically. The corresponding large deviation function is obtained by the Legendre transform $I(\dot{w},\dot{q})=\max_{\gamma,\lambda}\{\gamma\dot{w}+\lambda\dot{q}-\phi(\gamma,\lambda)\}$. The large deviation function for efficiency fluctuations is obtained from it using equation (6). Alternatively, it can be obtained using $J(\eta)=-\min_{\gamma}\phi(\gamma,\eta\gamma)$. The proof will be provided in a forthcoming publication. This latter minimization has been performed numerically to produce Fig. 3 in the study.

Alternative expression of $J(\eta)$. The three equations in the study for $J(\infty)$, $J(\eta_C)$ and $\bar{\eta}$ expressed in term of the covariance matrix close-to-equilibrium can be inverted to obtain

$$C_{qq}=\frac{8J(\eta_C)^2T_c^2}{(\bar{\eta}-\eta_C)^2J(\infty)}, \tag{25}$$

$$C_{wq}=-8J(\eta_C)T_c^2\frac{J(\infty)\bar{\eta}-J(\infty)\eta_C+\eta_CJ(\eta_C)}{J(\infty)(\bar{\eta}^2-2\bar{\eta}\eta_C+\eta_C^2)}, \tag{26}$$

$$C_{ww}=8J(\eta_C)T_c^2\frac{J(\infty)\bar{\eta}^2+\eta_C^2J(\eta_C)-J(\infty)\eta_C^2}{J(\infty)(\bar{\eta}^2-2\bar{\eta}\eta_C+\eta_C^2)}. \tag{27}$$

Using these coefficients, we recover equation (11) of the study.

References

1. Maxwell, J. C. Tait's "Thermodynamics". *Nature* **17,** 278–280 (1878).
2. Szilárd, L. On the decrease of entropy in a thermodynamic system by the intervention of intelligent beings. *Z. Phys.* **53,** 840–856 (1929).
3. Jarzynski, C. Equalities and inequalities: irreversibility and the second law of thermodynamics at the nanoscale. *Annu. Rev. Condens. Matter* **2,** 329–351 (2011).
4. Sevick, E. M., Prabhakar, R., Williams, S. R. & Searles, D. J. Fluctuation theorems. *Annu. Rev. Phys. Chem.* **59,** 603–633 (2008).
5. Campisi, M., Hänggi, P. & Talkner, P. Colloquium: quantum fluctuation relations: foundations and applications. *Rev. Mod. Phys.* **83,** 771–791 (2011).
6. Seifert, U. Stochastic thermodynamics, fluctuation theorems and molecular machines. *Rep. Prog. Phys.* **75,** 126001 (2012).
7. Van den Broeck, C. & Esposito, M. Ensemble and trajectory thermodynamics: a brief introduction. *Phys. A* doi:10.1016/j.physa.2014.04.035 (24 April 2014).
8. Esposito, M., Harbola, U. & Mukamel, S. Nonequilibrium fluctuations, fluctuation theorems, and counting statistics in quantum systems. *Rev. Mod. Phys.* **81,** 1665–1702 (2009).
9. Liphardt, J., Dumont, S., Smith, S. B., Tinoco, Jr I. & Bustamante, C. Equilibrium information from nonequilibrium measurements in an experimental test of Jarzynski's equality. *Science* **296,** 1832–1835 (2002).
10. Blickle, V., Speck, T., Helden, L., Seifert, U. & Bechinger, C. Thermodynamics of a colloidal particle in a time-dependent nonharmonic potential. *Phys. Rev. Lett.* **96,** 070603 (2006).
11. Küng, B. *et al.* Test of the fluctuation theorem for single-electron transport. *J. Appl. Phys.* **113,** 136507 (2013).
12. Saira, O.-P. *et al.* Test of the Jarzynski and Crooks fluctuation relations in an electronic system. *Phys. Rev. Lett.* **109,** 180601 (2012).
13. Blickle, V. & Bechinger, C. Realization of a micrometre-sized stochastic heat engine. *Nat. Phys.* **8,** 143–146 (2012).
14. Moffitt, J. R. *et al.* Intersubunit coordination in a homomeric ring ATPase. *Nature* **457,** 446–450 (2009).
15. Yasuda, R., Noji, H., Yoshida, M., Kinosita, K. & Itoh, H. Resolution of distinct rotational substeps by submillisecond kinetic analysis of F1-ATPase. *Nature* **410,** 898–904 (2001).
16. Toyabe, S., Sagawa, T., Ueda, M., Muneyuki, E. & Sano, M. Experimental demonstration of information-to-energy conversion and validation of the generalized Jarzynski equality. *Nat. Phys.* **6,** 988–992 (2010).
17. Bérut, A. *et al.* Experimental verification of Landauer's principle linking information and thermodynamics. *Nature* **483,** 187–189 (2012).
18. Alemany, A., Mossa, A., Junier, I. & Ritort, F. Experimental free-energy measurements of kinetic molecular states using fluctuation theorems. *Nat. Phys.* **8,** 688–694 (2012).
19. Collin, D. *et al.* Verification of the Crooks fluctuation theorem and recovery of RNA folding free energies. *Nature* **437,** 231–234 (2005).
20. Koski, J. V. *et al.* Distribution of entropy production in a single-electron box. *Nat. Phys.* **9,** 644–648 (2013).
21. Küng, B. *et al.* Irreversibility on the level of single-electron tunneling. *Phys. Rev. X* **2,** 011001 (2012).
22. Ciliberto, S., Imparato, A., Naert, A. & Tanase, M. Heat flux and entropy produced by thermal fluctuations. *Phys. Rev. Lett.* **110,** 180601 (2013).
23. Bustamante, C., Liphardt, J. & Ritort, F. The nonequilibrium thermodynamics of small systems. *Phys. Today* **58,** 43–48 (2005).
24. Matthews, J., Battista, F., Sanchez, D., Samuelsson, P. & Linke, H. Experimental verification of reciprocity relations in quantum thermoelectric transport. Preprint at http://arxiv.org/abs/1306.3694 (2013).
25. Touchette, H. The large deviation approach to statistical mechanics. *Phys. Rep.* **478,** 1–69 (2009).
26. García-García, R., Domnguez, D., Lecomte, V. & Kolton, A. B. Unifying approach for fluctuation theorems from joint probability distributions. *Phys. Rev. E* **82,** 030104 (2010).
27. Sinitsyn, N. A. Fluctuation relation for heat engines. *J. Phys. A:Math. Theor.* **44,** 405001 (2011).
28. Astumian, R. D. & Brody, R. Thermodynamics of gradient driven transport: application to single-particle tracking. *J. Phys. Chem. B* **113,** 11459–11462 (2009).
29. Rutten, B., Esposito, M. & Cleuren, B. Reaching optimal efficiencies using nanosized photoelectric devices. *Phys. Rev. B* **80,** 235122 (2009).
30. Jarzynski, C. Nonequilibrium equality for free energy differences. *Phys. Rev. Lett.* **78,** 2690–2693 (1997).
31. Crooks, G. E. Path-ensemble averages in systems driven far from equilibrium. *Phys. Rev. E* **61,** 2361–2366 (2000).

Acknowledgements

G.V. acknowledges insightful comments from Andreas Engel. This work was supported by the National Research Fund, Luxembourg under Project No. FNR/A11/02 and INTER/FWO/13/09 and also benefited from support by the ESF network 'Exploring the Physics of Small Devices'.

Author contributions

G.V. explicitly derived the central results of the study and suggested to study efficiency fluctuations using large deviation theory. T.W. was involved in preliminary studies of model systems which lead to this work. C.V.d.B. supervised the work at every stage and provided key contributions about the connection between the fluctuation theorem and efficiency fluctuations. M.E. supervised the work at every stage, proposed to study efficiency fluctuations and made key suggestions about the close-to-equilibrium limit.

Additional information

Competing financial interests: The authors declare no competing financial interests.

Reprints and permission information is available online at http://npg.nature.com/reprintsandpermissions/

How to cite this article: Verley, G. *et al.* The unlikely Carnot efficiency. *Nat. Commun.* 5:4721 doi: 10.1038/ncomms5721 (2014).

Efficiency Statistics at All Times: Carnot Limit at Finite Power

M. Polettini,* G. Verley,† and M. Esposito‡
Complex Systems and Statistical Mechanics, Physics and Materials Research Unit, University of Luxembourg, 162a Avenue de la Faïencerie, L-1511 Luxembourg, Luxembourg
(Received 16 September 2014; published 3 February 2015)

We derive the statistics of the efficiency under the assumption that thermodynamic fluxes fluctuate with normal law, parametrizing it in terms of time, macroscopic efficiency, and a coupling parameter ζ. It has a peculiar behavior: no moments, one sub-, and one super-Carnot maxima corresponding to reverse operating regimes (engine or pump), the most probable efficiency decreasing in time. The limit $\zeta \to 0$ where the Carnot bound can be saturated gives rise to two extreme situations, one where the machine works at its macroscopic efficiency, with Carnot limit corresponding to no entropy production, and one where for a transient time scaling like $1/\zeta$ microscopic fluctuations are enhanced in such a way that the most probable efficiency approaches the Carnot limit at finite entropy production.

DOI: 10.1103/PhysRevLett.114.050601 PACS numbers: 05.70.Ln, 05.70.Fh, 88.05.Bc

Efficiency quantifies how worth a local gain at the expense of a global loss is. In thermodynamics, "losses" are measured by the rate $\bar{\sigma}_2 > 0$ at which entropy is externalized to the environment in the form of a degraded form of energy, while "gain" is the rate $-\bar{\sigma}_1$ at which entropy is expelled from a system to upgrade its own state. Globally, entropy is produced at rate $\bar{\sigma} = \bar{\sigma}_2 + \bar{\sigma}_1$, and the second law of thermodynamics $\bar{\sigma} \geq 0$ conveys that locally one cannot earn more of what is globally lost. Then, the efficiency $\bar{\eta} = -\bar{\sigma}_1/\bar{\sigma}_2$ is bounded by the (scaled) Carnot efficiency $\eta_c = 1$. Alas, in craving this limit one is deluded by the fact that it occurs at zero power, which is useless for any activity to be accomplished in a reasonable time.

This picture is only tenable for macroscopic systems. For microscopic systems subject to random fluctuations, the concept of a stochastic efficiency has been recently introduced by Verley *et al.* [1,2]. The first notion one has to revise is that a fluctuating efficiency can indeed exceed the Carnot limit, when in a machine designed to convert in average a form of input power into a form of output power (e.g., an engine producing work at the expense of a heat flow), for a rare event the input and output are reversed (e.g., a pump that employs mechanical work to absorb heat). Moreover, it has been observed that for time-symmetric protocols in the long time limit the Carnot efficiency becomes the least probable in a "large deviation" sense [3]—a very counterintuitive and fascinating result that, in its time-asymmetric variant [2,4], is already subject to experimental inquiry [5]. Corrections at long finite times have been estimated in Ref. [4].

In this Letter, we derive the full probability density function (PDF) of the efficiency, under the assumption that thermodynamic fluxes are distributed with a multivariate Gaussian with cumulants growing linearly in time. The efficiency PDF displays quite peculiar features. In particular, it does not afford moments of any order so that there is no average efficiency and mean-square error. Experimentally, this implies that any data analysis should focus on most probable values. About the latter, after an initial transient the distribution becomes bimodal, as observed numerically in Ref. [6]. As time elapses, the more pronounced maximum drifts towards the always smaller macroscopic value of the efficiency, while a less pronounced maximum at higher efficiency moves in the super-Carnot region towards infinity. We provide a clear physical interpretation of these two peaks. Finally, we argue that the macroscopic framework fails to capture another way of approaching Carnot efficiency at finite entropy production, at finite time, when microscopic fluctuations are enhanced so as to affect the macroscopic behavior.

Macroscopic nonequilibrium thermodynamics [7] is rooted on two assumptions, both of which are today being challenged in the framework of the stochastic theory of nonequilibrium thermodynamics [8,9]: Certain fluxes $\boldsymbol{x} = (x_1, x_2)$, with units of an extensive physical quantity per time, take definite values $\bar{\boldsymbol{x}}$. Fluxes are linearly related to their conjugate thermodynamic forces $\boldsymbol{f}$ via $\bar{\boldsymbol{x}} = L\boldsymbol{f}$, where the linear response matrix L is assumed to be positive semidefinite and symmetric by virtue of the Onsager reciprocity relations, yielding a non-negative macroscopic entropy production rate $\bar{\sigma} = \boldsymbol{f} \cdot L\boldsymbol{f}$.

We relax the first assumption, by supposing that at a given time t fluxes $\boldsymbol{x}$ are distributed with law $P_t(\boldsymbol{x})$. Each current produces entropy at rate $\sigma_i = f_i x_i$, for a total entropy production rate $\sigma = \sigma_1 + \sigma_2$, with units of k_B per time. Then, the adimensional efficiency

$$\eta = -\frac{f_1 x_1}{f_2 x_2} = -\frac{\sigma_1}{\sigma_2} \tag{1}$$

is a stochastic variable distributed with PDF

$$P_t(\eta) = \int dx_1 dx_2 \delta\left(\eta + \frac{x_1 f_1}{x_2 f_2}\right) P_t(x_1, x_2) = \varphi \int dx |x| P_t(-\varphi\eta x, x), \tag{2}$$

where $\varphi = f_2/f_1$ can be assumed to be positive. A remarkable fact one immediately encounters is that the efficiency can fluctuate beyond the Carnot limit. The probability of an efficiency higher than that of Carnot coincides with the probability of negative entropy production rate,

$$P_t(\eta < 1) = P_t(\sigma > 0) = \langle \theta(\sigma) \rangle_t, \tag{3a}$$

$$P_t(\eta > 1) = P_t(\sigma < 0) = \langle \theta(\sigma) e^{-t\sigma} \rangle_t, \tag{3b}$$

where θ is Heaviside's step function. The rightmost equations follow from the fluctuation theorem [10,11]

$$\frac{P_t(\sigma)}{P_t(-\sigma)} = e^{t\sigma}, \tag{4}$$

which states that processes producing negative entropy are exponentially disfavored with respect to those producing positive entropy. Therefore, that super-Carnot efficiencies are unlikely compared to sub-Carnot efficiencies is an incarnation of the fluctuation theorem.

Exact results can be obtained by assuming that fluxes are distributed with normal multivariate density function

$$P_t(\boldsymbol{x}) = \frac{t}{4\pi\sqrt{|L|}} \exp\left[-\frac{t}{4}(\boldsymbol{x} - \bar{\boldsymbol{x}}) \cdot L^{-1}(\boldsymbol{x} - \bar{\boldsymbol{x}})\right], \tag{5}$$

where $|\cdot|$ is the determinant. That (one-half) the correlation matrix should be identified with the linear response matrix is corroborated by the Green-Kubo relations

$$L_{ij} = \frac{t}{2} \langle (x_i - \bar{x}_i)(x_j - \bar{x}_j) \rangle, \tag{6}$$

another well-known consequence of the fluctuation theorem [12]. The time dependence in Eq. (5) is due to the fact that the time-integrated fluxes $t\bar{\boldsymbol{x}}$ increase linearly in time, and correspondingly so do their cumulants. Under these assumptions, the efficiency PDF Eq. (2) can be exactly calculated (see the Supplemental Material [13]). It only depends on four adimensional parameters: The macroscopic efficiency $\bar{\eta}$, the coupling parameter $\zeta = |L|/(L_{11}L_{22}) \in [0, 1]$ that for thermoelectric devices [14] is related to the so-called figure of merit $zT = 1/\zeta - 1$, the average entropy production rate $\bar{\sigma}$, which sets the time scale and can be reabsorbed by a time reparametrization $\tau = t\bar{\sigma}$, and $\epsilon = \pm 1$. With $\bar{\sigma}$ being the only extensive parameter, large τ stands both for large times and the macroscopic limit. We obtain (Supplemental Material [13])

$$P_\tau(\eta) = \frac{e^{-\tau/4}}{\pi a(\eta)\sqrt{|C|}} \{1 + \sqrt{\pi\tau} h(\eta) e^{\tau h(\eta)^2} \mathrm{erf}[\sqrt{\tau} h(\eta)]\} \tag{7}$$

where erf is the error function and

$$a(\eta) = (1 - \eta)^2 + \frac{1}{|C|}\left(\frac{\eta - \bar{\eta}}{1 - \bar{\eta}}\right)^2, \tag{8a}$$

$$h(\eta) = \frac{1 - \eta}{2\sqrt{a(\eta)}}. \tag{8b}$$

Here, $|C| = |L| f_1^2 f_2^2/\bar{\sigma}^2$ is the determinant of the matrix with dimensionless entries $C_{ij} = L_{ij} f_i f_j/\bar{\sigma}$. It can be expressed in terms of our parameters as

$$|C| = \frac{zT}{2}\left(1 + \epsilon\sqrt{1 - \frac{4}{zT}\frac{\bar{\eta}}{(1 - \bar{\eta})^2}}\right) - \frac{\bar{\eta}}{(1 - \bar{\eta})^2}, \tag{9}$$

where $\epsilon = \pm$ accounts for the existence of two probability distributions corresponding to given parameters. For $|L|$ to be real, the known bound

$$\bar{\eta} \le \frac{1 - \sqrt{\zeta}}{1 + \sqrt{\zeta}} \tag{10}$$

must hold [14]. Importantly, $a(\eta)$ is positive semidefinite.

Let us study the efficiency PDF in detail. First, it is a power-law distribution with tails

$$P_\tau(\eta \to \pm\infty) \propto \eta^{-2}, \tag{11}$$

which, after submission of this Letter, has been proven to be a universal property of efficiency distributions [15]. As a consequence, it does not afford finite moments of any order. Hence, the macroscopic efficiency $\bar{\eta}$ is *not* the average efficiency $\langle \eta \rangle_t$, which is not finite.

In Fig. 1, the efficiency distribution is plotted as the bold curve. Remarkably, for a large class of parameters it displays two maxima at η_m, η_m^* and a minimum, the latter slightly off the Carnot efficiency. Hence, not only super-Carnot efficiencies are possible, but indeed, there appears a local maximum with an efficiency higher than that of Carnot. To understand its physical origin, we distinguish four operational regimes of the machine, according to the signs of the two contributions σ_1 and σ_2 to the entropy production rate. The two regimes contributing to positive efficiencies are the machine $-+$ that employs process 2 flowing along its spontaneous tendency, to drive process 1 against its spontaneous tendency (e.g., heat engine) and the dual machine $+-$ where the system's spontaneous tendency is used to drive the environment against its tendency (e.g., the heat pump). Correspondingly, we have $\theta(\eta) P_\tau(\eta) = P_\tau^{+-}(\eta) + P_\tau^{-+}(\eta)$ where

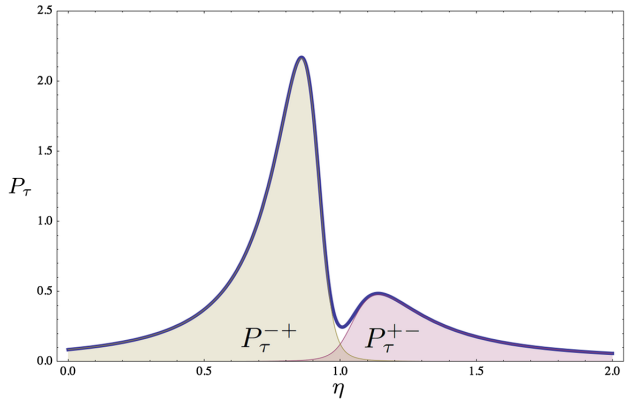

FIG. 1 (color online). Bold curve: efficiency distribution $P_\tau(\eta)$ for parameter values $\zeta = 0.01$, $\bar{\eta} = 0.6$, $\tau = 10$, $\epsilon = +1$. Filled curves beneath: $P_\tau^{-+}(\eta)$ and $P_\tau^{+-}(\eta)$, showing that each maximum is mostly due to one working mode of the engine.

$$P_\tau^{+-}(\eta) = \int_{\substack{+\sigma_1>0 \\ -\sigma 2>0}} dx_1 dx_2 P_t(x_1, x_2)\delta\left(\eta + \frac{f_1 x_1}{f_2 x_2}\right) \qquad (12)$$

and similarly for P_τ^{-+}. Shaded plots are provided in Fig. 1, showing that each of the two maxima is almost exclusively determined by one of the two modes of the machine, the second of which by inversion of input and output has typical efficiency $1/\eta_m^* < 1$. Regimes $++$ and $--$ contribute to the tail of the distribution at $\eta < 0$.

Let us now study the behavior of $P_\tau(\eta)$ in scaled time, depicted in Fig. 2. At $\tau = 0$ we obtain a Cauchy distribution $P_0(\eta) = 1/[\pi a(\eta)\sqrt{|C|}]$, with maximum at $\eta_0 = -L_{12}f_1/(L_{22}f_2)$. We have $\eta_0 \geq \bar{\eta}$, and equality can only occur for $|C| = 0$. This implies that the most probable efficiency decreases in time towards $\bar{\eta}$. Furthermore, at *thermodynamic equilibrium* where all the forces vanish,

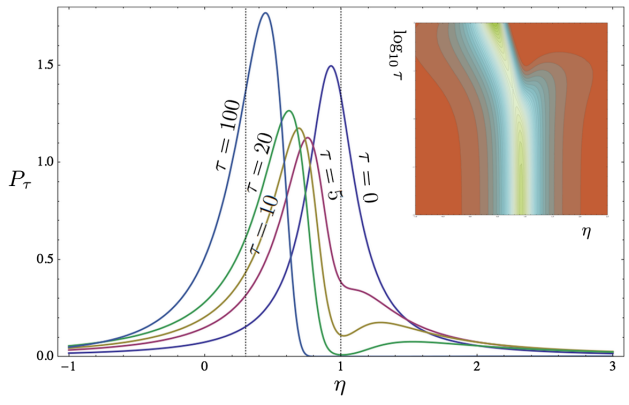

FIG. 2 (color online). Main frame: Efficiency distribution at various scaled times, for $\zeta = 0.05$, $\bar{\eta} = 0.3$, $\epsilon = +$. The vertical dotted lines correspond to $\bar{\eta}$ and η_c. Inset: Contour plot of the efficiency PDF as a function of η and τ (in log scale). Maxima are points where the level lines have horizontal tangents. After a critical time, a second maximum drifting to infinity appears.

$\boldsymbol{f} \to 0$ at finite φ, it can be shown that $P_\tau^{\rm eq}(\eta) = P_0(\eta)$, which means that systems at equilibrium do not evolve. As time elapses a transition to a bimodal distribution occurs, with the super-Carnot maximum drifting to infinity. We can define a critical time τ_c at which there appears an inflection point in $P_\tau(\eta)$. Numerical plots of τ_c in terms of $\bar{\eta}$ and c show that the critical time is higher the closer to the maximal efficiency and to the "loose coupling" condition $\zeta \to 1$ (Supplemental Material [13]). Finally, in the long time limit one has $\mathrm{erf}(\sqrt{\tau}h) \sim 1 - e^{-\tau h^2}/(\sqrt{\pi\tau}|h|)$ [16] and

$$P_{\tau\to\infty}(\eta) \sim \frac{e^{-\tau/4}}{\pi a(\eta)|C|}\left(1 - \frac{h}{|h|} + \sqrt{\pi\tau}e^{\tau h(\eta)^2}\right). \qquad (13)$$

The large-time behavior is captured by the large deviation rate function $I(\eta) = -\lim_{\tau\to\infty}\tau^{-1}\ln P_\tau(\eta) = 1/4 - h(\eta)^2 \geq 0$, which was first calculated and thoroughly analyzed by Verley *et al.* [1,2]. The rate function has only two extrema, a minimum $I(\bar{\eta}) = 0$ and a maximum $I(1) = 1/4$, and asymptotically $I(\pm\infty) = [4|C|(1-\bar{\eta})^2 + 4]^{-1} \leq I(1)$. Then, the more pronounced maximum tends to the macroscopic efficiency $\bar{\eta}$, while the minimum tends to the Carnot efficiency. The second maximum does not appear in the large deviation rate function because at infinite time it moves to infinity, since it belongs to a subdominant decay mode. This proves the existence of a critical time τ_c, as there must exist another maximum for the distribution to converge.

The quest for the Carnot limit is very subtle. By Eq. (10), the Carnot bound can be saturated in the limit $\zeta \to 0$, giving rise to two extreme situations related to the spectrum and eigenvectors of the response matrix $L \to L^\epsilon$. For $\epsilon = -$ ("tight coupling"), by Eq. (9) the correlation matrix becomes degenerate,

$$L^- = \begin{pmatrix} L_{11} & -\sqrt{L_{11}L_{22}} + O(\zeta) \\ -\sqrt{L_{11}L_{22}} + O(\zeta) & L_{22} \end{pmatrix}, \qquad (14)$$

where $O(\zeta)$ are terms of order ζ. For $\epsilon = +$ ("singular coupling"), L tends to the inverse of a degenerate matrix, i.e., $L^+ = L^-/O(\zeta)$, with $|L^+| \to \infty$.

To reach Carnot efficiency, a second independent condition ("self-duality") must hold: φ attains value $\varphi^* = \sqrt{L_{11}/L_{22}}$, which affords an interesting interpretation in terms of the probability of the inverse efficiency (Supplemental Material [13]). When $\zeta \to 0$, this condition makes $\boldsymbol{f}$ either the null eigenvector of L^- relative to its null eigenvalue or of L^+ relative to its finite eigenvalue. In the tight-coupling regime, this condition is known as the "stall force" [17].

Expressing the efficiency in terms of the adimensional parameters ζ and $\phi = \varphi/\varphi^*$ (for $L_{12} < 0$) as [18]

$$\bar{\eta}(\zeta, \phi) = -\frac{1 - \phi\sqrt{1-\zeta}}{\phi^2 - \phi\sqrt{1-\zeta}}, \qquad (15)$$

one finds that the two limits towards self-duality and towards tight or singular coupling do not commute,

$$1 = -\lim_{\zeta\to 0}\lim_{\phi\to 1}\bar{\eta} = +\lim_{\phi\to 1}\lim_{\zeta\to 0}\bar{\eta}\,. \tag{16}$$

Then, a macroscopic Carnot efficiency is "fragile," as the self-dual forces needed to attain it are those that slightly out of $\zeta = 0$ give a "dud" machine that dissipates to obtain nothing, with macroscopic efficiency $\bar{\eta} = -1$.

Nevertheless, the probabilistic level is richer. At tight coupling the bivariate Gaussian Eq. (5) becomes univariate with support along $x_1/x_2 = -\varphi^*$, and the efficiency PDF a Dirac delta centered at the macroscopic efficiency. Then tightly coupled machines work macroscopically at all scaled times.

More interesting is the singular coupling. Figure 3 shows that in this limit all extrema tend to accumulate towards the Carnot efficiency, where the density concentrates. Despite the fact that the two peaks survive, convergence to a Dirac delta can be proven by the following argument [19]: From Eqs. (7) and (8), $h \to 1/2$, $a \to (1-\eta)^2$, and the efficiency PDF converges to a distribution with support in $\eta = 1$, which is then necessarily a finite combination of derivatives of the Dirac delta $P_\tau(\eta) = \sum_{n=0}^{N} p_n \delta^{(n)}(1-\eta)$ [20]. Since $\langle g\rangle > 0$ for all positive test functions $g(\eta) > 0$, then necessarily $p_n = 0$ but for $p_0 = 1$ □. Then, singular coupling pushes the most probable efficiency towards the Carnot limit at fixed τ; the shadings in Fig. 3 suggest that in this limit the distribution is fairly insensitive to $\bar{\eta}$. Moreover, the contour plot in Fig. 3 supports that the most probable efficiency stays at the same value for probability densities evaluated at a fixed time $\tau \propto 1/\zeta$, showing that

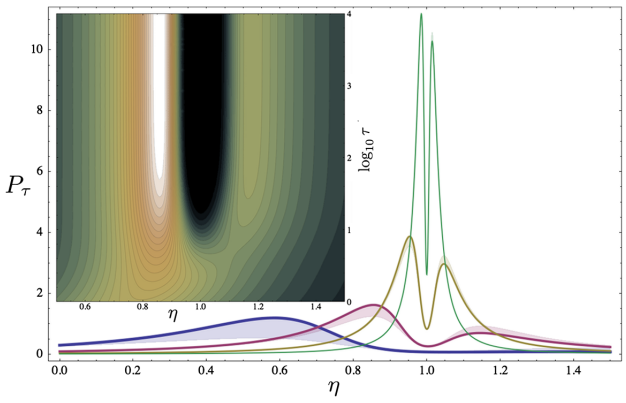

FIG. 3 (color online). Graphs of $(\eta, P_\tau(\eta))$ for $\tau = 10$, $\bar{\eta} = 0.3$, $\epsilon = +$ and for various coupling parameters (from bolder to thinner) $\zeta = 0.1, 0.01, 0.001, 0.0001$. The shading represents the distance to the corresponding curves for $\bar{\eta} = -1$. Inset: Contour plot of the efficiency PDFs corresponding to parameter $\zeta = 0.1/\tau$ as a function of the efficiency η and the scaled time τ (in log scale), showing that the PDF is invariant at all times, hence, that singular coupling stretches the relaxation times. Lighter tones for higher probabilities, darker for lower.

convergence to $\bar{\eta}$ is more and more delayed. However, it must be remembered that the physical time scale is set by the entropy production rate. Necessarily, the matrix entries of L^+ diverge; then in general $\bar{\sigma}$ also diverges. Still, L^+ admits a finite eigenvalue. Picking the forces along the relative eigenvector, $\phi = 1 + O(\zeta)$, one obtains a finite entropy production rate. Oddly, as discussed above, these conditions are met when the macroscopic machine is dud.

To resume: At singular coupling, the effect of fluctuations is macroscopically visible and permits us to work close to Carnot efficiency at finite entropy production rate for sufficiently long physical times. The conditions for which the entropy production rate can be held finite are those under which the machine eventually evolves towards a dud fate. Notice that in this regime the system might flip randomly across the close sharp peaks of the PDF. However, the inset in Fig. 3 suggests that at intermediate times reasonably high typical efficiencies will be favored and that a large separation between such peaks (the dark region of zero probability) occurs. Hence, to put it with a motto, a singular machine doomed to be useless might be efficiently useful for some time due to fluctuations; the better in the short run, the worse in the long. By the Green-Kubo relation of Eq. (6) the singular coupling limit is approached when correlations between the currents diverge and the inverse correlation matrix becomes degenerate. It is tempting to parallel this behavior to the paradigm of criticality at phase transitions, where fluctuations become macroscopic, correlations diverge, and the covariance matrix degenerates [21,22].

An important observation to be made here is that singular coupling pushes the system far from equilibrium. The framework of stochastic thermodynamics encompasses such systems by assuming that they are subtended by an underlying Markovian dynamics, giving rise to non-Gaussian current statistics. Gaussianity is only recovered in the linear regime at large times by the central limit theorem [23,24]. While the model of a Brownian particle in a tilted plane studied in Ref. [1] has the exact Gaussian propagators studied in this Letter, in general Markov processes have a more complex behavior in time; in particular, the average flux varies as the system evolves, depending on the initial ensemble. Then, the exact short- and large-time behavior of the efficiency distribution might become model dependent. For asymmetric protocols, a signature of non-Gaussian behavior is the off-Carnot least-probable efficiency [2,4,5].

Nevertheless, our study points out that in the simplest Gaussian scenario the efficiency PDF manifests peculiar features that might possibly be universal: power-law tails, no finite moments, a naturally occurring transition to a bimodal distribution due to reverse working regimes, etc. Particularly intriguing is the limit of a degenerate or singular covariance matrix. While the former case is intrinsically macroscopic and broadly studied [14,18],

we obtain a clear indication that the singular coupling regime displays an interesting behavior that could lead to the enhancement of the efficiency above its macroscopic value. More light is to be shed on these issues by future inquiry on the finite-time statistics of the efficiency in stochastic models [15,17] in their rich phenomenology, including maximum power generation [25,26], multiterminal machines [27], broken time-reversal symmetry [28], the insurgence of phase transitions, and in relation to the issue of efficiency enhancement by noise [29] or by decoherence [30]. Experimental setups that could test these predictions are already available [31–35]. The full statistics of the efficiency close to equilibrium has recently been sampled for a Carnot engine realized with a Brownian particle, in the quasistatic limit where the currents' statistics is Gaussian [5], and data analysis farther away from equilibrium might soon be available.

This research was supported by the National Research Fund Luxembourg in the frame of project FNR/A11/02 and of Postdoc Grant No. 5856127.

*matteo.polettini@uni.lu
†gatien.verley@th.u-psud.fr
‡massimilano.esposito@uni.lu

[1] G. Verley, T. Willaert, C. Van den Broeck, and M. Esposito, Nat. Commun. **5**, 4721 (2014).
[2] G. Verley, T. Willaert, C. Van den Broeck, and M. Esposito, Phys. Rev. E **90**, 052145 (2014).
[3] H. Touchette, Phys. Rep. **478**, 1 (2009).
[4] T. R. Gingrich, G. M. Rotskoff, S. Vaikuntanathan, and P. L. Geissler, New J. Phys. **16**, 102003 (2014).
[5] I. A. Martinez, E. Roldan, L. Dinis, D. Petrov, J. M. R. Parrondo, and R. Rica, arXiv:1412.1282.
[6] S. Rana, P. S. Pal, A. Saha, and A. M. Jayannavar, Phys. Rev. E **90**, 042146 (2014).
[7] S. R. De Groot and P. Mazur, *Non-equilibrium Thermodynamics* (Courier Dover Publications, New York, 2013).
[8] U. Seifert, Rep. Prog. Phys. **75**, 126001 (2012).
[9] C. Van den Broeck and M. Esposito, Physica (Amsterdam) **418A**, 6 (2015).
[10] G. N. Bochkov and Y. E. Kuzovlev, Physica (Amsterdam) **106A**, 443 (1981); G. N. Bochkov and Y. E. Kuzovlev, Physica (Amsterdam) **106A**, 480 (1981).
[11] M. Polettini and M. Esposito, J. Stat. Mech., (2014) P10033.
[12] D. Andrieux and P. Gaspard, J. Chem. Phys. **121**, 6167 (2004).
[13] See the Supplemental Material at http://link.aps.org/supplemental/10.1103/PhysRevLett.114.050601 for details regarding the derivation of the efficiency PDF, the parametrization, and the various limiting situations.
[14] G. Benenti, K. Saito, and G. Casati, Phys. Rev. Lett. **106**, 230602 (2011).
[15] K. Proesmans, B. Cleuren, and C. Van Den Broeck, arXiv:1411.3531.
[16] M. Abramowitz and I. A. Stegun, *Handbook of Mathematical Functions with Formulas, Graphs, and Mathematical Tables* (Dover, New York, 1965).
[17] F. Jülicher, A. Ajdar, and J. Prost, Rev. Mod. Phys. **69**, 1269 (1997).
[18] O. Entin-Wohlman, J.-H. Jiang, and Y. Imry, Phys. Rev. E **89**, 012123 (2014).
[19] Discussion with user Kostya_I on mathoverflow.net, http://mathoverflow.net/questions/178859/power-law-distribution-with-support-in-x-0.
[20] L. Hörmander, *The Analysis of Linear Partial Differential Operators I* (Springer, Berlin, 1983).
[21] P. Zanardi, P. Giorda, and M. Cozzini, Phys. Rev. Lett. **99**, 100603 (2007).
[22] M. Polettini, Eur. Phys. J. B **87**, 215 (2014).
[23] T. Speck and U. Seifert, Phys. Rev. E **70**, 066112 (2004).
[24] J. Hoppenau and A. Engel, J. Stat. Mech.: Theory Exp. (**2013**) P06004.
[25] M. Esposito, K. Lindenberg, and C. Van den Broeck, Phys. Rev. Lett. **102**, 130602 (2009).
[26] T. Schmiedl and U. Seifert, Europhys. Lett. **81**, 20003 (2008).
[27] F. Mazza, R. Bosisio, G. Benenti, V. Giovannetti, R. Fazio, and F. Taddei, New J. Phys. **16**, 085001 (2014).
[28] K. Saito, G. Benenti, G. Casati, and T. Prosen, Phys. Rev. B **84**, 201306 (2011).
[29] J. Spiechowicz, P. Hänggi, and J. Łuczka, Phys. Rev. E **90**, 032104 (2014).
[30] F. Caruso, A. W. Chin, A. Datta, S. F. Huelga, and M. B. Plenio, J. Chem. Phys. **131**, 105106 (2009).
[31] D. Collin, F. Ritort, C. Jarzynski, S. B. Smith, I. Tinoco, and C. Bustamante, Nature (London) **437**, 231 (2005).
[32] A. Bérut, A. Arakelyan, A. Petrosyan, S. Ciliberto, R. Dillenschneider, and E. Lutz, Nature (London) **483**, 187 (2012).
[33] J. V. Koski, T. Sagawa, O-P. Saira, Y. Yoon, A. Kutvonen, P. Solinas, M. Möttönen, T. Ala-Nissila, and J. P. Pekola, Nat. Phys. **9**, 644 (2013).
[34] S. Ciliberto, A. Imparato, A. Naert, and M. Tanase, Phys. Rev. Lett. **110**, 180601 (2013).
[35] C. Tietz, S. Schuler, T. Speck, U. Seifert, and J. Wrachtrup, Phys. Rev. Lett. **97**, 050602 (2006).

Efficiency Fluctuations of Stochastic Machines Undergoing a Phase Transition

Hadrien Vroylandt,[1] Massimiliano Esposito,[2] and Gatien Verley[1]
[1]*Université Paris-Saclay, CNRS/IN2P3, IJCLab, 91405 Orsay, France*
[2]*Complex Systems and Statistical Mechanics, Department of Physics and Material Science, University of Luxembourg, L-1511 Luxembourg, G.D. Luxembourg*

(Received 12 December 2019; accepted 13 May 2020; published 25 June 2020)

We study the efficiency fluctuations of a stochastic heat engine made of N interacting unicyclic machines and undergoing a phase transition in the macroscopic limit. Depending on N and on the observation time, the machine can explore its whole phase space or not. This affects the engine efficiency that either strongly fluctuates on a large interval of equiprobable efficiencies (ergodic case) or fluctuates close to several most likely values (nonergodic case). We also provide a proof that despite the phase transition, the decay rate of the efficiency distribution at the reversible efficiency remains largest one although other efficiencies can now decay equally fast.

DOI: 10.1103/PhysRevLett.124.250603

Introduction.—Small machines behave on average like macroscopic ones: a mean input flux is converted into a mean output flux with an efficiency bounded by the reversible efficiency due to the second law of thermodynamics [1]. However, their input and output fluxes fluctuate with root mean squares which can be larger than their averages. These fluctuations are constrained by the universal fluctuation relations that lead to the second law at the ensemble averaged level [2–4]. This implies that the efficiency η of the machine along a single realization of duration t is also a stochastic quantity characterized by a probability distribution $P(\eta)$. As recently discovered, its fluctuations also display universal statistical features in both classical [5–12] and quantum systems [13–16]. More specifically, for long trajectories of autonomous machines, the distribution $P(\eta)$ concentrates at the macroscopic efficiency $\bar{\eta}$ while the reversible efficiency $\eta_{\rm rev}$ becomes asymptotically the less likely. Also, the efficiency large deviation function (LDF), defined as the long time limit of $t^{-1}\ln P(\eta)$, has a characteristic smooth form with two extrema only and a well-defined limit for large efficiency fluctuations. These predictions were experimentally verified in Refs. [17,18]. However, these results focus on the efficiency statistics at long times and rely on the assumptions that the machine has a finite state space and thus cannot undergo a phase transition.

The performance of machines undergoing a nonequilibrium phase transition has attracted increasing attention [19–25]. In this Letter, we consider a model of N interacting machines first proposed in Ref. [26]. At the mean-field (MF) level, i.e., when $N \to \infty$, they may undergo a nonequilibrium phase transition caused by an asymmetric pitchfork bifurcation. Past the bifurcation point, ergodicity is broken and these machines exhibit multiple macroscopic efficiencies [27]. In practice this means that their initial condition will determine which stable steady state is eventually reached and its corresponding macroscopic efficiency. As a result fluctuations in performance only come from uncertainties in the initial state. Our main goal here is to characterize how efficiency fluctuations scale in size N and in time t in such critical machines using LDFs. We do so by developing a path integral method (in the spirit of [28–34]). Crucially two regimes must be distinguished depending on the order in which these scalings are taken, each yielding to a different LDF. The first, $J(\eta)$, characterizes the nonergodic regime and corresponds to taking first $N \to \infty$ and then $t \to \infty$ on $(Nt)^{-1}\ln P(\eta)$. The second, $J^{**}(\eta)$, characterizes the ergodic regime and corresponds to the opposite order of limits. While this latter remains smooth, its two extrema become degenerate, giving rise to strong efficiency fluctuations spanning over different operating modes. The former instead is not continuously differentiable anymore and displays steep minima located around the mean field efficiencies and multiple plateaux. Remarkably, despite significant qualitative changes in both types of LDF, the reversible efficiency, while not uniquely anymore, has the fastest decaying efficiency probability. While our method is presented for a specific model, it seems particularly well suited to study collections of interacting machines and characterizes critical nonequilibrium fluctuations.

Model.—We consider a machine made of a collection of N interacting unicyclic machines. Each of these is autonomous and converts heat into mechanical work by hopping between two discrete states of energy 0 or $E \geq 0$ via two different transition channels labeled by ν, where $\nu = 1$ is caused by a cold reservoir at temperature $T^{(1)} = 1/\beta^{(1)}$ and $\nu = 2$ by a hot one at $T^{(2)} = 1/\beta^{(2)}$ (we set $k_B = 1$). A nonconservative force promotes (represses) the transition from the lower to the higher energy state via channel $\nu = 1$ ($\nu = 2$), while the opposite is true for the transition from the

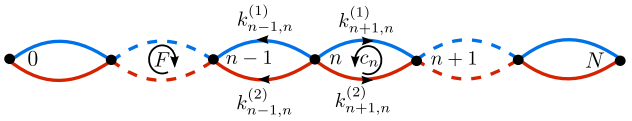

FIG. 1. Graph of the discrete state space of the collective machine. Blue edges are for channel 1 and red edges for channel 2.

higher to the lower state. These unicyclic machines interacts via a pair interaction energy V/N only when they are not in the same states. The energy of the collective machine thus reads $U_n = nE + n(N-n)V/N$, where n is the number of machines in the high energy state. The probability to find the collective machine in state n at time t follows a Markov master equation $\dot{p}_n = \sum_{\varepsilon=\pm1,0}\sum_\nu k^{(\nu)}_{n,n+\varepsilon}p_{n+\varepsilon}$, where $k^{(\nu)}_{n+\epsilon,n}$ is the Poisson rate with which a unicyclic machine hops to a high (low) energy state for $\epsilon = 1$ ($\epsilon = -1$) via channel ν and $k^{(\nu)}_{n,n} = -k^{(\nu)}_{n+1,n} - k^{(\nu)}_{n-1,n}$, see Fig. 1. To specify further the dynamics, we choose (for $\epsilon = \pm 1$)

$$k^{(\nu)}_{n+\epsilon,n} = N\left(\frac{1+\epsilon}{2} - \epsilon\frac{n}{N}\right)e^{-\frac{\beta^{(\nu)}}{2}(E_a + U_{n+\epsilon} - U_n - W^{(\nu)}_{n+\epsilon,n})}, \quad (1)$$

where E_a is an activation energy and $W^{(\nu)}_{n+\epsilon,n} \equiv -\epsilon(-1)^\nu F$ is the work done by the nonconservative force and received by the machine during the transition $n \to n+\epsilon$ via ν. Defining intensive quantities as being per unicyclic machine and per unit time, the intensive stochastic heat from the hot reservoir and the intensive work from the nonconservative force are, respectively,

$$q = \sum_{n=0}^{N-1}\phi_{\mathsf{q},n}j^{(2)}_n \quad \text{and} \quad w = \sum_{n=0}^{N-1}\phi_{\mathsf{w},n}j^{(2)}_n, \quad (2)$$

where $j^{(2)}_n$ counts the intensive net number of jumps from n to $n+1$ via channel 2 in a stochastic trajectory. Indeed, when $X = \mathsf{q}$ (respectively, $X = \mathsf{w}$), $\phi_{X,n}$ gives the amount of energy received from the hot reservoir (respectively, from the nonconservative force) when the system undergoes a cycle $c_n \equiv (n \underset{\nu=2}{\to} n+1 \underset{\nu=1}{\to} n)$:

$$\phi_{\mathsf{q},n} \equiv U_{n+1} - U_n - W^{(2)}_{n+1,n} \simeq V(1-2n/N) + F, \quad (3)$$

$$\phi_{\mathsf{w},n} \equiv W^{(1)}_{n,n+1} + W^{(2)}_{n+1,n} = -2F. \quad (4)$$

The intensive stochastic entropy production $\sigma \equiv \sigma^{\mathsf{w}} + \sigma^{\mathsf{q}}$ is the sum of the two partial entropy production $\sigma^{\mathsf{q}} \equiv [\beta^{(1)} - \beta^{(2)}]q$ and $\sigma^{\mathsf{w}} \equiv \beta^{(1)}w$. The stochastic efficiency is thus defined as $\eta \equiv -\sigma^{\mathsf{w}}/\sigma^{\mathsf{q}}$. Their local (i.e., along each cycle c_n) analogs read $\sigma^{\mathsf{q}}_n \equiv [\beta^{(1)} - \beta^{(2)}]\phi_{\mathsf{q},n}$, $\sigma^{\mathsf{w}}_n \equiv \beta^{(1)}\phi_{\mathsf{w},n}$,

$$\eta^{\mathsf{l}}_n \equiv -\frac{\beta^{(1)}\phi_{\mathsf{w},n}}{(\beta^{(1)} - \beta^{(2)})\phi_{\mathsf{q},n}} = -\frac{\sigma^{\mathsf{w}}_n}{\sigma^{\mathsf{q}}_n}. \quad (5)$$

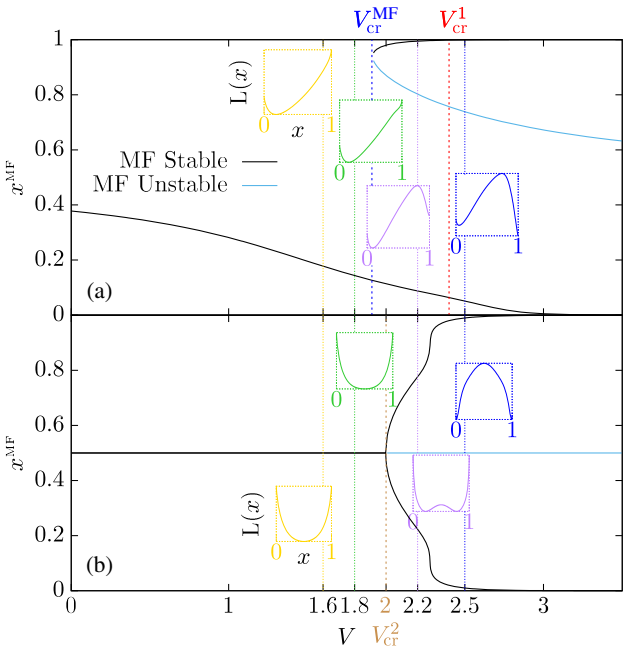

FIG. 2. Stable (black) and unstable (light blue) mean field steady state densities x^{MF} versus interaction energy V. Insets: density LDFs versus x for four values of V indicated by vertical dashed lines. The parameters are $E_a = 2$, $E = 0$, $\beta^{(1)} = 10$, $F = 0.5$ for panel (a) and $F = 0$ for panel (b). In all the Letter we take $\beta^{(2)} = 1$ to set the energy scales, while the timescale is set by Eq. (1).

In the macroscopic limit where N is very large and the density of units in the high energy state $x = n/N$ can be treated as a continuous variable, we denote them, respectively, by σ^{q}_x, σ^{w}_x and η^{l}_x.

Mean field dynamics.—When $N \to \infty$ but t remains finite, the master equation becomes a nonlinear MF master equation for x [26]. Ergodicity breaking is evidenced by the fact that its stationary solutions may take one, three (or even five) values x^{MF} depending on V and F, as shown on the branching diagrams of Fig. 2. Each of these solutions will give rise to a corresponding MF efficiency trough Eq. (5). The MF master equation is exact for this model, i.e., the extrema of the density LDF $L(x)$ [27,35] (shown in the insets) coincide with the MF densities. In panel (a) for $F = 0.5$, the abrupt change in the position of the minimum of the density LDFs around V^{1}_{cr} reveals a first order phase transition while in panel (b) for $F = 0$ the smooth appearance of two minima at V^{2}_{cr} reveals a second order phase transition.

Currents and efficiency fluctuations.—The quantity of interest is the cumulant generating function (CGF) for σ^{q} and σ^{w} expressed in terms of their conjugated Laplace parameter $\boldsymbol{\gamma} = (\gamma^{\mathsf{q}}, \gamma^{\mathsf{w}})$ which reads

$$\Phi(\boldsymbol{\gamma}) \equiv \lim_{Nt\to\infty}\frac{1}{Nt}\ln\langle e^{Nt(\gamma^{\mathsf{q}}\sigma^{\mathsf{q}} + \gamma^{\mathsf{w}}\sigma^{\mathsf{w}})}\rangle_{p_0}, \quad (6)$$

where $\langle \ldots \rangle_{p_0}$ is the mean on paths with initial condition drawn from probability density p_0. Using path integral technique [34,36,37], this CGF can be written as the maximum value taken by an action over trajectories $[x]_0^\infty$ of infinite duration

$$\Phi(\boldsymbol{\gamma}) = \max_{[x]_0^\infty} S([x]_0^\infty, \boldsymbol{\gamma}). \tag{7}$$

The action $S([x]_0^t, \boldsymbol{\gamma}) = (1/t)\int_0^t d\tau \mathcal{L}(x(\tau), \dot{x}(\tau), \boldsymbol{\gamma})$ is associated to the Lagrangian given by

$$\mathcal{L}(x,\dot{x},\boldsymbol{\gamma}) \equiv \sqrt{\dot{x}^2 + \varphi(x,\boldsymbol{\gamma})} - \sum_{\epsilon=\pm1,\nu=1,2} J_{\epsilon;\nu}(x) + \dot{x}\ln\left(\frac{-\dot{x}+\sqrt{\dot{x}^2+\varphi(x,\boldsymbol{\gamma})}}{2\sum_{\nu=1,2} J_{-1;\nu}(x) e^{-(\gamma^{\mathsf{q}}\sigma_x^{\mathsf{q}} + \gamma^{\mathsf{w}}\sigma_x^{\mathsf{w}})\delta_{\nu,2}}}\right), \tag{8}$$

where we introduced the transition rates in the continuous limit $J_{\epsilon;\nu} \equiv \lim_{N\to\infty} k^{(\nu)}_{xN+\epsilon,xN}/N$ and the function

$$\varphi(x,\boldsymbol{\gamma}) \equiv 4\prod_{\epsilon=\pm1}\sum_{\nu=1,2} J_{\epsilon;\nu}(x)\exp[\epsilon(\gamma^{\mathsf{q}}\sigma_x^{\mathsf{q}} + \gamma^{\mathsf{w}}\sigma_x^{\mathsf{w}})\delta_{\nu,2}]. \tag{9}$$

From extremum action principle, $\Phi(\boldsymbol{\gamma})$ is the action evaluated for the optimal trajectories satisfying the Euler-Lagrange equation based on Lagrangian (8) for given initial conditions $x(0)$ and $\dot{x}(0)$. The remaining optimization on initial conditions amounts to select stationary trajectories only since the CGF is bounded by

$$\max_{\text{stat.}[x]} S[x] \le \Phi(\boldsymbol{\gamma}) \le \max_{x,\dot{x}} \mathcal{L}(x,\dot{x},\boldsymbol{\gamma}). \tag{10}$$

The lower bound arises from restricting the maximization to the subset of stationary trajectories (i.e., trajectories with constant density), while the upper bound follows from exchanging the maximization and the time integration in the action. For Lagrangian (8), the maxima in the upper bound can be shown to coincide with the stationary solutions x^* of Euler-Lagrange equation. Hence, the upper and lower bounds match yielding the CGF

$$\Phi(\boldsymbol{\gamma}) = \max_{x^*} \mathcal{L}(x^*, 0, \boldsymbol{\gamma}). \tag{11}$$

The LDF for stochastic efficiency can be computed from the CGF of the partial entropy productions directly [5]. When x^* is not unique, the order of the limits $t\to\infty$ and $N\to\infty$ in (6) is of importance [38]. In the *ergodic case*, the initial probability density p_0 plays no role and the x^* maximizing the value of the Lagrangian is chosen in Eq. (11). The efficiency LDF then reads

$$J^{**}(\eta) \equiv -\min_{\gamma^{\mathsf{w}}} \max_{x^*} \mathcal{L}(x^*, 0, \gamma^{\mathsf{w}}\eta, \gamma^{\mathsf{w}}), \tag{12}$$

$$= -\min_{\gamma^{\mathsf{w}}} \Phi(\gamma^{\mathsf{w}}\eta, \gamma^{\mathsf{w}}) \ge 0, \tag{13}$$

where we used $\Phi(0,0) = 0$. In the *nonergodic case*, the system can be separated into ergodic regions and the number of regions accessible with the chosen initial condition p_0 will matter [38]. The x^* which belongs to those accessible regions and which maximizes the value of the Lagrangian must be picked. The efficiency LDF reads

$$J(\eta) \equiv -\max_{x^*} \min_{\gamma^{\mathsf{w}}} \mathcal{L}(x^*, 0, \gamma^{\mathsf{w}}\eta, \gamma^{\mathsf{w}}), \tag{14}$$

where the maximum holds on all x^* when choosing a uniform initial condition that makes all ergodic regions accessible.

Results.—The signature of a phase transition and/or ergodicity breaking is when x^* stops being unique. While the CGF is always continuous and convex, its derivatives may become singular [39]. A kink in the CGF signals a nonconvexity or a linear part in the currents LDF. We now proceed to prove that the reversible efficiency still corresponds to the faster decay rate of the efficiency probability without using the convexity of the LDF. The fluctuation relation $\Phi(\boldsymbol{\gamma}) = \Phi(-\boldsymbol{\gamma} - \mathbf{1})$ imposes that Φ is symmetric with respect to the point $\boldsymbol{\gamma} = (-1/2, -1/2)$ which we denote by C. Then, since Φ is convex, it has a minimum at C and the minima of $\mathcal{L}$ in Eqs. (12) or (14) are reached at this point when the efficiency is the reversible one ($\eta = 1$) leading to $J(\eta) \le J(1)$. However, since Φ is not necessarily strictly convex, the minima may be degenerate and other efficiencies can give rise to equally large LDF.

We now turn to our numerical results. In Figs. 3(d)–(f), we show the efficiency LDFs obtained from Eqs. (12)–(14) (for $N\to\infty$) or from numerical evaluation of the CGF for σ^{q} and σ^{w} (for finite N) using standard spectral techniques [40,41]. We clearly see that both $J(\eta)$ and $J^{**}(\eta)$ are substantially different than the efficiency LDF of finite machines discussed in Ref. [5]. In both cases their maximum is degenerate and comprises the reversible efficiency as we will explain below. We remark that $J(\eta) > J^{**}(\eta)$ for all η, as expected since $J^{**}(\eta)$ can be derived from the convex hull of the nonconvex LDF for partial entropy productions from which $J(\eta)$ is derived [38]. The minimum of both LDF that correspond to the MF efficiency is unique for $V < V_{\text{cr}}^{\text{MF}}$, while for higher V, a plateau connects the different MF efficiencies $\eta^l_{x^{\text{MF}}}$ in the ergodic case or several minima appear in $J(\eta)$ in the nonergodic case. The plateaux signify that ergodicity enables large fluctuations between MF efficiencies while nonergodicity prevents them. Interestingly, our numerical computations for increasing N show a faster convergence of $J^{**}(\eta)$ toward the plateau lying between two *stable* MF efficiencies. Efficiency LDFs with multiple minima (or even a plateau) had not been reported before. Finding these plateaux and relating them to the existence of a phase transition in the machine constitutes a key finding of this Letter.

We now discuss the physical origin of the degenerate maximum of efficiency LDF. In tightly coupled finite

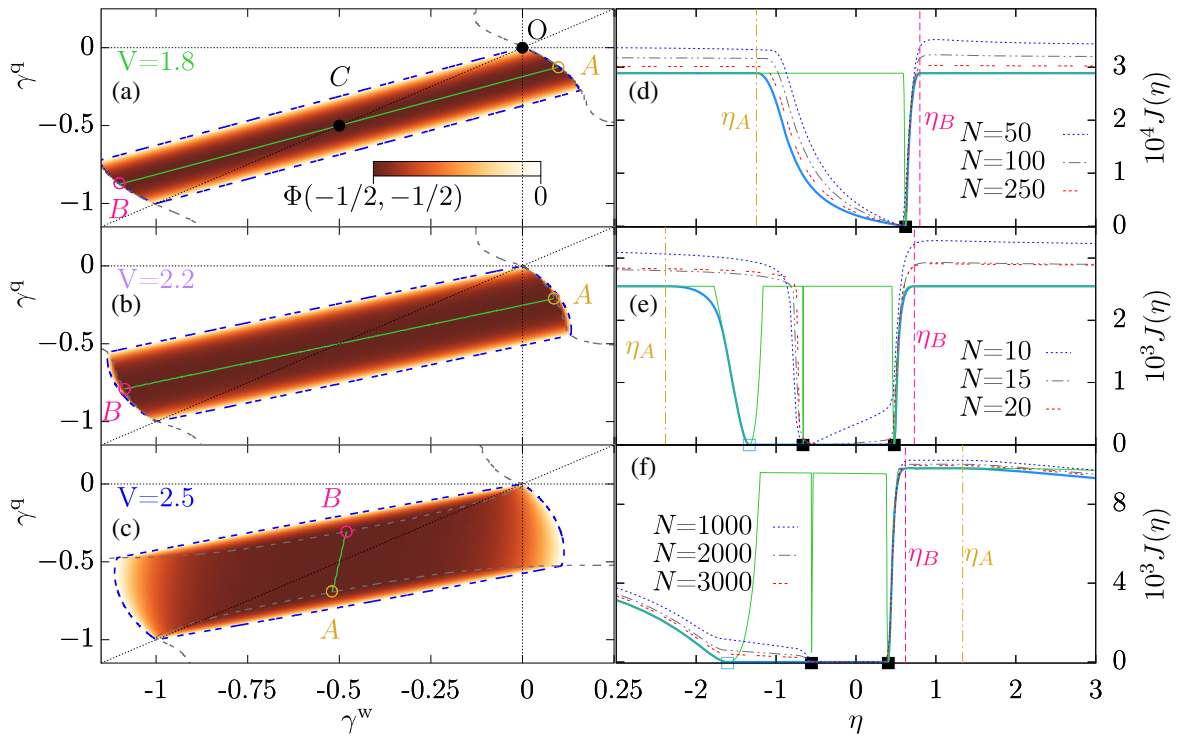

FIG. 3. Left column, CGFs Φ defined in (11) as a function of γ^{q} and γ^{w} for three different V (a)–(c). Right column, the corresponding efficiency LDF (d)–(f). On the left, the diagonal black dotted line of slope one is there to guide the eye and the blue dashed line is the contour line $\Phi = 0$ enclosing the $\Phi < 0$ region that is relevant to calculate (13). The green solid line between A and B defines the degenerate minimum of the CGF. Its boundaries belong to the dashed gray critical lines separating regions with different dominant stationary solutions x^*. The slopes η_A and η_B, of the lines (OA) and (OB), respectively, give the efficiencies delimiting the higher plateaux of the efficiency LDFs on the right. When $V > V_{\mathrm{cr}}^{\mathrm{MF}} = 1.92$, one critical line touches the origin indicating bistability in the MF dynamics. On the right, $J^{**}(\eta)$, $J(\eta)$, and the finite N efficiency LDFs are given, respectively, by the light blue thick solid line, the thin green solid line and the different dashed lines. The solid black (empty blue) squares show the location of the stable (unstable) MF efficiencies. The parameters are those of Fig. 2(a).

machines [42,43], the input and output fluxes are proportional at the stochastic trajectory level ($-\sigma^{\mathrm{q}}\alpha = \sigma^{\mathrm{w}}$) and $\bar{\eta} = \alpha$. As a result, the CGF $\Phi(\boldsymbol{\gamma})$ displays a translation invariance: it is zero on the line $\gamma^{\mathrm{q}} - \alpha\gamma^{\mathrm{w}} = 0$ and constant on any other parallel line. Using (13), the efficiency LDF has a singular minimum zero at efficiency α and a degenerate maximum everywhere else [9]. This results from the fact that the stochastic efficiency is either a constant number α or undefined when both σ^{q} and σ^{w} are zero (or more precisely subextensive in Nt). The degenerate LDF value thus corresponds to the LDF of the probability of having no extensive hot heat input and work output. However, when such machines have infinite state spaces, the notion of tight coupling softens as extensive entropy fluctuations can arise and compromises the translation invariance of the CGF (in fact it remains valid in a bounded region and the CGF diverges elsewhere). As a result the efficiency LDF still displays a degenerate maximum but that does not cover anymore all the efficiencies since the minimum is not singular anymore and is reached continuously [44,45]. In our model, similar plateaux are observed in Figs. 3(d)–3(f). However the mechanism responsible for softening the tight coupling is different and is the phase transition. The CGF has no global translation invariance anymore, but the Lagrangian keeps some invariance upon change of $\boldsymbol{\gamma}$ as one can check directly

$$\mathcal{L}\left(x, 0, -\frac{1}{2} + \left[\gamma^{\mathrm{w}} + \frac{1}{2}\right]\eta_x^l, \gamma^{\mathrm{w}}\right) = \mathcal{L}\left(x, 0, -\frac{1}{2}, -\frac{1}{2}\right). \quad (15)$$

For each density x^* over which the maximization is taken in (12) and (14) and for given $\eta \neq \eta_{x^*}^l$, the Lagrangian minimizer $\gamma^{\mathrm{w}} = (\eta_{x^*}^l - 1)/(2\eta - 2\eta_{x^*}^l)$ is yielding the same minimum $\mathcal{L}(x^*, 0, -1/2, -1/2)$ as long as the phase transition induces no change of maximizer x^* (this happens at efficiency η_A and η_B). This degeneracy is illustrated for the absolute minimum $\Phi(-\frac{1}{2}, -\frac{1}{2})$ on Figs. 3(a)–3(c). In the end, several ηs share the same Lagrangian's minimum associated to the same maximum $J(1)$ of the efficiency LDF in both the ergodic and nonergodic cases. As in tightly

coupled finite machines, these degenerate LDF maxima correspond to the LDF of the probability for no extensive work and hot heat to arise.

In summary, using a simple model, we found that efficiency fluctuations are strongly affected by the existence of a phase transition and depend on the order in which the long time and large size limit are taken. Nonetheless, the efficiency probability still decay the faster at the reversible efficiency, but maybe decay equally fast at other efficiencies. Our large deviation theory techniques are general and opens the way to a more systematic study of efficiency fluctuations in energy converters undergoing a phase transition.

We dedicate this work to Christian Van den Broeck who initiated this research project. We thank Alexandre Lazarescu for his comments on path action extremization. M. E. is funded by the European Research Council project NanoThermo (ERC-2015-CoG Agreement No. 681456).

[1] H. B. Callen, *Thermodynamics and an Introduction to Thermostatistics*, 2nd ed. (Wiley, New York, 1985).
[2] N. A. Sinitsyn, Fluctuation relation for heat engines, J. Phys. A **44**, 405001 (2011).
[3] M. Campisi, Fluctuation relation for quantum heat engines and refrigerators, J. Phys. A **47**, 245001 (2014).
[4] R. Rao and M. Esposito, Detailed fluctuation theorems: A unifying perspective, Entropy **20**, 635 (2018).
[5] G. Verley, T. Willaert, C. Van den Broeck, and M. Esposito, Universal theory of efficiency fluctuations, Phys. Rev. E **90**, 052145 (2014).
[6] T. R. Gingrich, G. M. Rotskoff, S. Vaikuntanathan, and P. L. Geissler, Efficiency and large deviations in time-asymmetric stochastic heat engines, New J. Phys. **16**, 102003 (2014).
[7] H. Vroylandt, A. Bonfils, and G. Verley, Efficiency fluctuations of small machines with unknown losses, Phys. Rev. E **93**, 052123 (2016).
[8] G. Verley, T. Willaert, C. Van den Broeck, and M. Esposito, The unlikely carnot efficiency, Nat. Commun. **5**, 4721 (2014).
[9] M. Polettini, G. Verley, and M. Esposito, Efficiency Statistics at all Times: Carnot Limit at Finite Power, Phys. Rev. Lett. **114**, 050601 (2015).
[10] K. Proesmans and C. V. den Broeck, Stochastic efficiency: five case studies, New J. Phys. **17**, 065004 (2015).
[11] K. Proesmans, B. Cleuren, and C. V. den Broeck, Stochastic efficiency for effusion as a thermal engine, Europhys. Lett. **109**, 20004 (2015).
[12] K. Proesmans, C. Driesen, B. Cleuren, and C. Van den Broeck, Efficiency of single-particle engines, Phys. Rev. E **92**, 032105 (2015).
[13] M. Esposito, M. A. Ochoa, and M. Galperin, Efficiency fluctuations in quantum thermoelectric devices, Phys. Rev. B **91**, 115417 (2015).
[14] J.-H. Jiang, B. K. Agarwalla, and D. Segal, Efficiency Statistics and Bounds for Systems with Broken Time-Reversal Symmetry, Phys. Rev. Lett. **115**, 040601 (2015).
[15] B. K. Agarwalla, J.-H. Jiang, and D. Segal, Full counting statistics of vibrationally assisted electronic conduction: Transport and fluctuations of thermoelectric efficiency, Phys. Rev. B **92**, 245418 (2015).
[16] T. Denzler and E. Lutz, Efficiency fluctuations of a quantum otto engine, arXiv:1907.02566.
[17] I. A. Martinez, É. Roldán, L. Dinis, D. Petrov, J. M. R. Parrondo, and R. Rica, Brownian Carnot engine, Nat. Phys. **12**, 67 (2015).
[18] K. Proesmans, Y. Dreher, M. Gavrilov, J. Bechhoefer, and C. Van den Broeck, Brownian Duet: A Novel Tale of Thermodynamic Efficiency, Phys. Rev. X **6**, 041010 (2016).
[19] A. Imparato, Stochastic thermodynamics in many-particle systems, New J. Phys. **17**, 125004 (2015).
[20] N. Golubeva and A. Imparato, Efficiency at Maximum Power of Interacting Molecular Machines, Phys. Rev. Lett. **109**, 190602 (2012).
[21] N. Golubeva and A. Imparato, Efficiency at maximum power of motor traffic on networks, Phys. Rev. E **89**, 062118 (2014).
[22] M. Campisi and R. Fazio, The power of a critical heat engine, Nat. Commun. **7**, 11895 (2016).
[23] P.-S. Shim, H.-M. Chun, and J. D. Noh, Macroscopic time-reversal symmetry breaking at a nonequilibrium phase transition, Phys. Rev. E **93**, 012113 (2016).
[24] T. Herpich, J. Thingna, and M. Esposito, Collective Power: Minimal Model for Thermodynamics of Nonequilibrium Phase Transitions, Phys. Rev. X **8**, 031056 (2018).
[25] T. Herpich and M. Esposito, Universality in driven potts models, Phys. Rev. E **99**, 022135 (2019).
[26] B. Cleuren and C. V. den Broeck, Ising model for a brownian donkey, Europhys. Lett. **54**, 1 (2001).
[27] H. Vroylandt, M. Esposito, and G. Verley, Collective effects enhancing power and efficiency, Europhys. Lett. **120**, 30009 (2017).
[28] J. Ross, *Thermodynamics and Fluctuations Far From Equilibrium* (Springer Berlin Heidelberg, New York, 2008).
[29] F. Ritort, Work and heat fluctuations in two-state systems: A trajectory thermodynamics formalism, J. Stat. Mech. (2004) P10016.
[30] J. Tailleur, J. Kurchan, and V. Lecomte, Mapping out-of-equilibrium into equilibrium in one-dimensional transport models, J. Phys. A **41**, 505001 (2008).
[31] T. Grafke and E. Vanden-Eijnden, Non-equilibrium transitions in multiscale systems with a bifurcating slow manifold, J. Stat. Mech. (2017) 093208.
[32] A. Suárez, J. Ross, B. Peng, K. L. C. Hunt, and P. M. Hunt, Thermodynamic and stochastic theory of nonequilibrium systems: A lagrangian approach to fluctuations and relation to excess work, J. Chem. Phys. **102**, 4563 (1995).
[33] M. F. Weber and E. Frey, Master equations and the theory of stochastic path integrals, Rep. Prog. Phys. **80**, 046601 (2017).
[34] A. Lazarescu, T. Cossetto, G. Falasco, and M. Esposito, Large deviations and dynamical phase transitions in stochastic chemical networks, J. Chem. Phys. **151**, 064117 (2019).
[35] T. L. Hill, *Free Energy Transduction and Biochemical Cycle Kinetics* (Springer-Verlag New York, Inc., New York, 1989).

[36] H. Vroylandt, D. Lacoste, and G. Verley, Degree of coupling and efficiency of energy converters far-from-equilibrium, J. Stat. Mech. (2018) 023205.
[37] H. Vroylandt, Thermodynamics and fluctuations of small machines, thesis, Université Paris-Saclay, 2018, https://tel.archives-ouvertes.fr/tel-01968075#.
[38] H. Vroylandt and G. Verley, Non-equivalence of dynamical ensembles and emergent non-ergodicity, J. Stat. Phys. **174**, 404 (2019).
[39] H. Touchette, The large deviation approach to statistical mechanics, Phys. Rep. **478**, 1 (2009).
[40] R. Chétrite and H. Touchette, Nonequilibrium markov processes conditioned on large deviations, Ann. Henri Poincaré **16**, 2005 (2015).
[41] M. Esposito, U. Harbola, and S. Mukamel, Entropy fluctuation theorems in driven open systems: Application to electron counting statistics, Phys. Rev. E **76**, 031132 (2007).
[42] M. Esposito, K. Lindenberg, and C. Van den Broeck, Universality of Efficiency at Maximum Power, Phys. Rev. Lett. **102**, 130602 (2009).
[43] B. Cleuren, B. Rutten, and C. Van den Broeck, Universality of efficiency at maximum power, Eur. Phys. J. Special Topics **224**, 879 (2015).
[44] J.-M. Park, H.-M. Chun, and J. D. Noh, Efficiency at maximum power and efficiency fluctuations in a linear brownian heat-engine model, Phys. Rev. E **94**, 012127 (2016).
[45] S. K. Manikandan, L. Dabelow, R. Eichhorn, and S. Krishnamurthy, Efficiency Fluctuations in Microscopic Machines, Phys. Rev. Lett. **122**, 140601 (2019).

Bibliography

[1] G. Verley, K. Mallick, and D. Lacoste. Modified fluctuation-dissipation theorem for non-equilibrium steady states and applications to molecular motors. *Europhys. Lett.*, 93:10002, 2011. (Cited on pages 4 and 5.)

[2] G. Verley, R. Chétrite, and D. Lacoste. Modified fluctuation-dissipation theorem for general non-stationary states and application to the Glauber-Ising chain. *J. Stat. Mech: Theory Exp.*, 10:P10025, 2011. (Cited on pages 4, 5 and 6.)

[3] G. Verley and D. Lacoste. Fluctuation theorems and inequalities generalizing the second law of thermodynamics out of equilibrium. *Phys. Rev. E*, 86:051127, 2012. (Cited on pages 4 and 5.)

[4] G. Verley and D. Lacoste. Fluctuations and response from a Hatano and Sasa approach. *Phys. Scr.*, 86:058505, 2012. (Cited on pages 4 and 5.)

[5] Gatien Verley. Nonequilibrium thermodynamic potentials for continuous-time markov chains. *Phys. Rev. E*, 93:012111, 2016. (Cited on pages ii, 4, 5, 12, 67, 68, 69, 74, 93 and 112.)

[6] G. Verley and D. Lacoste. Fluctuation relations and fluctuation-response for molecular motors. In *AIP Conf. Proc.*, volume 1332, pages 247–248, 2011. (Cited on page 4.)

[7] G. Verley, R. Chétrite, and D. Lacoste. Inequalities generalizing the second law of thermodynamics for transitions between non-stationary states. *Phys. Rev. Lett.*, 108:120601, 2012. (Cited on page 4.)

[8] Hadrien Vroylandt, Massimiliano Esposito, and Gatien Verley. Collective effects enhancing power and efficiency. *Europhys. Lett.*, 120(3):30009, nov 2017. (Cited on pages 4, 9, 19 and 122.)

[9] Hadrien Vroylandt, David Lacoste, and Gatien Verley. Degree of coupling and efficiency of energy converters far-from-equilibrium. *J. Stat. Mech: Theory Exp.*, 2018. (Cited on pages 4, 8, 13, 16, 22, 29, 33, 34 and 112.)

[10] Hadrien Vroylandt, David Lacoste, and Gatien Verley. An ordered set of power-efficiency trade-offs. *J. Stat. Mech: Theory Exp.*, 2019(5):054002, may 2019. (Cited on pages 4, 8, 14 and 112.)

[11] Paul Raux, Christophe Goupil, and Gatien Verley. Thermodynamic circuits i: Association of devices in stationary nonequilibrium. September 2023. (Cited on pages 4, 7, 8, 16, 33 and 35.)

[12] Hadrien Vroylandt and Gatien Verley. Non-equivalence of dynamical ensembles and emergent non-ergodicity. *J. Stat. Phys.*, 174(2):404–432, Jan 2018. (Cited on pages 4, 8, 13, 68 and 122.)

[13] G. Verley, T. Willaert, C. Van den Broeck, and M. Esposito. The unlikely carnot efficiency. *Nat. Commun.*, 5:4721, 2014. (Cited on pages 4, 9 and 120.)

[14] G. Verley, T. Willaert, C. Van den Broeck, and M. Esposito. Universal theory of efficiency fluctuations. *Phys. Rev. E*, 90:052145, 2014. (Cited on pages 4, 9, 12 and 121.)

[15] M. Polettini, G. Verley, and M. Esposito. Efficiency statistics at all times: Carnot limit at finite power. *Phys. Rev. Lett.*, 114:050601, 2015. (Cited on pages 4, 9 and 121.)

[16] H. Vroylandt, A. Bonfils, and G. Verley. Efficiency fluctuations of small machines with unknown losses. *Phys. Rev. E*, 93:052123, 2016. (Cited on pages 4, 9 and 121.)

[17] Hadrien Vroylandt, Massimiliano Esposito, and Gatien Verley. Efficiency fluctuations of stochastic machines undergoing a phase transition. *Phys. Rev. Lett.*, 124(25), jun 2020. (Cited on pages 4, 9, 13 and 122.)

[18] Gatien Verley. Dynamical equivalence classes for markov jump processes. *J. Stat. Mech: Theory Exp.*, 2022(2):023211, 2022. (Cited on pages 4, 12, 68, 71 and 120.)

[19] Lydia Chabane, Raphaël Chétrite, and Gatien Verley. Periodically driven jump processes conditioned on large deviations. *J. Stat. Mech: Theory Exp.*, 2020(3):033208, mar 2020. (Cited on pages 4, 10, 13, 112 and 118.)

[20] Lydia Chabane, Alexandre Lazarescu, and Gatien Verley. Effective hamiltonians and lagrangians for conditioned markov processes at large volume. *J. Stat. Phys.*, 187(1), feb 2022. (Cited on pages 4, 6, 10, 11, 13, 74 and 122.)

[21] G. Verley, C. Van den Broeck, and M. Esposito. Modulated two-level system: Exact work statistics. *Phys. Rev. E*, 88:032137, 2013. (Cited on pages 4, 12 and 121.)

[22] G. Verley, C. Van den Broeck, and M. Esposito. Work statistics in stochastically driven systems. *New J. Phys.*, 16(9):095001, 2014. (Cited on pages 4, 12 and 121.)

[23] S. Tusch, A. Kundu, G. Verley, T. Blondel, V. Miralles, D. Démoulin, D. Lacoste, and J. Baudry. Energy versus information based estimations of dissipation using a pair of magnetic colloidal particles. *Phys. Rev. Lett.*, 112:180604, 2014. (Cited on pages 4 and 5.)

[24] Albert Messiah. *Mécanique quantique*, volume 2. Dunod, Paris, 1995. (Cited on page 5.)

[25] Jean-Marcel Rax. *Mécanique analytique : Adiabaticité, résonances, chaos.* Dunod (Malakoff), 2020. (Cited on page 5.)

[26] R. Kubo. The fluctuation-dissipation theorem. *Rep. Prog. Phys.*, 29(1):255, 1966. (Cited on page 5.)

[27] P. Hänggi. Stochastic processes ii: Response theory and fluctuation theorems. 51:202, 1978. (Cited on page 5.)

[28] N. G. van Kampen. The case against linear response theory. *Physica Norvegica*, 5(3-4), 1971. (Cited on page 5.)

[29] P. Pietzonka, A. C. Barato, and U. Seifert. Universal bounds on current fluctuations. *Phys. Rev. E*, 93:052145, May 2016. (Cited on pages 5 and 13.)

[30] T. R. Gingrich, J. M. Horowitz, N. Perunov, and J. L. England. Dissipation bounds all steady-state current fluctuations. *Phys. Rev. Lett.*, 116:120601, Mar 2016. (Cited on pages 5 and 13.)

[31] A C Barato, R Chétrite, A Faggionato, and D Gabrielli. A unifying picture of generalized thermodynamic uncertainty relations. *Journal of Statistical Mechanics: Theory and Experiment*, 2019(8):084017, aug 2019. (Cited on page 5.)

[32] T. Harada and S. Sasa. Equality connecting energy dissipation with a violation of the fluctuation-response relation. *Phys. Rev. Lett.*, 95(13):130602, 2005. (Cited on page 5.)

[33] Andreas Dechant and Shin-ichi Sasa. Fluctuation-response inequality out of equilibrium. *Proceedings of the National Academy of Sciences*, 117(12):6430–6436, March 2020. (Cited on page 5.)

[34] L. F. Cugliandolo, J. Kurchan, and G. Parisi. Off equilibrium dynamics and aging in unfrustrated systems. *J. Phys.*, 4(11):1641–1656, 1994. (Cited on page 5.)

[35] T. Speck and U. Seifert. Restoring a fluctuation-dissipation theorem in a nonequilibrium steady state. *Europhys. Lett.*, 74:391, 2006. (Cited on page 5.)

[36] M. Baiesi, C. Maes, and B. Wynants. Fluctuations and response of nonequilibrium states. *Phys. Rev. Lett.*, 103:010602, 2009. (Cited on page 5.)

[37] R. Chétrite and K. Gawedzki. Eulerian and Lagrangian pictures of non-equilibrium diffusions. *J. Stat. Phys.*, 137:890, 2009. (Cited on page 5.)

[38] Denis J. Evans, E. G. D. Cohen, and G. P. Morriss. Probability of second law violations in shearing steady states. *Phys. Rev. Lett.*, 71:2401–2404, 1993. (Cited on page 6.)

[39] G. Gallavotti and E. G. D. Cohen. Dynamical ensembles in nonequilibrium statistical mechanics. *Phys. Rev. Lett.*, 74(14):2694–2697, 1995. (Cited on page 6.)

[40] Giovanni Gallavotti. Nonequilibrium and Fluctuation Relation. *Journal of Statistical Physics*, 180(1-6):172–226, aug 2019. (Cited on page 6.)

[41] J. L. Lebowitz and H. Spohn. A Gallavotti-Cohen-type symmetry in the large deviation functional for stochastic dynamics. *J. Stat. Phys.*, 95:333, 1999. (Cited on page 6.)

[42] K. Kurchan. Fluctuation theorem for stochastic dynamics. *J. Phys. A: Math. Gen.*, 31(16):3719, 1998. (Cited on page 6.)

[43] C. Jarzynski. Nonequilibrium equality for free energy differences. *Phys. Rev. Lett.*, 78(14):2690–2693, 1997. (Cited on page 6.)

[44] T. Hatano and S. I. Sasa. Steady-state thermodynamics of Langevin systems. *Phys. Rev. Lett.*, 86(16):3463–3466, 2001. (Cited on page 6.)

[45] Riccardo Rao and Massimiliano Esposito. Conservation laws and work fluctuation relations in chemical reaction networks. *The Journal of chemical physics*, 149(24):245101, 2018. (Cited on page 6.)

[46] Riccardo Rao and Massimiliano Esposito. Detailed fluctuation theorems: A unifying perspective. *Entropy*, 20(9):635, 2018. (Cited on page 6.)

[47] U. Seifert. Generalized Einstein or Green-Kubo relations for active biomolecular transport. *Phys. Rev. Lett.*, 104(13):138101, 2010. (Cited on page 6.)

[48] U. Seifert and T. Speck. Fluctuation-dissipation theorem in nonequilibrium steady states. *Europhys. Lett.*, 89(1):10007, 2010. (Cited on page 6.)

[49] Alexandre Lazarescu. Einstein's fluctuation relation and gibbs states far from equilibrium. February 2020. (Cited on page 6.)

[50] Pedro E. Harunari, Alberto Garilli, and Matteo Polettini. Beat of a current. *Phys. Rev. E*, 107:L042105, Apr 2023. (Cited on page 6.)

[51] Pedro E. Harunari, Annwesha Dutta, Matteo Polettini, and Édgar Roldán. What to learn from a few visible transitions' statistics? *Phys. Rev. X*, 12:041026, Dec 2022. (Cited on page 6.)

[52] P. Baerts, U. Basu, C. Maes, and S. Safaverdi. Frenetic origin of negative differential response. *Phys. Rev. E*, 88:052109, Nov 2013. (Cited on page 6.)

[53] Gianmaria Falasco, Tommaso Cossetto, Emanuele Penocchio, and Massimiliano Esposito. Negative differential response in chemical reactions. *New Journal of Physics*, 21(7):073005, jul 2019. (Cited on page 6.)

[54] Christophe Goupil. *Continuum theory and modeling of thermoelectric elements*. John Wiley & Sons, 2015. (Cited on page 6.)

[55] Ora Kedem and Roy S. Caplan. Degree of coupling and its relation to efficiency of energy conversion. *Trans. Faraday Soc.*, 61:1897–1911, 1965. (Cited on pages 7, 8, 14 and 16.)

[56] Aharon Katchalsky and Peter F. Curran. *Nonequilibrium Thermodynamics in Biophysics*. Harvard University Press, Cambridge, MA and London, England, 1965. (Cited on page 7.)

[57] Leonardo Peusner. *Studies in network thermodynamics*, volume 5. Elsevier, Studies in modern thermodynamics., 1986. (Cited on page 7.)

[58] Leonardo Peusner. Network thermostatics. *The Journal of Chemical Physics*, 83(3):1276–1291, 08 1985. (Cited on page 7.)

[59] Jean U. Thoma and Henri Atlan. Network thermodynamics with entropy stripping. *Journal of the Franklin Institute*, 303(4):319–328, 1977. (Cited on page 7.)

[60] Yann Apertet, Henni Ouerdane, Olga Glavatskaya, Christophe Goupil, and Philippe Lecoeur. Optimal working conditions for thermoelectric generators with realistic thermal coupling. *Europhysics Letters*, 97(2):28001, jan 2012. (Cited on page 7.)

[61] Yann Apertet, Henni Ouerdane, Christophe Goupil, and Philippe Lecoeur. Efficiency at maximum power of thermally coupled heat engines. *Phys. Rev. E*, 85:041144, Apr 2012. (Cited on page 7.)

[62] Yann Apertet, Henni Ouerdane, Christophe Goupil, and Philippe Lecoeur. Equivalent parameters for series thermoelectrics. *Energy Conversion and Management*, 93:160–165, 2015. (Cited on page 7.)

[63] C. Goupil, H. Ouerdane, E. Herbert, G. Benenti, Y. D'Angelo, and Ph. Lecoeur. Closed-loop approach to thermodynamics. *Phys. Rev. E*, 94:032136, Sep 2016. (Cited on page 7.)

[64] F. L. Curzon and B. Ahlborn. Efficiency of a Carnot engine at maximum power output. *Am. J. Phys.*, 43(1):22–24, 1975. (Cited on page 7.)

[65] George Oster, Alan Perelson, and Aharon Katchalsky. Network thermodynamics. *Nature*, 234(5329):393–399, dec 1971. (Cited on page 7.)

[66] William Sutherland. LXXV. a dynamical theory of diffusion for non-electrolytes and the molecular mass of albumin. *The London, Edinburgh, and Dublin Philosophical Magazine and Journal of Science*, 9(54):781–785, jun 1905. (Cited on page 8.)

[67] A. Einstein. Über die von der molekularkinetischen theorie der wärme geforderte bewegung von in ruhenden flüssigkeiten suspendierten teilchen. *Annalen der Physik*, 322(8):549–560, 1905. (Cited on pages 8, 119 and 121.)

[68] Lars Onsager. Reciprocal relations in irreversible processes. i. *Phys. Rev.*, 37:405–426, Feb 1931. (Cited on page 8.)

[69] Lars Onsager. Reciprocal relations in irreversible processes. ii. *Phys. Rev.*, 38:2265–2279, Dec 1931. (Cited on page 8.)

[70] M. Toda R. Kubo and N. Hashitsume. *Statistical Physics II.* Springer, 1985. (Cited on page 8.)

[71] Hadrien Vroylandt. *Thermodynamics and fluctuations of small machines.* Theses, Université Paris-Saclay, September 2018. (Cited on pages 8 and 10.)

[72] Hugo Touchette. Methods for calculating nonconcave entropies. *J. Stat. Mech: Theory Exp.*, (05):P05008, 2010. (Cited on pages 8, 13 and 122.)

[73] B. Cleuren and C. Van den Broeck. Ising model for a brownian donkey. *Europhys. Lett.*, 54(1):1, 2001. (Cited on pages 9, 13 and 122.)

[74] R. Chétrite and T. Touchette. Variational and optimal control representations of conditioned and driven processes. *J. Stat. Mech: Theory Exp.*, 2015(12):P12001, 2015. (Cited on page 9.)

[75] R. Chétrite and H. Touchette. Nonequilibrium markov processes conditioned on large deviations. *Annales Henri Poincaré*, 16(9):2005–2057, 2015. (Cited on pages 9 and 14.)

[76] R. Chétrite and H. Touchette. Nonequilibrium microcanonical and canonical ensembles and their equivalence. *Phys. Rev. Lett.*, 111:120601, Sep 2013. (Cited on pages 9 and 14.)

[77] Raphaël Chétrite. *Périgrinations sur les phénomènes aléatoires dans la nature.* Habilitation à diriger des recherches, Université de Nice. Laboratoire J.A. Dieudonné, 2018. (Cited on page 9.)

[78] J. Ross. *Thermodynamics and fluctuations far from equilibrium.* Springer Berlin Heidelberg NewYork, 2008. (Cited on page 10.)

[79] Lydia Chabane. *From rarity to typicality : the improbable journey of a large deviation.* Theses, Université Paris-Saclay, November 2021. (Cited on page 10.)

[80] Alexandre Lazarescu, Tommaso Cossetto, Gianmaria Falasco, and Massimiliano Esposito. Large deviations and dynamical phase transitions in stochastic chemical networks. *J*, 151(6):064117, 2019. (Cited on page 10.)

[81] Y Oono and M Paniconi. Steady state thermodynamics. *Prog. of Theo. Phys. Supplement*, 130:29–44, 1998. (Cited on page 10.)

[82] M. Polettini. Nonequilibrium thermodynamics as a gauge theory. *Europhys. Lett.*, 97(3):30003, 2012. (Cited on page 12.)

[83] R. K. P. Zia and B. Schmittmann. Probability currents as principal characteristics in the statistical mechanics of non-equilibrium steady states. *J. Stat. Mech: Theory Exp.*, (P07012), 2007. (Cited on page 12.)

[84] Julien Tailleur, Jorge Kurchan, and Vivien Lecomte. Mapping nonequilibrium onto equilibrium: The macroscopic fluctuations of simple transport models. *Phys. Rev. Lett.*, 99:150602, Oct 2007. (Cited on page 12.)

[85] Christian Maes. Frenesy: Time-symmetric dynamical activity in nonequilibria. *Physics Reports*, 850:1–33, mar 2020. (Cited on page 12.)

[86] C. Maes and K. Netočný. Canonical structure of dynamical fluctuations in mesoscopic nonequilibrium steady states. *Europhys. Lett.*, 82(3):30003, 2008. (Cited on page 12.)

[87] David Andrieux. Equivalence classes for large deviations. *arXiv*, August 2012. (Cited on pages 12 and 68.)

[88] Sara Dal Cengio, Vivien Lecomte, and Matteo Polettini. Geometry of nonequilibrium reaction networks. *Phys. Rev. X*, 13:021040, Jun 2023. (Cited on page 12.)

[89] Riccardo Rao and Massimiliano Esposito. Conservation laws shape dissipation. *New Journal of Physics*, 20(2):023007, feb 2018. (Cited on pages 12 and 21.)

[90] Cecile Monthus. Inverse problem in the conditioning of markov processes on trajectory observables: what canonical conditionings can connect two given markov generators ? August 2023. (Cited on page 12.)

[91] Andre C Barato and Raphael Chétrite. Current fluctuations in periodically driven systems. *J. Stat. Mech: Theory Exp.*, 2018(5):053207, may 2018. (Cited on page 13.)

[92] Patrick Pietzonka and Udo Seifert. Universal trade-off between power, efficiency, and constancy in steady-state heat engines. *Phys. Rev. Lett.*, 120:190602, May 2018. (Cited on page 13.)

[93] P. Pietzonka, A. C. Barato, and U. Seifert. Universal bound on the efficiency of molecular motors. *J. Stat. Mech: Theory Exp.*, 2016(12):124004, 2016. (Cited on page 13.)

[94] Andre C. Barato and Udo Seifert. Cost and precision of brownian clocks. *Phys. Rev. X*, 6:041053, Dec 2016. (Cited on page 13.)

[95] Timur Koyuk, Udo Seifert, and Patrick Pietzonka. A generalization of the thermodynamic uncertainty relation to periodically driven systems. *Journal of Physics A: Mathematical and Theoretical*, 52(2):02LT02, December 2018. (Cited on page 14.)

[96] Navinder Singh and Bram Wynants. Dynamical fluctuations for periodically driven diffusions. *J. Stat. Mech: Theory Exp.*, (03):P03007, 2010. (Cited on page 14.)

[97] Lorenzo Bertini, Raphael Chetrite, Alessandra Faggionato, and Davide Gabrielli. Level 2.5 large deviations for continuous-time markov chains with time periodic rates. *Annales Henri Poincaré*, 19(10):3197–3238, Oct 2018. (Cited on pages 14 and 112.)

[98] C. Van den Broeck. Stochastic thermodynamics: a brief introduction. *Proceedings of the International School of Physics "Enrico Fermi", Course CLXXXIV Physics of Complex Colloids, C. Bechinger, F. Sciortino and P. Ziherl eds., Italian Physical Society*, 2013. (Cited on page 16.)

[99] L. Peliti and S. Pigolotti. *Stochastic Thermodynamics: An Introduction.* Princeton University Press, 2021. (Cited on page 16.)

[100] M. Esposito. Stochastic thermodynamics under coarse graining. *Phys. Rev. E*, 85:041125, 2012. (Cited on page 20.)

[101] Jean-Marcel Rax. *Physique de la conversion d'énergie.* EDP Science et Edition CNRS, 2015. (Cited on pages 22 and 25.)

[102] D Andrieux and P Gaspard. Fluctuation theorem and Onsager reciprocity relations. *J. Chem. Phys.*, 121(13):6167–6174, 2004. (Cited on page 22.)

[103] D. Lacoste, A. W.C. Lau, and K. Mallick. Fluctuation theorem and large deviation function for a solvable model of a molecular motor. *Phys. Rev. E*, 78(1):011915, 2008. (Cited on pages 25, 119 and 120.)

[104] B. Cleuren, B. Rutten, and C. Van den Broeck. Universality of efficiency at maximum power. *Eur. Phys. J. Special Topics*, 224(5):879–889, 2015. (Cited on page 28.)

[105] J. Schnakenberg. Network theory of microscopic and macroscopic behavior of master equation systems. *Rev. Mod. Phys.*, 48:571–585, 1976. (Cited on page 29.)

[106] T. L. Hill. *Free Energy Transduction and Biochemical Cycle Kinetics.* Springer-Verlag New York, Inc., 1989. (Cited on page 29.)

[107] Matteo Polettini and Massimiliano Esposito. Irreversible thermodynamics of open chemical networks. i. emergent cycles and broken conservation laws. *J. Chem. Phys.*, 141(2), 2014. (Cited on page 29.)

[108] Matteo Polettini, Gregory Bulnes-Cuetara, and Massimiliano Esposito. Conservation laws and symmetries in stochastic thermodynamics. *Phys. Rev. E*, 94:052117, Nov 2016. (Cited on page 29.)

[109] Matteo Polettini. *Geometric and Combiatorial Structures in Nonequilibrium Statistical Mechanics*. PhD thesis, Universita di Bologna, 2012. (Cited on page 30.)

[110] David Andrieux. Nonequilibrium large deviations are determined by equilibrium dynamics. *arXiv*, 2012. (Cited on page 68.)

[111] David Andrieux. Making sense of nonequilibrium current fluctuations: A molecular motor example. June 2023. (Cited on page 68.)

[112] Matteo Polettini. Best statistics of markovian fluxes: a tale of eulerian tours and fermionic ghosts. *J. Phys. A: Math. Theor.*, 48(36):365005, 2015. (Cited on page 68.)

[113] Adrián A Budini, Robert M Turner, and Juan P Garrahan. Fluctuating observation time ensembles in the thermodynamics of trajectories. *J. Stat. Mech: Theory Exp.*, 2014(3):P03012, 2014. (Cited on pages 68, 71, 72 and 74.)

[114] H. Touchette. The large deviation approach to statistical mechanics. *Phys. Rep.*, 478:1–69, 2009. (Cited on page 71.)

[115] Herbert B. Callen. *Thermodynamics and an Introduction to Thermostatistics*. Wiley, New York, 2nd edition, 1985. (Cited on page 74.)

[116] Todd R Gingrich, Grant M Rotskoff, and Jordan M Horowitz. Inferring dissipation from current fluctuations. *Journal of Physics A: Mathematical and Theoretical*, 50(18):184004, April 2017. (Cited on pages 112 and 115.)

[117] Lorenzo Bertini, Alessandra Faggionato, and Davide Gabrielli. Flows, currents, and cycles for markov chains: Large deviation asymptotics. *Stochastic Processes and their Applications*, 125(7):2786–2819, jul 2015. (Cited on page 114.)

[118] Andre C Barato, Raphael Chétrite, Alessandra Faggionato, and Davide Gabrielli. Bounds on current fluctuations in periodically driven systems. *New Journal of Physics*, 20(10):103023, oct 2018. (Cited on pages 115 and 118.)

[119] K. Proesmans and C. Van den Broeck. Onsager coefficients in periodically driven systems. *Phys. Rev. Lett.*, 115:090601, Aug 2015. (Cited on page 118.)

[120] Giorgio Parisi. Brownian motion. *Nature*, 433(7023):221–221, January 2005. (Cited on page 119.)

[121] A. W. C. Lau, D. Lacoste, and K. Mallick. Nonequilibrium fluctuations and mechanochemical couplings of a molecular motor. *Phys. Rev. Lett.*, 99:158102, Oct 2007. (Cited on page 119.)

[122] Anatoly B. Kolomeisky and Michael E. Fisher. Molecular motors: A theorist's perspective. *Annu. Rev. Phys. Chem.*, 58(1):675–695, 2007. (Cited on page 119.)

[123] U. Seifert. Stochastic thermodynamics, fluctuation theorems and molecular machines. *Rep. Prog. Phys.*, 75(12):126001, 2012. (Cited on page 119.)

[124] E. Herbert, H. Ouerdane, Ph. Lecoeur, V. Bels, and Ch. Goupil. Thermodynamics of animal locomotion. *Physical Review Letters*, 125(22):228102, nov 2020. (Cited on page 119.)

[125] H. Wang and George Oster. Energy transduction in the F1 motor of ATP synthase. *Nature*, 396:279–282, 1998. (Cited on page 119.)

[126] Ryohei Yasuda, Hiroyuki Noji, Kazuhiko Kinosita, and Masasuke Yoshida. F1-ATPase is a highly efficient molecular motor that rotates with discrete 120° steps. *Cell*, 93(7):1117–1124, 1998. (Cited on page 119.)

[127] K. Hayashi, H. Ueno, R. Lino, and H. Noji. Fluctuation theorem applied to F1-ATPase. *Phys. Rev. Lett.*, 104(21):218103, 2010. (Cited on page 119.)

[128] Eva Zimmermann and Udo Seifert. Efficiencies of a molecular motor: a generic hybrid model applied to the F1-ATPase. *New Journal of Physics*, 14(10):103023, October 2012. (Cited on page 119.)

[129] Sosuke Ito and Takahiro Sagawa. Maxwell's demon in biochemical signal transduction with feedback loop. *Nature Communications*, 6(1), June 2015. (Cited on page 119.)

[130] I. A. Martinez, E. Roldán, L. Dinis, D. Petrov, J. M. R. Parrondo, and R. Rica. Brownian Carnot engine. *Nat. Phys.*, 12:67, 2015. (Cited on page 120.)

[131] John P. S. Peterson, Tiago B. Batalhão, Marcela Herrera, Alexandre M. Souza, Roberto S. Sarthour, Ivan S. Oliveira, and Roberto M. Serra. Experimental characterization of a spin quantum heat engine. *Phys. Rev. Lett.*, 123:240601, Dec 2019. (Cited on page 120.)

université
PARIS-SACLAY

Titre: Fluctuations hors de l'équilibre et processus de conversion
Mots clés: Thermodynamique stochastique, Courants Couplés, Théorie des grandes déviations, Fluctuations d'Éfficacité, Production d'Entropie

Résumé: Cette thèse d'habilitation présente une étude approfondie des processus de conversion aux niveaux moyen et fluctuant. Elle s'appuie sur la thermodynamique stochastique pour modéliser de petits convertisseurs couplant différents courants. La théorie des grandes déviations fournit des outils méthodologiques pour les travaux présentés, mais est également considérée pour ses interactions profondes avec la physique statistique. Le chapitre d'introduction approfondit une description globale de mes recherches, en zoomant sur divers sous-domaines tels que : la théorie des réponses hors d'équilibre, les relations de fluctuation, les transitions de phase dynamiques, la transformation et la rectification de Doob, ou le calcul exact de fonctions génératrices des cumulants. Le deuxième chapitre introduit la thermodynamique stochastique et la physique des courants couplés en régime linéaire et non linéaire au niveau moyen. Nous décrivons le concept de conductance non linéaire et appliquons ce concept pour développer une théorie des circuits de dispositifs hors d'équilibre. Le troisième chapitre se concentre sur des résultats de la théorie des grandes déviations appliquée aux processus de saut markovien. Nous étendons au niveau 2.5 le lien existant entre les grandes déviations à asymptotiquement grand temps d'observation ou à asymptotiquement grande activité. Dans ce contexte, nous relions les processus transformés de Doob obtenus à temps continu et discret. Par la suite, nous décrivons la difficulté qui se pose lorsqu'on tente de relier, par transformations de Doob, des dynamiques d'équilibre et hors d'équilibre de type Arrhenius. Nous terminons ce chapitre en généralisant pour les états périodiques dans le temps nos travaux sur les matrices de conductance non linéaires. Le dernier chapitre met l'accent sur la cohérence de nos travaux qui visent à caractériser le rendement stochastique de convertisseurs très fluctuants.

Title: Nonequilibrium fluctuations and conversion processes
Keywords: Stochastic Thermodynamics, Coupled Currents, Large Deviations Theory, Efficiency Fluctuations, Entropy Production

Abstract: This professorial thesis presents a comprehensive study of conversion processes at the mean and fluctuating levels. It relies on stochastic thermodynamics to model small converters coupling different currents. Large deviation theory provides methodological tools for the presented works, but it is also considered for its profound interplay with statistical physics. The introductory chapter delves into an overall description of my research, zooming into various subfields such as nonequilibrium response theory, fluctuation relations, dynamical phase transitions, Doob transformation, and rectification, or exact computation of cumulant generating function. The second chapter introduces stochastic thermodynamics and the physics of coupled currents in the linear and nonlinear regime at the mean level. We describe the concept of nonlinear conductance and apply this concept to develop a circuit theory of nonequilibrium devices. The third chapter focuses on results in large deviation theory. We extend to level 2.5 the existing relation between large deviations with asymptotically long observation times or asymptotically large activity. In this context, we relate the Doob-transformed processes in continuous and discrete time. Next, we describe the difficulty arising when trying to relate, by Doob transforms, the arrhénius dynamics of in- and out-of-equilibrium systems. We end this chapter by generalizing our work on nonlinear conductance matrices for time-periodic states. The last chapter emphasizes the coherence of our works that aim to characterize the stochastic efficiency of highly fluctuating converters.